FILAMENTARY OXIDE FORMATION ON IRON

A thesis presented for the Degree of
Doctor of Philosophy in Mechanical Engineering
in the University of Canterbury, Christchurch,
New Zealand.

by B.L. Rhoades, B.E. (Hons)

University of Canterbury,
December, 1975.

ACKNOWLEDGEMENTS

My sincere thanks are due to Dr L.A. Erasmus who has supervised this work. His guidance and encouragement throughout the duration of the project have been much appreciated.

The support of Professor D.C. Stevenson and the staff of the Department of Mechanical Engineering is gratefully acknowledged. Many members of the academic, technical and secretarial staff have assisted the project; but, in particular, my thanks go to my colleague, Mr J. S. Smaill, for his interest, assistance with many aspects of computer programming, and for provision of a copy of a computer program to generate stereographic projections; to the workshop staff directed by Mr E.D. Retallick, especially Mr O. Bolt for his skill in constructing the gas reaction chamber described in Chapter 3; to Mr H.J. Anink for design and construction of the electronic control systems for the reaction chamber; to Mrs J. Ritchie for her care in preparation of many diagrams and photographs; and to Mrs D. Jeal for her enthusiastic and meticulous typing of the thesis.

Appreciation is also due to Dr S.R. Keown of the Department of Metallurgy, University of Sheffield, for his interest, helpful comments and assistance with part of the experimental programme.

Construction of the gas reaction chamber was supported by a grant from the University Grants Committee which is gratefully acknowledged.

The continual encouragement and assistance given by my wife, Merilyn, has enabled me to undertake and complete this study programme.

ABSTRACT

The oxidation of iron in air or oxygen at temperatures between 300°C and 800°C is accompanied by the growth of filamentary crystals from the outer oxide surface. Below 470°C the predominant crystal habit is pointed platelets of approximately 10 μm thickness and 1-4 μm length, while above 470°C ribbon-like whiskers of 5 μm to 2 μm thickness and lengths up to 30 μm are observed.

The structure of these crystals has been examined by transmission electron microscopy and electron diffraction. Selected area electron diffraction spot patterns have been indexed using a rapid computer technique which has been developed to compare the geometry of diffraction patterns with reciprocal lattice planes of any crystal. Both platelets and whiskers are shown to consist of αFe_2O_3 with $\langle 10\bar{1} \rangle$ structural rhombohedral growth direction. A feature of diffraction from the platelet crystals is the presence of continuous reciprocal lattice streaks, which indicate the existence of a high density of planar defects lying parallel to the (010) platelet face. Most of the whisker filaments consist of multiple crystals with a common $\langle 10\bar{1} \rangle$ growth direction; and no evidence of lattice twist, to indicate the existence of screw dislocations, is provided by the diffraction patterns.

The construction of a high temperature controlled atmosphere specimen chamber for the JEM 7A electron microscope has enabled the growth process of the oxide filaments to be directly observed. Specimen motion includes tilting to a limit of 15° about any axis in the plane of the specimen and continuous observation is possible at temperatures up to 1000°C and gas pressures up to 30 kPa. After an initial induction period both whisker and platelet crystals are preferentially nucleated on surface protruberances and exhibit a linear rate of growth with respect to time The linear growth is abruptly terminated at a variety of filament lengths.

At 500°C a variation of growth rates of 1.6 μm/min to 0.1 μm/min is observed between adjacent filaments on a single specimen; and a maximum growth rate of 15 μm/min has been observed at approximately 800°C. Platelet crystals maintain a constant shape and broaden at the base as the length increases.

Arguments are presented in support of the proposal that the growth of both platelets and whiskers occurs by transport of oxide molecules to the filament tips by surface diffusion over whisker and platelet side-walls of high crystalline perfection; rate control being attributed to the generation and propagation of growth steps at the filament tips.

CONTENTS

LIST OF FIGURES

LIST OF TABLES

CHAPTER 1

INTRODUCTION

1.1 SCOPE OF THESIS

With the exception of gold, no pure metal or alloy is stable in air at room temperature. All metals tend to form oxides and, although the rate of reaction is very slow at low temperatures in many instances, the utilisation of metals at high temperatures is severely limited by reactions with their gaseous environment.

Over the past three decades considerable research has been directed towards the development of oxidation-resistant alloys capable of providing the improved performance demanded by high-temperature technology. The primary basis for much of this effort has been the work of Carl Wagner who demonstrated in the 1930's the importance of point defects in the diffusion processes controlling the formation of what were observed to be coherent uniform oxidation layers on metal surfaces. Development of this theory led to optimism that it would become possible to predict the manner in which alloying elements would modify the defect structure of oxide layers, and hence to predict the high temperature behaviour of new materials rather than rely on a purely empirical approach.

Many workers in the field were surprised when early electron microscopes and other improved experimental techniques revealed a degree of complexity in oxidation mechanisms and structures which was previously uncontemplated. These observations revealed that the oxide grows normally as discrete particles and crystallites in a variety of shapes and forms during the initial stages of oxidation. Even after a thin base film of oxide has been formed on the metal, the surface is often covered with dense growths of crystallites in the form of mounds, polyhedra, columnar crystals, whiskers and platelets. As the number of observations

of such particles increased, the tendency to regard the whisker and platelet growth as either exceptional or unessential to the course of the oxidation reaction was replaced by the acknowledgement that these are quite normal features of certain stages of most oxidation processes. Consequently, the diffusion-controlled theory of oxide layer formation had to be reconsidered in terms of nucleation processes, phase boundary processes and crystal growth kinetics. It also became evident that the development of alloys based on the interpretation of oxidation behaviour in terms of simple diffusion models is unlikely to be accomplished.

Despite considerable research effort applied to the elucidation of the structure and growth mechanism of these surface particles, their occurrence and their relation to oxide layer formation remain largely unexplained. The discovery of the exceptional mechanical properties of filamentary particles and their potential for utilisation as strengthening agents in composite materials has provided additional impetus for this research effort.

This project was commenced with the objective of determining the structure and growth mechanism of filamentary oxide particles by examination with electron microscopy and electron diffraction techniques. The scope of this thesis is suggested by this objective, although the extent of the investigation has been largely restricted to the oxide formations on iron surfaces. The vast literature on whisker and allied growth phenomena has been surveyed and numerous reported observations of oxide particulate growth have been examined in terms of the existing theory. The difficulties in successfully observing successive stages in the growth of a single whisker particle, by alternate observation and oxidation in a furnace external to the electron microscope, led to the design and development of a controlled atmosphere high-temperature specimen stage for a transmission electron microscope which allows *in situ* observation of oxidation reactions. This stage provides for tilting of

the specimen to enable effective utilisation of selected area electron diffraction as the reaction proceeds. The development of computer techniques to interpret electron diffraction patterns from non-cubic structures has also been an integral part of this study, as no experience of electron diffraction from these materials existed in New Zealand at the commencement of this project in 1970.

1.2 INITIAL STAGES OF OXIDE FORMATION

The first step in the reaction between a metal and oxygen is the adsorption of gas on the metal surface. Observations of this process are rare, owing to the difficulties in producing "clean" metal surfaces and the stringent high-vacuum requirements needed to maintain them, but low-energy electron diffraction (LEED) studies [1] on clean surfaces have established that the adsorbed molecules of oxygen are dissociated and may form a variety of two-dimensional structures depending on the nature of the adsorbent and adsorbate; the exposed crystal face; degree of coverage; temperature; and the presence of impurity atoms or surface defects. The adsorbed layer may range from the amorphous, like that found in adsorption of oxygen on silicon, to the regular ordered structures such as are formed on nickel surfaces.

After the metal surfaces have become completely covered with chemisorbed oxygen, LEED observations revealed that isolated oxide nuclei appear at what seem to be random positions on the surface. These nuclei grow laterally by surface diffusion, in the form of small expanding islands of fairly constant height, until the entire metal surface is covered with an oxide film less than 10 monolayers thick. The end of this first stage is indicated by an abrupt decrease in the rate of oxygen uptake. Observations of these early stages of oxidation are summarised by Rhodin *et al*[2], Kofstad[3], Benard[4], and Kubaschewski and Hopkins[5].

As soon as the nucleation behaviour became known, a number of

researchers asserted that the locations of the nuclei are controlled by the presence of defects. However, further research has shown that although the presence of surface defects is important when the reaction takes place at low temperatures the influence decreases at higher temperatures. At high temperatures all the characteristics of homogeneous nucleation are exhibited, the number of nuclei being determined only by the temperature and concentration of the oxidising agent.

Although the effect of nucleation is most pronounced at the commencement of the reaction, its existence greatly influences the texture, structure, and epitaxy of the thick oxide films and surface growths which form later. Nucleation and surface diffusion processes at the metal/oxide interface may control the rate of oxidation when porous non-protective films are formed at high temperatures, or when new phases are nucleated on the surface of an initial layer. For example: under certain conditions the oxidation rate of iron has an unusual dependence on the oxygen pressure owing to the nucleation and growth of Fe_2O_3 crystals on the surface of the initial layer of Fe_3O_4 [6].

1.3 GROWTH OF OXIDE LAYERS

1.3.1 Low Temperatures

The initial stage of oxidation results in a compact oriented layer of oxide crystals covering the metal surface. Thi layer constitutes a physical barrier separating the reactants. When such a film has formed it is assumed in most theories that the reaction rate of further oxidation is determined by transport of the reacting ions through the film. At high temperatures this transport is assumed to involve diffusion due to a chemical potential gradient across the scale, but at lower temperatures ion transport is facilitated by an electrical potential gradient. It is assumed that oxygen atoms are adsorbed on the oxide surface, and that an equilibrium between the metal and adsorbed oxygen is established by the

rapid tunnelling of electrons through the thin oxide film. This process establishes the electrical potential gradient which provides the driving force for diffusion.

A characteristic feature of low temperature oxidation is that the oxidation reaction is initially very rapid but that it gradually decreases to very low levels. The extent of the reaction is often proportional to the logarithm of elapsed time, which results in a thin protective film covering the metal surface. To explain this behaviour a large number of theories have been developed[3, 7], most of which attempt to relate the influence of a number of competing mechanisms. These mechanisms include electric field-induced transport; chemical diffusion; space charges in the oxide film; rate control by electron tunnelling; preferential diffusion along grain boundaries and other low resistance paths; adsorption; and nucleation and growth mechanisms. The rapid rate of change and the experimental difficulties associated with the study of thin film formation makes it difficult or impossible to verify the validity of the various models and the parameters in the derived equations. Most of the theories also assume the existence and formation of uniform plane-parallel oxide films but, as indicated previously, this is not a generally acceptable assumption. The mechanisms of low temperature oxidation, therefore, remain poorly understood.

1.3.2 High Temperatures

The classical theory of oxidation at high temperatures, proposed by Wagner[8, 9], assumes a volume diffusion of the reacting ions or a transport of electrons across the growing compact layer is the rate-determining process of the total reaction. Reactions at phase boundaries are considered to be very rapid, and it is assumed that thermodynamic equilibrium is established between the oxide and the oxygen gas at the oxide/gas interface and between the metal and the oxide at the metal/oxide interface. The driving force for the reaction is the free-energy change

associated with formation of the oxide, and concentration gradients of the components are formed in the oxide layer as a result of the reaction.

On the basis of this model of ionic transport through a film lattice of different concentrations at the two interfaces, Wagner derived an expression for the rate of thickening which predicted the increase in the film thickness with time to be inversely proportional to the film thickness. Hence the thickness at a given time is proportional to the square root of time which is in accordance with parabolic rate laws that are frequently obtained experimentally. However, attempts to relate the observed growth rates to the thermodynamic parameters which control diffusion through the oxide have met with many difficulties. Numerous complications have been revealed which may modify reaction kinetics to such an extent that the theory has very limited value as a means of predicting oxidation behaviour in most systems. The most significant complicating factors are as follows:

(a) Multilayered Scales:

If a metal has several oxidation states and forms a number of compounds with oxygen, these compounds are arranged in layers with the compound richest in oxygen at the oxide-gas interface and the compound richest in metal in contact with the metallic base. The total oxidation behaviour will be determined by the nature of the oxide in the different layers. It is not unusual to find that the higher oxide forms a porous non-protective scale growing on a compact scale of a lower oxide.

(b) Grain Boundary and Short Circuit Diffusion:

The polycrystalline nature of oxide layers implies that enhanced diffusion will occur along grain boundaries and other low resistance paths and may be the predominant mode of transport, particularly at low temperatures. Grain boundary diffusion is normally a function of grain orientation, which provides an additional factor to be considered.

(c) Orientation Relationships between Phases:

The existence of well defined crystallographic relationships between the metal and its oxide, or between adjacent oxide layers, may improve the adherence of the oxide and increase the rate at which ions can transfer across the phase boundaries.

(d) Accumulation of Impurities:

Electron microscopic examination of oxide/metal interfaces reveals that the interface morphology is very dependent on the metal porosity. In the case of iron the metal/oxide interface is a smooth plane when the iron is of very high (zone melted) purity, but may be highly irregular when small quantities of impurities are present. The irregularity is due to the accumulation of less easily oxidised impurities in the metal adjacent to the interface. This change of metal composition in the vicinity of the interface becomes more significant as the impurity level increases. When the level of impurities is of the order of one percent rapid modification of the metal composition may occur, leading to numerous possible changes in the reaction kinetics.

(e) Porosity:

In addition to the accumulation of impurities at the interface, the accumulation of vacancies in the oxide frequently creates cavities at the metal/oxide interface and porosity in the oxide. In such cases the cavities may act as barriers to the solid state diffusion process or may cause rupture of the oxide scale. In either case, solid-state diffusion through the scale is no longer rate-determining.

(f) Stress in the Oxide Layer:

Stresses in oxide films may be generated by epitaxial relationships, oxide-metal lattice mismatch, the formation of cavities, the growth morphology of the oxide, differences in oxidation rates between neighbouring grains, the presence of foreign inclusions which are oxidised at different rates from the parent metal, differences in thermal expansion, and other factors. These stresses may lead to cracking and rupture of the layer or stripping of the layer from the metal surface, particularly after it has reached a certain critical thickness. In these circumstances the oxidation kinetics commonly revert to a linear relationship. Such kinetics may reflect that phase boundary relationships involving adsorption and nucleation have become rate-determining, that gas diffusion through the pores is limiting the reaction, or that successive cycles of diffusion-controlled oxidation followed by layer breakdown are occurring. Hence, the course of the reaction is dependent to a major extent on the mechanical properties of the oxide layers, their ability to plastically deform under load, and their adherence to the substrate.

A different type of oxidation reaction kinetics occurs in the case where the rate-determining step is no longer diffusion through the oxide, but is some phase boundary process. The most common examples involve adsorption or dissociation of adsorbed molecules at the gas/oxide interface in atmospheres with low oxygen partial pressure. In such circumstances the reaction takes place at a constant rate and resembles the behaviour when the oxide is not compact.

1.4 OXIDATION BEHAVIOUR OF IRON

The outstanding technological importance of iron and its alloys has resulted in considerable expenditure of effort to understand its oxidation

behaviour. Surveys of this work appear in the oxidation texts[3-5,10], and the following discussion is confined to aspects of the oxidation of iron under conditions which promote the growth of surface particles such as whiskers and platelets.

Iron forms three stable oxides, namely: wustite, FeO (face centred cubic), magnetite Fe_3O_4 (face centred cubic), and hematite α Fe_2O_3 (rhombohedral). Details of the structure of these compounds and of maghemite γFe_2O_3, goethite αFeOOH, and lepidocrocite γFeOOH, are provided in Appendix 4.

The equilibrium diagram of the iron-oxygen system in Figure 1.1 shows that two distinct temperature regions must be considered for the oxidation of iron. Below 570°C the greatest part of the oxide layer consists of Fe_3O_4, which is covered with thin outer layers of γFe_2O_3 and αFe_2O_3 as shown in Figure 1.2. FeO is not stable in bulk below 570°C, but it may continue to be present as a thin film adjacent to the metal surface at temperatures down to 400°C. Above 570°C the oxide layer consists primarily of FeO, with thin outer layers of Fe_3O_4 and Fe_2O_3 as shown in Figure 1.3. The FeO proportion of the total oxide produced increases with increasing temperature until significant quantities of Fe_3O_4 and Fe_2O_3 can no longer be detected above 750°C. From many observations, Hauffe[10] presents the simplified schematic representation of the oxidation mechanism in this temperature range which is shown in Figure 1.4.

Kinetic investigations have been paralleled by studies to determine the structure of the oxide films and their orientation relationships. Electron microscopic investigations by Gulbransen and co-workers[11] showed that the course of high temperature oxidation can be separated into four stages, as is shown in Figure 1.5. The initial stage involves the chemisorption of a layer of oxygen atoms which rapidly grows into a compact film of fine oxide crystallites approximately 10nm thick. This is followed by the nucleation and growth of larger crystals which grow in rows

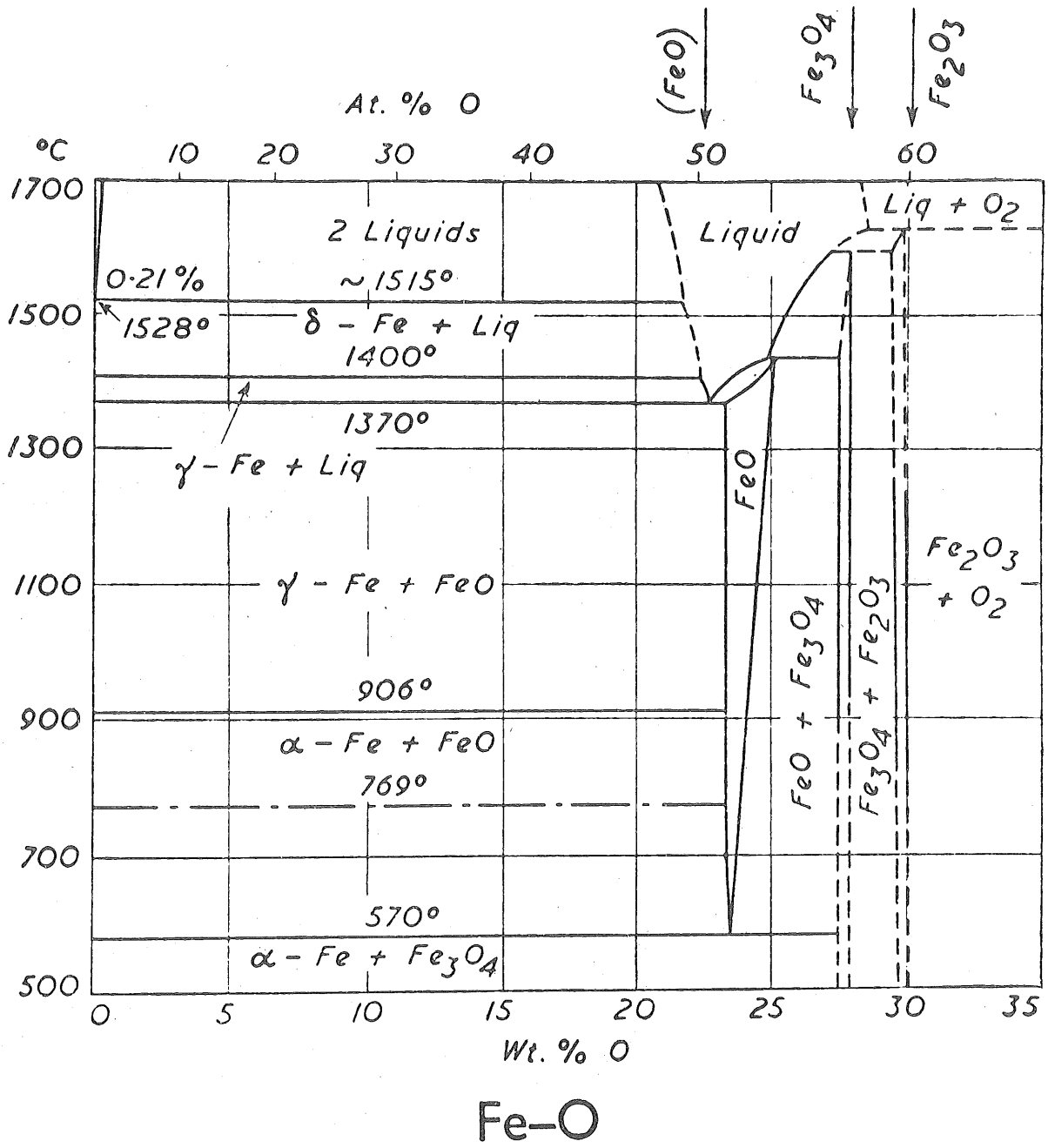

Fig. 1.1 Iron - Oxygen phase diagram. From Smithells[127].

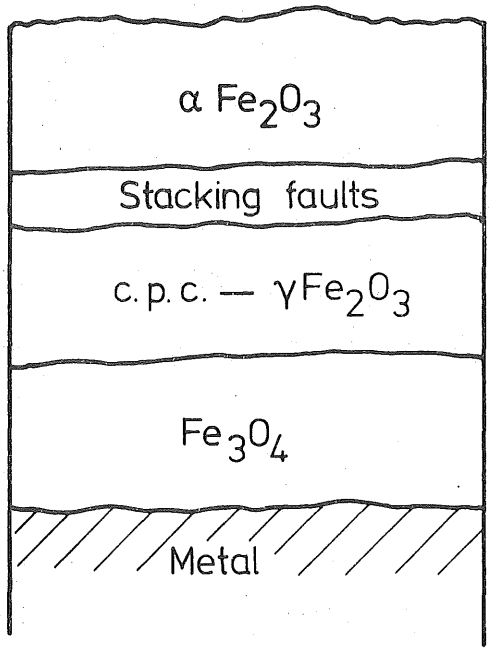

Fig. 1.2 Composition of thin iron oxide film on single crystal surfaces below 570°C. c.p.c. designates a close-packed cubic array of oxygen planes with a distribution of cations resembling that of γFe_2O_3. From Sewell and Cohen[16].

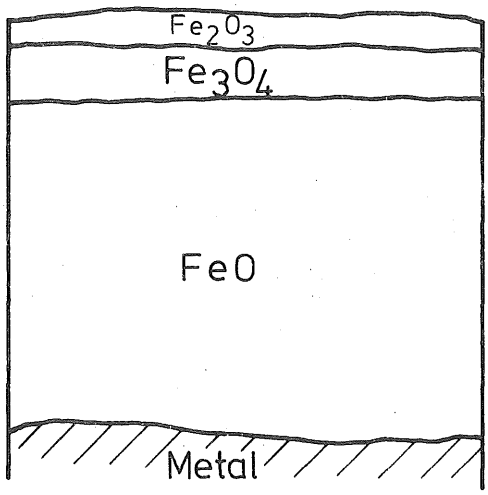

Fig. 1.3 Composition of oxide layers on iron above 570°C.

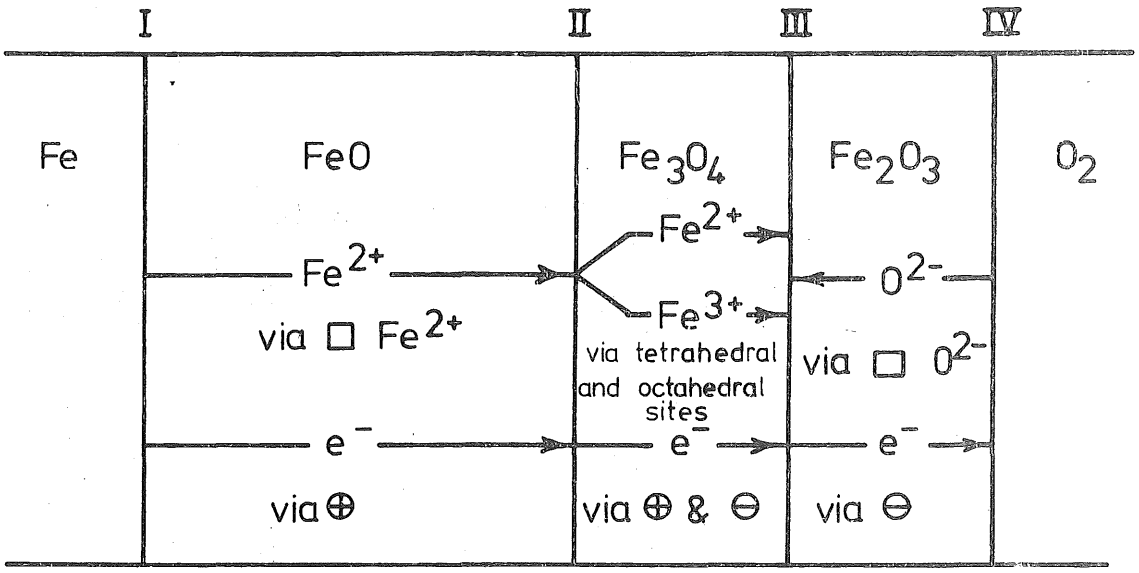

Fig. 1.4 Schematic representation of the diffusion processes and phase boundary reactions during the oxidation of iron in oxygen. From Hauffe[10].

Phase Boundary Reactions:

I. $Fe + [\square Fe^{2+} + 2\,\oplus]_{FeO} \rightleftharpoons$ zero

II. $Fe_3O_4 \rightleftharpoons [4FeO + \square Fe^{2+} + 2\,\oplus]_{FeO}$

$[\oplus]_{FeO} + [\square Fe^{2+} + \square Fe^{3+}]_{Fe_3O_4} \rightleftharpoons 2[Fe^{2+}]_{FeO}$

III. $12\ Fe_2O_3 \rightleftharpoons 9\ Fe_3O_4 + [\square Fe^{2+} + 2\square Fe^{3+} + 8\,\oplus]_{Fe_3O_4}$

$2\ Fe_3O_4 \rightleftharpoons 3\ Fe_2O_3 + [\square O^{2-} + 2\,\ominus]_{Fe_2O_3}$

IV. $\frac{1}{2}\ O_2^{(g)} + [\square O^{2-} + 2\,\ominus]_{Fe_2O_3} \rightleftharpoons$ zero

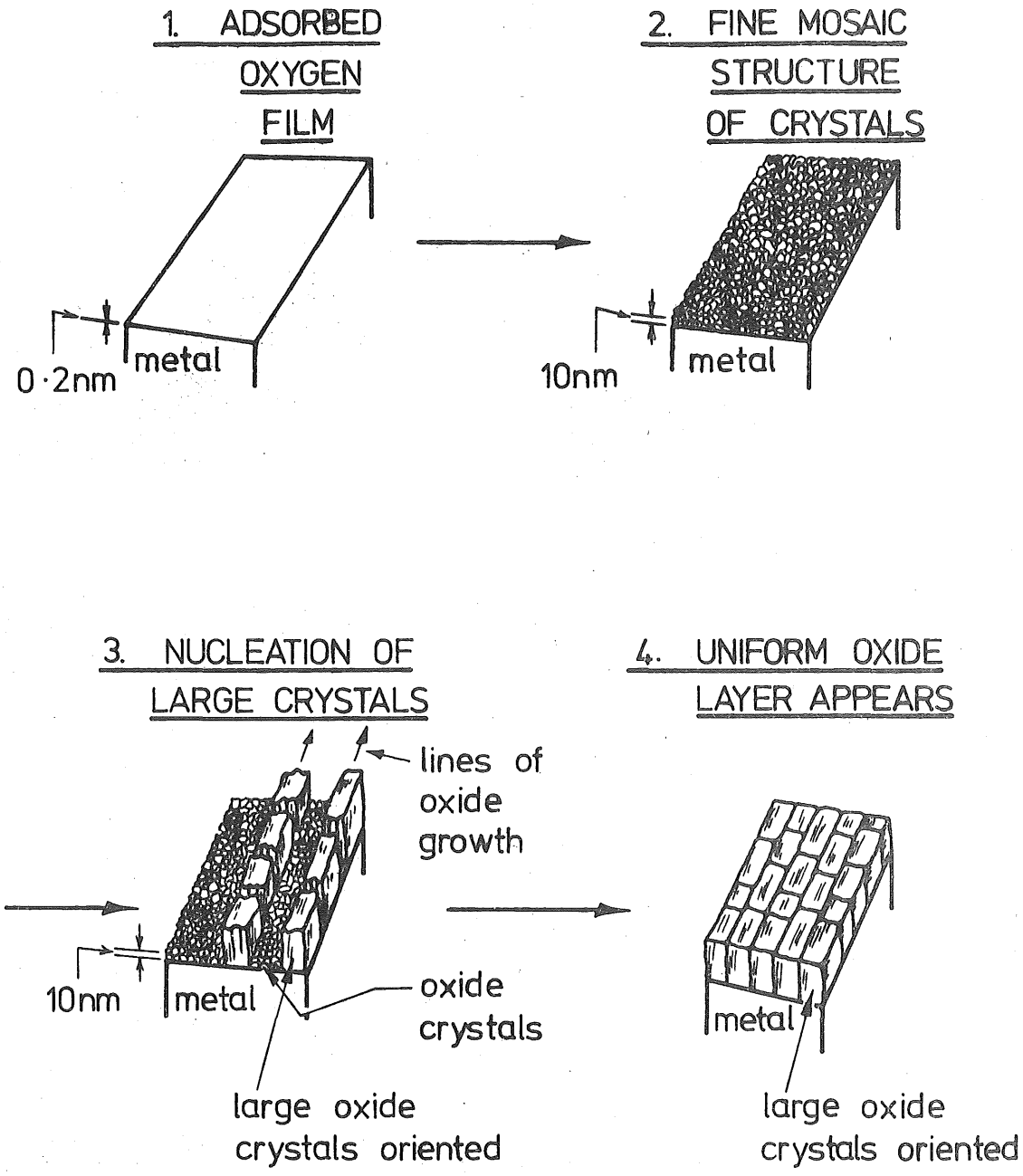

Fig. 1.5 Model of early stage oxide formation on iron at 850°C. From Gulbransen and Tallman[11].

along preferred directions on the iron surface, thus forming a granular oxide film oriented to the metal surface, but with several oxide crystals to each metal grain. Bardolle and Benard[12] showed that the number of FeO nuclei formed at 850°C is a function of the temperature, oxygen pressure, and the orientation of the underlying surface. Hondros [13] oxidised thin foils at 500°C and made simultaneous observations of the foil dislocation structure and surface nuclei to demonstrate that the nucleation sites are essentially independent of the emergence of dislocations at the surface. These observations were verified by Rönnquist and Thomas[14], at temperatures as low as 200°C, who found no preferential nucleation at grain or sub-grain boundaries, but who also observed that nucleation appeared to be easier on cold-worked specimens than on annealed specimens.

At temperatures below 570°C the nuclei generally consist of Fe_3O_4, although a number of electron diffraction investigations have revealed the presence of reflections forbidden by the Fe_3O_4 lattice[14,15,16]. These reflections are characteristic of the cubic γFe_2O_3 phase and show the same orientation as the Fe_3O_4 crystals. However, not all reflections expected for the γFe_2O_3 phase are observed. (A discussion of the similarities between the Fe_3O_4 and γFe_2O_3 structures is included in Appendix 4.) A similar oxide phase, composed of cubic close-packed oxygen planes with a cation distribution resembling that of γFe_2O_3, is frequently found in a thin film separating the Fe_3O_4 and γFe_2O_3 layers in later stages of oxidation at temperatures between 200°C and 570°C. The presence of this phase is shown in Figure 1.2.

The reason for the ordered growth sites, which favour nucleation on certain rows of the metal grain as shown in Figure 1.5, is not clear. Gulbransen and co-workers determined that ordering of these nucleation sites was influenced by the composition of the atmosphere in which specimens were annealed prior to oxidation. In particular, the presence of hydrogen promoted ordering of the oxide nuclei. Laukonis and Coleman[17,18]

demonstrated this effect by oxidising single crystal iron whiskers between 300°C and 800°C. Although the oxide nuclei were randomly oriented on unannealed specimens, electron microscope examination of replicas from hydrogen annealed crystals showed ordered mosaic patterns of oriented nuclei, indicating preferential nucleation at very fine growth steps which were not previously observable by the replica technique.

Boggs *et al*[15] demonstrated that the orientation of the inital Fe_3O_4 layer, formed between 200°C and 400°C, may also affect the nucleation and growth of layers of higher order oxide phases which may form subsequently. Herringbone textures, suggestive of a Widmanstätten structure, were observed on the surface of early-stage oxide formed in this temperature range. Electron diffraction indicated the textured growth to be acicular αFe_2O_3 crystals growing into a fine grained Fe_3O_4 base layer from sites of αFe_2O_3 nucleation at the Fe_3O_4/gas interface. The number of αFe_2O_3 crystals formed and their lateral growth rate is a function of the orientation of the Fe_3O_4 matrix and the oxygen pressure. The model proposed for the arrangement of the oxide layers on the four iron crystal faces studied is shown in Figure 1.6.

1.5 WHISKER AND PLATELET FORMATION

The formation of whiskers and platelets on oxide surfaces occurs over a wide range of conditions during the oxidation of many metals. Table 1.1 illustrates the diversity of the observations of the phenomena, and, although it is not intended to provide a complete summary of such observations, it does indicate the range of conditions under which whisker and allied growth forms are observed and the range of research activity in this field. The table has been restricted to gas-metal reactions involving oxygen, although sulphides, hydroxides and nitrides commonly exhibit similar growth forms. A number of oxides can also be prepared in filamentary form by growth from molten salt solutions ("flux growth").

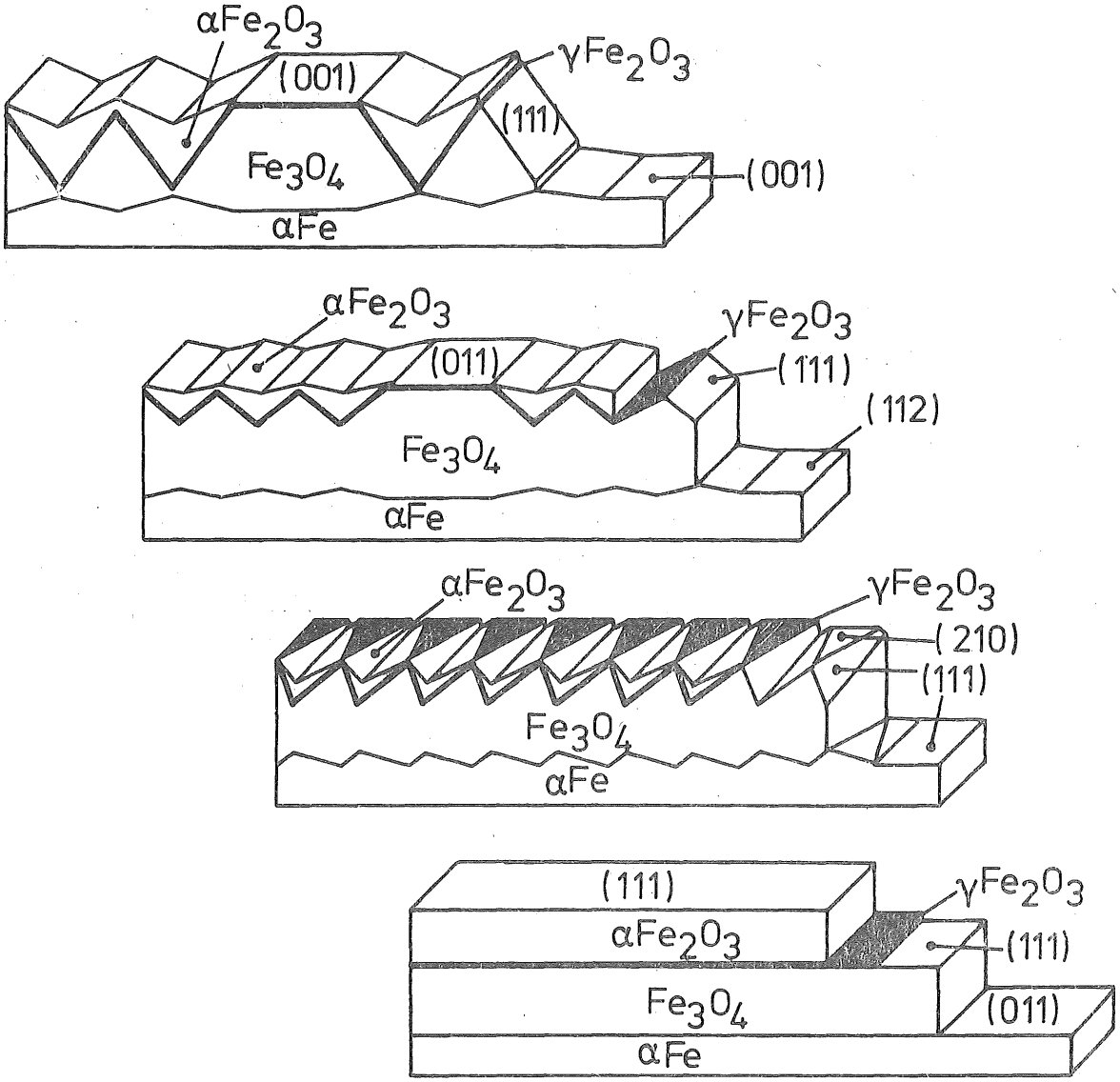

Fig. 1.6 Concept of the arrangement of the oxide layers on four low index iron crystal faces. From Boggs *et al* [15].

METAL	FILAMENT TYPE	CONDITIONS FOR GROWTH	REFS.
Beryllium	BeO whiskers of hexagonal cross-section. Many hollow, growth direction <0001> and <10$\bar{1}$0> Thickness <1.5 μm, length <15 mm. A few platelets.	1450 - 1500°C Moist argon plus impurities.	19
Magnesium	Spikes length 1 - 8 μm	400°C for 60 - 100 hours in air	20
Aluminium	(i) αAl_2O_3 whiskers mostly of hexagonal cross-section with [0001] growth direction Many hollow with axial cavities of 0.5 - 3.0 μm diameter. Thickness 3 - 50 μm length 1 - 30 mm. Platelets up to several mm in width also observed.	(i) Heating Al or $TiAl_3$ in moist H_2 at 1300 - 1450°C.	21 - 29
	(ii) αAl_2O_3 whiskers and ribbons of similar dimensions to (i) above, terminated by droplets of Al.	(ii) Evaporation and condensation of aluminium on alumina at 1250°C in vacuum of 6.7 mPa (5×10^{-5} mm Hg)	30
	(iii) αAl_2O_3 platelets of thickness 15 nm and length <3 μm. Growth direction [1000]	(iii) Al in steam at 540°C and 4.1 MPa pressure.	31
Titanium	Whiskers	500 - 50°C in air	20,32
Chromium	Thin rounded platelets of thickness 10 nm, width 7 μm and length 3 μm. Structure may be Cr_2O_3. Also whiskers of 10 - 20 nm thickness and 3 μm length.	500°C in 0.1 atm. dry O_2 for 120 hours	33

TABLE 1.1 Summary of oxide whisker and platelet growth on metal surfaces at elevated temperature.

continued ...

METAL	FILAMENT TYPE	CONDITIONS FOR GROWTH	REFS.
Iron	(i) αFe_2O_3 whiskers thickness <15 nm, length <50 μm	(i) 300-850°C in dry air or O_2.	11,17 33-44.
	(ii) Blade-shaped platelets	(ii) 400°C in O_2 or in air with traces of H_2O.	11,37, 39,45, 46.
	(iii) Broad rounded platelets, thickness 10 nm, width 7.5μm length 7.5 μm	(iii) Cold worked iron at 400°C in dry O_2.	11,47.
Austenitic Stainless Steels	(i) Irregular whiskers of thickness 160 nm, length 2 μm	(i) 600 - 900°C in dry air or O_2.	21,33, 40.
	(ii) Angular platelets,thickness 10 nm, width 6 μm, length 3 μm	(ii) 500°C in wet O_2 for 24 hours	48
Nickel	(i) NiO whiskers of thickness <1 μm, length <200 μm. At higher pO_2 larger whiskers of hexagonal and blade-shaped cross-section formed with thicknesses 5 - 15 μm, length <10 mm.	(i) Pure Ni heated to 1450°C in argon with low pO_2.	49
	(ii) NiO needles thickness 200nm length 7 μm	(ii) 400 - 600°C in air or O_2 for 60 - 120 hours.	20,21, 33,40, 49.
Copper	CuO needles of thickness 20 - 100 nm, length 1 - 10 μm. Many whiskers broaden into platelets near base. Generally have [110] growth direction	300 - 800°C in air or O_2.	34,40 50-57.
Zinc	ZnO whiskers, platelets and dendrites typically of width 1 μm, length 10 μm.	350 - 850°C in air or O_2 (also at 960 - 980°C. under close atmosphere control)	20,21, 34,40 58.
Niobium	αNb_2O_5 whiskers	900°C in air at 1.3 Pa (0.01 mm Hg) for 25 hours	20,62.

TABLE 1.1 (continued)

continued...

METAL	FILAMENT TYPE	CONDITIONS FOR GROWTH	REFS.
Molybdenum	MoO_3 needles	580°C in $N_2 + O_2 + H_2O$	20,21.
Tantalum	Needles	Between 200°C and 700°C in air	20,21.
Tungsten	(i) γ-tungsten oxide ($WO_{2.72}$) needles with bundle structure. Thickness <50 nm	(i) 700-1000°C under vacuum of 0.05 - 9.3 Pa (4×10^{-4} - 7×10^{-2} mm Hg)	20,21, 59.
	(ii) γ-tungsten oxide ribbons and whiskers (some whiskers of irregular section with droplets on tips).	(ii) decomposition of ammonium tungstate at 700°C.	60,61.
	(iii) $W_{20}O_{58}$, $W_{18}O_{49}$, WO_2 & WO_3 whiskers of length <8mm	(iii) Tungsten coil heated in temperature gradient from 100°C to 1200°C in argon containing approx. 200 Pa (1.5 mm Hg) H_2O.	49.
Lead	Pb_3O_4 needles of length <10 μm	140-300°C in air	20,40.

TABLE 1.1 (continued)

Although the observations reported in Table 1.1 include a wide variety of particle shapes, sizes and growth conditions, a number of common features are observed in many of them:

(a) The majority of whiskers and platelets are reported to be single crystals of high perfection, although many irregular filaments are also formed.

(b) In the vast majority of cases, whiskers occur only after a base oxide film of substantial thickness has formed, and do not grow directly on the metal surface. However, Pfefferkorn[63] observed oxide whiskers on copper after five seconds at 400°C in air.

(c) The presence of a thick oxide substrate suggests that the rate of formation of surface particles will, in most instances, be controlled by the diffusion of cations through the base oxide layer. Consequently, it is assumed that surface whisker growth will not significantly affect the overall kinetics of the metal-gas reaction.

(d) Whenever whiskers have been positively identified, they have been found to consist of the highest oxide which is stable under the conditions of the experiment. For example, copper oxide whiskers are invariably found to consist of CuO, even under conditions where the base oxide layer is Cu_2O.

(e) Different growth morphologies, such as whiskers, ribbons or platelets of varying cross-sections, commonly occur simultaneously.

The larger crystals of Al_2O_3 and BeO are amenable to study by optical techniques, and by X-ray diffraction, and also have potential for use as strengthening agents in composite materials. Most of the smaller filaments can only be observed by electron microscopy, however, and their growth process has not been directly observed.

CHAPTER 2

GROWTH OF CRYSTAL WHISKERS AND ASSOCIATED MORPHOLOGIES

2.1 TYPES OF WHISKER GROWTH

Filamentary crystal forms have been the subject of considerable investigation for many years. Observations on whiskers were reported as early as 1574 by Erker[64] who noted hairlike growths emerging from copper and silver halide ores. Many studies of filamentary particles, which were treated as laboratory curiosities, continued to be reported spasmodically until the 1940's when the growth of metal whiskers from metal surfaces was found to be the cause of short circuits in miniaturised communications equipment, and extensive efforts were made to suppress their formation.

In 1952, however, the study of filamentary crystals obtained a new significance when Herring and Galt[65] experimentally determined the strength of tin whiskers to be an order of magnitude higher than that of bulk tin and approaching the strength of perfect crystals. This discovery immediately stimulated extensive research into this crystal form, not only with a view to utilising the potential of whiskers as strengthening agents, but also because they provide convenient defect-free single crystal specimens for examination of the general physical properties of solids. The extent of this effort is indicated in a report by Campbell[66], in 1970, that more than thirty elements and fifty compounds had been grown in whisker form.

The extensive literature on whisker observations has been surveyed in many comprehensive reviews, including those by Brenner[67,68], Nabarro and Jackson[21], and Coleman[18]. These reviews encompass an enormous variety of observations on the growth forms, crystal structure, growth conditions, growth mechanisms, and physical properties of whiskers. The

major part of an International Conference on Crystal Growth, held in Cooperstown, New York in 1958, was devoted to filamentary forms of crystal growth, and the reviews by Brenner and by Nabarro and Jackson are articles from the conference proceedings. Despite the optimism at that time that some rational theory of crystal growth would encompass the variety of crystal types observed, subsequent years of observation and a proliferation of proposed growth mechanisms have left the phenomenon of whisker growth largely unexplained. It is now quite clear that a wide variety of mechanisms are involved, and that each case must be studied individually. It also seems likely that two or more quite different mechanisms may operate simultaneously under some conditions.

Nabarro and Jackson divide observations into a series of categories based on the physical conditions under which whisker growth occurred. These categories are:

(a) Proper whiskers (growth from the solid without the atoms which form the whisker experiencing a change of phase).

(b) Growth from vapour.

(c) Precipitation from solution.

(d) Chemical deposition (including oxidation).

(e) Formation under mechanical stress.

(f) Formation by electrolysis.

Since it is plain that many of these growth forms are interrelated, and that factors such as mechanical stress, vapour pressure, and purity of the substrate have a profound influence on many different growth mechanisms, it seems appropriate to discuss the processes responsible for the filamentary growth in more general terms, namely:

(a) Growth from the base.

(b) Growth from the tip.

2.2 WHISKER GROWTH FROM THE BASE

Metal whiskers, notably those of tin, zinc and cadmium, grow spontaneously from the solid state at room temperature, when conditions are appropriate, by a process resembling extrusion from the base. These whiskers generally have diameters of 0.05-5.0 μm and lengths ranging from 100 μm to several centimetres. They grow most readily from thin plated coatings (0.25 μm thick), less readily from heavy coatings (12 μm thick); only with difficulty from solid polycrystalline materials; and never on single crystals. The growth rate is higher at increased temperature and is not uniform. There is normally an induction period followed by a period of rapid growth which ceases abruptly. The growth rate is increased by the presence of atmospheric oxygen, water vapour or organic contaminants, but continues at a slower rate under ultra high vacuum. It is not inhibited by protective coatings of oil or lacquer. Pressure applied to the substrate substantially increases the growth rate; in some cases by many orders of magnitude.

These 'proper' whiskers grow in a large variety of shapes and sizes. Most are single crystals of high crystalline perfection with their axes parallel to a prominent crystal direction. They are usually of polygonal cross-section with low index planes as their side faces. Although most whiskers are straight, kinked, straight, and spiral growths frequently occur simultaneously, the kink angles being grouped around the principal crystallographic directions.

2.2.1 Growth Theories based on Dislocation Mechanisms

Most of the theories of growth of "proper" whiskers from metallic substrates require:

(a) Dislocations in the substrate which meet the surface with a component of the Burgers vector normal to the surface.

(b) A dislocation mechanism for generating vacancies at the whisker base.

(c) A driving force to enable the transport mechanism to work.

(d) A sink for the vacancies.

Frank[69] proposed the first mechanism for whisker growth from the base as a process in which oxidation of the metal surface provides the driving force. The surface oxidation effectively reduces the surface free energy to a negative value, and so encourages the spontaneous increase of the surface area of the body by movement of the dislocations which terminate on the surface. For a screw dislocation this motion is a glide, raising a new step in the surface, whereas for an edge dislocation the motion is a climb, exposing a new row of atoms in the surface which still remains flat. The dislocation end will travel over the metal surface until it finds a position of equilibrium, and if it encounters a groove in the surface it will be constrained to move along the groove since it has effectively a line tension. The underside of any projection from the smooth surface will form a closed path similar to a groove to which the dislocation end may attach and, unless it reaches a position of equilibrium in this closed path, it will move round and round the base of the projection indefinitely. For each circuit made by the dislocation end, the projection will be displaced by a distance and direction corresponding to the Burgers vector of the dislocation. The result of many circuits will be the growth of a cylinder from the surface which is based on the original peripheral groove, and with axis parallel to a possible Burgers vector of a dislocation in the crystal. In general, this will be a close-packed direction.

A similar theory, proposed by Eshelby[70], is also based on a negative-free energy as a result of oxidation. The surface tension forces on a small hump existing on the surface are shown in Figure 2.1. A Frank-Read source of length l and vertical Burgers vector b lies in a horizontal plane (b) some distance below the surface. The stress τ_{zz} (Figure 2.1 (c)) makes the source emit dislocation loops which expand

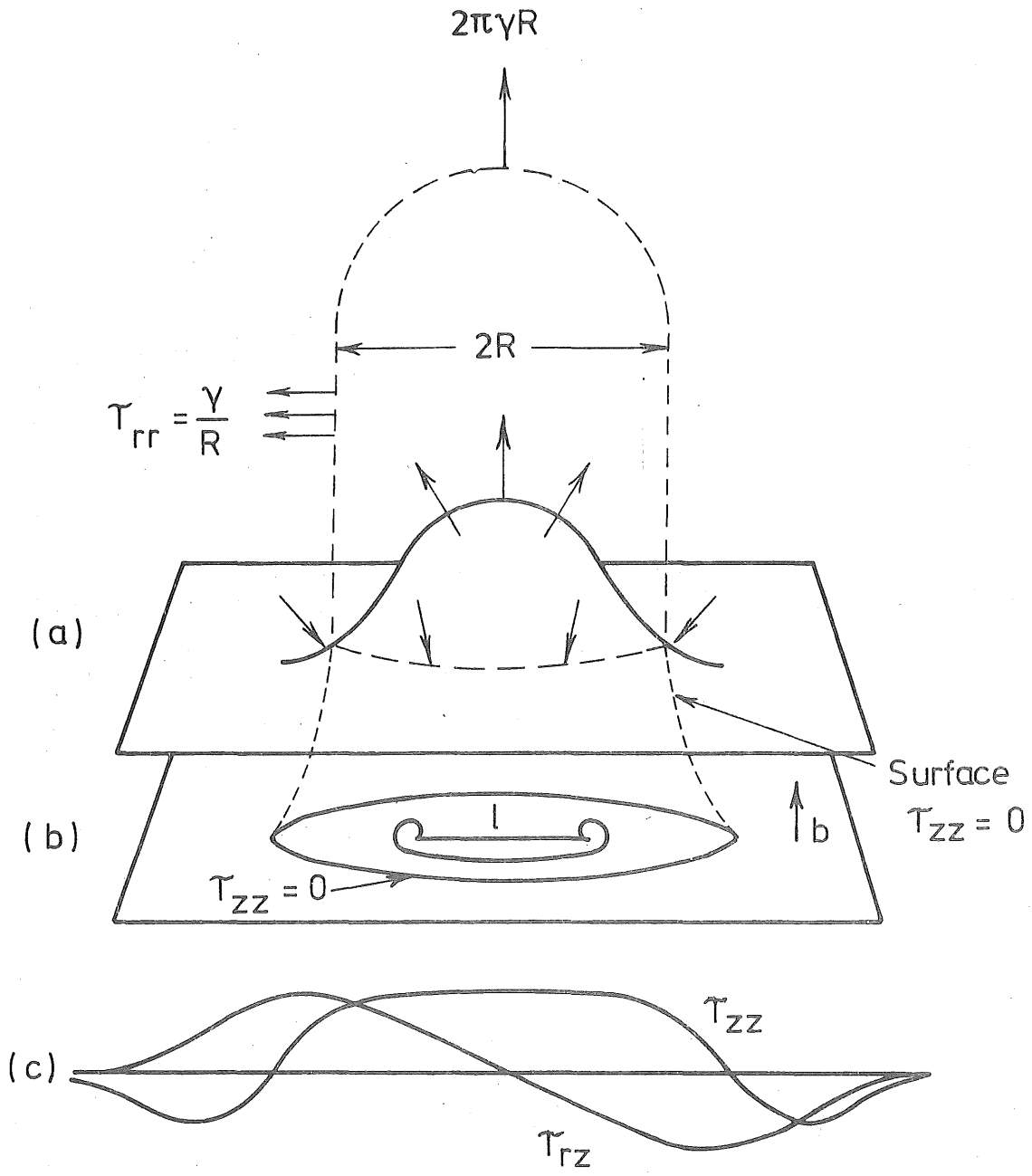

Fig. 2.1 Dislocation model of whisker growth from the base. From Eshelby[70].

until they reach a radius where $\tau_{zz} = 0$. Here the stress τ_{zz} forces the loops to glide vertically so adding atomic planes to the base of the hump which eventually becomes a whisker. It is assumed that the surface tension-produced stresses are appreciably larger than those required to operate the Frank-Read source. Nabarro and Jackson[21] estimate that these forces will usually be of the same order of magnitude, for commonly observed whisker sizes, but that it is difficult to imagine any other source of stress of comparable magnitude.

The rate of whisker growth by both Frank's and Eshelby's mechanisms would be controlled by the rate of migration of vacancies from the generating dislocation to the surface, and calculations based on this vacancy diffusion show a reasonable agreement with observed growth rates.

Amelinckx *et al*[71] proposed a further growth mechanism, similar to those of Frank and Eshelby, based on the concept of spiral prismatic dislocations and helical dislocations. In Figure 2.2 (a) the vertical line AB represents a screw dislocation of Burgers vector b which terminates at a ridge on the surface and at a node point within the solid. In the presence of an excess or deficiency of vacancies, the screw can climb into a helical form as illustrated in Figure 2.2 (b). Rotation of the helix about its axis, or transformation of the helical dislocation into a procession of prismatic loops which may glide to the surface in a similar manner to that proposed by Eshelby, will produce growth of a whisker at the surface. The whisker formed is shown in Figure 2.2 (c) and has a screw dislocation along its axis.

An elegant explanation for the presence of kinked whiskers, which are frequently observed, was provided in terms of this mechanism. The model assumes that most of the dislocations near the surface are involved in network structures and do not have the simple form shown in Figure 2.2 (a). Figure 2.3 (a) shows such a dislocation network terminating at the surface. All dislocations should be transformed to helices if the

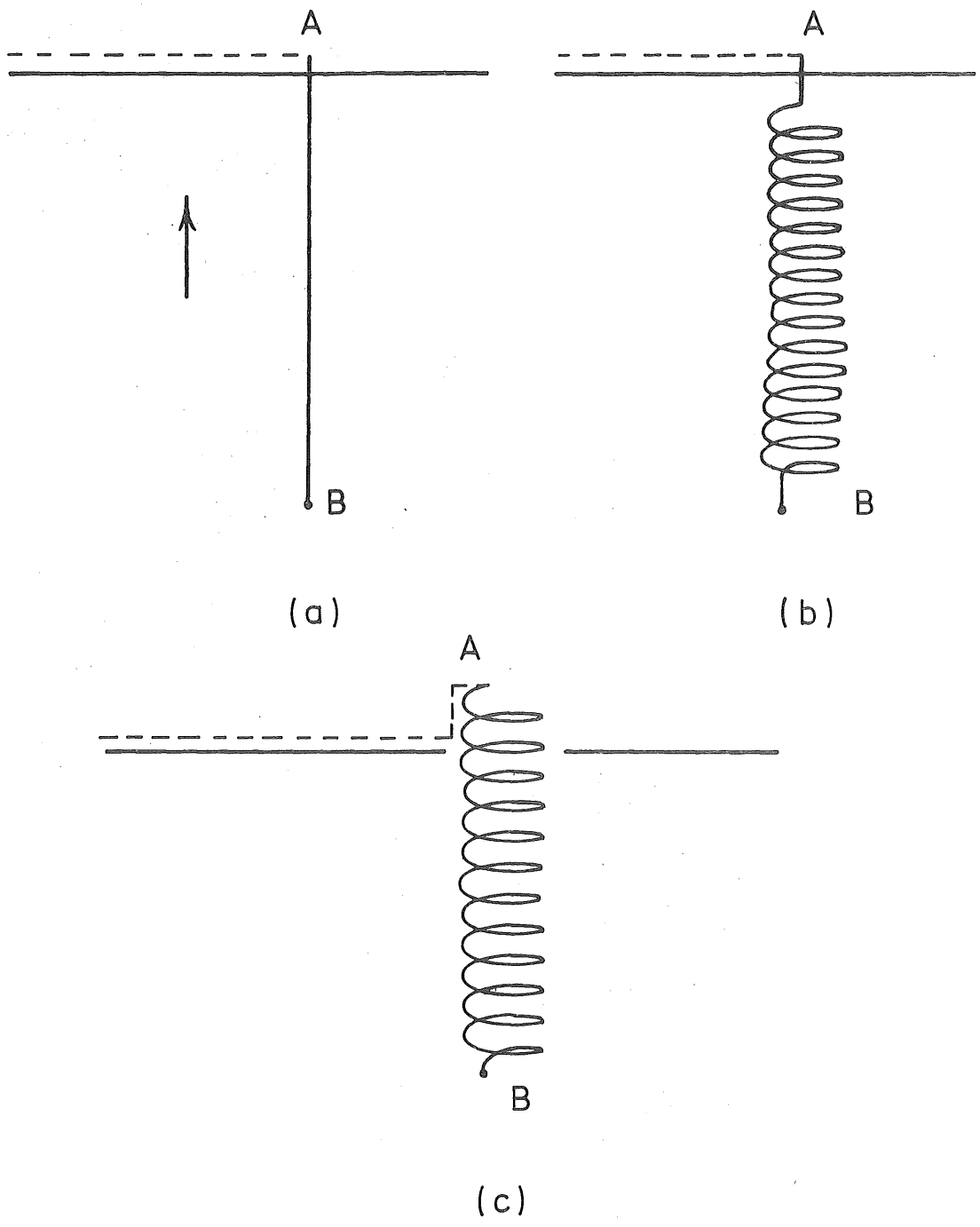

Fig. 2.2 Schematic diagram of the development of a whisker from a spiral or helical prismatic dislocation. From Amelinckx *et al* [71].

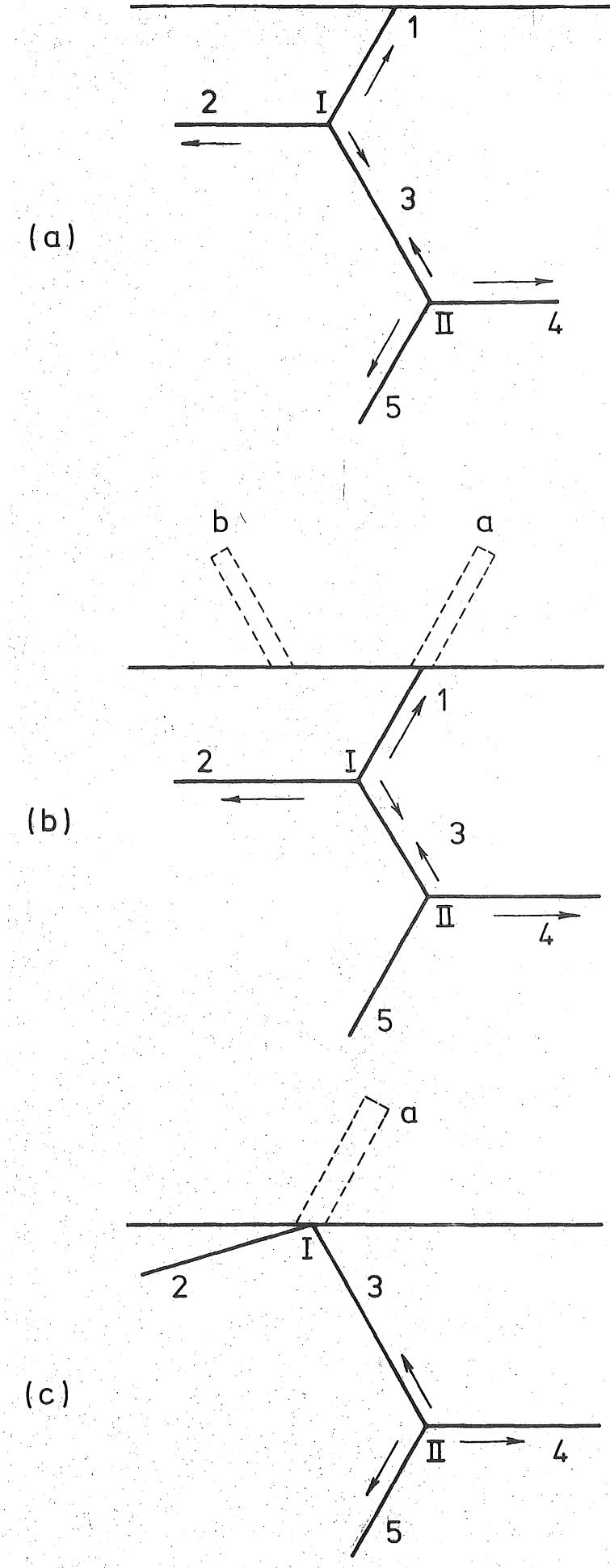

Fig. 2.3 Growth of whiskers containing kinks from a dislocation network terminating in the surface. From Amelinckx *et al*[71].

environment favours climb, and the helix formed by dislocation 1 could produce a whisker of the type described above, as shown in Figure 2.3(b). The Burgers vectors for dislocations 3 and 5 are in favourable directions so that the helices formed from them could produce whiskers if they are able to reach the surface. If the compressive forces between successive turns of the helix formed from dislocation 3 become strong enough, they could glide to the surface in the direction of the Burgers vector and form a new whisker (b), as shown in Figure 2.3 (c). It is also possible that the node I would be induced to climb to the surface, as a result of forces upon it, so that the whisker (a) formed from dislocation 1 would stop growing and be joined to a whisker oriented in a different direction. The angle of kink should, therefore, be closely related to the angles between the Burgers vectors of dislocations 1 and 3. Other more complex growth shapes can be explained in terms of similar mechanisms

2.2.2 Growth by Recrystallisation

The observations of Arnold and Koonce[20] of whisker growth on the surfaces of noble metals at elevated temperatures, including gold at 300^{o}C, and the growth of whiskers of tin at pressures of 1.3 μPa (10^{-8} mm Hg), suggested that the driving force for dislocation sources was not provided by a negative surface free energy. However, no other driving force of sufficient strengthto activate such sources could be envisaged. These observations, the presence of fluted, hollow, and other irregular cross-sections, and the greatly enhanced growth rate under applied compressive stress led Ellis *et al*[72] to propose that the growth of "proper" whiskers is a process of grain growth, or recrystallisation and growth, entailing mass transport. It was postulated that given a recrystallised surface grain of critical size,

whisker growth provides a more favourable path for relaxation of stored strain energy and external stress than does bulk recrystallisation and growth. The nucleating grain, which must have stable boundaries with the surrounding surface, is assumed to be the size of the whisker cross-section. Growth outwards from the surface occurs either by dislocation action within the grain or by atoms in the surrounding material shifting their allegiance to the more strain-free environment of the whisker grain. If a nucleating grain of suitable size does not exist at first, such a grain forms by re-crystallisation before the whisker is generated. This point is supported by experiments with large-grain substrates and single crystals. Whiskers do not grow on such surfaces unless the substrates are first heavily stressed and allowed to recrystallise. Ellis *et al* suggest a number of atomic mechanisms for generating the whisker growth, including mechanisms based on dislocations in the nucleating grain, but the growth process does not necessarily require dislocation action.

This theory has received widespread support and is thought to account for many observations of the growth of metal whiskers from the base. Although there is little direct experimental evidence to support the theory, experiments involving compressive stressing of the substrate; surface coatings; and the effects of irradiation, produce results which can be explained in terms of the recrystallisation mechanism.

2.3 GROWTH FROM THE TIP

The majority of whiskers are observed to grow by incorporation of material at the growing tip rather than by extrusion from the base. These observations include metallic whiskers formed by condensation from the vapour phase; whiskers grown from solution and porous

substrates; growth from the melt and within solids; growth by electrolysis; and whisker formation by chemical decomposition which includes both oxidation and reduction reactions.

The characteristic features of whiskers grown from the tip are reported to be the absence of thickening or growth on the whisker side faces, and growth rates far greater than are predicted by classical theories of crystal growth involving two-dimensional nucleation on growing surfaces. Three types of detailed growth mechanisms have been proposed to account for tip growth:

(a) Growth based on the presence of an axial screw dislocation in each whisker.

(b) The vapour-liquid-solid (VLS) mechanism.

(c) Growth by surface diffusion to the whisker tip.

2.3.1 Axial Screw Dislocation Theory

(i) Crystal Growth from the Vapour

The general theory of crystal growth from the vapour has been summarised by Burton *et al* [73]. If the lattice of the crystal is perfect, growth can only occur by two-dimensional nucleation on low index crystal faces, followed by incorporation of mobile adsorbed atoms at the energetically favoured sites around the projecting nucleus. A complete new lattice plane, bounded by low index densely-packed faces, is thus formed. Two dimensional nucleation must then again take place before further growth can proceed. The rate of two dimensional nucleation was shown to be far too small

to account for the observed rates of crystal growth under moderate supersaturations; and Frank[74] resolved the discrepancy by suggesting that all real crystals contain screw dislocations capable of providing a continual source of surface steps, of the type shown in Figure 2.4, which are energetically favoured sites for adsorbed atoms to be incorporated into the crystal. The important feature of a screw dislocation is that the step cannot be eliminated as growth proceeds, but extends in length to reach an equilibrium shape as a spiral growth hill centred on the dislocation, as shown in Figure 2.5. When the curvature at the centre reaches a critical value the step ceases to advance, but the whole spiral rotates steadily with constant shape presenting a continuous step as growth proceeds.

(ii) Dislocation Mechanism of Whisker Growth

The significance of emergent screw dislocations in crystal growth has been well verified experimentally in many crystal growth situations. In 1953, Sears[75] made a logical extension of this proposal to include filamentary crystal growth by suggesting that whiskers grown from the vapour contained one or more screw dislocations parallel to their axes. It was proposed that this mechanism required three steps consisting of:

(a) adsorption of atoms on perfect sidewalls of the whisker;

(b) surface diffusion to the whisker tip; and

(c) incorporation into the lattice at a step in the tip associated with the emergence of a single axial screw dislocation.

The emergent step, or steps, at a whisker tip provide the energetically favoured sites for growth to continue indefinitely below the

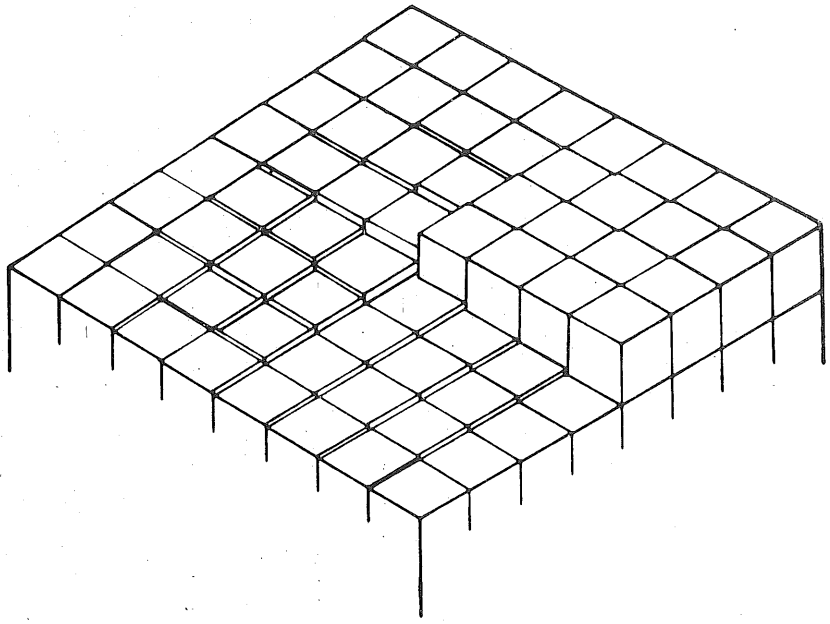

Fig. 2.4 Source of growth steps associated with the emergence of a screw dislocation from a crystal surface.

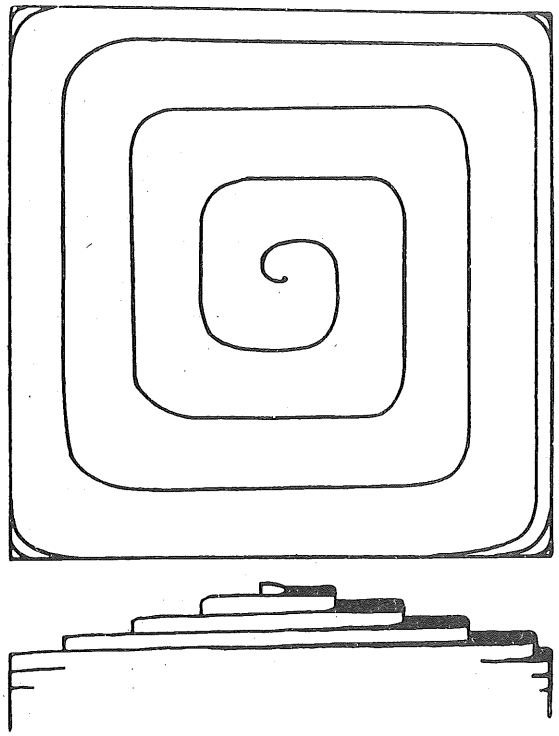

Fig. 2.5 Growth pyramid resulting from a single screw dislocation.

critical supersaturation level for two-dimensional nucleation, while the sides of the whisker remain atomically smooth. Growth ceases if the screw dislocation ceases to emerge from the tip and reaches a surface parallel to its Burgers vector. Growth should also cease if the critical supersaturation for two-dimensional nucleation is exceeded, as nucleation on the whisker sidewalls leads to thickening of the whiskers into pyramid-shaped crystal forms[76].

Experiments by Sears[75,77] and by Gomer[78] on mercury whiskers have shown that steps (a) and (b) above are indeed correct. The observed growth rates are up to 5000 times that calculated on the assumption that only mercury atoms striking the advancing whisker tip contribute to axial growth. The verification of step (c) has proved a more difficult problem and is discussed in Section (iv) below. Melmed and Gomer[79] have also shown that at low temperatures whiskers can grow at very high supersaturations, when, according to Sears, thickening into a pyramid shape should rapidly occur.

(iii) The Role of Impurities

The presence of a screw dislocation does not in itself lead to whisker growth. Under conditions of high purity the advancing crystal surfaces which contain screw dislocations should remain practically flat, and it seems likely that this growth pattern is modified by impurities in a manner which leads to the whisker profile. It has been demonstrated[102] that the presence of adsorbed impurities may modify the nature of growth steps in a complex manner, and the screw dislocation mechanism is critically dependent on the nature of the growth step generated by the dislocation. The action of the impurities is not well understood, but attempts have been made to examine two limiting cases[103], namely:

(a) impurities which are immobile, i.e. impurity molecules which remain adsorbed at the points where they strike the crystal surface; and

(b) completely mobile adsorbed impurities.

Immobile impurity atoms may slow the movement of growth steps, or may block the motion completely if the separation between them is less than a critical distance. Thus, the advance of growth steps moving away from the dislocation source will be slowed and the continuing generation of steps at the source will produce a much steeper growth hill. If the impurity concentration is such that the advance of growth steps is completely stopped, the mechanism may cause the crystal to grow out into a whisker as impinging atoms from the vapour diffuse to the centre of the spiral.

Mobile impurities are assumed to act in a different manner but may also give rise to steeper growth profiles which favour whisker growth. Impurities that establish an equilibrium concentration along the steps may considerably lower the edge free energy so that the core portion of the step is driven as though the supersaturation of the vapour is higher at the region of the core than elsewhere. The rate of step advance elsewhere is simultaneously inhibited. A screw dislocation so poisoned should, therefore, give rise to a steeply pitched growth cone. There have been numerous observations of such growth cones, terminated by whisker crystals, under conditions where impurities may be a contributing factor, but the details of these impurity effects require much further study.

(iv) Detection of Screw Dislocations in Whiskers

A whisker containing an axial screw dislocation is illustrated in Figure 2.6. This figure assumes a circular cross-section with no displacement of the dislocation from the axis. The angle σ results

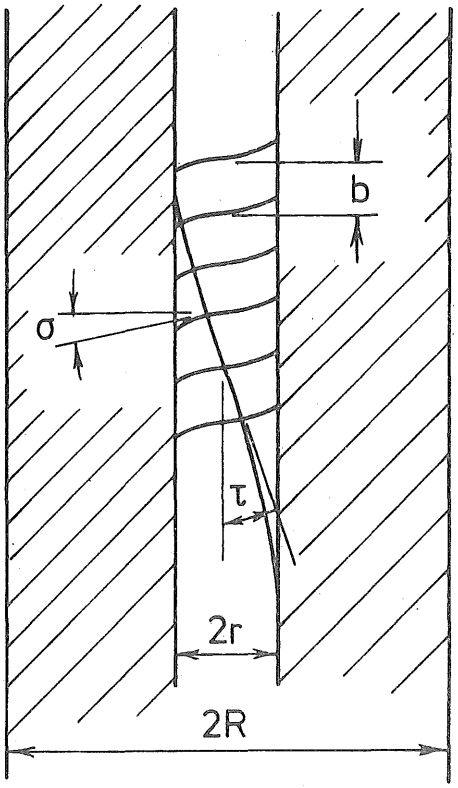

Fig. 2.6 Lattice distortion by a single screw dislocation lying on the axis of a cylindrical rod.

from the spiral climb of the lattice plane about the screw dislocation, and

$$\tan \sigma = \frac{b}{2\pi r} \qquad \ldots.(2.1)$$

where b is the magnitude of the Burgers vector and r is the effective radius of the dislocation core. In the neighbourhood of the dislocation this shear cannot correspond to elastic deformation of the real structure, and the structure of the whisker in this region remains undefined. Eshelby[80] derived the torsional strain, which is illustrated by the angle τ in Figure 2.6, resulting from the presence of such a screw dislocation lying parallel to the axis in an elastically isotropic thin cylindrical rod of circular section. The twist per unit length is given by

$$\alpha(\xi) = \frac{b}{\pi R^2}\left[1 - \frac{\xi^2}{R^2}\right] \qquad \ldots.(2.2)$$

where ξ is the displacement of the dislocation line from the rod axis, and R is the whisker radius. For an axial dislocation this becomes

$$\alpha = \frac{b}{\pi R^2} \qquad \ldots.(2.3)$$

Hence, in a sufficiently thin whisker crystal, for example, R = 1.0 μm, the lattice twist due to a screw dislocation of Burgers vector of reasonable magnitude should be of the order of degrees per millimetre of length. In addition, Eshelby showed that the dislocation remains stable along the axis of the rod so long as it remains within a distance of 0.54R from the rod axis. This theory has been extended to include screw dislocations in whiskers of arbitrary cross-section[81].

Attempts to detect axial twist in whiskers grown from the tip, and so verify the screw dislocation growth mechanism, have involved a number of experimental techniques. The most comprehensive approach has been that of Webb and co-workers[24-26,82-84] using a modified

Laue X-ray diffraction method, employing a microfocus X-ray tube with a cylindrical camera coaxial with the whisker growth axis. The lattice twist was inferred from the observed tilt of the equatorial diffraction spots. Attempts were also made to verify the results by imaging the dislocations by X-ray diffraction microscopy techniques. Whiskers of αAl_2O_3 showed axial twists corresponding to a variety of Burgers vectors which were thought to be multiples of the appropriate unit cell dimension. Edwards and Happel[23] added further evidence to support these observations by growing αAl_2O_3 whiskers on single crystal alumina substrates. The whiskers grew coherently with the substrate, with axes either parallel to the c-axis, or in one of 12 equally spaced directions in the basal plane. These growth directions are the screw dislocation directions in alumina, hence, it seems plausible that the whiskers grew coherently with the substrate at the site of emergent screw dislocations.

Some alkali halide whiskers studied by Webb and co-workers also exhibited lattice twist. However, other whiskers with similar appearance from the same batch clearly had undistorted lattices. Despite these isolated cases, the vast majority of whiskers examined which included those of zinc, copper, iron, nickel, manganese, and silver, failed to provide any evidence for the presence of a single axial screw dislocation. Similar X-ray and optical investigations by other workers[85-89] have generally confirmed these results, but have also indicated that multiple dislocations and complex lattice disorder are often present in whisker structures.

The direct observation of dislocation contrast images in the electron microscope, and electron diffraction studies[11,41,59,90-94], has provided similarly variable results which are often ambiguous. Some of these studies are examined in greater detail in Chapter 6,

however, they do not generally confirm or deny the existence of screw dislocations in whiskers.

Amelinckx[95] decorated dislocations in alkali halide whiskers of larger size with gold chloride and directly observed, by optical techniques, large numbers of dislocations in some specimens and the apparent complete absence of dislocations in others. Etching of the tips of larger crystals produced pits corresponding to the emergence of the dislocations observed by the decoration technique, thus confirming the result.

Gomer[96] attempted a very elegant field emission observation of mercury whiskers vapour grown on the tungsten emission filament. By increasing the emission voltage, tensile stress could be applied to the whiskers until fracture occurred. When the voltage was close to that required for fracture, the emission patterns from approximately 20% of the whiskers rotated by amounts varying from a few degrees to 360^{o}. Gomer assumed this rotation to be evidence of axial twist in the original lattice. After fracture, emission from a whisker stump showed the same orientation as the original tip, rather than the random orientation expected if the lattice twist were of the order of ten complete turns in the whisker length, as calculated from Equation (2.3). It was proposed that this indicated a periodic weakness in the crystal related to the pitch of the Eshelby twist but verification of the presence of such a feature is lacking. Unequivocal evidence of lattice twist, to support the screw dislocation mechanism is, therefore, available for very few materials which exhibit the whisker growth form. This does not entirely eliminate the possibility of the operation of such a growth mechanism as a number of factors might conceal the presence of the dislocation:

(a) the dislocation could absorb trapped vacancies which allow it to climb out of the whisker during or after the growth process; and

(b) two screw dislocations of equal and opposite sign might be present, equally spaced from the whisker axis. Such a pair can glide together and annihilate themselves by combination, thus leaving a dislocation-free crystal.

Some evidence for the second of these two possibilities has been provided by Müller[97], who applied the field ion microscopy technique to untwisted iron whiskers of 10 μm to 30 μm diameter. The tip planes of whiskers with [001]growth direction collapsed in a manner which suggested the presence of paired axial screw dislocations of opposite sign.

2.3.2 Vapour - Liquid - Solid Growth Mechanism

In 1964, detailed study of the morphology and growth of silicon whiskers[90,98] led to a new concept of crystal growth from the vapour, termed the vapour-liquid-solid (VLS) mechanism. Silicon whiskers, grown by the disproportionation of SiI_2 and by the hydrogen reduction of $SiCl_4$ and which did not contain an axial screw dislocation, were shown to grow with a small globule or liquid droplet on their tips. The presence of a suitable impurity was found to be essential for the growth to occur. It was shown that, at supersaturation ratios well below that required for two-dimensional nucleation, molecules from the vapour can deposit in the liquid droplet which has a high accommodation coefficient for impinging molecules. The whisker then grows by precipitation of silicon from the supersaturated droplet, and a screw dislocation is not required to generate growth steps. The mechanism is illustrated in Figure 2.7.

The main requirements which must be met simultaneously for VLS growth are as follows:

(a) The alloying agent or impurity must form a liquid solution with the whisker material at the growth temperature.

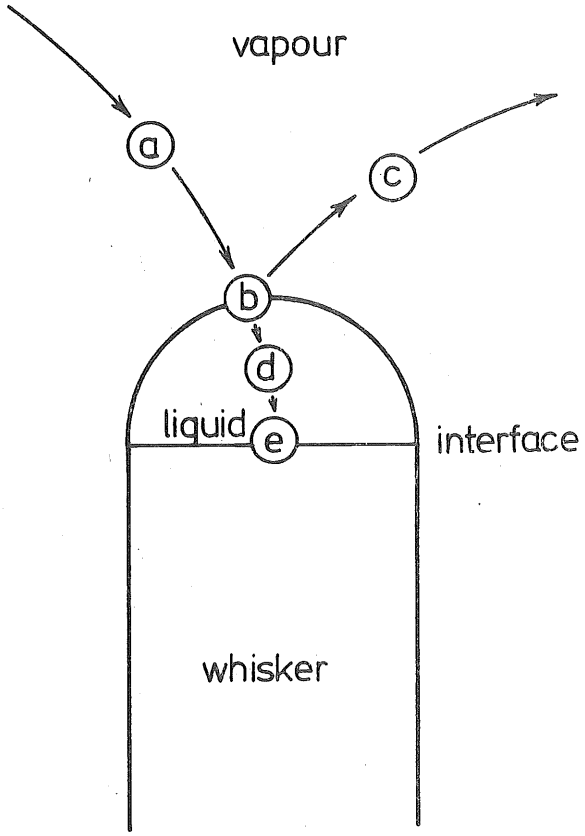

Fig. 2.7 Atomic processes at the whisker tip during VLS growth.

(a) Diffusion of gas phase molecules to the droplet.

(b) Vapour deposition at the droplet which frequently involves a chemical reaction to produce a new phase.

(c) Diffusion of the reaction by-products (if any) away from the droplet.

(d) Transport of the vapour molecules or new phase through the droplet to the interface.

(e) Precipitation at the droplet/substrate interface to form the whisker.

(b) The distribution coefficient of the impurity must be such that the impurity concentration remains higher in the liquid than in the crystalline solid.

(c) The equilibrium pressure of the alloying agent over the liquid alloy must be low at the growth temperature. Loss of agent from solution changes the droplet volume, and hence also changes the whisker diameter.

(d) The agent must be inert to the chemical reaction products.

(e) The various V-S, V-L, and L-S interfacial energies are critical, since it is important to achieve the correct wetting angle for whisker formation.

(f) The temperature of the system must remain constant. Small fluctuations may cause large diameter variations.

It is evident that the stability of the droplet, which is a function of diameter, surface tension, and supersaturation, is the critical growth factor. Wagner[99] shows that this condition imposes a limitation on the minimum radius of a VLS grown crystal.

$$r_{min} = \frac{2\sigma_{LV} V_L}{RT.\ell n \sigma} \qquad \ldots\ (2.4)$$

where r_{min} is the limiting radius, σ_{LV} is the liquid-vapour interfacial energy, V_L is the liquid molar volume, and σ is the degree of supersaturation. For most materials the minimum critical radius (r_{min}) is approximately 0.1 μm for $\sigma = 1.02$.

Materials which have been grown by the VLS technique include[99] Al_2O_3, boron, GaAs, GaP, $Ga(As_{1-x} P_x)$, germanium, MgO, $NiBr_2$, NiO, selenium, silicon, and SiC. Crystalline defects are not essential for VLS growth. However, defects present at the solid-liquid interface may reduce the required supersaturation in the liquid solution during growth, and an emergent dislocation from a suitable substrate may provide a preferred site

for the initial location of the formation of the liquid phase.

2.3.3 Growth by Surface Diffusion

The measured rates of growth of whisker crystals growing by vapour deposition are orders of magnitude higher than would be predicted from the rate of impingement of molecules on the whisker tips alone. It is, therefore, clear that surface diffusion of the depositing species must provide the predominant transport mechanism for tip growth. Most growth models assume this to be the case and provide an additional mechanism to explain the high rate at which atoms are incorporated into the whisker lattice.

In 1966 Schwoebel[100] proposed a surface diffusion mechanism for filamentary growth, based on the manner in which diffusing species are incorporated into steps on crystal surfaces. The model does not require the presence of either screw dislocations or impurities. Schwoebel and Shipsey[101] advised experimental results which indicated that surface steps of different crystallographic orientations incorporate diffusing atoms into the advancing step face with different probabilities, this probability being dependent on the direction from which a diffusing atom approaches the step. It was shown that the spacing between surface steps can be stabilised for certain relative values of these capture probabilities, and for other relative values the steps can coalesce with one another to form steps of greater than minimum height. Schwoebel's whisker growth model develops this idea by considering the relative motion of a number of concentric circular steps, as shown in Figure 2.8(a). The relative motion of the steps, based on assumed values of the capture probability for atoms approaching a step from either side, is described by a set of coupled differential equations which can be simultaneously solved by computer. If suitable initial conditions and capture probabilities are assumed, whisker type growth can be predicted. Although the model clearly requires considerable development and experimental verification, it does indicate the possibility that the limitation of diffusion processes may

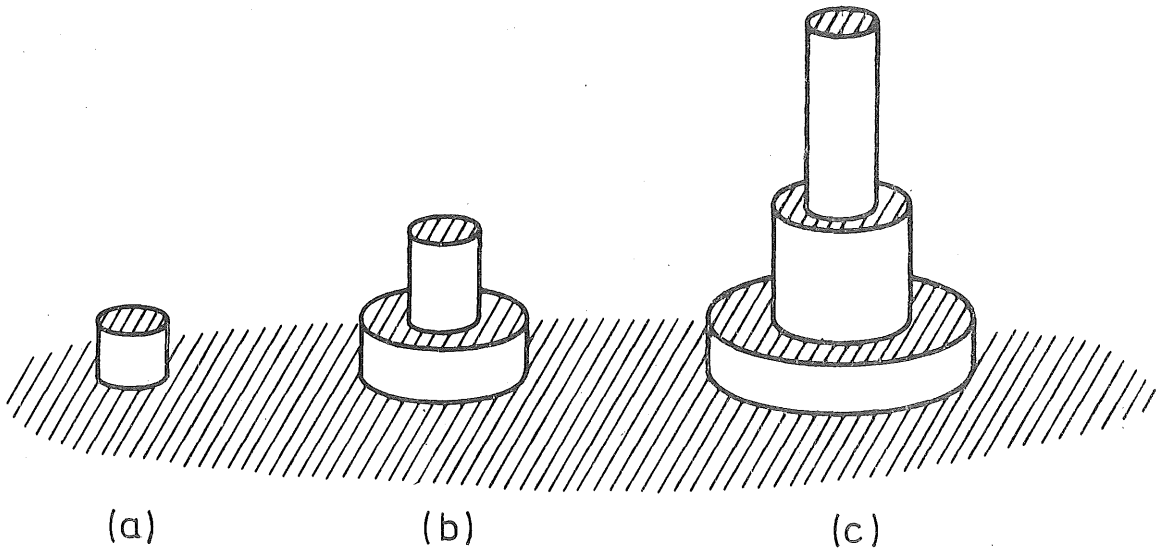

Fig. 2.8 An assumed configuration of a filamentary crystal in an early stage of growth by surface diffusion. Atoms adsorbed on unshaded surfaces are assumed to have greater mobility than those on shaded portions of the figure. Filamentary growth occurs through capture of adsorbed atoms at one of the two steps bordering each cylindrical region on which atoms are initially adsorbed.
From Schwoebel[100].

enable the growth of filamentary particles without the requirement for a screw dislocation to generate growth steps.

2.3.4 Structural Anisotropy

Structural anisotropy is an additional feature which is almost certainly a contributory factor in much non-cubic whisker growth. Many crystals have anisotropic structures so that the external surfaces have differing surface energies. These differences alone may be sufficient to produce filament growth by favouring growth on a high energy face and exposing side faces of low surface energy. No detailed theory exists and the relative contribution of this factor is not known.

2.4 MECHANISMS FOR OXIDE WHISKER GROWTH

The growth of oxide whiskers on metal surfaces at elevated temperatures may be considered in terms of the mechanisms discussed previously, with the additional requirement of cation transport from the substrate to the whisker tip where the reaction with atmospheric oxygen and incorporation into the whisker crystal is thought to take place. The three mechanisms which have been proposed to account for this ion transport are as follows:

(a) vapour transport;

(b) surface diffusion on the sides of the whisker; and

(c) internal diffusion in a hole or screw dislocation.

A fourth possibility, extrusion from the base oxide layer, has been discounted by most workers as Takagi[34] and Drott[104] have observed growth from the tip in samples which were alternately oxidised and examined by electron microscopy.

2.4.1 Vapour Transport

A number of observations of whiskers of αAl_2O_3[23,30], BeO[19], MoO_3[105,106], and γ-tungsten oxide[61] appear to be well described by the vapour-liquid-solid mechanism discussed in Section 2.3.2, although the nature of the vapour phase transport and chemical reactions have not been

determined in all instances. These crystals are distinguished from most other oxide filaments by their relatively large size, i.e. diameter > 0.5μm, and by the small liquid droplets which are present on the growing whisker tips. Whiskers of ZnO have also been observed growing on surfaces other than zinc or zinc oxide at 450°C [34]. This indicates vapour transport, presumably of zinc which has a high vapour pressure at this temperature.

2.4.2 Surface Diffusion

The high growth rates for oxide whiskers indicate that oxygen adsorbed on the whisker sidewalls is incorporated into the growing crystal. It is generally assumed that this oxygen migrates to the whisker tip via the outer surfaces. The migration of cations to the tip by surface diffusion has also been proposed by Pfefferkorn[63] and by Takagi[34]. The mechanism has received little favour from many authors, as it is difficult to envisage a concentration gradient of metal atoms between the base and the tip of the whisker when the migrating ions would be everywhere exposed to the gaseous reactant. Metal ions would also have to migrate long distances, not only over the side faces of the whisker but also over the base oxide, without any alternative growth site being encountered.

2.4.3 Internal Diffusion

Gulbransen[38] and Fischmeister[107] proposed two similar models for metal atoms to reach the whisker tip by a path which protects them from atmospheric effects, i.e. by way of a hollow centre, grain boundary, or axial screw dislocation. Gulbransen's model applies to both whisker and platelet growths which are formed during the oxidation of iron at 400°C, and is illustrated in Figure 2.9. The essential feature of the model is an internal defect, the nature of which is not specified, which would allow rapid diffusion of iron from the base oxide layer to the tip where the reaction with oxygen occurs.

The cation mobility in the core is required to be much greater than in the lattice to obtain whiskers of uniform cross-section. A high lattice

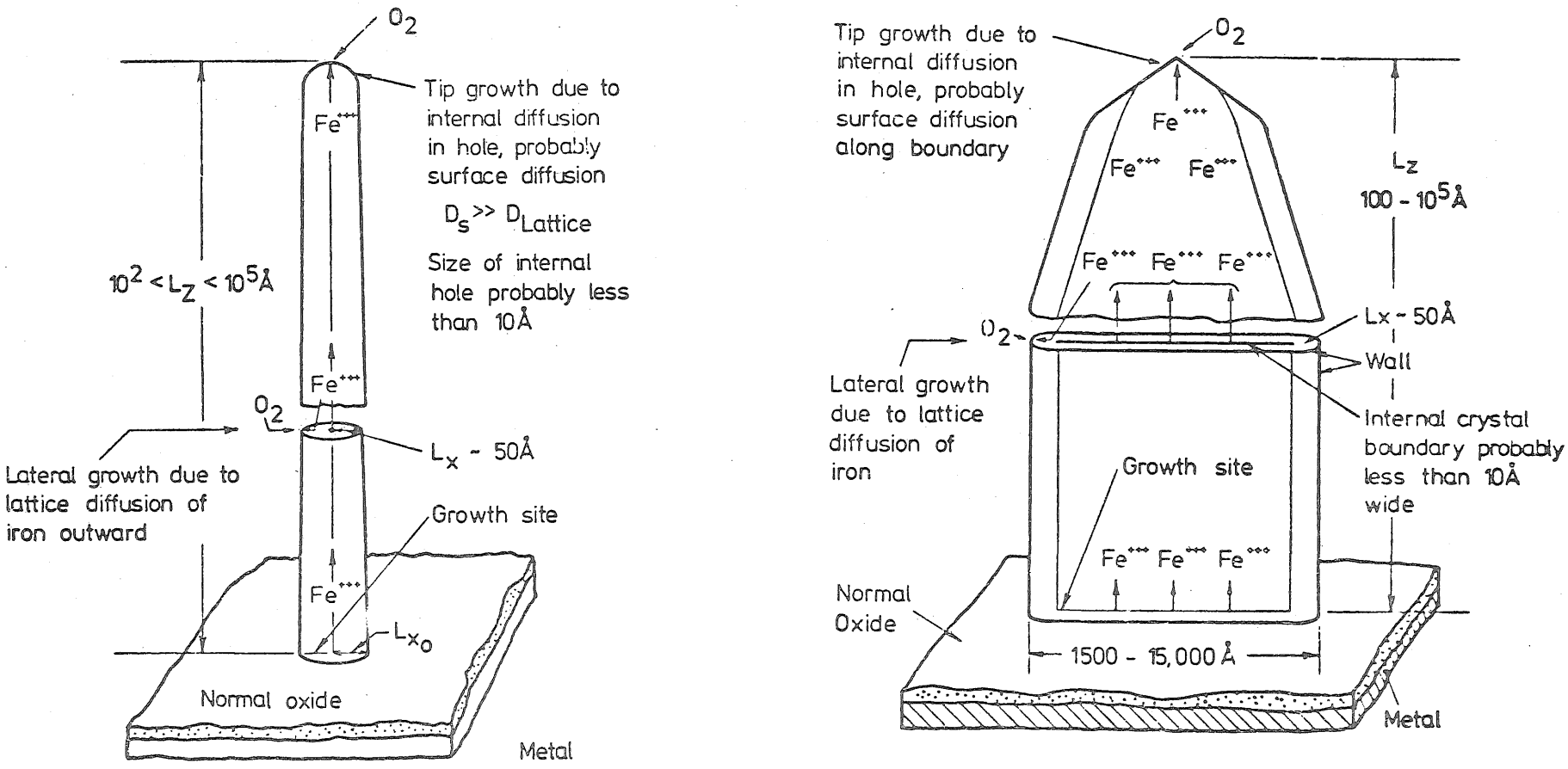

Fig. 2.9 Model of iron oxide whisker and platelet growth mechanism based on internal diffusion of cations to the filament tip. From Gulbransen and Tallman[11].

diffusion coefficient would result in lateral growth and broadening of the filaments near the base. The driving force for the diffusion process is assumed to be the oxidation of the base layer of Fe_3O_4 to Fe_2O_3. A further driving force may result from stresses developed in the oxide layer as the reaction proceeds, and it is possible that such stresses may create a pressure gradient to assist a liquid-like flow of both oxygen and iron atoms within the dislocation core.

Fischmeister's model assumes the primary driving force for cation diffusion to be this stress build-up in the base oxide layers, and a mechanism is proposed by which these stresses may be relieved by whisker growth processes. The mismatch between the metal and oxide lattices will be accommodated by dislocations with Burgers vectors parallel to the metal/oxide interface, and the climb of these dislocations will result in stress relief. In Figure 2.10, a dislocation at position A is linked to two vertical dislocations, one of which terminates at the surface. The dislocation may eliminate a sheet of atoms by climbing through positions B and C if a supply of vacancies is available. A relatively inexhaustible supply of such vacancies may be assumed, as these may diffuse along the dislocation core from the surface with great facility. The displaced atoms, both iron and oxygen, therefore enter the dislocation core and diffuse to the surface where a new whisker is formed which contains an axial screw dislocation. If the base film is of a lower oxide than the whisker there will be an additional reaction with oxygen at the tip.

There are many similarities between this proposal and a dislocation model for solid state whisker growth which was proposed by Peach[108], in 1952, before it was verified that such whiskers grew from the base. Peach's proposal indicates that not only does the screw dislocation provide an inexhaustible growth step at the whisker tip, but that the supply of atoms from the dislocation core might lead to the whisker profile without the need for impurity poisoning of the outer turns of the growth step. The

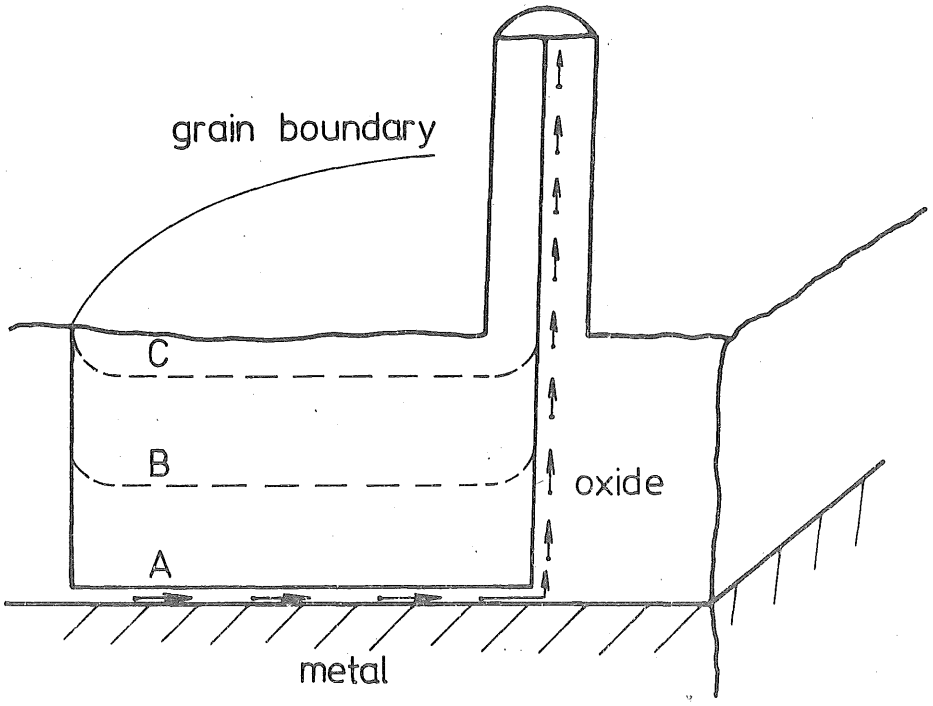

Fig. 2.10 Model of whisker growth by dislocation pipe diffusion combined with stress relief by dislocation climb. From Fischmeister[107].

parts of the growth spiral nearest to the core are very favourably situated to receive atoms which emanate from this source, and, after a few turns, the outer portions of the spiral are completely shielded from the source and cease to grow. This is in direct contrast to the formation of a crystal from its vapour, where the atoms are randomly distributed over the crystal surface and growth of the outer turns of the spiral is favoured. The cessation of growth of these outer turns leads to a steep growth hill and whisker formation in a manner similar to that described in Section 2.3.1 (iii) under the action of impurities.

CHAPTER 3

TILTING GAS REACTION CHAMBER FOR J.E.M. 7A ELECTRON MICROSCOPE

Reaction products resulting from the interaction of materials with a gaseous environment may be examined by transmission electron microscopy either *post situ*, i.e. after reaction external to the electron microscope, or *in situ*, as the reaction proceeds in a specially designed specimen chamber. The *post situ* technique allows for precise control of reaction conditions, but in many instances experimental difficulties make it impossible to observe a particular area of specimen at successive stages of reaction. Also, the removal of a specimen from its reaction environment, for the purposes of examination in the electron microscope, may drastically alter the course of subsequent stages of the reaction.

The growth of oxide whiskers is ideally suited to the *in situ* approach, as interesting features of the specimen may be continuously observed as the reaction proceeds. In 1972 a decision was made to obtain a commercially available gas reaction stage (JEM-AGI), of proven performance, for the JEM 7A transmission electron microscope. The failure of the manufacturers to supply this unit led to a decision to design and construct a gas reaction specimen chamber suited to the range of experimental conditions appropriate for oxide whisker growth, and the specimen chamber produced as a result of that decision is described below.

3.1 DESIGN CONCEPT

There are several difficulties associated with the presence of a gaseous atmosphere surrounding a specimen during observation by electron microscopy. These are:

(a) Scattering of electrons by the gas molecules leads to a reduction in image intensity and resolution.

(b) The gaseous environment is difficult to control without introducing contamination into the electron optical column which interferes with electron gun operation.

(c) Space is very limited inside the bore of the objective lens polepiece where the specimen must be precisely positioned.

(d) The electron beam irradiating the specimen may affect the course of the reaction by introducing radiation damage, chemical changes or contamination.

To perform *in situ* investigations of oxidation reactions the specimen must be enclosed at elevated temperature in a controlled atmosphere chamber with entry and exit windows for the electron beam. The length of the path of the electron beam through the chamber must be small to minimise the reduction of image quality which results from interaction of the electron beam with the gas molecules. Temperature, pressure, and gas composition should be subject to close control.

Flower[109] has surveyed environmental reaction chambers for transmission electron microscopes which have been described in the literature. These designs fall into three groups as follows:

(a) The specimen may be contained in a sealed chamber with a pair of electron transparent membranes placed on either side to seal the atmosphere surrounding the specimen from the vacuum of the electron optical column. Reaction chambers of this type are frequently used for room temperature studies, and their simple construction allows excellent control of the pressure around the specimen. However, the membranes are normally less than 50 nm thick, and are made from plastic materials which are unable to withstand elevated temperatures. They are also subject to damage resulting from pressure fluctuations. These deficiencies render chambers of this type unsuitable for the study

of most oxidation reactions. The presence of the membranes also contributes to the loss of image quality.

(b) Another group of environmental chamber designs is based on the introduction of small quantities of gas from a jet in the vicinity of the specimen. The residual gas is removed from the microscope column by the normal pumping system which may be supplemented by additional pumps or by cryogenic traps positioned around the specimen. Specimen stages based on this principle have proved useful for *in vivo* studies of biological material but have little application at the higher pressures desired for oxidation reactions.

(c) The third group of specimen stages utilises a sealed chamber with a pair of small apertures placed above and below the specimen, through which the electron beam may pass, in preference to the electron transparent windows of the type (a) cells. The gas which leaks from the specimen chamber into the microscope through these apertures is limited by the "throttling" effect, and may be removed by auxiliary vacuum pumps without significant degradation of microscope performance. Reaction chambers of this type permit high temperature reactions to be observed as the noble metal apertures which are employed are not subject to thermal damage. The operating pressure is limited by the diameter of the apertures, the pumping speed of the auxiliary vacuum system, and the ability of the electron beam to penetrate the gas atmosphere. The reaction chamber described in the following sections is of this type.

3.2 DESIGN EVOLUTION

3.2.1 The JEM-AGI Reaction Stage

The initial design concept was based on a notably successful gas reaction chamber designed by Hashimoto *et al*[105] for the JEM 7A trans-

mission microscope. This device was marketed commercially as the JEM-AGI Gas Reaction Stage, and allows observation of specimens at temperatures up to 1000°C in atmospheres at pressures up to 40 kPa (300 mm Hg). Figure 3.1 is a schematic diagram of the Hashimoto stage which illustrates the important features of its construction. The specimen is placed over a small hole in a platinum ribbon which is supported on a mica ring, the ribbon being heated by the passage of direct current. The gas atmosphere is supplied around the specimen through a pipe and overflows into the vacuum of the electron microscope column through the two platinum apertures of 50 μm to 100 μm diameter on either side of the ribbon. A fine thermocouple wire spot-welded to the platinum heater ribbon completes the specimen assembly, the thermocouple being located adjacent to the hole through which the electron beam passes to enable temperature measurement as close as possible to the area of observation. This specimen assembly, shown in Figure 3.2, is mounted on four stainless steel electrodes which form part of a central specimen holder assembly. This complete assembly may be removed from the microscope through an airlock. Provision is made for water cooling of the stage, but this is not normally utilised unless the stage is operated for more than one hour at temperatures above 700°C. The field of view available for examination is limited to the area of the apertures as there is no provision for movement of the specimen within the chamber. Maintenance of the normal microscope vacuum is assisted by an auxiliary vacuum pump, with a port near the specimen chamber, which augments the normal pumping system.

3.2.2 Differentially Pumped Chamber

Although a device similar to the Hashimoto stage would provide experimental conditions suitable for oxide whisker growth, an attempt was made to improve the performance to enable reactions at higher gas pressures to be observed. This attempt led to the second design concept shown in Figure 3.3.

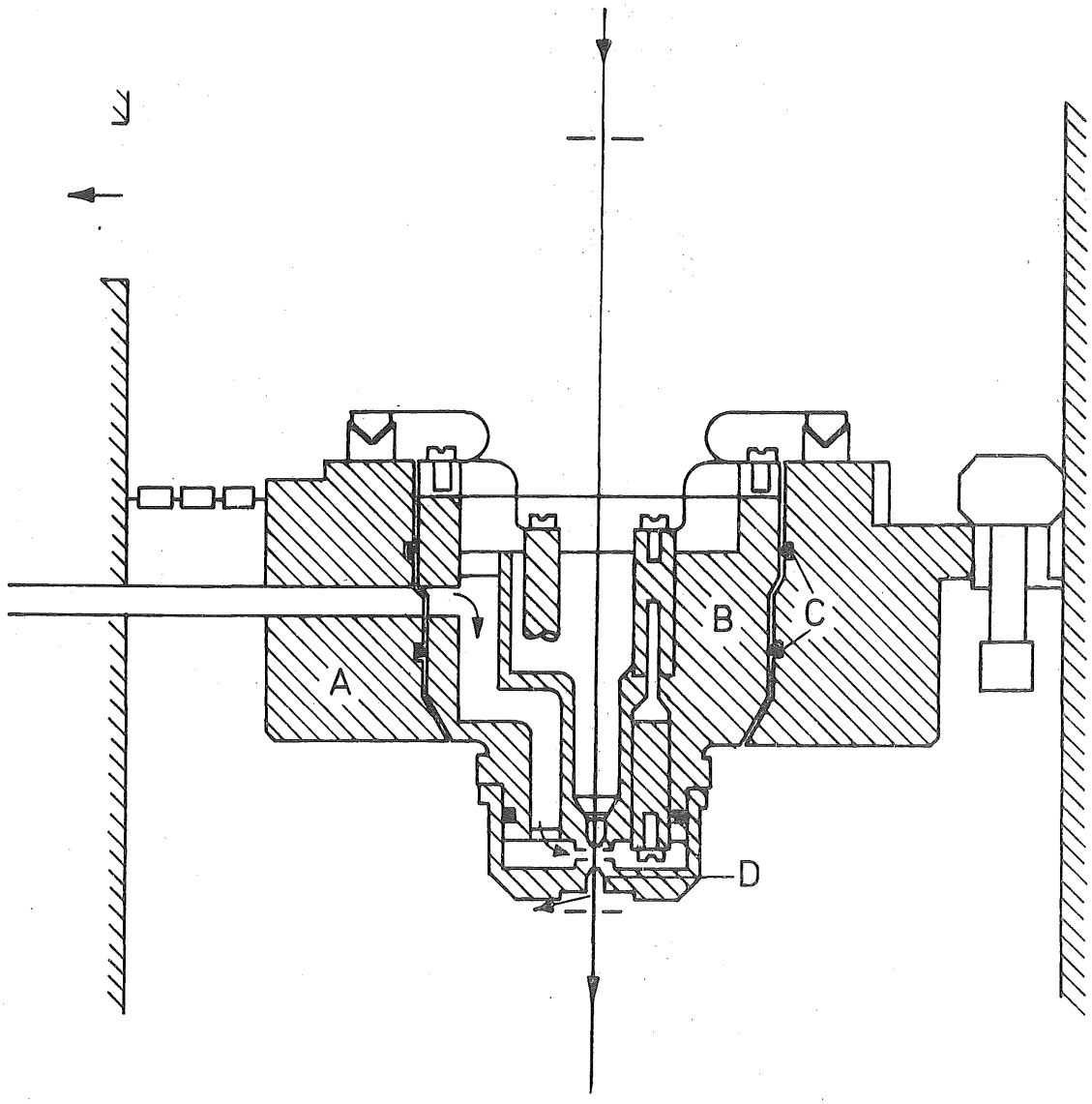

Fig. 3.1 Schematic diagram of the JEM AGI gas reaction stage developed by Hashimoto.

The stage A is permanently mounted on the specimen translation platform of the microscope, while cell B containing the specimen can be removed through an airlock. This cell is sealed into the stage by two 'O' rings C which create a channel through which gas can gain access to the specimen. The gas flows out into the microscope vacuum through an aperture mounted in the body of the cell and another D mounted in a removable cap.

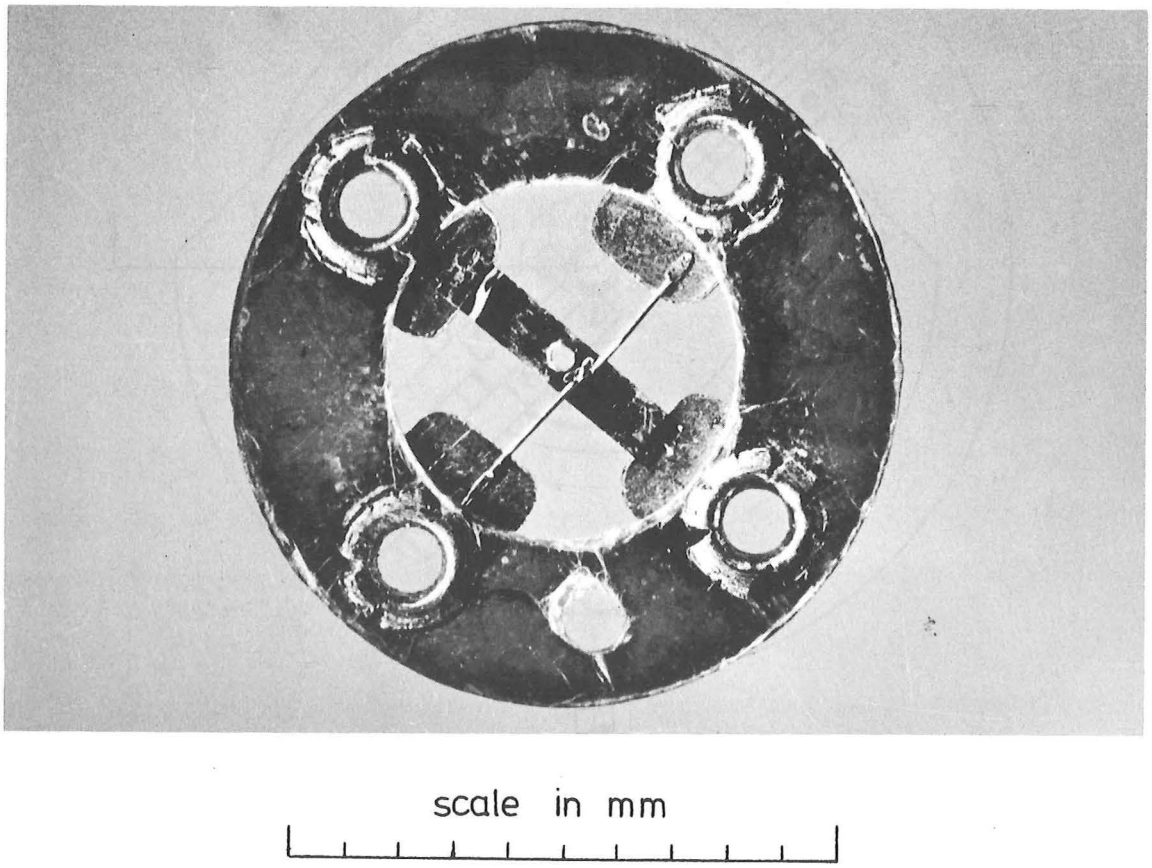

Fig. 3.2 Hashimoto stage specimen assembly. Platinum heater ribbon and thermocouple wires are spot-welded to platinum tabs which are riveted to a mica ring for support. The thermocouple junction is spot-welded to the heater ribbon adjacent to the hole through which the electron beam passes.

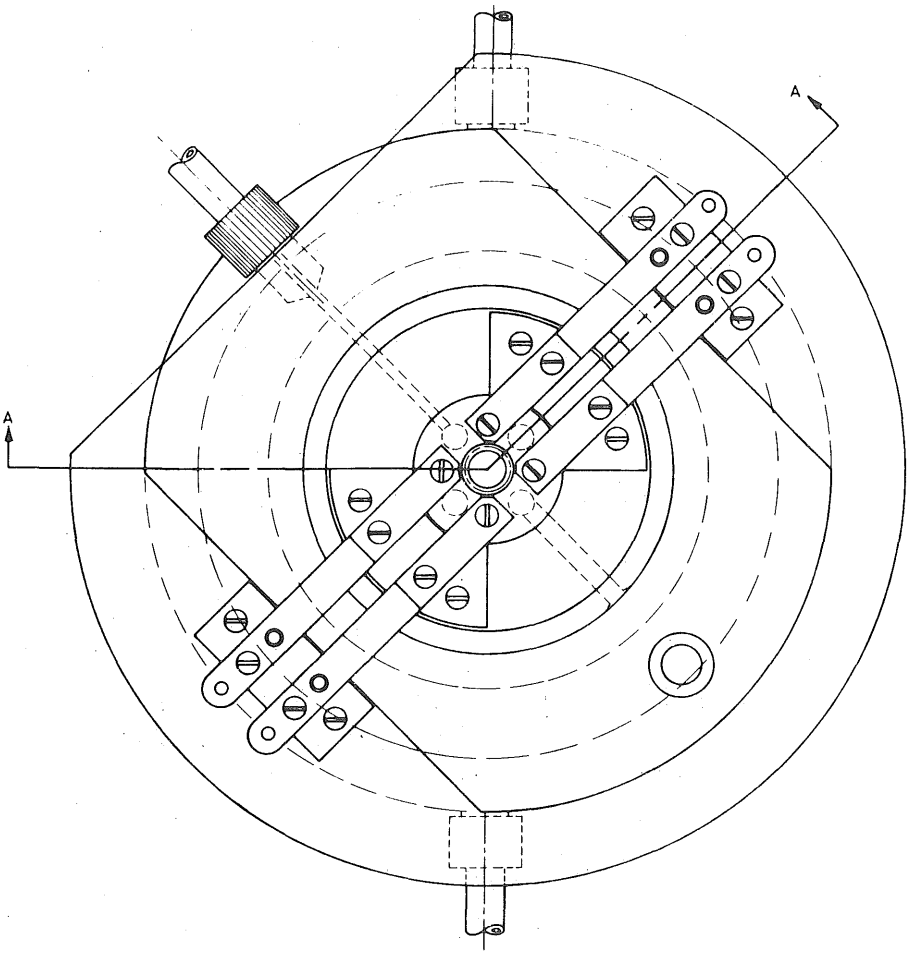

PLAN VIEW

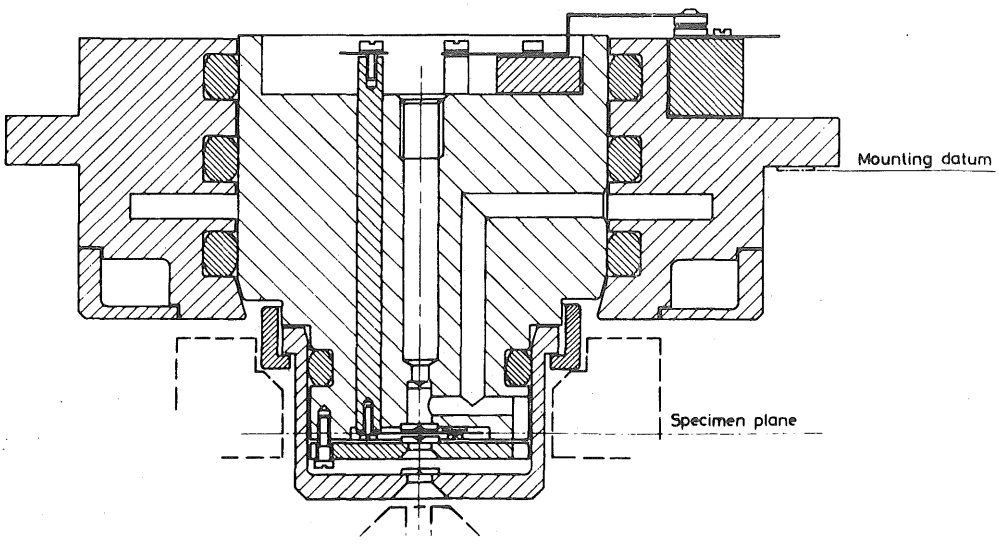

SECTION A-A

Fig. 3.3 Differentially pumped reaction chamber design. (Not constructed).

This design incorporates a second pair of apertures which constrains the gas overflowing from the specimen chamber to a second chamber which is pumped separately from the microscope column. This pumping action should maintain the pressure in the outer chamber at a very low level, thus reducing the quantity of gas which would leak through the outer apertures into the microscope. The differentially pumped chamber would, therefore, permit higher gas pressures around the specimen without excessive microscope contamination.

The outer section of the reaction stage is permanently mounted in the microscope and contains gas inlet and vacuum pumping manifolds, water-cooling jacket, electrical connections and 'O' ring seals to accept the removable specimen carrier. The apertures may be pre-aligned optically before insertion of the specimen carrier in the microscope and the specimen assembly is of a type similar to that shown in Figure 3.2.

Considerable detail design was required for each concept before the feasibility of the concept could be determined in terms of the limited space available inside the objective lens polepiece of the JEM 7A microscope. The problems of aperture and specimen alignment associated with this design had been largely solved when the realisation was made that the sonic velocity gas jet emerging from an inner aperture into the differentially pumped chamber would remain undisturbed for a considerable distance from the inner aperture. If the apertures are close together, the majority of the escaping gas will pass directly through the differentially pumped chamber and on through the outer aperture into the microscope column. Although the theory of turbulent flow of a gas jet is not sufficiently developed to calculate the characteristics of this flow at any great distance from the inner aperture, observations of jets[110] reveal that the flow from the aperture could be expected to remain as a slender column of gas with similar diameter to the aperture for a distance greater than 40 times the aperture diameter. Hence, for an aperture

diameter of 100 μm the spacing between inner and outer apertures should exceed five millimetres for the differential pumping system to be effective.

The maximum spacing between inner and outer apertures which is possible with the design of Figure 3.3 is limited by the projector pole-piece dimensions to approximately three millimetres, and even at this distance diffracted beams from crystal lattice planes of spacing less than 0.11 nm will not be passed by a lower aperture of 100 μm diameter. Subsequent tests have also shown that the 100 kV electron beam is not capable of producing images of useful intensity at gas pressures higher than those obtainable with the Hashimoto type stage.

Although these considerations indicate that it is not feasible to utilise a differentially pumped chamber for microscopy at 100 kV, a versatile reaction cell based on these principles has been successfully designed by Swann[111] for high voltage (1000 kV) microscopes. At 1000 kV the electron beam can successfully penetrate a longer column of gas at higher pressure and the apertures of the cell may be placed much further apart. The space available within the objective lens is also much greater than in 100 kV microscopes and permits independent specimen translation and tilt.

3.2.3 Specimen Tilting Stage

The absence of specimen tilting seriously restricts the scope of structural investigations involving electron diffraction. Tilting enables diffraction contrast experiments to be performed; the acquisition of diffraction patterns for a variety of crystal orientations; and the enhancement of three-dimensional effects by stereo photography. The most useful specimen tilting devices provide accurately measured inclination in any direction without lateral or vertical movement of the specimen area under observation. The provision of this type of movement requires that the tilt axis lies in the plane of the specimen and in line with the area

of the specimen under observation but very few commercially available tilting devices meet these requirements in full owing to the fundamental lack of space available within the objective lens.

Figure 3.4 illustrates the first development of a design concept for a reaction chamber with specimen tilting geometry based on the above criteria. This design allows for the removal of the central portion of the stage through an airlock in the microscope column. Subsequent development of this concept resulted in the abandonment of this airlock feature on recognition that insertion and removal of such a complicated device through an airlock would present numerous problems. These problems could be avoided at the expense of a small increase in microscope evacuation time if the stage were bodily removed from the microscope to change specimens. The specimen chamber shown in Figure 3.5 has similar tilting geometry but may be completely removed from the microscope through a side port after bringing the electron optical column to atmospheric pressure. The following sections describe details of the construction, development and operation of this device.

The specimen is mounted on a platinum ribbon heater similar to the type shown in Figure 3.2 which is attached with stainless steel screws to four insulated stainless steel electrodes passing through a 14.3 mm diameter bronze ball. The ball is machined so that the midpoint between the specimen area under observation and one of the gas containment apertures, which is also mounted on the face of the ball, is accurately located at the ball centre. The ball and ball-socket are machined and lapped to provide a gas seal as well as a bearing surface for specimen tilting. The second gas containment aperture is mounted on a removable cap, the separation between the two apertures being 0.28 mm. The reacting gas is circulated around the specimen from an inlet pipe which enters through the side of this cap, a viton 'O' ring ensuring that the

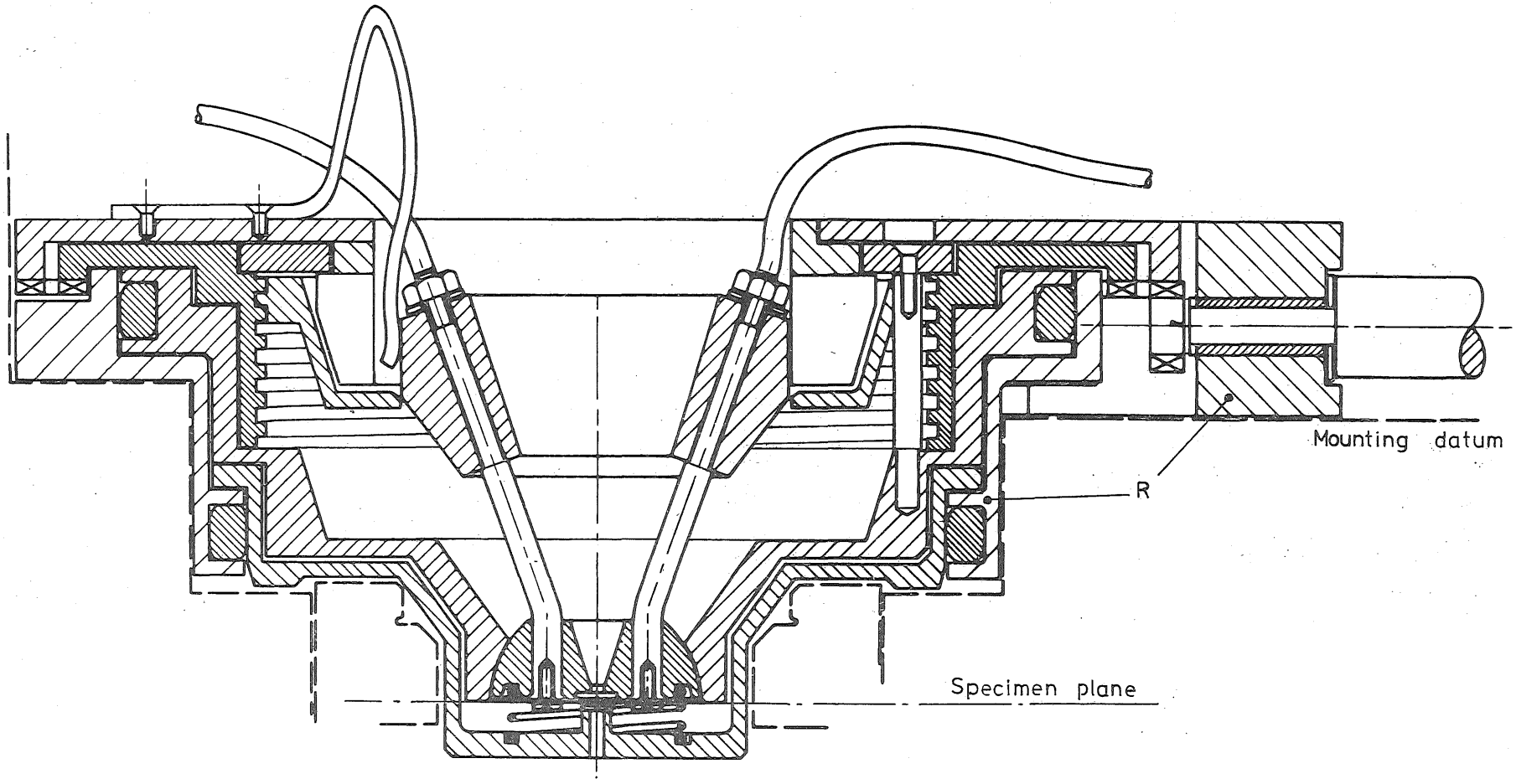

Fig. 3.4 Initial concept of tilting gas reaction specimen chamber. The outer ring (R) which contains an 'O' ring seal and tilt drive shafts is designed to be permanently mounted in the electron microscope, the remainder of the stage being removable through an airlock. (Not constructed).

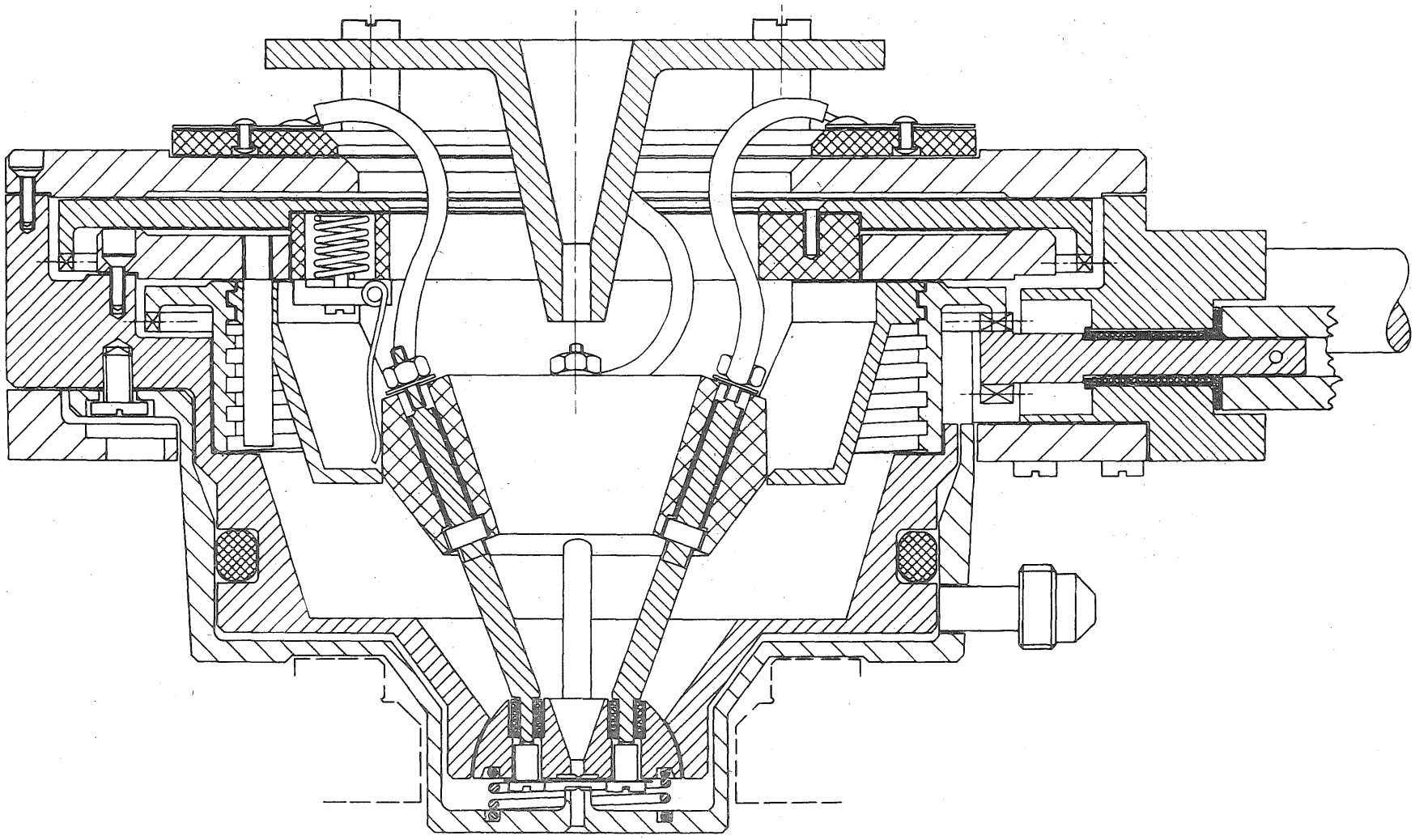

Fig. 3.5 Final design of the tilting high temperature controlled atmosphere specimen chamber.

gas atmosphere is contained within the specimen chamber. A spring mounted in the cap maintains contact between the ball and its socket when the chamber pressure is low.

The two apertures are lightly held in position with silver-conducting paint to enable them to be easily removed for cleaning purposes and to avoid the build-up of electric charge resulting from irradiation by the electron beam, and electrical contact between the apertures and the heater ribbon is prevented by thin sheets of mica cemented on the aperture surfaces. Alignment of the specimen and apertures is performed under an optical microscope when the specimen is inserted in the chamber. The specimen area of interest is first positioned over the centre of the aperture fixed to the tilting ball using the four current-carrying mounting screws. The removable cap containing the lower aperture is then replaced with three compressible lead shims positioned under its outer flange. The three screws which secure this cap are then progressively tightened on the shims until slight tilting of the cap brings the apertures into alignment.

The majority of the specimen chamber components are machined from continuously-cast phosphor bronze to specification BS 1400: 1973, grade PB4. This material is chosen for its good machining properties; relative freedom from porosity; and low contents of zinc and lead which have high vapour pressures at elevated temperatures.

3.3 ATMOSPHERE CONTROL

The complete gas flow system is shown in Figure 3.6. Gas mixtures are admitted to the reaction chamber through controlled leak valves V18, V19 and V20 which allow flow rate control from 500 ml/min to less than 1.0 ml/hr. The majority of oxidation experiments have been performed in tank oxygen atmospheres preceded by a hydrogen anneal, but any atmosphere compatible with the construction materials of the reaction chamber and

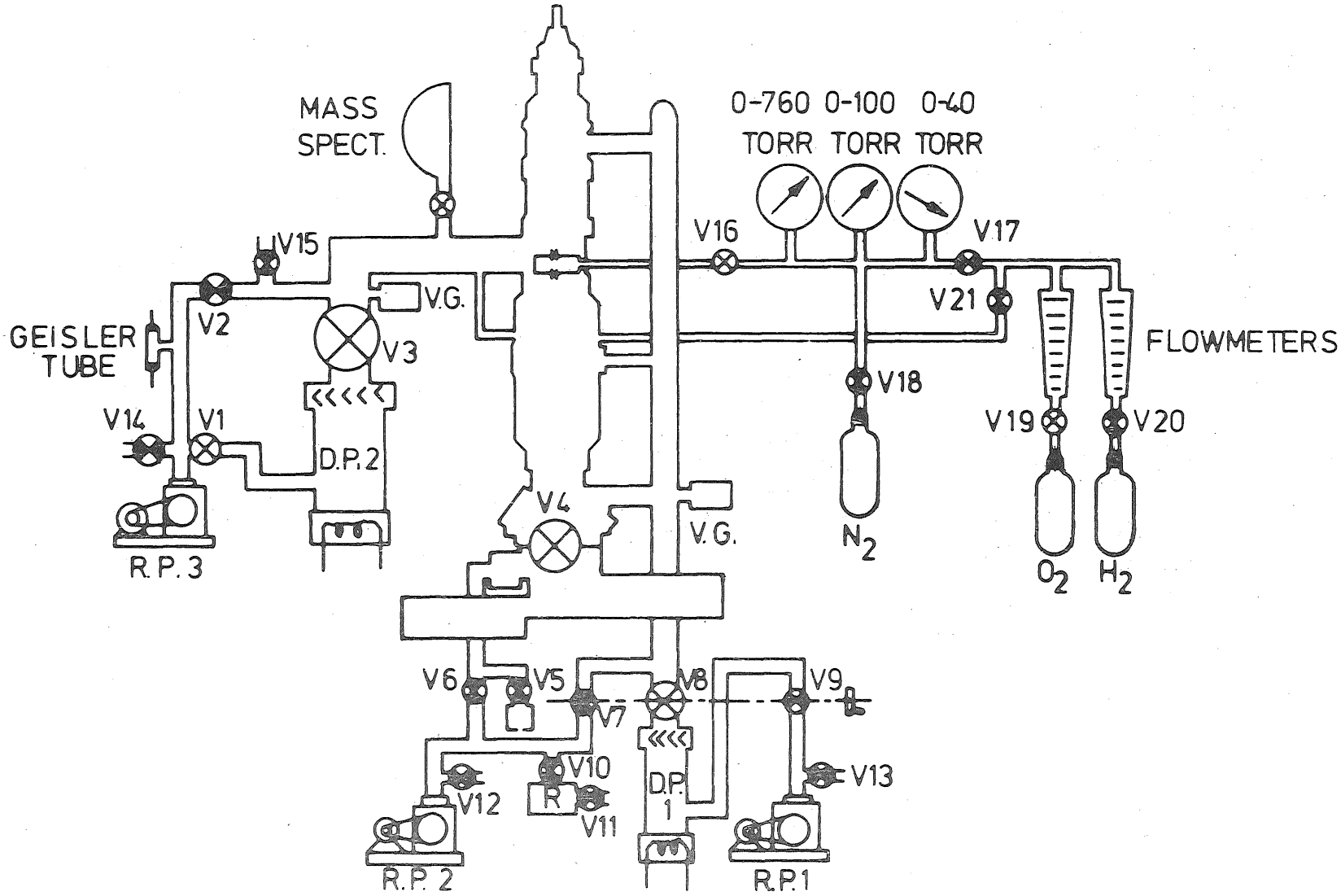

Fig. 3.6 Schematic diagram of the gas flow system of the reaction chamber

electron microscope may be utilised. The composition of the reacting atmosphere is monitored by flow meters on the gas inlet or by the use of an A.E.I. Minimass mass spectrometer which is mounted in the auxiliary vacuum system. This instrument has a sensitivity of 1.3 nPa (10^{-11} mm Hg), a mass range of 2 to 240, and a maximum operating pressure of 130 mPa (10^{-3} mm Hg). This maximum operating pressure restricts use of the mass spectrometer to reaction stage operating pressures less than approximately 5 kPa (40 mm Hg), but below this limit the identification and partial pressure of each component of the atmosphere leaking from the specimen chamber may be determined. The spectrometer readings are influenced by residual gases in the vacuum systems and by contamination from the oil diffusion pumps and must be interpreted with care.

The pressure in the reaction chamber is assumed to be identical to the pressure in the inlet pipe which is measured by three barometrically compensated capsule-type gauges. Although this reading is only an approximation to the pressure in the vicinity of the area of the specimen under observation, which may be affected by the aperture leakage, Hashimoto *et al*[105] have demonstrated that the difference between these pressures can be ignored for pressures greater than 1.3 Pa (10^{-2} mm Hg) provided a large reservoir of gas exists close to the specimen.

The relation between the pressure of introduced gas and the intensity of 80 kV and 100 kV electron beams passed through the Hashimoto chamber has been examined[105] for apertures of 50 µm, 100 µm and 150 µm diameter. These intensities are expected to be similar to those for the tilting stage which has a clearance between the apertures of 0.28 mm compared with 0.30 mm for the Hashimoto chamber. The larger column of escaping gas associated with the larger apertures is shown to produce a more severe intensity reduction than is experienced using a smaller aperture at the same pressure. Hashimoto also estimates that image resolution in air at 40 kPa (300 mm Hg) is degraded to 5-10nm. Initial experience with the

tilting stage suggests similar performance. Images of useful intensity and contrast may be obtained at oxygen pressures up to 20 kPa (150 mm Hg) using apertures of 100 μm diameter and resolution appears to be limited by Brownian motion of the oxide particles rather than by scattering of the electron beam. The JEM 7A microscope is normally capable of 0.6 nm point to point resolution but the reaction cell necessitates use of a wide bore objective polepiece which in itself limits resolution to approximately 1.2 nm.

To achieve a satisfactory electron emission filament life a vacuum of the order of 1.3 mPa (10^{-5} mm Hg) must be maintained in the vicinity of the electron gun. To maintain this vacuum the gas leakage from the specimen stage must be removed from the electron optical column by an auxiliary vacuum pump separate from the normal microscope evacuation system. The normal pumping port for the specimen area of the microscope is blanked off and the microscope volume immediately above the specimen chamber is evacuated by a separate ULVAC YV2 pumping system, which consists of a three-stage oil diffusion pump backed by a gas-ballasted rotary pump. Figures 3.7 and 3.8 illustrate the 100 mm diameter vibration isolating pipe connection from this pump to the microscope column which ensures a high pumping speed estimated at 33 l/s in the vicinity of the specimen chamber. To further reduce contamination of the electron gun an additional gas sealed aperture of 600 μm diameter was fitted in a specially designed holder below the condenser lens polepiece. The design, which incorporated sliding 'O' ring seals to allow manipulation of the aperture from outside the microscope column, did not prove entirely satisfactory. The aperture showed a tendency to collect contamination from the sliding seals which led to a build-up of static charge and instability of the electron beam. Subsequent operation of the reaction stage without this aperture has proved perfectly satisfactory at pressures up to 10 kPa (75 mm Hg) which are suitable for oxide whisker growth; however, higher pressure reactions may require a gas constrictor at this point for satisfactory electron gun

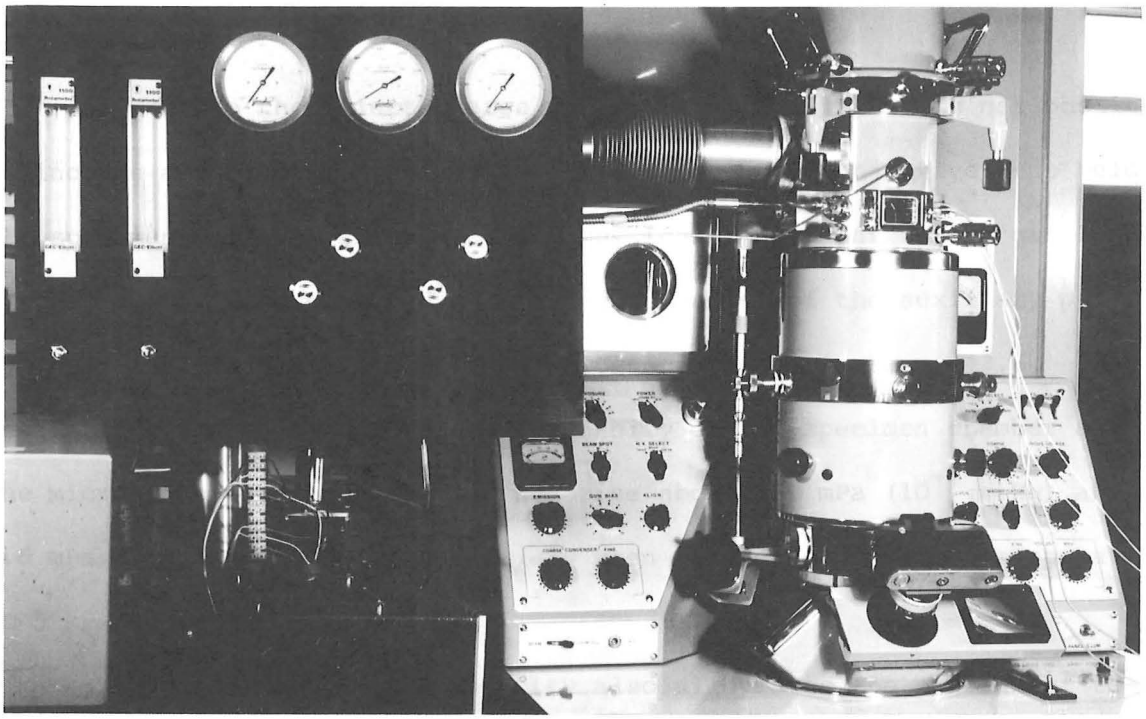

Fig. 3.7 View of gas mixing and control panel. Vibration isolated auxiliary vacuum coupling to the electron microscope is also visible.

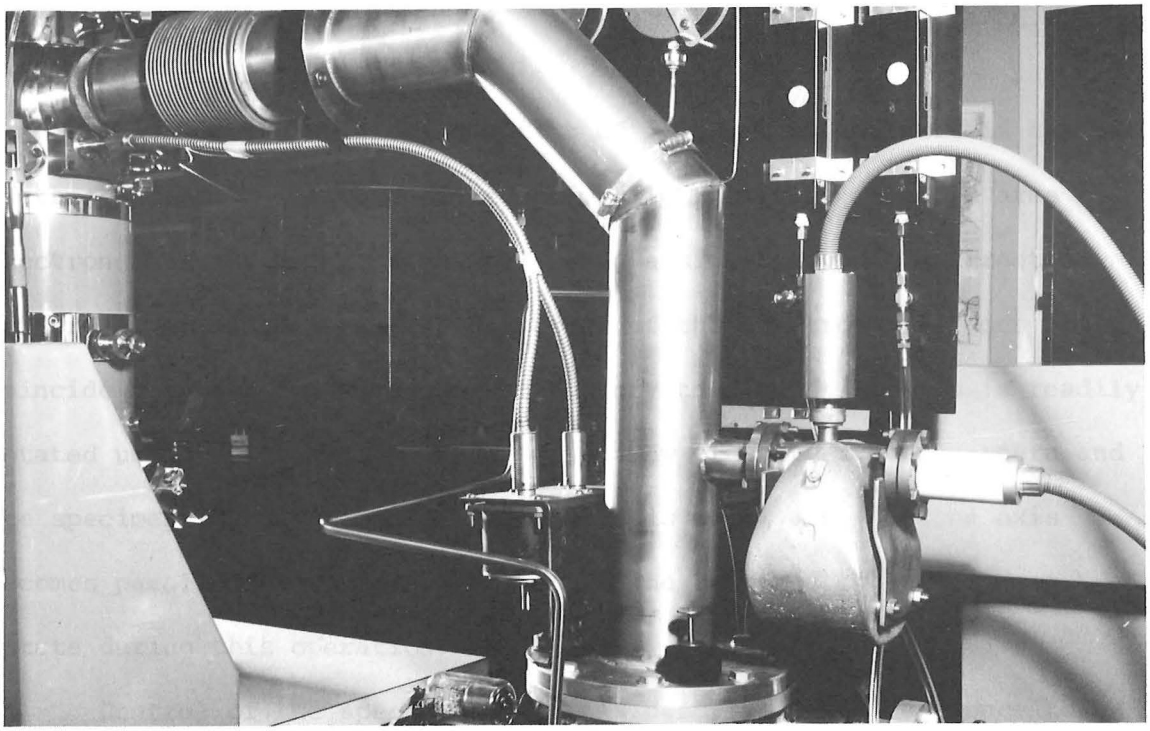

Fig. 3.8 View of rear of gas control panel showing mounting of mass spectrometer head in auxiliary vacuum system and dual stepper motor drives for control of specimen orientation.

filament life.

To retain the selected area diffraction facility it is not possible to include a further gas containment aperture in the objective lens below the specimen, but the absence of any physical constraint to the gas leakage at this point is compensated by the high capacity of the auxiliary pumping system. The two vacuum gauges, positioned as shown in Figure 3.6, indicate that the pressures in the vicinity of the specimen chamber and in the microscope pumping system do not rise above 130 mPa (10^{-3} mm Hg) and 6.6 mPa (5×10^{-5} mm Hg) respectively when the reaction stage is operating at 5 kPa (40 mm Hg).

The auxiliary pumping capacity also alleviates the problem of re-evacuation of the complete system each time a new specimen is inserted. Normal operating pressure is achieved in less than five minutes pumping time and is a small proportion of the total specimen changeover time of approximately 30 minutes.

3.4 SPECIMEN TILTING

The geometry which allows tilt of $\pm 15^{o}$ about any axis in the plane of the specimen has been designed primarily to assist selected area electron diffraction. For example, when a single crystal diffraction pattern is obtained where the direction of the electron beam does not coincide with a major zone axis of the crystal, the tilt axis is readily rotated until it coincides with a major row of spots in the pattern and the specimen is then tilted about this axis until a major zone axis becomes parallel to the electron beam. The specimen image does not rotate during this operation.

Control of the specimen motion is described with reference to Figure 3.9. The upper aperture and specimen, which are separated by a sheet of mica 0.01 mm thick, are attached to the bronze ball A such that the mid point between them is positioned to within 0.01 mm of the ball

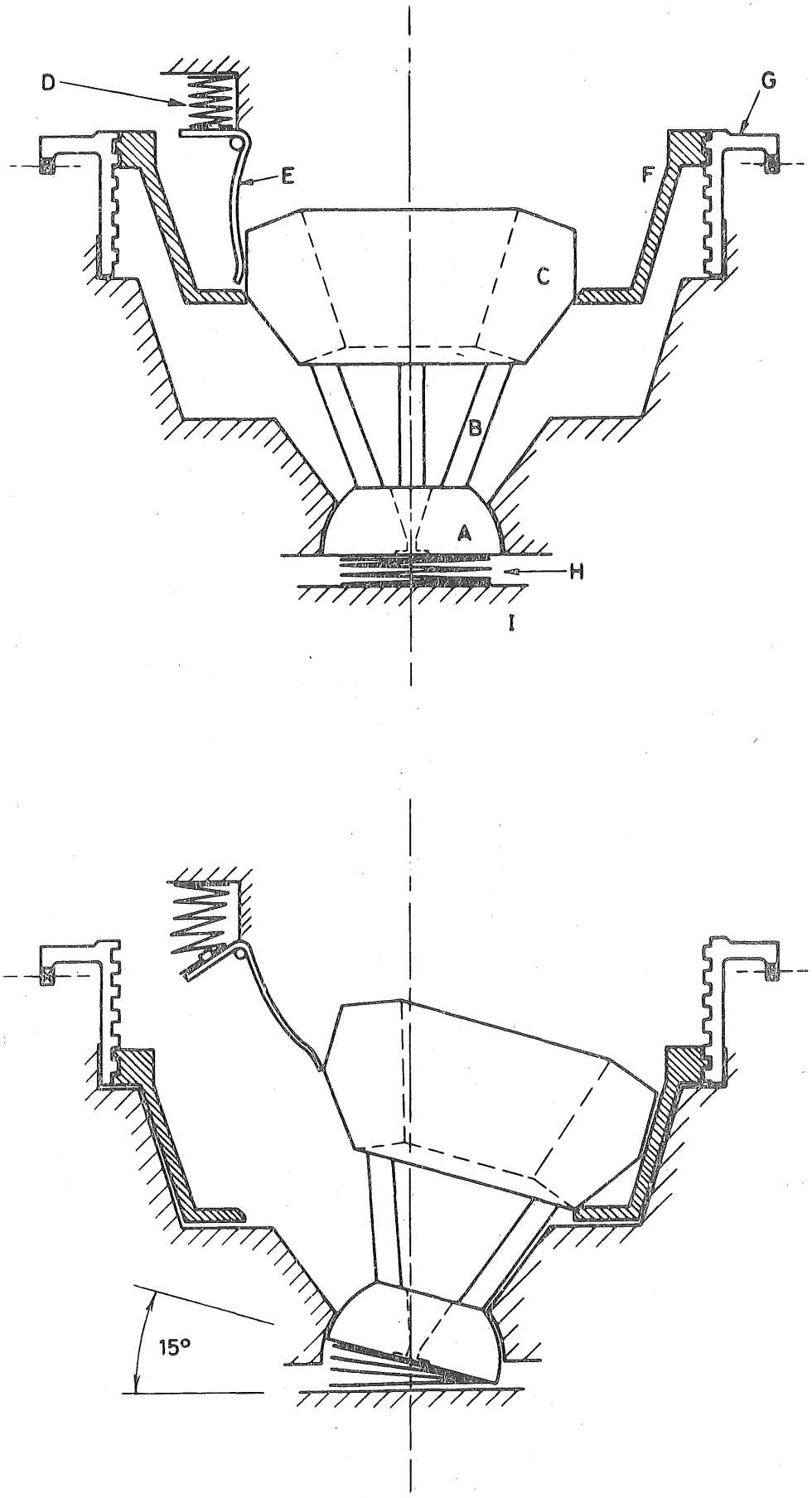

Fig. 3.9 Geometry of the specimen tilting mechanism.

centre. The tilt axis therefore passes very close to the area under observation, which is limited to the cross-section of the apertures. This geometry results in minimal easily controlled translation of the image as tilting occurs, and a maximum vertical displacement of the observed area of the specimen of 13 μm.

The stainless steel electrodes B passing through the ball are attached at the upper end to a P.T.F.E. ring C which is machined with an inclined outer surface. This ring is constrained to move laterally in one direction only by a pair of P.T.F.E. jaws which are not shown in Figure 3.9 but are visible in Figure 3.10. These jaws are attached to a geared ring which can rotate through 360° and thus alter the direction of tilt of the complete specimen holder assembly. The low friction P.T.F.E. contact between jaws and specimen holder assembly produces little torque to rotate the ball A in its seating during rotation of the geared ring, but additional protection is provided by fitted ends on spring H which couple the ball to the covering cap I . A spring D , acting on one side of the ring C through lever arm E , maintains constant contact between the inclined outer edge of the opposite side of the ring and the inside surface of a circular hole machined in part F . Part F does not rotate but is raised and lowered by a rotating ring G acting on its threaded outer surface. As part F is lowered, spring D constrains the specimen holder assembly to tilt about the ball seating, the degree of tilt being limited by the position of part F , and the direction of tilt by the orientation of the P.T.F.E. jaws. The maximum tilt available by this mechanism is limited by the geometry of the objective polepiece to approximately 15°.

The two geared rings which control tilt and azimuth orientation are driven by two stepper motors through flexible drive shafts external to the microscope, and by universally jointed drive shafts and pinions within the microscope to allow specimen translation. The pinion drives are mounted

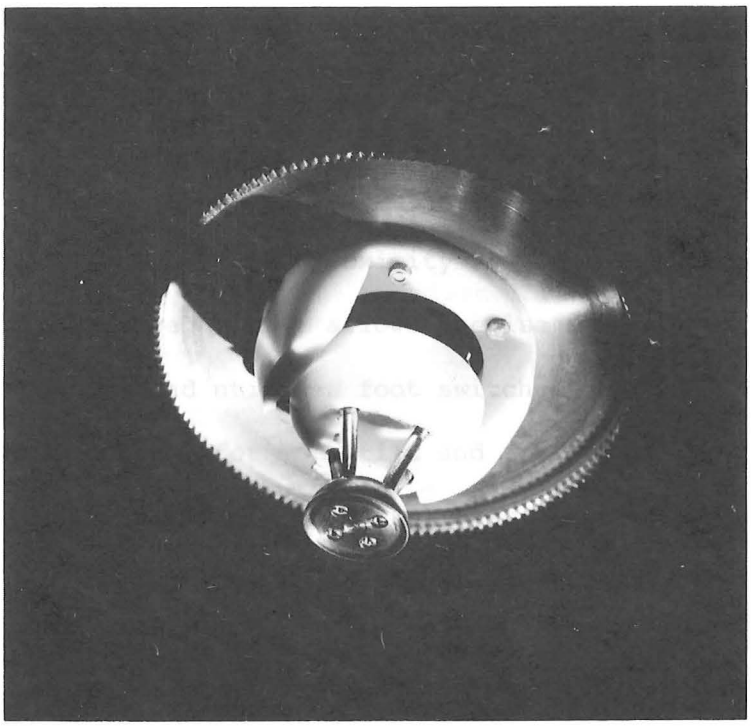

Fig. 3.10 P.T.F.E. jaws mounted on the geared azimuth control ring determine the direction of tilt. The spring and lever arm which force the specimen holder assembly to tilt about the ball centre are obscured. (Scale of photograph approximately full size).

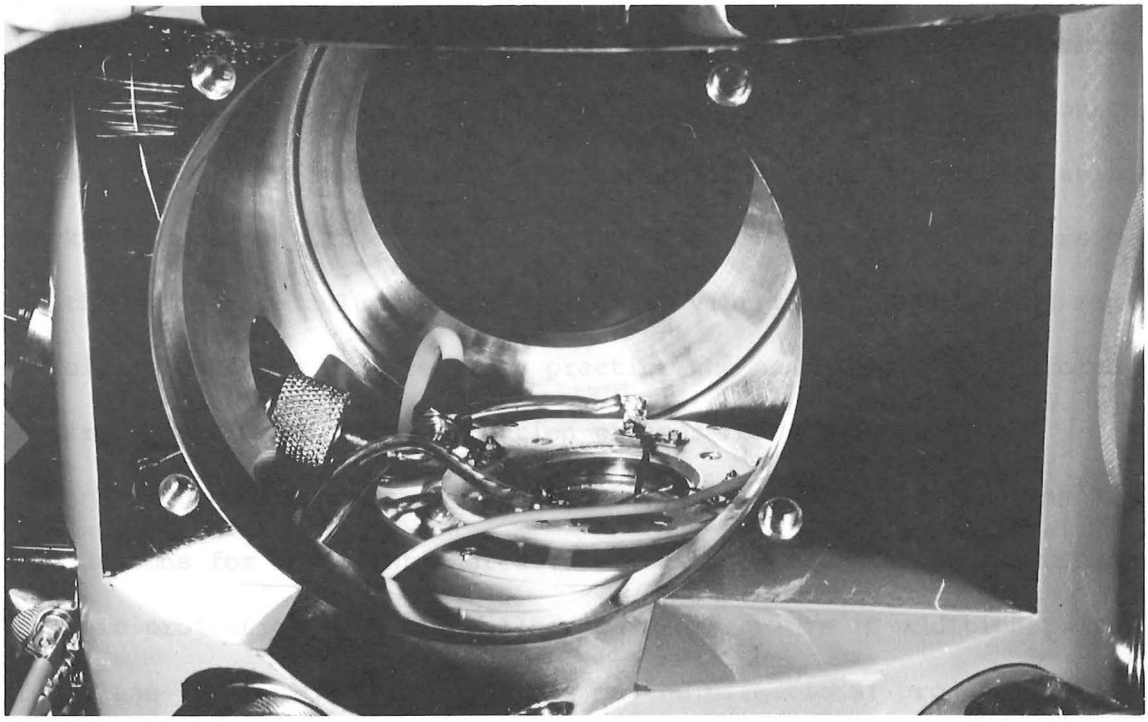

Fig. 3.11 Mounting of the specimen chamber in the electron microscope. Note the detachable gas inlet pipe and the proximity of the large diameter vacuum port.

permanently in the microscope on the normal specimen translation platform and mesh directly with the geared rings when the reaction chamber is inserted. Figure 3.11 shows the mounting of the specimen chamber in the microscope and illustrates the proximity of the large diameter vacuum port. The stepper motor drive system allows precise open loop control over the specimen orientation and utilises foot switches to provide forward/reverse and a 10:1 speed control for both tilt and axis rotation. The operator's hands, therefore, remain free to adjust specimen translation, focus, and all normal microscope controls. Any desired orientation may be preset on the control panel using thumbwheel switches, and the specimen may then be driven to this position at any desired speed using the foot controls, the motors automatically stopping when the desired position is reached. Digital counters provide a continuous readout of tilt and azimuth position at all times.

Accuracy of positioning is limited by backlash in the flexible drive shafts and gears, but calibration, on the basis that desired positions will always be approached from the same direction, provides for positioning tolerances of $\pm$ 0.1 degrees of tilt and $\pm$ 0.5 degrees of axis rotation. Backlash could be largely eliminated by mounting the stepper motors close to the microscope column, but substantial vibration isolation and magnetic shielding would be required. In practice the need always to approach a desired position from one direction creates few difficulties.

A computer program by Smaill[140], which produces stereographic projections for any crystal structure, has been modified to produce stereographic projections for crystallographic directions in addition to those for plane poles. Low index spots on the directional projection represent poles of reciprocal lattice planes (zone axes) which may give rise to diffraction patterns and may be used to assist crystal manipulation using the goniometer. An example of this application is provided by the directional projection for the rhombohedral αFe_2O_3 cell with axis

$[10\bar{1}]$ which is shown in Figure 3.12. The growth direction of most αFe_2O_3 whiskers is $[10\bar{1}]$, therefore, the spots around the perimeter of this projection represent the reciprocal lattice planes likely to produce diffraction patterns with the electron beam perpendicular to a whisker axis. Once a single pattern is recognised the projection facilitates manipulation of the crystal with the tilt controls to obtain additional patterns for structural confirmation.

3.5 TEMPERATURE CONTROL

The specimen is heated by passage of direct current through a metal ribbon which is of reduced cross-section near the point of observation. For most oxide whisker growth experiments the heater ribbon is manufactured from the metal to be oxidised and is observed directly; but for thin foil studies a platinum ribbon is used with a 0.3 mm diameter hole at the centre the foil being placed over this hole. Figure 3.13 shows production of a specimen assembly by spot welding. A thermocouple is spot-welded to the heater ribbon as close as possible to the point of observation, and ribbon and thermocouple are attached to a supporting mica ring to form a complete specimen assembly similar to that shown in Figure 3.2. The thermocouple registers the temperature of the heater ribbon at a short distance from the point of observation, the effective cold junction being inside the reaction cell. The thermocouple e.m.f. may be calibrated against the known melting points of metals, or by a method described by Martin and Boyd[112] which makes use of the image shift caused by phase changes in magnetic materials, but calibration for oxidation experiments has been simply achieved against a second thermocouple spot-welded alongside the first and with reference junction at $0^{o}C$.

The method of temperature measurement is not entirely satisfactory as the temperature distribution in the heater ribbon is not known. Baker and Harris[113] have used optical pyrometry to determine that the temperature

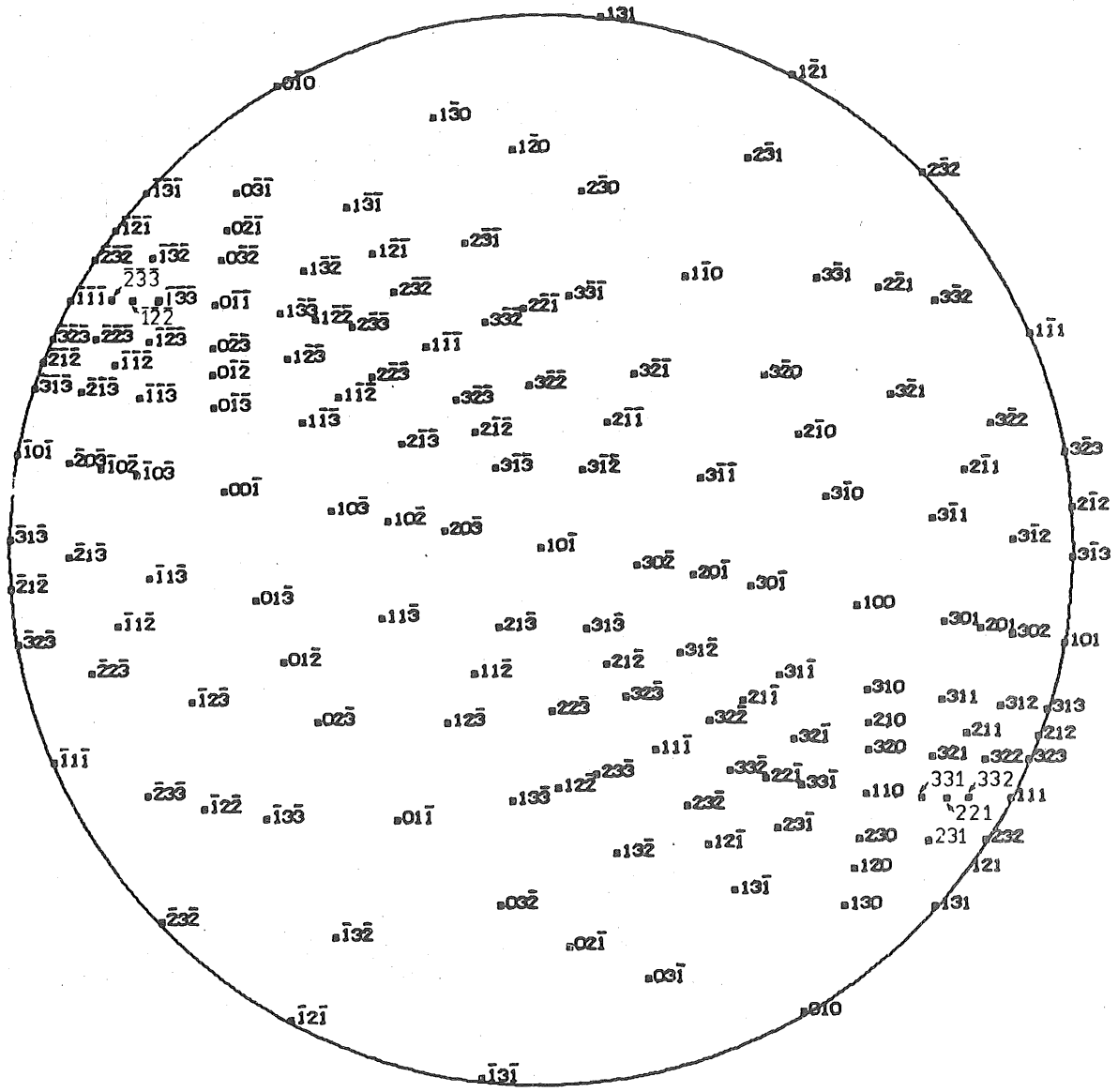

Fig. 3.12 Stereographic projection for αFe_2O_3 (structural rhombohedral cell) crystallographic directions with $[10\bar{1}]$ as pole. Points around the periphery of this projection represent the zone axes of diffraction patterns obtained with the electron beam perpendicular to a whisker of $[10\bar{1}]$ growth direction.

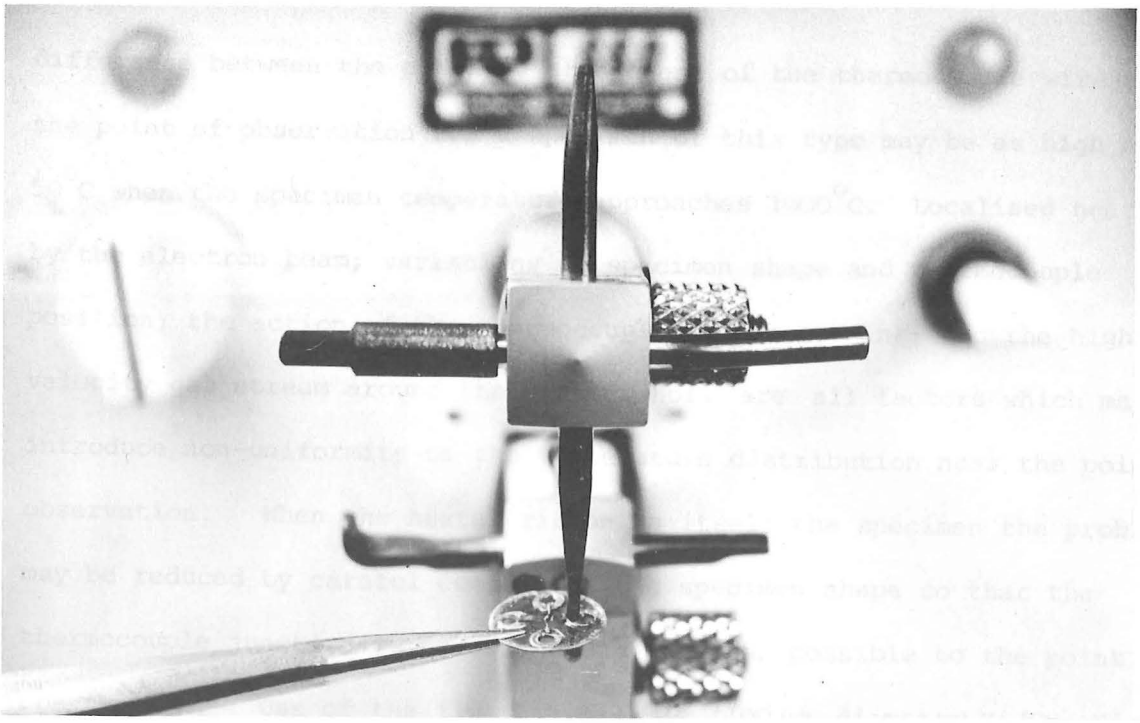

Fig. 3.13 Construction of a specimen assembly by spot welding. (Scale 1.5 times full size.)

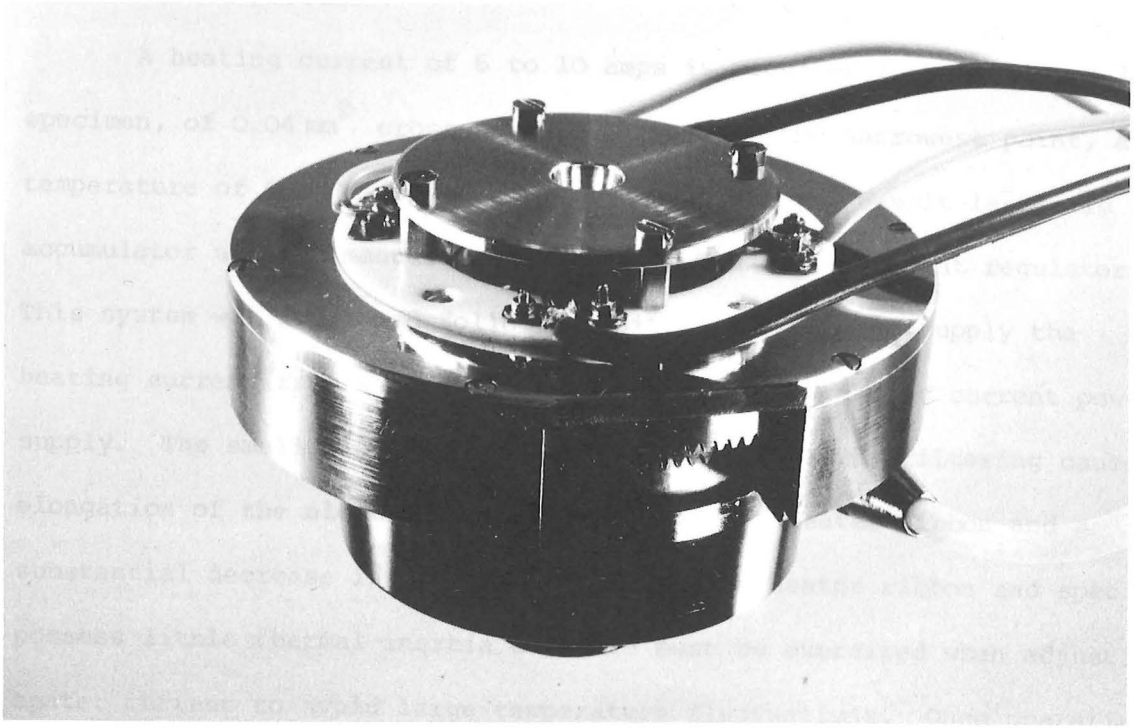

Fig. 3.14 The complete tilting gas reaction chamber. The geared rings engage automatically with pinion drives when the chamber is inserted into the microscope but manual connection of gas inlet pipe and electrical leads is required. (Scale approximately 1.5 times full size.)

difference between the point of attachment of the thermocouple wire and the point of observation for a specimen of this type may be as high as 50°C when the specimen temperature approaches 1000°C. Localised heating by the electron beam; variations in specimen shape and thermocouple position; the action of the thermocouple as a heat-sink; and the high velocity gas stream around the central hole are all factors which may introduce non-uniformity of the temperature distribution near the point of observation. When the heater ribbon is itself the specimen the problem may be reduced by careful control of the specimen shape so that the thermocouple junction is positioned as close as possible to the point of observation. Use of the finest available (100 μm diameter) Ni/Cr: Ni/Al thermocouple wire also reduces heat dissipation by the thermocouple. Despite these precautions the effect of electron beam heating remains a serious unknown, and accurate calibration of the temperature measurement system is not possible.

A heating current of 6 to 10 amps is required to maintain an iron specimen, of 0.04 mm^2 cross-sectional area, at the narrowest point, at a temperature of 600°C. The current is supplied by a 6-volt lead acid accumulator using a manually controlled solid state current regulator. This system was developed following initial attempts to supply the heating current from a rectified and filtered alternating current power supply. The small ripple voltage which remained after filtering caused elongation of the electron beam parallel to the heater ribbon and a substantial decrease in image resolution. The heater ribbon and specimen possess little thermal inertia and care must be exercised when adjusting heater current to avoid large temperature fluctuations. Once operating conditions are established, however, the temperature remains stable and requires few adjustments.

Re-alignment of the electron beam and objective aperture is required when the heating current is altered to compensate for the beam

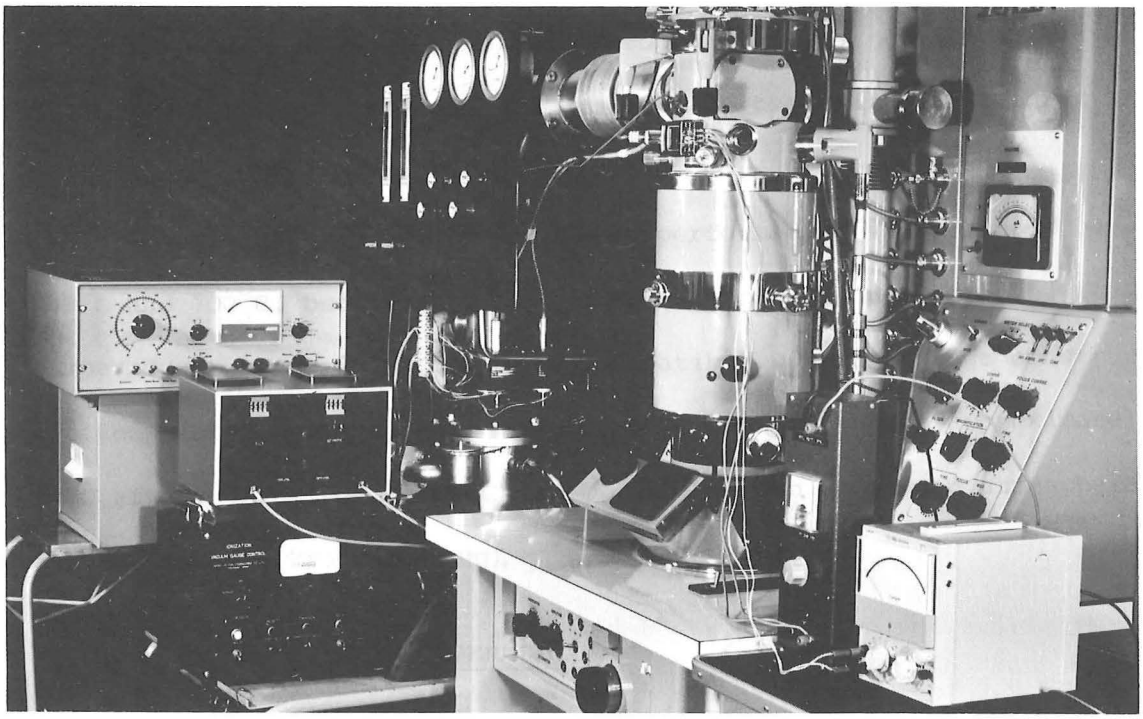

Fig. 3.15 General view of the JEM 7A electron microscope with the tilting gas reaction stage installed.
Control panels for stepper motors and mass spectrometer are on the operator's left; millivolt meter and current regulator for temperature measurement and control are on the right.

deflection created by the changing magnetic field associated with this current. Little thermal drift of the specimen is observed and the image generally remains stable under stable operating conditions. The image drift normally associated with magnetic specimens is observed whenever the objective lens field strength is altered to focus the specimen, and it is possible that magnetic effects contribute to the small image shift which occurs when the specimen is tilted.

Oxidation experiments have been performed at temperatures between 250°C and 700°C, but it is anticipated that continuous operation at temperatures up to 1000°C would be compatible with the stage construction. The temperature of the outer body of the chamber reaches approximately 50°C after operation at 600°C for two hours with an oxygen atmosphere at a pressure of 5 kPa (40 mm Hg).

3.6 COMMISSIONING AND OPERATION

An operational problem became evident on first insertion of the specimen chamber into the electron microscope with no specimen fitted. Apparent misalignment of the gas containment apertures and microscope viewing system indicated considerable tilting of the electron beam while passing through the chamber. This deflection was traced to the current-carrying electrodes which were manufactured from type 304 stainless steel and had become slightly magnetic during manufacture. Prior testing of the stock from which the electrodes were machined had not provided any evidence of paramagnetism in a strong magnetic field, and it is assumed that a small proportion of austenite was transformed to ferrite or martensite by cold work associated with the manufacturing processes. The austenite structure was regained by a homogenising anneal, consisting of heating to 1000°C followed by a water quench, and no further trace of the problem was observed.

The initial testing of the reaction chamber was performed without

the insulation shield which covers the electrical wiring at the top of the stage. Non-conducting parts in close proximity to the electron beam were coated with silver conducting paint and earthed to avoid electrostatic charging by the electron beam. The tilting ball and P.T.F.E. ring which is part of the tilting specimen holder assembly were similarly earthed through one of the stainless steel electrodes. Despite these precautions, uncontrollable beam drift occurred owing to charging of the lacquer insulation on the flexible wires which provide electrical connection to the tilting sections of the stage. Charging of these wires persisted, even when they were constrained a minimum distance of 10 mm from the electron beam; but the problem was rectified by the addition of the earthed conducting shield which projects into the stage to separate the insulated portions of the wires from the beam.

The efficiency of the ball and socket gas seal was initially open to doubt. The oxygen flow rate at an operating pressure of 2.5 kPa (20 mm Hg with 100 μm diameter apertures is approximately 80 ml/min, but there is no observable change in this flow rate, which is measured by rotameter, when the ball and socket joint in the reaction cell is coated with a layer of vacuum grease. This indicates that leakage past this joint in the dry operating condition is negligible at this pressure, and at higher pressures the seal efficiency should increase as the ball is held more firmly against its seating.

A number of different heater ribbon configurations were examined for their suitability as oxidation specimens. The ribbon shapes in Figure 3.16 illustrate a number of variations which were examined. The ribbon configuration is critical, as there is a need to localise the area of high temperature to lower the heating power required and reduce specimen drift and the risk of thermal damage to reaction stage components. However, excessive reduction in the cross-section reduces the degree of temperature control and introduces instability since it is not possible to

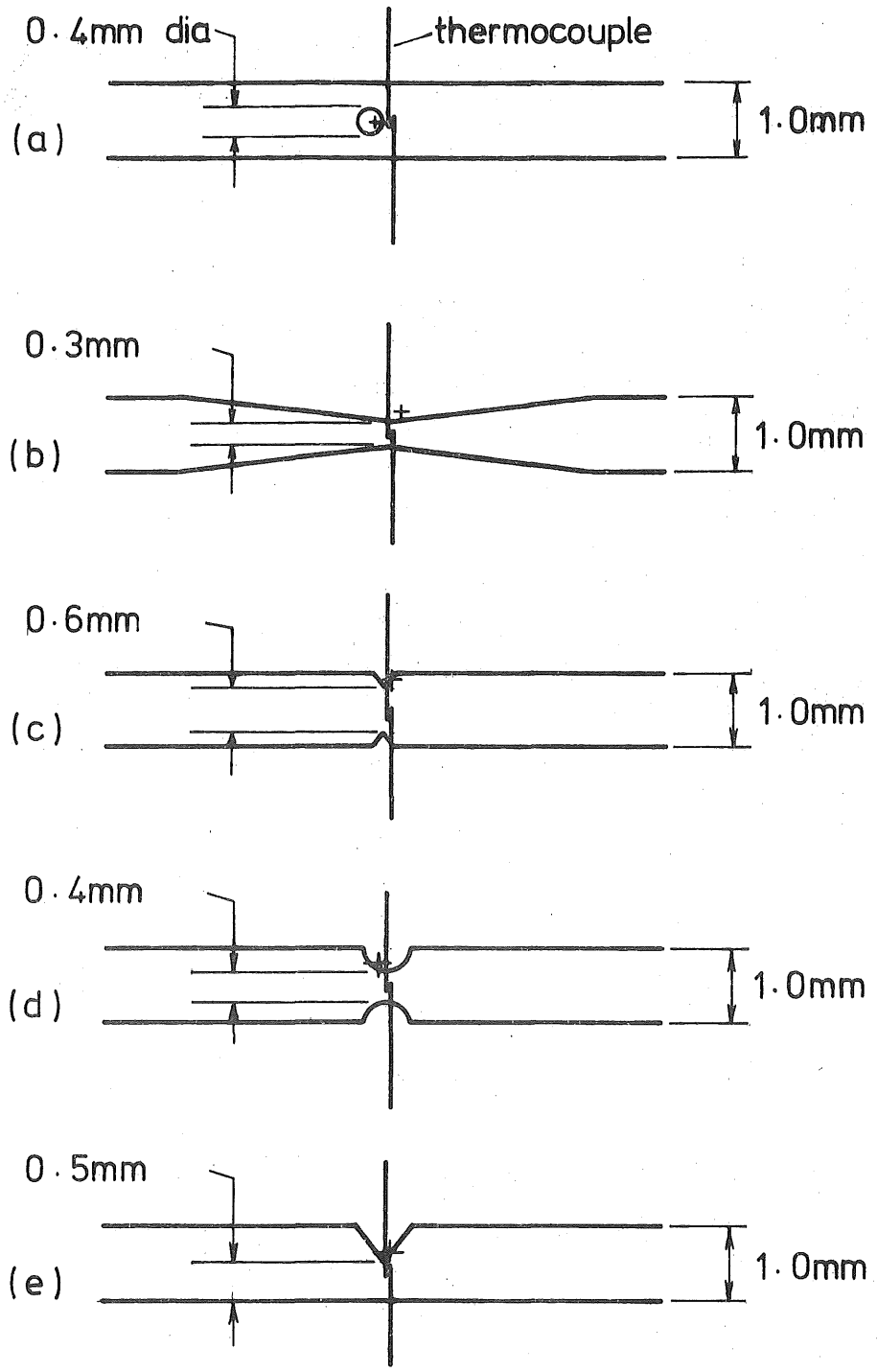

Fig. 3.16 Iron heater ribbon configurations examined. The position of the point of observation is indicated with a cross. All ribbons are of 0.01 thickness.

accurately measure the temperature at the point where maximum temperature occurs. Instability of this type is of particular significance when the heater ribbon is manufactured from a material liable to oxidation as local overheating may cause rapid oxidation leading to further localised reduction in cross-section and rapid destruction of the specimen. Specimens of type (a) with a central hole are particularly prone to thermal runaway, as any reduction in cross-section at one side of the hole is more severe than in a specimen of type (c) with the same cross-sectional area. Type(d) specimens are most commonly used, and provide a satisfactory compromise between localisation of the high temperature region, precise positioning of the thermocouple junction, and ease of construction.

The recording of dynamic experiments using glass photographic plates has proved satisfactory but cumbersome. The camera chamber capacity of the JEM 7A of 24 plates is rapidly exhausted despite the relatively slow growth rate of oxide whiskers, and re-evacuation of the chamber following insertion of additional plates requires a minimum interruption to photography of four minutes. To avoid this delay a motorised 35 mm camera has been mounted to observe the viewing screen in place of the normal focussing telescope, and the continuous recording of 250 images at rates up to four exposures per second is possible. Photographic plates are used in preference to this recording system wherever possible, however, as the 35 mm images are of lower resolution and contrast and suffer from an exaggerated perspective in one direction as a result of the inclination of the viewing screen to the electron beam.

One significant advantage to be gained from the observation of specimens in a controlled environment is freedom from contamination resulting from reaction of the specimen with residual gases in the microscope column while under observation. The most serious form of contamination, which may build up at very high rates under normal operation, is that due to hydrocarbon vapour arising from greases or oils in the

vacuum system. Incidental leaks and volatile matter absorbed in the photographic plate emulsions also contribute to the problem. The high velocity gas stream emerging from the reaction chamber apertures protects the specimen from these contaminants most effectively.

3.7 CONCLUSIONS

The reaction chamber described has been used to observe *in situ* formation of oxidation products at temperatures up to 700°C and in gas pressures up to 20 kPa (150 mm Hg). Stable operating conditions may be maintained with a minimum of operator attention, and the powered tilt facility, although limited in range, is a versatile aid to selected area electron diffraction. The reaction chamber should have application to the study of a broad range of chemical reactions under controlled atmosphere conditions.

CHAPTER 4

COMPUTER INDEXING OF ELECTRON DIFFRACTION PATTERNS

4.1 THE COMPUTER APPROACH

The indexing of electron diffraction patterns from simple known structures presents few problems for the experienced metallographer. However, the identification of non-cubic materials from spot patterns remains a difficult and tedious task if it is necessary to calculate lattice spacings and interplanar angles for a large number of possible diffracting phases. In addition, diffraction patterns from non-cubic structures with low symmetry can frequently be described by many non-equivalent indexing systems within the limits of experimental accuracy, and without computer assistance it is difficult to ensure that all such possible solutions are examined. Many of the oxide phases encountered in this study are non-cubic, and an additional complication is created by the publication of experimental results using a variety of unit cells to describe any one phase. For example, five different unit cells are commonly used to describe the αFe_2O_3 structure, these being: structural hexagonal, morphological hexagonal, structural rhombohedral, morphological rhombohedral, and face-centred rhombohedral[11].

At the time of commencement of this study a limited number of computer techniques were available to assist electron diffraction analysis[11] These programs performed the calculation of d-spacings for crystal lattices; the calculation of interplanar angles; and the simulation of electron diffraction patterns by plotting reciprocal lattice sections[115-118]. These simulated patterns could be manually matched to observed patterns to aid identification.

The computer approach adopted in this study has involved the

preparation of one major program XIDENT, and two lesser programs ANGLES and DSPACING.

(a) Program XIDENT directly indexes electron diffraction spot patterns by matching of the diffraction pattern to reciprocal lattice planes of prospective materials.

(b) ANGLES is designed to be used with a minicomputer in an interactive mode to compute the angles between crystal planes and directions for any crystal structure. The primary purpose of ANGLES is to determine the orientation relationships between a number of diffraction patterns and crystal features of interest.

(c) DSPACING produces lists of crystal d-spacings to assist with the identification of diffracting phases from ring type patterns, but has an important dual purpose in that it indexes diffraction patterns which result when more than one reciprocal lattice plane intersects the sphere of reflection.

4.2 PROGRAM XIDENT

XIDENT is a FORTRAN IV computer program which has been developed to directly index electron diffraction spot patterns from any crystal structure using a computer of at least 64K words of core storage capacity. A rapid identification technique is used which enables a large number of prospective structures to be examined while accommodating the experimental error which is inherent in selected area electron diffraction using an electron microscope. The speed of the program is such that all possible orientations of each phase are considered, and every reciprocal lattice plane which corresponds to the diffraction pattern, within the prescribed limits of accuracy, will be identified.

An outline flow diagram of XIDENT is shown in Figure 4.1, and a FORTRAN listing, which contains detailed input specifications, is included in Appendix 1. Figure 4.2 is a typical diffraction pattern from the tip

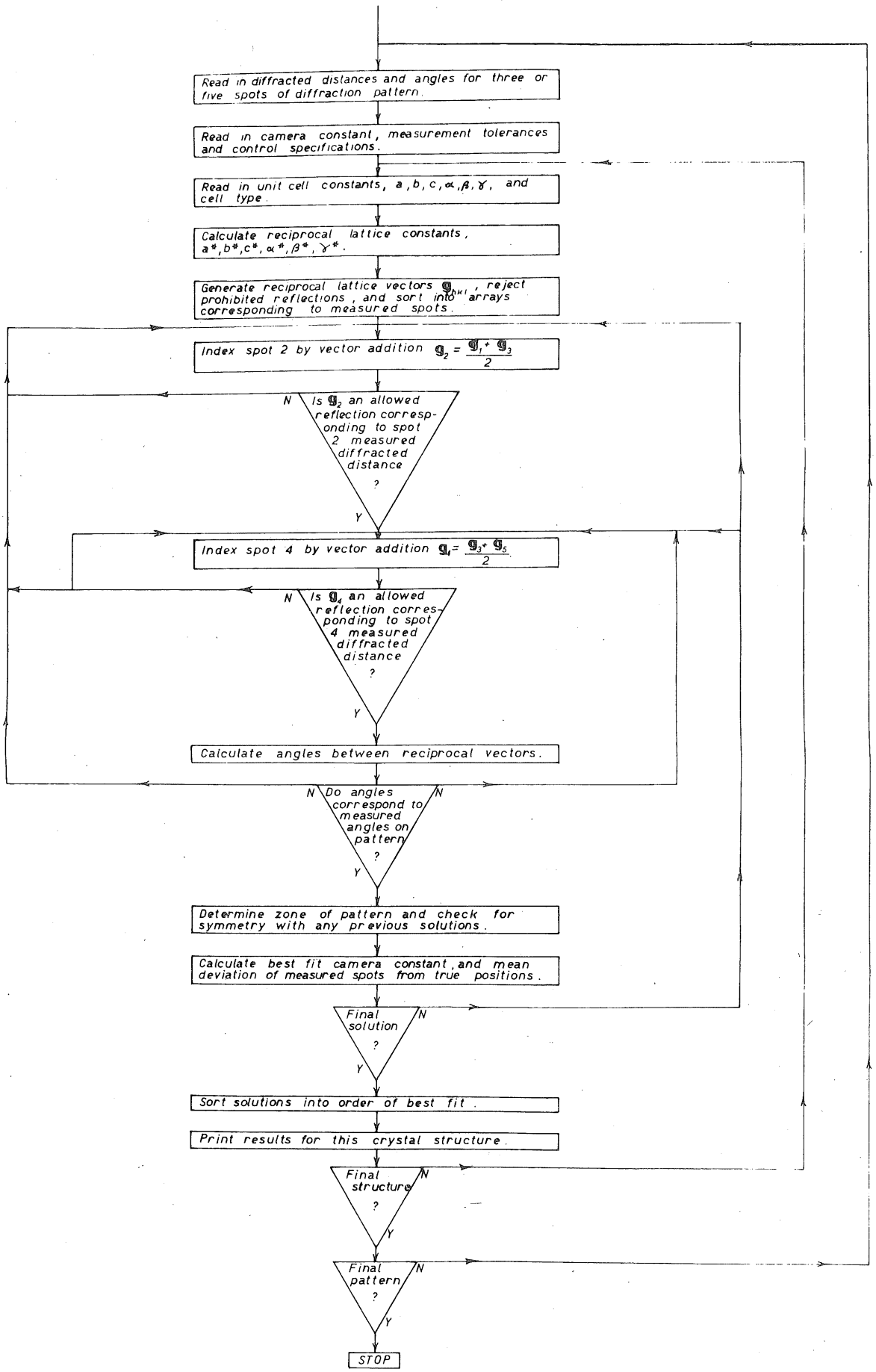

Fig. 4.1 Outline flow diagram of program XIDENT.

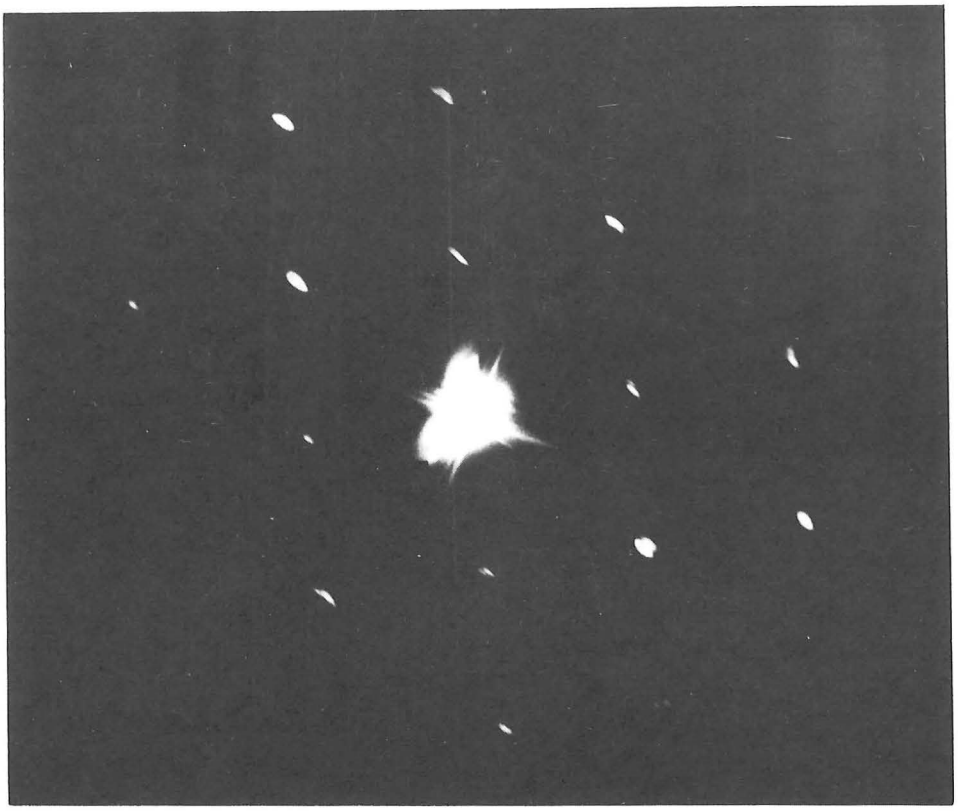

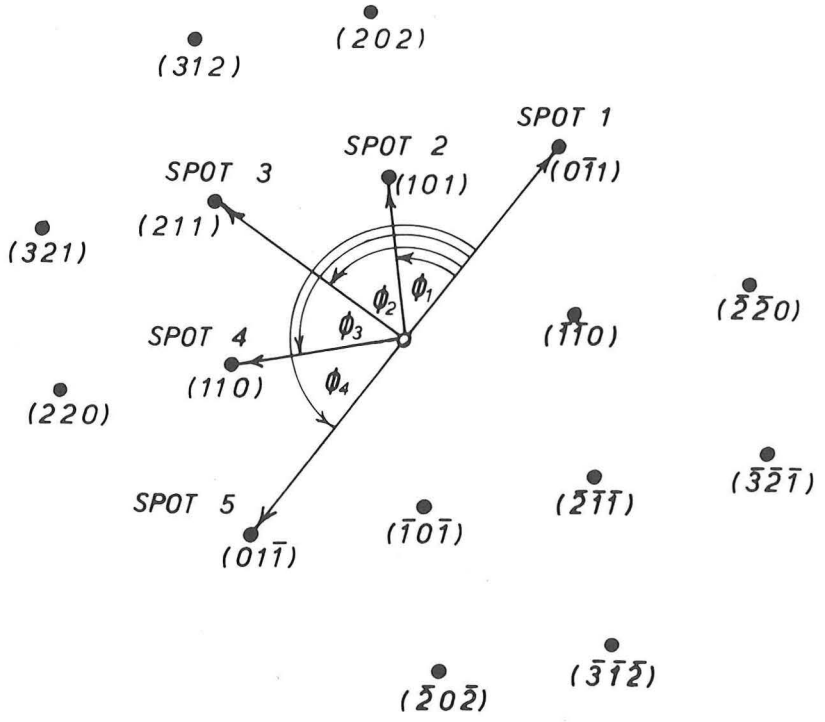

Fig. 4.2 Selected area electron diffraction pattern from αFe_2O_3 whisker. The [$\bar{1}$11] zone (structural rhombohedral cell) is shown, with streaks perpendicular to [0$\bar{1}$1] whisker growth direction.

of an iron oxide whisker crystal and will be used to illustrate a typical application of the program.

4.2.1 Data Input

The reciprocal lattice net of the spot pattern is represented to the computer by the input of the diffracted distances of either three or five diffraction spots, an approximate camera constant, and the measured angles ϕ_1, ϕ_2, etc. between these spots. The spots are chosen in groups of three to represent rows of the reciprocal lattice; spots 1, 2 and 3 being three equi-spaced points in any non-central row of the diffraction pattern, and spots 4 and 5 being chosen in conjunction with spot 3 to represent another non-central row in a similar manner. Figure 4.2 illustrates the choice of five spots according to this criterion, and it will be seen that the geometry of a single zone diffraction pattern may be completely characterised by these five spots except for the positions of possible forbidden reflections. The innermost spots on the pattern are normally used as input data since these represent the crystal lattice planes of greatest separation. These planes are fewer in number and are more characteristic of a particular structure than are the planes represented by spots further from the centre. It is not essential to choose the innermost spots, however, as these may frequently be obscured by a superimposed pattern from a diffraction standard or from a specimen support film, but computation times are lower and there is less likelihood of ambiguous results when the innermost spots are chosen.

Any three equi-spaced spots in any non-central row of the pattern may be chosen as an alternative form of input; spots 1, 2 and 3 from Figure 4.2 being acceptable input. It is plain from the figure that such an input may not completely describe the two-dimensional nature of a diffraction net and, although XIDENT will index the pattern normally, there is a possibility that incorrect solutions will be produced. This form of input may be useful for the indexing of imperfect patterns which

are produced when the zone axis of the pattern is inclined to the electron beam but it is generally preferable to use five spots to avoid erroneous solutions.

Experimental error is accommodated by the input of three tolerances which relate to the following:

(a) errors in the camera constant (expressed as a percentage);

(b) errors in measurement of the diffracted distances of individual spots (expressed in millimetres); and

(c) errors in the measured interplanar angles from the diffraction pattern (expressed in degrees).

It is necessary to separate tolerances (a) and (b). Errors in the determination of the camera constant; owing to variation of objective lens current, specimen position, or other instrument factors; tend to dominate for spots with large diffracted distances; whereas errors in individual spot positions, attributable to the presence of reciprocal lattice streaks inclined to the direction of the electron beam and other factors which lead to poor measurement precision, are of greater significance for spots nearer the centre of the pattern.

4.2.2 Generation of Reciprocal Vectors

Indexing of the five diffraction spots is accomplished by matching of the measured diffracted distances and interplanar angles to the magnitudes of vectors $\vec{g}_{hkl}$ in the reciprocal lattice and the angles ϕ_1, ϕ_2, etc. between these vectors. Reciprocal vectors are generated for all possible combinations of Miller indices by successive decrementing of the values of (hkl) from (nnn) to $(\bar{n}\bar{n}\bar{n})$, where the value of n is chosen so that only vectors with magnitudes small enough to correspond with one of the input diffracted distances will be generated.

To determine the magnitude of the reciprocal vectors it is first necessary to define the reciprocal unit cell in terms of the unit cell

vectors $\vec{a}$, $\vec{b}$ and $\vec{c}$ for the crystal being considered. The reciprocal lattice unit cell is defined by the vectors $\vec{a}^*$, $\vec{b}^*$, $\vec{c}^*$, where $\vec{a}^*$ is the axis normal to the plane containing $\vec{b}$ and $\vec{c}$, the $\vec{b}^*$ axis is normal to the plane containing $\vec{c}$ and $\vec{a}$, and the $\vec{c}^*$ axis is normal to the plane containing $\vec{a}$ and $\vec{b}$.

hence $$\vec{a}^*.\vec{a} = \vec{b}^*.\vec{b} = \vec{c}^*.\vec{c} = 1 \qquad \ldots.(4.1)$$

and $$\vec{a}^*.\vec{b} = \vec{b}^*.\vec{c} = \vec{c}^*.\vec{a} = \vec{a}^*.\vec{c} = 0 \qquad \ldots.(4.2)$$

The reciprocal vectors can thus be determined from the direct cell vectors by the relationships

$$\vec{a}^* = \frac{\vec{b} \times \vec{c}}{V}; \quad \vec{b}^* = \frac{\vec{c} \times \vec{a}}{V}; \quad \vec{c}^* = \frac{\vec{a} \times \vec{b}}{V} \qquad \ldots.(4.3)$$

where V is the volume of the direct unit cell bounded by a, b, and c and is given by the triple product,

$$V = \vec{a}.(\vec{b} \times \vec{c})$$

$$= abc\,(1 + 2\cos\alpha\cos\beta\cos\gamma - \cos^2\alpha - \cos^2\beta - \cos^2\gamma)^{\frac{1}{2}} \qquad \ldots.(4.4)$$

where α, β, γ are respectively the angles between

$\vec{b}$ and $\vec{c}$, $\vec{c}$ and $\vec{a}$, and $\vec{a}$ and $\vec{b}$.

The angles α^*, β^* and γ^* between $\vec{b}^*$ and $\vec{c}^*$, $\vec{c}^*$ and $\vec{a}^*$, and $\vec{a}^*$ and $\vec{b}^*$ respectively are given by the scalar product:

$$\cos\alpha^* = \frac{\vec{b}^*.\vec{c}^*}{b^*c^*}, \quad \text{etc.}$$

That is $$\cos\alpha^* = \frac{\cos\beta\cos\gamma - \cos\alpha}{\sin\beta\sin\gamma}$$

$$\cos\beta^* = \frac{\cos\alpha\cos\gamma - \cos\beta}{\sin\alpha\sin\gamma}$$

$$\cos\gamma^* = \frac{\cos\alpha\cos\beta - \cos\gamma}{\sin\alpha\sin\beta} \qquad \ldots.(4.5)$$

It can be shown that the reciprocal vector

$$\vec{g}_{hkl} = h\vec{a}^* + k\vec{b}^* + l\vec{c}^* \qquad \ldots.(4.6)$$

is normal to the crystal lattice plane with Miller indices (hkl), and that

$$|\vec{g}_{hkl}| = \frac{1}{d_{hkl}}$$

where d_{hkl} is the spacing of these lattice planes.

Three vectors $\frac{\vec{a}}{h}$, $\frac{\vec{b}}{k}$, and $\frac{\vec{c}}{l}$ determine the position of the crystal lattice plane (hkl) which passes through their end points A, B and C as shown in Figure 4.3. Vector $\vec{AB}$ is $\frac{\vec{b}}{k} - \frac{\vec{a}}{h}$, and the scalar products of $\vec{AB}$ and $\vec{g}_{hkl}$ is

$$(\frac{\vec{b}}{k} - \frac{\vec{a}}{h}).(h\vec{a}^* + k\vec{b}^* + l\vec{c}^*) = 0 \qquad \ldots.(4.7)$$

from equations (4.1) and 4.2). Hence $\vec{g}_{hkl}$ is perpendicular to $\vec{AB}$, and similarly is perpendicular to $\vec{BC}$, $\vec{CA}$, or any vector in this plane; i.e. $\vec{g}_{hkl}$ is perpendicular to the plane (hkl). Also, if d_{hkl} is the length of the normal to this plane from the origin of the coordinates and if $\vec{n}$ is a unit vector along the normal,

$$d_{hkl} = \vec{n}.\frac{\vec{a}}{h} = \frac{(h\vec{a}^* + k\vec{b}^* + l\vec{c}^*)}{|\vec{g}_{hkl}|}.\frac{\vec{a}}{h} = \frac{1}{|\vec{g}_{hkl}|} \qquad \ldots.(4.8)$$

Therefore $\vec{g}_{hkl}$ is normal to the crystal plane (hkl) and its magnitude $|\vec{g}_{hkl}| = \frac{1}{d_{hkl}}$. Hence

$$\vec{g}.\vec{g} = \frac{1}{d_{hkl}^2} = h^2(\vec{a}^*.\vec{a}^*) + 2hk(\vec{a}^*.\vec{b}^*) + 2hl(\vec{a}^*.\vec{c}^*) + k^2(\vec{b}^*.\vec{b}^*) + 2kl(\vec{b}^*.\vec{c}^*) + l^2(\vec{c}^*.\vec{c}^*) \qquad \ldots.(4.9)$$

From the properties of the scalar product

$$|\vec{g}_{hkl}| = \frac{1}{d_{hkl}} = (h^2a^{*2} + 2hka^*b^*\cos\gamma^* + 2hla^*c^*\cos\beta^* + k^2b^{*2} + 2klb^*c^*\cos\alpha^* + l^2c^{*2})^{\frac{1}{2}} \qquad \ldots.(4.10)$$

4.2.3 Indexing of Spots by Vector Addition

Vectors with magnitudes falling within the prescribed tolerances for the measured diffracted distances for spots 1, 3 and 5 are sorted into

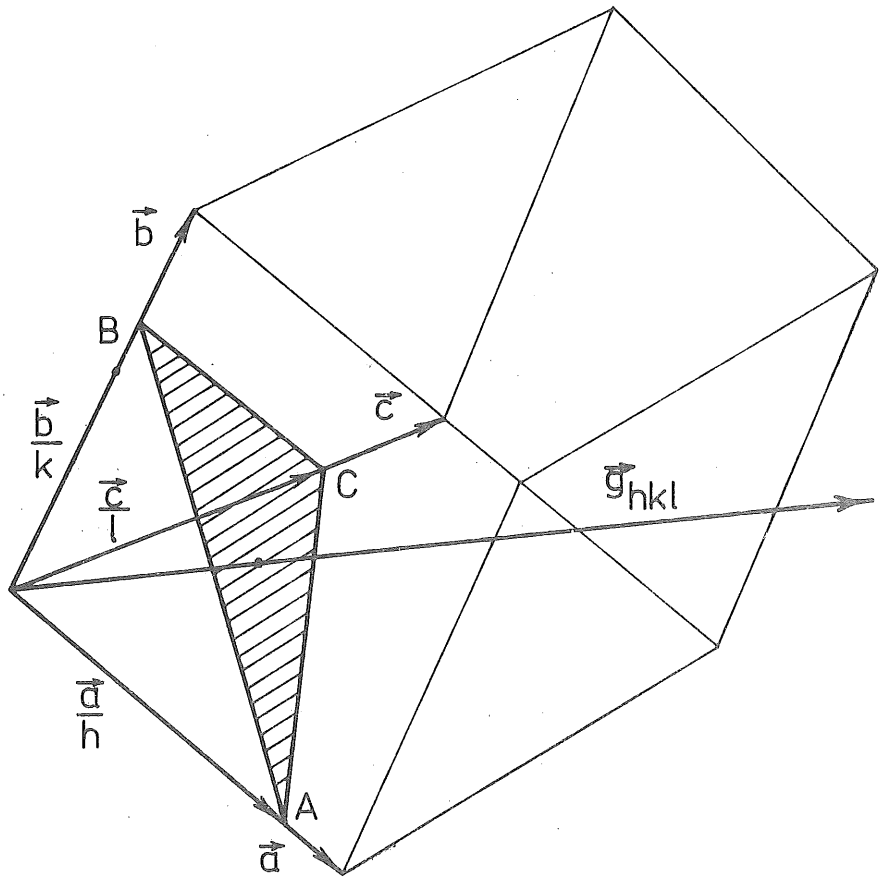

Fig. 4.3 Relation between the reciprocal lattice vector $\vec{g}_{hkl}$ and the unit cell vectors $\vec{a}$, $\vec{b}$, $\vec{c}$.

three arrays as they are generated. In the listed version of the program provision has been made for up to 800 reciprocal vectors corresponding to each spot. However, this number may be readily altered to match the available core storage on any computer system. In the unusual event that more than 800 reciprocal vectors may be matched to any one diffraction spot, it is necessary to either choose new input data spots nearer to the centre of the pattern or reduce the tolerance on camera constant or measured diffracted distance.

During this loading operation reciprocal vectors corresponding to prohibited reflections for the lattice types listed in Table 4.1 may be automatically removed. The appropriate control information (SYM) to initiate this procedure is contained in the first column of the data card describing the crystal structure. If forbidden reflections are removed in this way the input data diffraction spots must be chosen with care, as it is possible that two-dimensional diffraction and secondary scattering may mask the extinction laws for a structure and lead to the appearance of forbidden reflections in the diffraction pattern[119]. If a forbidden spot is chosen as input data, and reciprocal vectors for forbidden reflections have been removed, the correct indexing will be automatically rejected by XIDENT.

Indexing of the pattern proceeds by considering the spots in groups of three. All $\vec{g}_{h_1k_1l_1}$ vectors corresponding to point 1 are sequentially matched with $\vec{g}_{h_3k_3l_3}$ vectors corresponding to point 3, and a tentative indexing of point 2 is performed by vector addition:

$$h_2 = \frac{h_1 + h_3}{2}, \quad k_2 = \frac{k_1 + k_3}{2}, \quad l_2 = \frac{l_1 + l_3}{2} \qquad \ldots.(4.11)$$

If $\vec{g}_{h_2k_2l_2}$ corresponds to an allowed reflection, its magnitude is calculated and compared with the measured diffracted distance for point 2. If $\left|\vec{g}_{h_2k_2l_2}\right|$ falls within the allowed tolerance for spot 2 an attempt is

CLASS OF REFLECTIONS	LATTICE TYPE	LATTICE SYMBOL	FORBIDDEN REFLECTIONS	SYM
hkl	Primitive	P	none	0
"	All faces centred	F	$h + k \neq 2n$ $k + l \neq 2n$ $h + l \neq 2n$	1
"	Body centred	I	$h + k + l \neq 2n$	2
"	A face centred	A	$k + l \neq 2n$	3
"	B face centred	B	$h + l \neq 2n$	4
"	C face centred	C	$h + k \neq 2n$	5
"	Rhombohedral, obverse	R	$-h + k + l \neq 3n$	6
"	Rhombohedral, reverse	R	$h - k + l \neq 3n$	7

TABLE 4.1 Prohibited reflections removed by subroutine PROHIB.

made to index spot 4 by a similar process. (If three spots only are input the program moves directly to the angles check described in Section 4.2.4.)

$$h_4 = \frac{h_3 + h_5}{2}, \quad k_4 = \frac{k_3 + k_5}{2}, \quad l_4 = \frac{l_3 + l_5}{2}$$

The magnitude of $\vec{g}_{h_4k_4l_4}$ is then compared with the measured diffracted distance for spot 4.

4.2.4 Comparison of Interplanar Angles

If five reciprocal vectors are found with magnitudes corresponding to the measured diffracted distances and with hkl values satisfying the vector inter-relationships implied by the geometry of the input data spots, then the angles between these vectors ϕ_1', ϕ_2', etc., are calculated and compared with the angles ϕ_1, ϕ_2, etc., measured from the diffraction pattern.

These angular relationships are determined by consideration of the scalar product of the relevant reciprocal vectors.

$$\vec{g}_1 . \vec{g}_2 = \left|\vec{g}_1\right| \left|\vec{g}_2\right| \cos \phi^1 \qquad \ldots.(4.12)$$

therefore

$$\cos \phi' = \frac{(h_1\vec{a}^* + k_1\vec{b}^* + l_1\vec{c}^*).(h_2\vec{a}^* + k_2\vec{b}^* + l_2\vec{c}^*)}{\left|\vec{g}_1\right| \left|\vec{g}_2\right|}$$

$$= [h_1h_2a^{*2} + k_1k_2b^{*2} + l_1l_2c^{*2} + (k_1l_2 + l_1k_2)b^*c^*\cos\alpha^*$$

$$+(l_1h_2 + h_1l_2)c^*a^*\cos\beta^* + (h_1k_2 + k_1h_2)a^*b^*\cos\gamma^*](\left|\vec{g}_1\right| \left|\vec{g}_2\right|)^{-1}$$

$\ldots.(4.13)$

Evaluation of $\left|\vec{g}_1\right|$ and $\left|\vec{g}_2\right|$ from Equation 4.10 provides the required

angle in terms of the reciprocal cell constants and the Miller indices of the relevant crystal planes.

If all angles correspond with those measured, within the specified tolerance, the indexing of the spots is recognised as a valid solution. The zone axis of the pattern [uvw] is then determined by cross multiplication of $\vec{g}_{h_1k_1l_1}$ and $\vec{g}_{h_2k_2l_2}$ and division by the highest common factor.

$$u = k_1l_2 - k_2l_1 \ , \quad v = l_1h_2 - l_2h_1 \ , \quad w = h_1k_2 - h_2k_1 \qquad \ldots(4.14)$$

No attempt is made to check that spots 3, 4 and 5 lie in the same reciprocal lattice plane as 1 and 2 as XIDENT may index spots across overlapping Laue zones if the vector additive relationships are satisfied. (A detailed discussion of the indexing of such spots is contained in Section 4.4.1.)

4.2.5 Sorting of Results and Output

If more than one successful indexing is found for a given phase, the indexed solutions are sorted into order of accuracy based on the mean deviation of the measured spots from their true positions which are determined on the basis of a calculated best fit camera constant.

$$C_{\text{best fit}} = C\left[\frac{\sum_{n=1}^{m}\left\{d_n - \frac{C}{2r_n}\right\}}{\sum_{n=1}^{m}\frac{C}{2r_n}} - 1\right] \qquad \ldots.(4.15)$$

Where $C_{\text{best fit}}$ is the 'best fit' diametral camera constant, C is the input diametral camera constant; r_n is the measured diffracted distance to spot n ; d_n is the calculated d-spacing corresponding to spot n ; and m is the number of spots being considered (either three or five).

Figure 4.4 illustrates the procedure for determining the mean deviation of the measured spots from their "true positions". Since spot 1 is the datum for the measurement of angles ϕ_1, ϕ_2, etc., it is necessary

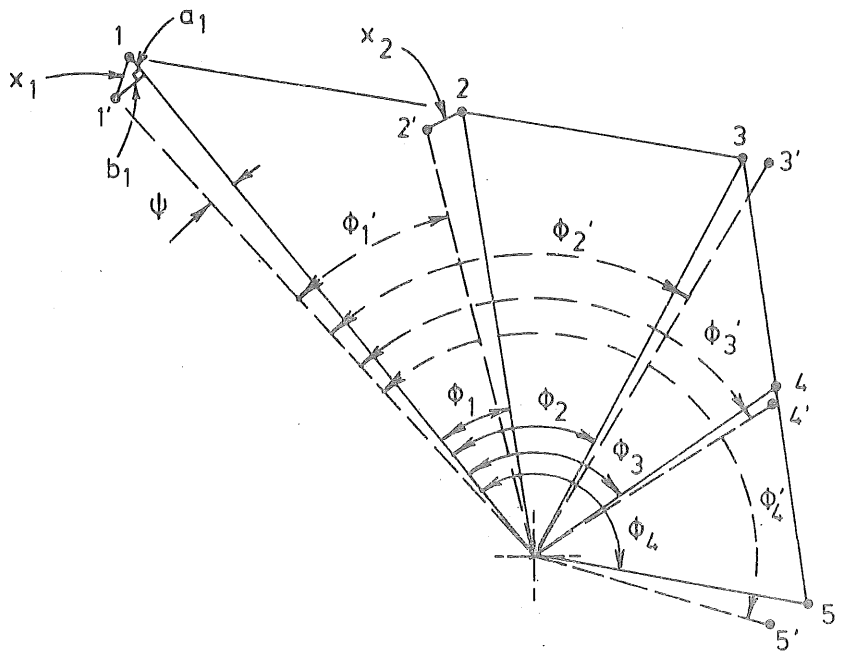

Fig. 4.4 Determination of mean deviation of diffraction spots from "true positions".

1, 2, 3, etc. are the measured positions of input data spots. 1', 2', 3', etc. are calculated "true positions" based on the best fit camera constant.

to make correction for any small initial error in the angular position of spot 1 relative to the other spots; i.e. the pattern is effectively rotated by an angle ψ to obtain the best average correspondence between the measured angles ϕ_1, ϕ_2, etc., and the calculated angles ϕ'_1, ϕ'_2, etc. between the relevant reciprocal vectors. The required rotation is given by:

$$\psi = \frac{-\sum_{n=1}^{m} (\phi'_n - \phi_n)}{m} \qquad \ldots.(4.16)$$

The mean deviation of the spots from their true positions $\frac{\Sigma x}{m}$ is now calculated with reference to the notation of Figure 4.4,

$$\frac{\Sigma x}{m} = \frac{\sum_{n=1}^{m} (a_n^2 + b_n^2)^{\frac{1}{2}}}{m} \qquad \ldots.(4.17)$$

where $$a_n = r_n - \frac{C_{\text{best fit}} \cdot \cos(\phi'_{n-1} - \phi_{n-1} - \psi)}{2d_n} \qquad \ldots.(4.18)$$

and $$b_n = \frac{C_{\text{best fit}} \cdot \sin(\phi'_{n-1} - \phi_{n-1} - \psi)}{2d_n} \qquad \ldots.(4.19)$$

A sample printout from program XIDENT is shown in Figure 4.5. This printout corresponds to the diffraction pattern of Figure 4.2. If more than one set of equivalent solutions is detected, the symmetrical equivalent solutions are grouped together and are printed out in order of accuracy. The printing of equivalent solutions may be suppressed if desired.

The 180° rotation ambiguity which exists for the indexing of each reciprocal lattice plane is resolved during the indexing process so that only one valid indexing is recognised for each zone. This is achieved by the termination of loading of reciprocal vectors into the array corresponding to spot 3 when the (hkl) values are decremented through (000). This expediency halves the number of reciprocal vectors corresponding to

```
PHOTO 5502 IRON OXIDE WHISKER
* * * * * * * * * * * * * * * *

CAMERA CONSTANT = 44.75
POSITION TOLERANCE = 1.00 MILLIMETRES (MINIMUM OVER-RIDING TOLERANCE OF + OR - 5.0 PERCENT OF DIFF.
                     DISTANCE PREVAILS)
DIFFRACTED DISTANCES OF SPOTS ARE
  9.05    6.10    8.40    6.15    9.05 (MILLIMETRES)
ANGLE TOLERANCE = 3.00 DEGREES
MEASURED ANGLES BETWEEN SPOTS ARE
  45.00   90.00   135.00   180.00

ALPHA FE 203 RHOMBOHEDRAL
* * * * * * * * * * * * * *

REAL CELL CONSTANTS

    A       B       C      ALPHA      BETA       GAMMA
 5.427   5.427   5.427   55.260     55.260     55.260

      MAXIMUM INDICES ARE       3  3  3
      MAXIMUM DIMENSIONS OF ARRAYS ARE      20    6    20

SET 1  ZONE AXIS  [-1   1   1]   (SET 1 HAS 6 SYMMETRICAL EQUIVALENT SOLUTIONS)
* * * * * * * * * * * * * * * * *

   SPOT          PLANE          DSPACE        ESTIMATED DSPACE FROM DIFF.PATTERN
     1        ( 0 -1  1)         2.517                      2.502
     2        ( 1  0  1)         3.682                      3.713
     3        ( 2  1  1)         2.699                      2.696
     4        ( 1  1  0)         3.682                      3.682
     5        ( 0  1 -1)         2.517                      2.502
N.B.  BEST FIT CAMERA CONSTANT USED IN ABOVE ESTIMATES OF D SPACINGS = 45.294
                                          (INPUT CAMERA CONSTANT  = 44.750)
      MEAN DEVIATION OF MEASURED SPOTS FROM TRUE POSITIONS = 0.110 MILLIMETRES


ANGLE BETWEEN PLANES  1 & 2 =   43.00 (MEASURED  45.00) DEGREES
ANGLE BETWEEN PLANES  1 & 3 =   90.00 (MEASURED  90.00) DEGREES
ANGLE BETWEEN PLANES  1 & 4    137.00 (MEASURED 135.00) DEGREES
ANGLE BETWEEN PLANES  1 & 5 =  180.00 (MEASURED 180.00) DEGREES

SYMMETRICAL EQUIVALENT SOLUTIONS FOR SET 1

  ZONE AXIS      POINT 1      POINT 2      POINT 3      POINT 4      POINT 5
[ 1  1 -1]    (-1  1  0)   ( 0  1  1)   ( 1  1  2)   ( 1  0  1)   ( 1 -1  0)
[ 1 -1  1]    ( 1  0 -1)   ( 1  1  0)   ( 1  2  1)   ( 0  1  1)   (-1  0  1)
[ 1 -1 -1]    ( 0  1 -1)   ( 1  1  0)   ( 2  1  1)   ( 1  0  1)   ( 0 -1  1)
[-1 -1  1]    ( 1 -1  0)   ( 1  0  1)   ( 1  1  2)   ( 0  1  1)   (-1  1  0)
[-1  1 -1]    (-1  0  1)   ( 0  1  1)   ( 1  2  1)   ( 1  1  0)   ( 1  0 -1)
```

Fig. 4.5 Printout from program XIDENT corresponding to the diffraction pattern of Fig. 4.2. Burroughs computation time for this identification = 1.25 seconds.

this spot as vectors of the type $(00\bar{\ell})$, $(0\bar{k}\ell)$ and $(\bar{h}k\ell)$ are rejected. The result of this action is that duplicate solutions for each zone are eliminated and program execution time is substantially decreased.

4.2.6 Application of Program XIDENT

XIDENT has proved a most useful technique for the indexing of most electron diffraction spot patterns, although the primary field of application is envisaged as the indexing of patterns from non-cubic structures when the identity of the diffracting phase is not known. The testing of published spot patterns, when the original identification is in doubt, can also be rapidly accomplished in a similar manner to the example shown. An approximate camera constant may be obtained from the original indexing and a search for alternative identification may then be performed over wide experimental limits.

It will be observed from Figure 4.5 that wide limits of error have been allowed in the indexing process. A camera constant tolerance of $\pm$ 2% to $\pm$ 5% has been routinely used for diffraction patterns from oxide whisker crystals as it is generally impossible to position a diffraction standard co-planar with specimens of this type. Wide measurement error limits of $\pm$ 1.0 mm on diffracted distance and $\pm$ 3.0^{o} on measured angles have also been routinely utilised to accommodate the displacement of spots resulting from pronounced reciprocal lattice streaks in diffraction patterns from filamentary crystals. Despite these large tolerances most materials can be checked within a few seconds of processing time on the Burroughs B6718 computer system and unambiguous results are generally obtained.

A number of alternative computer indexing techniques have been examined within the basic structure of program XIDENT. The indexing method described in Section 4.2.3 has a significant advantage over most other possible methods of vector addition in that it is not necessary to utilise the innermost spots on the diffraction pattern which may

frequently be obscured by a superimposed pattern. Indexing of patterns by the matching of interplanar angles alone, in the manner described by Wilkes[120] and by Booth *et al*[121], has also been attempted. It was found that the matching of reciprocal vectors and diffraction spots on the basis of an angles comparison was considerably slower than the indexing technique of Section 4.2.3 owing to the complexity of the matrix manipulations required to calculate such angles compared to the simple vector addition technique of XIDENT. The absence of any attempt to compare the relative positions of reciprocal lattice vectors and diffraction spots by vector addition also resulted in the production of large numbers of incorrect solutions which required manual verification.

4.3 PROGRAM ANGLE

The angle ρ between two vectors in the crystal lattice $\vec{L}_{(u_1v_1w_1)} = u_1\vec{a} + v_1\vec{b} + w_1\vec{c}$ and $\vec{L}_{(u_2v_2w_2)} = u_2\vec{a} + v_2\vec{b} + w_2\vec{c}$ may be determined in terms of the direct cell constants from the scalar product of the vectors in a similar manner to that described for reciprocal lattice vectors in Section 4.2.4

$$\cos\rho = \left(\begin{array}{l} u_1u_2a^2 + v_1v_2b^2 + w_1w_2c^2 \\ \quad +(v_1w_2 + w_1v_2)bc\cos\alpha \\ \quad +(w_1v_2 + u_1w_2)ca\cos\beta \\ \quad +(u_1v_2 + v_1u_2)ab\cos\gamma \end{array} \right) \Big/ \left| \vec{L}_{(u_1v_1w_1)} \right| \left| \vec{L}_{(u_2v_2w_2)} \right| \qquad \ldots.(4.20)$$

where the magnitude of the lattice vector $\vec{L}_{(uvw)}$ is given by

$$\left| \vec{L}_{(uvw)} \right|^2 = u^2a^2 + v^2b^2 + w^2c^2 + 2vwbc\cos\alpha + 2wuca\cos\beta + 2uvab\cos\gamma \qquad \ldots.(4.21)$$

The angle between a zone axis and a plane normal, which are represented by a direct cell vector and a reciprocal cell vector respectively, may also be readily obtained from this relationship by transformation of the reciprocal vector into components in the direct lattice as follows:

Consider the two coordinate systems with unit cell vectors a,b,c and a*, b*, c* for direct and reciprocal cells respectively. A reciprocal lattice vector

$$\vec{g} = h\vec{a}^* + k\vec{b}^* + l\vec{c}^* \qquad \ldots.(4.22)$$

has components in the direct lattice

$$\vec{g} = u\vec{a} + v\vec{b} + w\vec{c} \qquad \ldots.(4.23)$$

By taking the scalar product of (4.23) and $\vec{a}^*$

$$\vec{a}^*.\vec{g} = u\vec{a}^*.\vec{a} + v\vec{a}^*.\vec{b} + w\vec{a}^*.\vec{c}$$

$$= u \qquad \ldots.(4.24)$$

by definition of the reciprocal lattice in Equations (4.1) and (4.2).

Similarly, by taking the scalar product of (4.22) and a*

$$u = \vec{a}^*v$$

Therefore $$u = h\vec{a}^*.\vec{a}^* + k\vec{b}^*.\vec{a}^* + l\vec{c}^*.\vec{a}^*$$

and similarly $$v = h\vec{a}^*.\vec{b}^* + k\vec{b}^*.\vec{b}^* + l\vec{c}^*.\vec{b}^*$$

$$w = h\vec{a}^*.\vec{c}^* + k\vec{b}^*.\vec{c}^* + l\vec{c}^*.\vec{c}^* \qquad \ldots.(4.25)$$

These transformation relationships may be represented in the simplified notation

$$u = s_{11}h + s_{12}k + s_{13}l$$

$$v = s_{21}h + s_{22}k + s_{23}l$$

$$w = s_{31}h + s_{32}k + s_{33}l \qquad \ldots.(4.26)$$

where $s_{11} = \vec{a}^*.\vec{a}^* = |\vec{a}^*|^2$

$$= \left(\frac{bc \sin\alpha}{V}\right)^2 \quad \text{from Equation (4.3)}$$

$$= b^2c^2 \sin^2\alpha V^{-2}$$

Similarly $s_{22} = a^2c^2 \sin^2\beta V^{-2}$

$s_{33} = a^2b^2 \sin^2\gamma V^{-2}$

and $s_{12} = s_{21} = \vec{a}^*.\vec{b}^*$

$$= |\vec{a}^*||\vec{b}^*|\cos\gamma^*$$

$$= \frac{bc \sin\alpha \, ac \sin\beta(\cos\alpha\cos\beta - \cos\gamma)}{V^2 \sin\alpha\sin\beta}$$

$$= abc^2(\cos\alpha \cos\beta - \cos\gamma)V^{-2}$$

Similarly $s_{23} = s_{32} = a^2bc(\cos\beta \cos\gamma - \cos\alpha)V^{-2}$

$s_{13} = s_{31} = ab^2c(\cos\gamma \cos\alpha - \cos\beta)V^{-2}$ ....(4.27)

By transformation of two reciprocal vectors $\vec{g}_1$ and $\vec{g}_2$ into direct lattice components using (4.26) and (4.27) the interplanar angle ϕ'_{12} can also be determined from Equation (4.20).

The flow diagram shown in Figure 4.6 describes the manner by which program ANGLE utilises these relationships to determine the angles between zone axes and crystal planes. Angles are calculated individually using a minicomputer in an interactive mode. The indices of the zone axis or plane are typed into the minicomputer on command from the program on a visual display unit. The constant IPLAN indicates to the program whether the indices of the two vectors are related to the direct lattice or to the reciprocal lattice, so that all reciprocal lattice vectors can

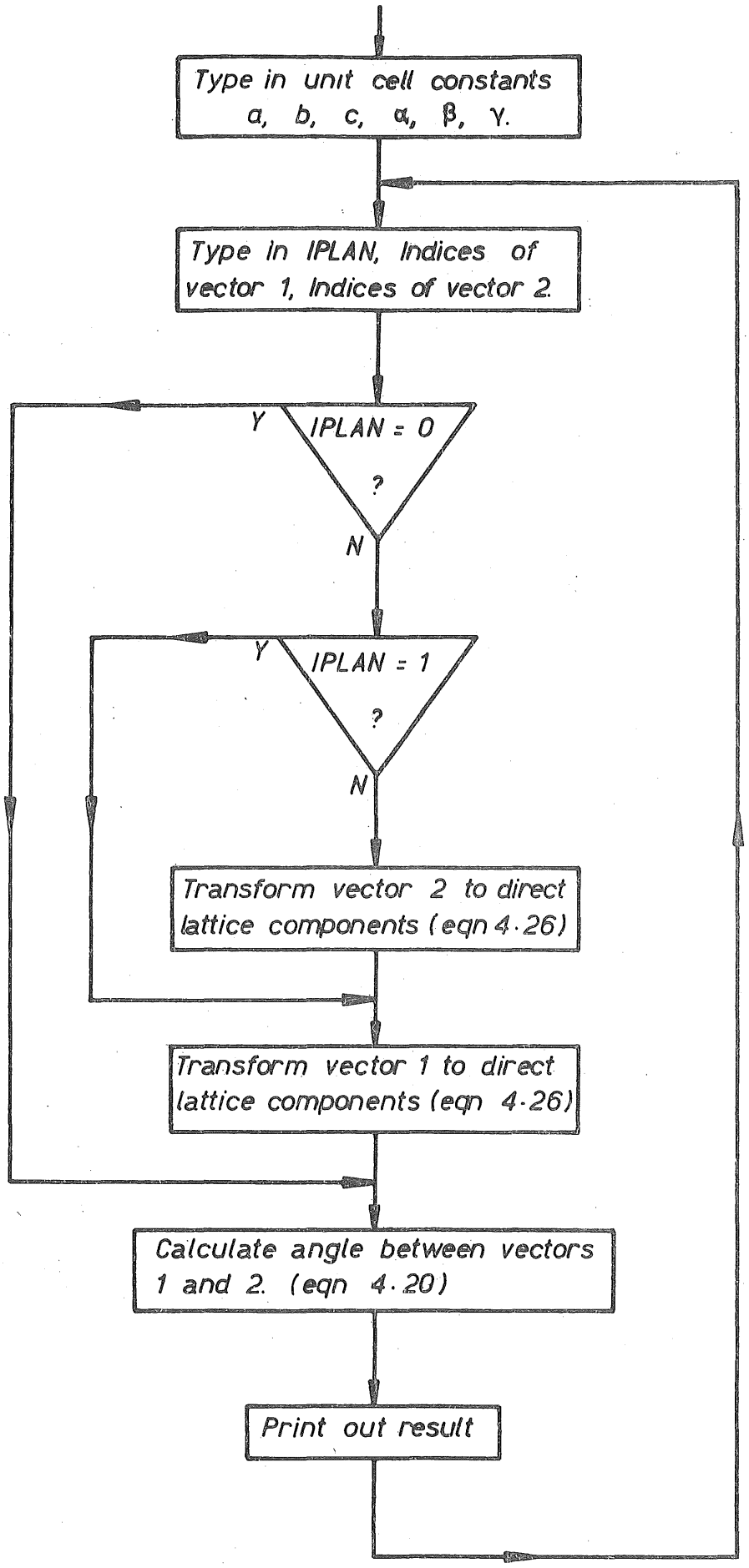

Fig. 4.6 Flow Diagram of program ANGLE

be transformed into the direct lattice basis before the angle is calculated. A complete listing of ANGLE, together with a sample of output, is included in Appendix 2.

4.4 PROGRAM DSPACING

Program DSPACING was developed from XIDENT for the production of formatted lists of crystal d-spacings to assist the identification of diffracting phases from ring type patterns. The addition of a subroutine LSPOTS, which calculates and compares the angles between reciprocal vectors, has extended application of the program to assist with the indexing of diffraction spots which are related to higher order Laue zones than the primary zone of a pattern.

Reference to the outline flow diagram of DSPACING in Figure 4.7 and the FORTRAN listing in Appendix 3, shows that the sections of the program which produce lists of d-spacings are an almost direct transcription of the equivalent sections of program XIDENT, described in Sections 4.2.1 and 4.2.2, with the addition of sorting and formatting routines (subroutines SORT and OUTPUT). The nature of the output from this portion of the program is shown in Figure 4.8 which is a list of d-spacings for the structural rhombohedral cell for αFe_2O_3.

Additional spots which are not directly related to the primary diffracting zone frequently arise in spot patterns. The presence of such spots may be attributed to a number of factors, including:

(a) curvature of the specimen;

(b) misaligned fragments of crystal; and

(c) the intersection of one or more reciprocal lattice planes with the sphere of reflection in addition to the plane giving rise to the primary pattern. These planes are either parallel to the plane giving the primary pattern or are inclined at a slight angle to it.

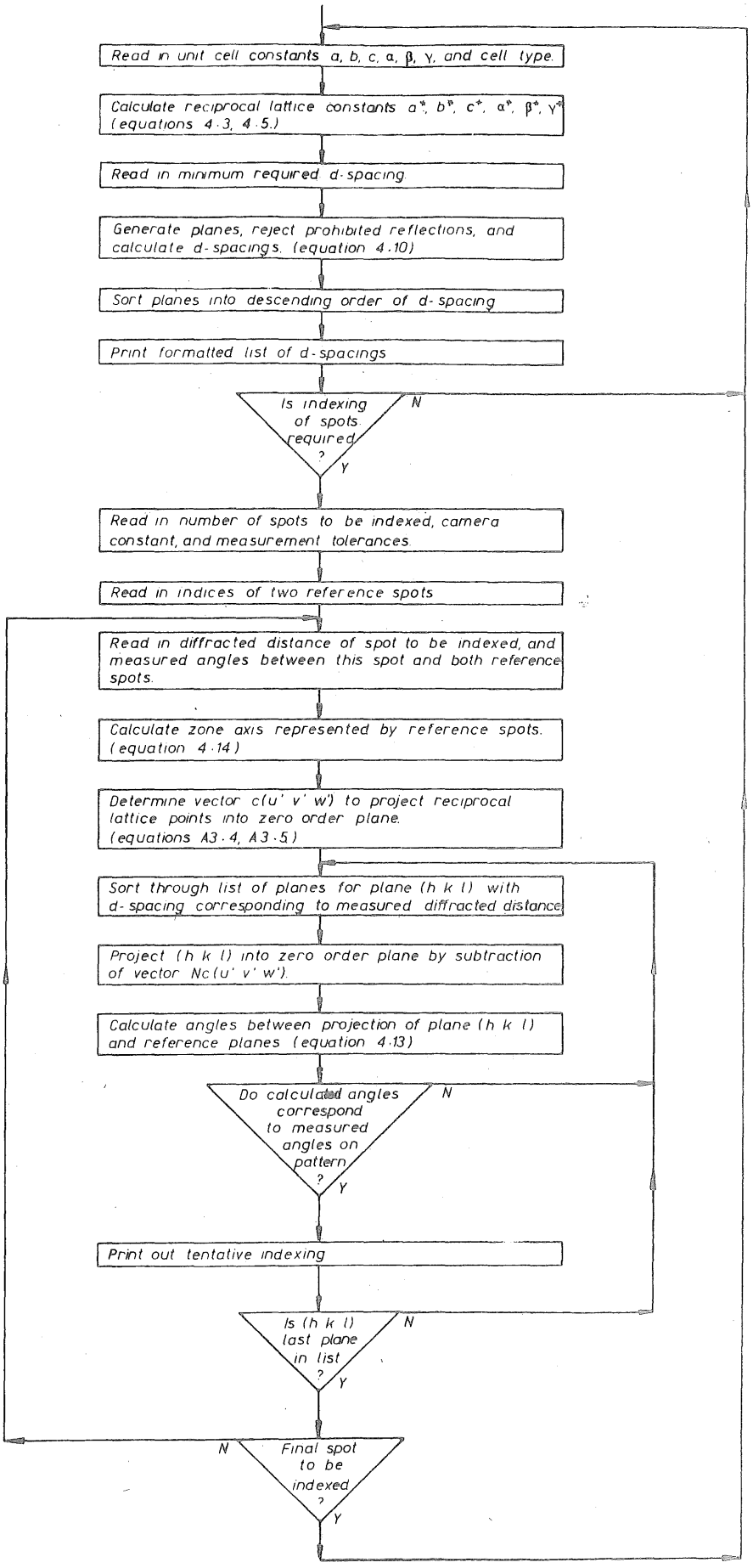

Fig. 4.7 Outline flow diagram of program DSPACING.

ALPHA FE2O3 STRUCTURAL RHOMBOHEDRAL

REAL CELL CONSTANTS

A	B	C	ALPHA	BETA	GAMMA
5.427	5.427	5.427	55.260	55.260	55.260

MINIMUM DSPACE DESIRED = 1.000 ANGSTROMS

LIST OF D SPACINGS (UNIT = ANGSTROMS)

SHEET 1 OF 2 SHEETS

H	K	L	DSPACE
-1	-1	-1	4.583
1	1	1	
0	0	1	4.155
0	0	-1	
0	1	0	
1	0	0	
0	-1	0	
1	0	0	
-1	1	0	3.682
0	-1	-1	
-1	1	0	
1	0	1	
-1	0	-1	
0	1	1	
-1	1	-2	2.699
1	1	2	
-2	-1	-1	
2	-1	1	
-1	-2	1	
1	2	1	
-1	0	1	2.517
-1	1	0	
1	-1	0	
0	1	1	
0	-1	-1	
1	0	-1	
-1	-2	-2	2.326
1	2	2	
-2	-1	-2	
2	-1	2	
-2	-2	-1	
2	2	1	
2	2	2	2.292
-2	-2	-2	
-2	-1	0	2.206
2	0	1	
0	1	2	
0	-2	1	
-1	2	0	
1	-2	-2	
0	-2	-1	
0	-1	-2	
2	1	0	
-1	-2	0	
-2	0	-1	
1	0	2	
1	-1	-1	2.153
-1	1	-1	
1	-1	1	
1	-1	-1	

H	K	L	DSPACE
1	-1	1	2.153
-1	1	-1	
0	-2	0	2.078
0	0	2	
0	2	0	
0	0	-2	
2	0	0	
-2	0	0	
0	-2	-2	1.841
0	2	2	
-2	0	-2	
2	0	2	
2	2	0	
-2	-2	0	
2	2	3	1.791
-2	-2	-3	
2	3	2	
3	2	2	
-3	-2	-2	
-2	-3	-2	
-1	-3	-1	1.708
-1	-1	-1	
1	3	1	
1	1	3	
-1	-1	-3	
3	1	1	
1	2	3	1.694
1	3	2	
3	1	2	
-2	-1	-3	
-2	-3	-1	
2	3	1	
-1	-2	-3	
3	2	1	
-2	-1	-2	1.636
0	0	-2	
0	-2	1	
-2	0	1	
0	2	-1	
1	-2	0	
-1	2	0	
1	0	-2	
2	-1	0	
0	-1	2	
-1	0	2	
2	0	-1	

H	K	L	DSPACE
2	1	-1	1.602
-1	-1	2	
2	-1	1	
-2	1	-1	
-2	-1	1	
1	-2	1	
-1	1	2	
1	1	-2	
-1	-1	-2	
1	-2	-1	
-1	2	1	
-3	-2	-3	1.599
3	3	2	
-2	-3	-3	
2	3	3	
3	2	3	
3	3	3	1.528
-3	-3	-3	
0	-3	-1	1.486
-1	3	0	
0	-1	-3	
0	1	3	
-1	0	-3	
3	1	0	
1	0	3	
3	0	1	
-3	0	-1	
-3	-1	0	
0	3	-1	
-1	-3	0	
-3	-3	-1	1.459
-1	-3	-3	
3	1	3	
-1	-3	3	
-3	-1	-3	
-3	-2	-1	1.453
-1	-2	-1	
2	-1	-1	
1	-1	2	
-2	1	-2	
-1	-1	2	
3	2	0	1.413
2	3	0	
-3	-2	0	
-2	0	-3	
2	0	3	
0	-3	-2	

H	K	L	DSPACE
-2	-3	0	1.413
3	0	2	
0	3	2	
-3	0	-2	
0	-2	-3	
0	2	3	1.385
0	0	3	
2	-1	2	
3	0	0	
2	2	-1	
0	-3	0	
1	-2	-2	
-1	2	2	
-2	1	-2	
0	0	-3	
-2	-2	1	
-3	0	0	
0	3	0	
-2	-2	-4	1.350
4	2	2	
-2	-4	-2	
2	2	4	
2	4	2	
4	-2	-2	
-3	-4	-3	1.311
4	-3	-3	
4	3	3	
3	3	4	
-3	-3	-4	
3	4	3	
3	2	4	1.306
-3	-4	-2	
4	3	2	
-4	-3	-2	
2	4	-3	
-2	3	4	
-3	-4	-4	
3	4	2	
-2	-3	-4	
-4	-2	-3	
2	4	3	1.262
4	1	2	
-2	-1	-4	
1	4	-2	
-2	-4	-1	
2	1	4	
1	4	2	
-4	-1	-2	
-4	-2	-1	

Fig. 4.8 Typical output from program DSPACING.
List continued on next page.

ALPHA FE2O3 STRUCTURAL RHOMBOHEDRAL

LIST OF D SPACINGS (UNIT = ANGSTROMS)

SHEET 2 OF 2 SHEETS

H	K	L	DSPACE
1	2	4	1.262
-1	-2	-4	
4	2	1	
2	4	1	
2	0	-2	1.258
-2	2	0	
0	2	-2	
2	-2	0	
0	-2	2	
-2	0	2	
3	3	0	1.227
0	-3	-3	
-1	-1	-4	
-4	-1	-1	
1	1	4	
-3	0	-3	
0	3	3	
-1	-4	-1	
3	0	3	
1	4	1	
4	1	1	
-3	-3	0	
1	3	-1	1.214
-3	1	-1	
1	-1	-3	
-1	1	3	
-3	-1	1	
3	1	-1	
3	-1	1	
-1	3	1	
1	-3	-1	
1	-1	3	
-1	1	-3	
-1	-3	1	
2	-2	-1	1.204
1	2	-2	
2	-1	-2	
2	-2	1	
2	1	-2	
-2	-1	2	
1	-2	2	
-1	2	-2	
-2	2	1	
-2	2	-1	
-1	-2	2	
-2	1	2	
4	3	4	1.202
-3	-4	-4	
-4	-3	-4	
3	4	4	

H	K	L	DSPACE
-4	-4	-3	1.202
4	4	3	
-1	3	0	1.191
1	0	-3	
0	-1	3	
-3	1	0	
3	0	-1	
-3	0	1	
3	-1	0	
0	3	-1	
0	-3	1	
0	1	-3	
-1	0	3	
1	-3	0	
-4	-1	-3	1.189
-3	-4	-1	
1	3	4	
-1	-4	3	
-3	-1	-4	
-4	-3	-1	
1	4	3	
4	3	1	
3	1	4	
3	4	1	
4	1	3	
-1	-3	-4	
2	4	4	1.163
-4	-4	-2	
4	2	4	
4	4	2	
-4	-2	-4	
-2	-4	-4	
4	4	4	1.146
-4	-4	-4	
-3	1	-2	1.141
1	-3	-2	
-3	-2	1	
-1	2	3	
3	-1	2	
2	-1	3	
3	2	-1	
1	-2	-3	
-2	-3	1	
2	3	-1	
-1	3	2	
-2	1	-3	
0	1	4	1.107
1	0	4	
-4	0	-1	
4	1	0	

H	K	L	DSPACE
-1	0	-4	1.107
0	-4	-1	
-4	-1	0	
1	4	0	
4	0	1	
-1	-4	0	
0	4	1	
0	-1	-4	
0	4	2	1.103
4	0	2	
4	2	0	
2	4	0	
2	0	4	
-2	0	-4	
-4	0	-2	
0	-4	-2	
-2	-4	0	
0	2	4	
-4	-2	0	
0	-2	-4	
1	1	-3	1.086
-1	3	-1	
-1	-1	3	
3	-1	-1	
1	-3	1	
-3	1	1	
2	-2	-2	1.076
-2	2	2	
-2	2	-2	
2	2	-2	
2	-2	2	
-2	-2	2	
-4	-1	-4	1.053
-4	-4	-1	
4	1	4	
4	4	1	
-1	-4	-4	
1	4	4	
0	-4	0	1.039
0	0	4	
4	0	0	
-4	0	0	
0	4	0	
0	0	-4	
3	4	0	1.030
-3	0	-4	
0	4	3	
-3	-4	0	
-4	-3	0	
3	0	4	

H	K	L	DSPACE
0	-4	-3	1.030
0	3	4	
4	0	3	
4	3	0	
0	-3	-4	
-4	0	-3	
1	-3	-3	1.013
-3	1	-3	
-1	3	3	
3	-1	3	
-3	-3	1	
3	3	-1	

Fig. 4.8 continued.

It is often important to be able to distinguish which of these factors is active in producing the extra spots, especially to determine whether or not the pattern can be interpreted as arising from a single crystal fragment; and to do so requires an attempt to index the spots in relation to the primary or central diffraction network.

4.4.1 Indexing of Spots in Laue Zones

The effect of curvature of the sphere of reflection is discussed by Hirsch *et al*[122] and by Andrews *et al*[123] and is illustrated in Figure 4.9. At 100 kV the radius of this sphere is sufficiently small to intersect a number of reciprocal lattice planes within the region which may be recorded on a selected area diffraction pattern, and a circular band of spots, known as a Laue zone, is formed on the pattern for each such intersection. The zero order Laue zone corresponds to the (uvw) reciprocal lattice plane which passes through the origin, all spots in this zone satisfying the relation

$$hu + kv + lw = 0 \qquad \ldots.(4.28)$$

The higher order zones of spots arise from (uvw) reciprocal lattice planes displaced from the origin, the Nth parallel plane from the origin consisting of (hkl) lattice points such that

$$hu + kv + lw = \pm N \qquad \ldots.(4.29)$$

Although the spots within each zone are arranged in identical networks, the higher order zones may consist of very narrow bands so that this order may not be evident on inspection of the diffraction pattern. For this reason the computer technique described was developed to relate the spots from non-zero order Laue zones to the indexed pattern of the zero order zone.

The flow diagram of Figure 4.7 shows the method by which this indexing is accomplished. The central or zero order diffraction pattern is initially indexed using program XIDENT, and two spots, shown as

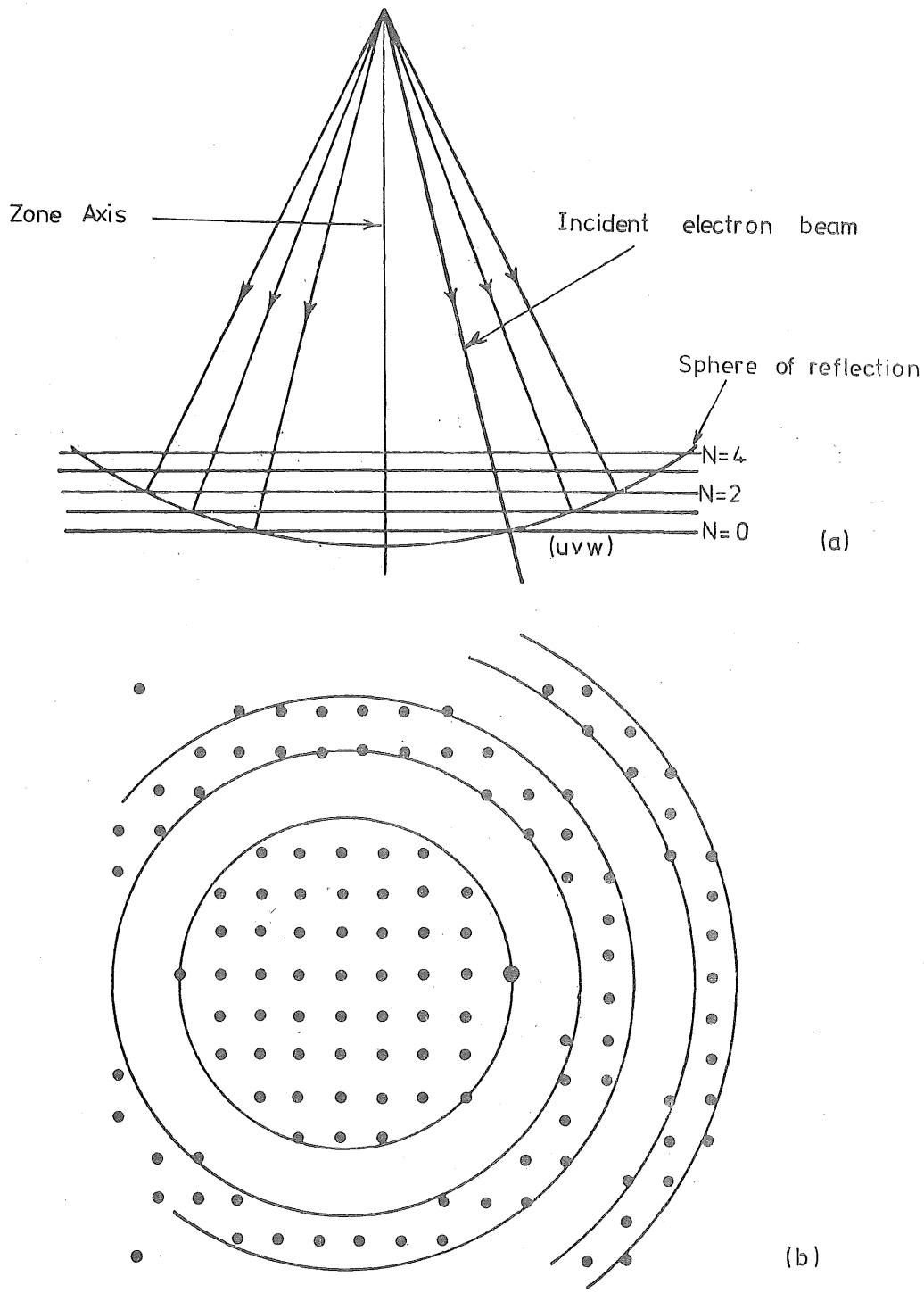

Fig. 4.9 The effect of curvature of the sphere of reflection.

(a) Intersection between sphere of reflection and reciprocal lattice planes.

(b) Corresponding diffraction pattern exhibiting Laue zones.

$(h_1k_1l_1)$ and $(h_2k_2l_2)$ in Figure 4.10 are chosen as reference spots to which higher order zones may be related. The indices of these two spots are input to subroutine LSPOTS and the (uvw) reciprocal lattice plane represented by the central pattern is determined from Equation 4.14.

The measured position of a diffraction spot S to be indexed is then input, the position being defined by the diffracted distance D and the two measured angles ψ_1 and ψ_2 between S and the two reference spots. A search of the previously generated list of crystal d-spacings is then made for (hkl) planes with d-spacings corresponding to the diffracted distance for spot S, within the desired tolerance. Each such plane is tested in relation 4.29, and all planes producing values of N greater than 12 are rejected. The reciprocal lattice vector $\vec{g}_{hkl}$, corresponding to the plane (hkl), is then projected into the zero order plane by the technique described in Section 4.4.2, and the angles between the projected reciprocal vector and $\vec{g}_{h_1k_1l_1}$ and $\vec{g}_{h_2k_2l_2}$ are calculated from Equation 4.13. If the two calculated angles correspond to the two measured angles ψ_1 and ψ_2, within the desired tolerance, a possible indexing of spot S is recognised and the solution is printed out. Up to 50 spots may be indexed in this way during any single application of the program.

4.4.2 Projection of Reciprocal Vectors into the Zero Order Plane

The simultaneous intersection of the zero order reciprocal lattice plane and the Nth order plane with the sphere of reflection results in superimposed diffraction patterns from both planes. However, the angular relationships measured from the diffraction pattern represent the angles between the projections of the spots in the zero order plane rather than the true angles between the reciprocal vectors for the corresponding crystal planes. In order to calculate the angles on the pattern the N-plane must be projected into the zero order plane by addition of a vector, representing the separation of these two planes,

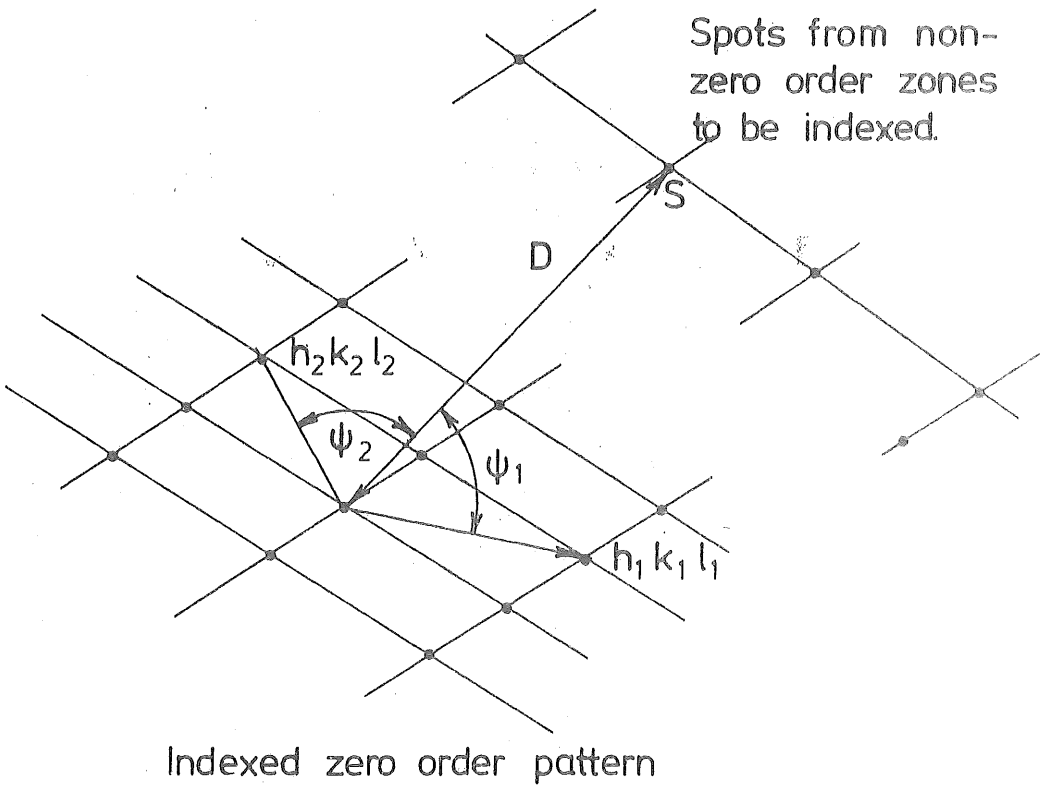

Fig. 4.10 Indexing of spots in Laue zones.

to each position vector defining a reciprocal lattice point in the N-plane. This projection should be performed along the direction of the particular diffracted beam for each spot, but the error resulting from projection along a direction perpendicular to the (uvw) plane can normally be neglected and the use of this method is justified by its simplicity. Hirsh *et al* describe this projection technique for cubic crystals where the crystal lattice and reciprocal lattice are parallel, and the procedure has been extended below to enable the more complex case of non-cubic lattices to be handled by subroutines LSPOTS and ZONES of program DSPACING.

From the properties of the reciprocal cell described in Section 4.2.2 it can be demonstrated that the (uvw) reciprocal lattice planes shown in Figure 4.11 are perpendicular to a direct cell vector $\vec{L}_{(uvw)}$ which has components $\vec{ua} + \vec{vb} + \vec{wc}$ and magnitude equal to $\frac{1}{d^*_{uvw}}$, where d^*_{uvw} is the interplanar spacing for the (uvw) reciprocal lattice planes.

Therefore $$d^*_{uvw} = (u^2a^2 + v^2b^2 + w^2c^2)^{-\frac{1}{2}} \quad \ldots.(4.30)$$

The components of $\vec{L}_{(uvw)}$ in the reciprocal lattice $(u'\vec{a}^* + v'\vec{b}^* + w'\vec{c}^*)$ may be obtained from the inverse transformation relationships

$$\begin{aligned} u' &= ua^2 + vab\cos\gamma + wac\cos\beta \\ v' &= uab\cos\gamma + vb^2 + wbc\cos\alpha \\ w' &= uac\cos\gamma + vbc\cos\alpha + wc^2 \end{aligned} \quad \ldots.(4.31)$$

which provide direction coordinates for the reciprocal lattice vector perpendicular to plane (uvw). The [u'v'w'] reciprocal lattice vector will intersect the first order (uvw) plane at point P given by c(u'v'w') when vector $\vec{OP}$ with components $c(u'\vec{a}^* + v'\vec{b}^* + w'\vec{c}^*)$ has a magnitude of d^*_{uvw}, therefore, from Equation 4.30

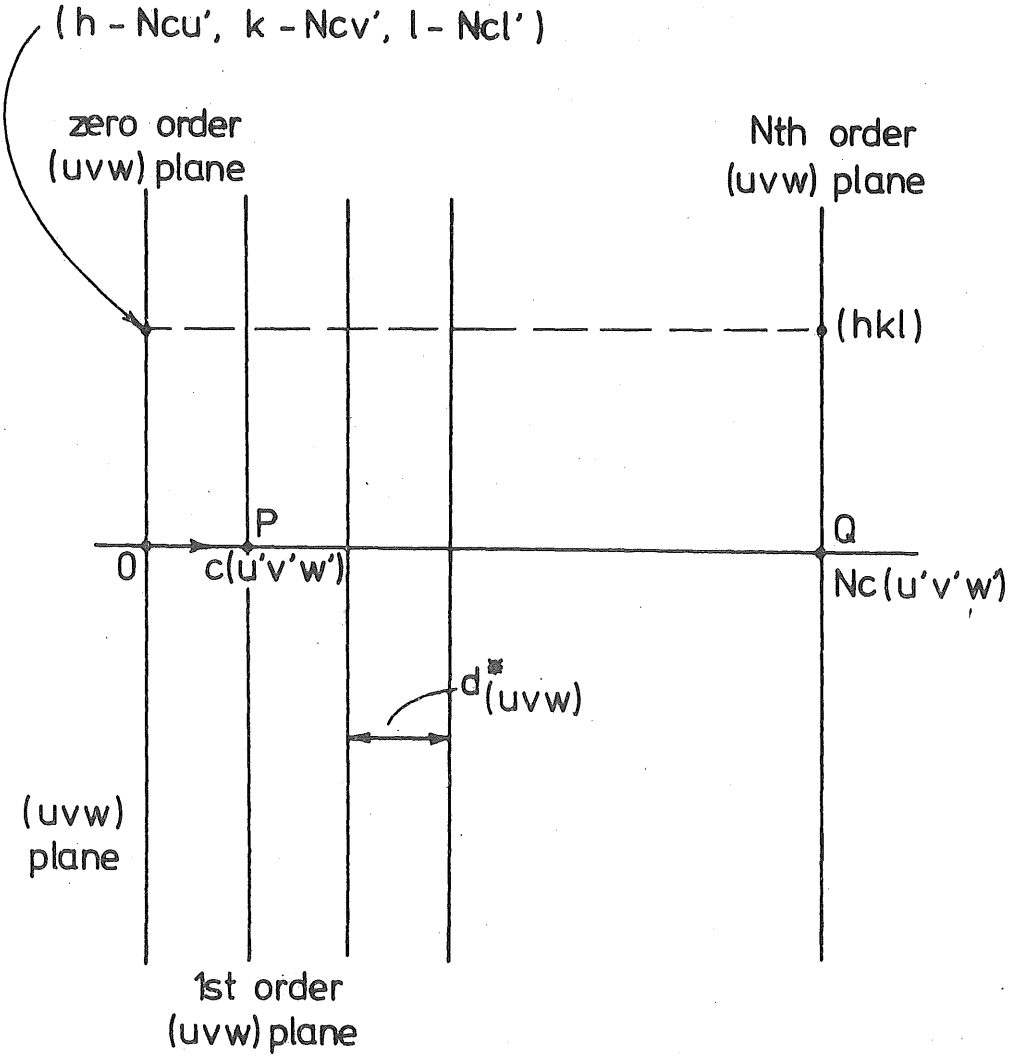

Fig. 4.11 Projection of spots into zero order (uvw) reciprocal lattice plane.

$$c(u'^2a^2 + v'^2b^2 + w'^2c^2)^{\frac{1}{2}} = (u^2a^2 + v^2b^2 + w^2c^2)^{-\frac{1}{2}}$$

$$\text{and} \quad c = (u^2a^2 + v^2b^2 + w^2c^2)^{-\frac{1}{2}} \cdot (u'^2a^2 + v'^2b^2 + w'^2c^2)^{-\frac{1}{2}} \quad \ldots.(4.32)$$

Hence, the projection of any point in the Nth order (uvw) plane into the zero order plane, along a direction perpendicular to these planes, may be performed by subtraction of a vector $\vec{OQ}$ which has components $Nc(u'\vec{a}^* + v'\vec{b}^* + w'\vec{c}^*)$. Thus the point (hkl) projects into the position (h - Ncu', k - Ncv', l - ncw'), and the angles between the reciprocal vector $\vec{g}_{(h - Ncu', k - Ncv', l - Ncw')}$ and $\vec{g}_{(h_1k_1l_1)}$ and $\vec{g}_{(h_2k_2l_2)}$ may be calculated from Equation 4.13 for comparison with the measured angles ψ_1 and ψ_2 from the diffraction pattern.

4.4.3 Application of Program DSPACING

The application of DSPACING is demonstrated with reference to Figure 4.12 which represents a diffraction pattern published by Andrews *et al*[123] exhibiting four successive overlapping Laue zones. The pattern arises from an M_6C particle found in low alloy steels, where M represents a fixed total of unspecified metal atoms. Indexing of the pattern may be completed with the assistance of two computer runs. The first run involves the application of XIDENT to the central zone of spots, and the output is shown in Figure 4.13. The spots labelled A - E in Figure 4.12 were used as input data for this operation. Two of these spots, with indices $(51\bar{1})$ and $(\bar{2}6\bar{2})$ were chosen as reference points for the subsequent indexing of all other spots in the second computer run with program DSPACING, and Figure 4.14 contains the output from DSPACING which corresponds to the first 20 spots which were indexed. These spots are labelled in Figure 4.12.

The discriminating power of the program is evident from the print-out. Sufficient information is provided to enable ready selection of the most likely diffracting planes from low order zones, and manual

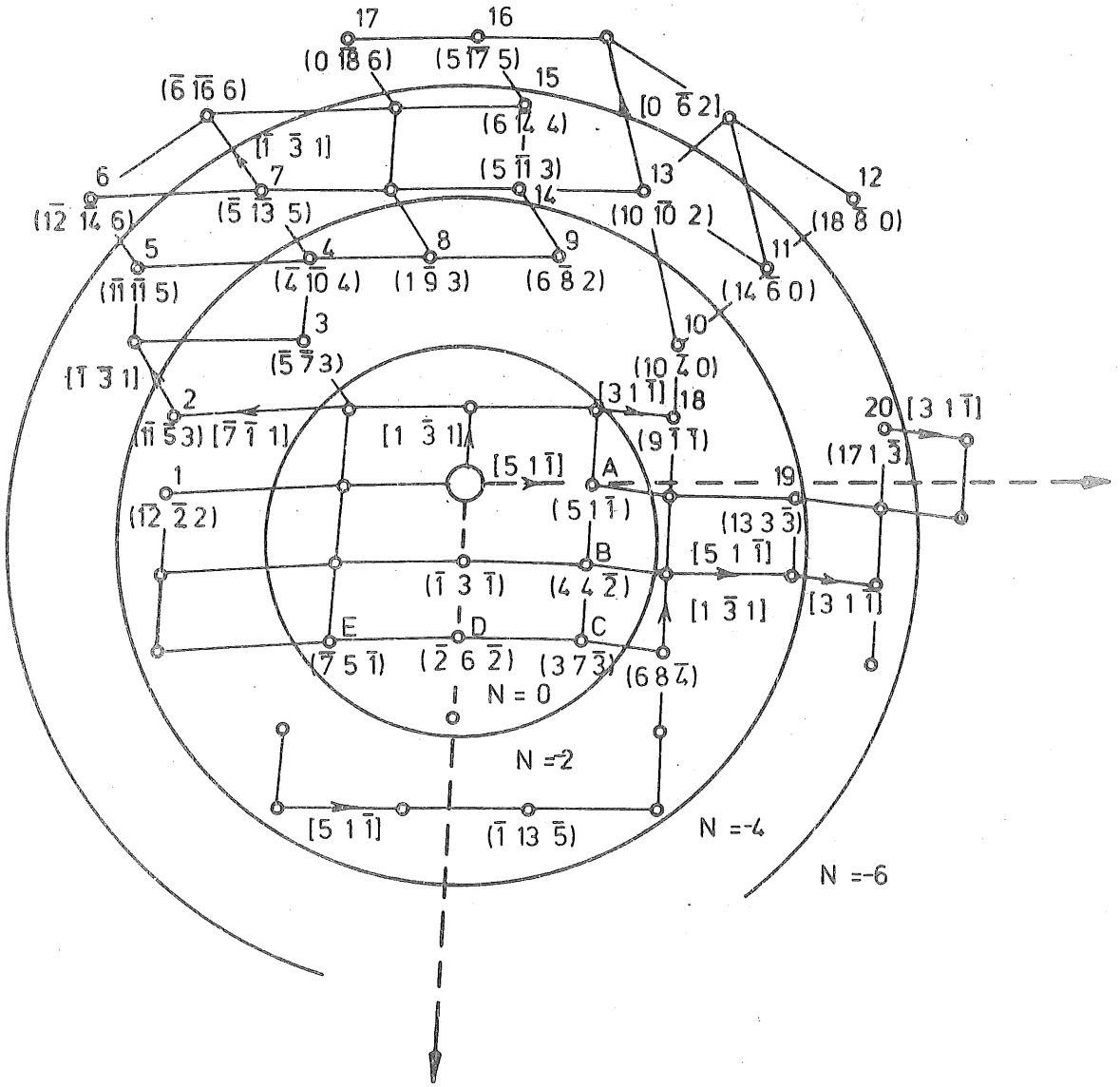

Fig. 4.12 Indexing of diffraction pattern containing four overlapping Laue zones. Spots A - E are input data for indexing of the zero order zone using program XIDENT, and spots 1 - 20 in higher order zones are indexed using program DSPACE. The computer output corresponding to these operations is shown in figures 4.13 and 4.14.

```
PROGRAM CRYSTAL IDENTIFICATION


PLATE 5 ANDREWS DYSON AND KEOWN      (CENTRAL PATTERN)
**********************************************************
**********************************************************
**********************************************************

CAMERA CONSTANT= 71.3000

POSITION TOLERANCE = 1.000 MILLIMETRES  (MINIMUM OVER-RIDING TOLERANCE OF + OR - 5.0 PERCENT OF DIFF. DISTANCE PREVAILS)

DIFFRACTED DISTANCES OF SPOTS ARE

    16.90     19.00     25.80     21.00     28.00   (MILLIMETRES)

ANGLE TOLERANCE =  3.00 DEGREES

MEASURED ANGLES BETWEEN SPOTS ARE

    34.60     54.60     93.90    131.60


M6C CARBIDE (FACE CENTRED CUBIC)(PARAMETERS FROM ANDREWS ET AL P.202)
**********************************************************************

                REAL CELL CONSTANTS

                    A         B         C      ALPHA      BETA     GAMMA

                 11.082    11.082    11.082    90.000    90.000    90.000

                MAXIMUM INDICES ARE  10  10  10

                MAXIMUM DIMENSIONS OF ARRAYS ARE      32    75   212

                PROHIBITED REFLECTIONS FOR THE FACE CENTRED CELL TYPE F HAVE BEEN OMITTED


SET  1    ZONE AXIS (  1  3  8)          (SET  1 HAS 24 SYMMETRICAL EQUIVALENT SOLUTIONS)
******    ************************

                POINT          PLANE          DSPACE          ESTIMATED DSPACE FROM DIFF. PATTERN

                  1          (  5  1 -1)       2.133                  2.096
                  2          (  4  4 -2)       1.847                  1.864
                  3          (  3  7 -3)       1.354                  1.373
                  4          ( -2  6 -2)       1.671                  1.687
                  5          ( -7  5 -1)       1.280                  1.265

                N.B. BEST FIT CAMERA CONSTANT USED IN ABOVE ESTIMATES OF D SPACINGS =  70.834
                                                          (INPUT CAMERA CONSTANT =  71.300)

                MEAN DEVIATION OF MEASURED SPOTS FROM TRUE POSITIONS = 0.326 MILLIMETRES

                ANGLE BETWEEN PLANES 1 & 2 =  33.49  MEASURED  34.60 DEGREES
                ANGLE BETWEEN PLANES 1 & 3 =  54.00  MEASURED  54.60 DEGREES
                ANGLE BETWEEN PLANES 1 & 4 =  93.33  MEASURED  93.90 DEGREES
                ANGLE BETWEEN PLANES 1 & 5 = 130.12  MEASURED 131.60 DEGREES

                SYMMETRICAL EQUIVALENT SOLUTIONS FOR SET  1

                ZONE AXIS          POINT 1          POINT 2          POINT 3          POINT 4          POINT 5

                (  3  8  1)      (  1 -1  5)      (  4 -2  4)      (  7 -3  3)      (  6 -2 -2)      (  5 -1 -7)
                (  8  1  3)      (  1 -5 -1)      (  2 -4 -4)      (  3 -3 -7)      (  2  2 -6)      (  1  7 -5)
                ( -1  8  3)      (  5  1 -1)      (  4  2 -4)      (  3  3 -7)      ( -2  2 -6)      ( -7  1 -5)
                (  3 -1  8)      (  1 -5 -1)      (  4 -4 -2)      (  7 -3 -3)      (  6  2 -2)      (  5  7 -1)
                (  8  3 -1)      (  1 -1  5)      (  2 -4  4)      (  3 -7  3)      (  2 -6 -2)      (  1 -5 -7)
                (  1  8 -3)      (  5 -1 -1)      (  4 -2 -4)      (  3 -3 -7)      ( -2 -2 -6)      ( -7 -1 -5)
                (  8 -3  1)      (  1  1 -5)      (  2  4 -4)      (  3  7 -3)      (  2  6  2)      (  1  5  7)
                ( -3  1  8)      (  1 -5  1)      (  4 -4  2)      (  7 -3  3)      (  6  2  2)      (  5  7  1)
                ( -1 -3  8)      (  5  1  1)      (  4  4  2)      (  3  7  3)      ( -2  6  2)      ( -7  5  1)
                ( -3  8 -1)      (  1  1  5)      (  4  2  4)      (  7  3  3)      (  6  2 -2)      (  5  1 -7)
                (  8 -1 -3)      (  1  5  1)      (  2  4  4)      (  3  3  7)      (  2 -2  6)      (  1 -7  5)
                (  1 -8  3)      (  5  1  1)      (  4  2  4)      (  3  3  7)      ( -2  2  6)      ( -7  1  5)
                ( -8  3  1)      (  1  1  5)      (  2  4  4)      (  3  7  3)      (  2  6 -2)      (  1  5 -7)
                (  3  1 -8)      (  1  5  1)      (  4  4  2)      (  7  3  3)      (  6 -2  2)      (  5 -7  1)
                ( -1  3 -8)      (  5 -1 -1)      (  4 -4 -2)      (  3 -7 -3)      ( -2 -6 -2)      ( -7 -5 -1)
                (  3 -8 -1)      (  1  1 -5)      (  4  2 -4)      (  7  3 -3)      (  6  2  2)      (  5  1  7)
                ( -8 -1  3)      (  1 -5  1)      (  2 -4  4)      (  3 -3  7)      (  2  2  6)      (  1  7  5)
                (  1 -3 -8)      (  5 -1  1)      (  4 -4  2)      (  3 -7  3)      ( -2 -6  2)      ( -7 -5  1)
                ( -3 -8  1)      (  1 -1 -5)      (  4 -2 -4)      (  7 -3 -3)      (  6 -2  2)      (  5 -1  7)
                ( -8  1 -3)      (  1  5 -1)      (  2  4 -4)      (  3  3 -7)      (  2 -2 -6)      (  1 -7 -5)
                ( -1 -8 -3)      (  5 -1  1)      (  4 -2  4)      (  3 -3  7)      ( -2 -2  6)      ( -7 -1  5)
                ( -8 -3 -1)      (  1 -1 -5)      (  2 -4 -4)      (  3 -7 -3)      (  2 -6  2)      (  1 -5  7)
                ( -3 -1 -8)      (  1  5 -1)      (  4  4 -2)      (  7  3 -3)      (  6 -2 -2)      (  5 -7 -1)
```

Fig. 4.13 Output from program XIDENT corresponding to zero order zone of diffraction pattern shown in Figure 4.12.

```
MGC CARBIDE (FACE CENTRED CUBIC)(PARAMETERS FROM ANDREWS ET AL P.202)
**********************************************************************

REAL CELL CONSTANTS

     A        B        C      ALPHA     BETA     GAMMA
  11.082   11.082   11.082   90.000   90.000   90.000

MINIMUM DSPACE DESIRED = 0.500 ANGSTROMS


LOOSE SPOTS FROM PLATE 5 ANDREWS ET AL
**************************************

                CAMERA CONSTANT = 70.590    ANGLE TOLERANCE = 3.00 DEGREES    POSITION TOLERANCE = 1.00 MILLIMETRES
                      (N.B.  MINIMUM OVER-RIDING TOLERANCE OF 0 OR - 5.0 PERCENT OF DIFF. DISTANCE PREVAILS)
                DATUM PLANES ARE          5  1 -1       -2  6 -2
                ZONE REPRESENTED BY DATUM PLANES IS     1  3  8

POINT  1  MEASURED DSPACE  0.880                          MEASURED ANGLES   177.90   85.00
          IDENTIFIED AS PLANE (-12 -2  2)   DSPACE = 0.899    TRUE ANGLES   177.71   84.39   ORDER OF REFLECTION =  -2


POINT  2  MEASURED DSPACE  0.887                          MEASURED ANGLES   166.70  100.20
          IDENTIFIED AS PLANE (-11 -5  3)   DSPACE = 0.890    TRUE ANGLES   166.91   99.76   ORDER OF REFLECTION =  -2


POINT  3  MEASURED DSPACE  1.230                          MEASURED ANGLES   138.00  129.00
          IDENTIFIED AS PLANE ( -5 -7  3)   DSPACE = 1.216    TRUE ANGLES   137.70  128.98   ORDER OF REFLECTION =  -2


POINT  4  MEASURED DSPACE  0.959                          MEASURED ANGLES   125.00  141.90
          IDENTIFIED AS PLANE ( -4-10  4)   DSPACE = 0.965    TRUE ANGLES   124.72  141.95   ORDER OF REFLECTION =  -2


POINT  5  MEASURED DSPACE  0.675                          MEASURED ANGLES   146.90  120.00
          IDENTIFIED AS PLANE (-11-11  5)   DSPACE = 0.678    TRUE ANGLES   146.78  119.89   ORDER OF REFLECTION =  -4
          IDENTIFIED AS PLANE (-11-11  7)   DSPACE = 0.650    TRUE ANGLES   145.72  120.95   ORDER OF REFLECTION =  12


POINT  6  MEASURED DSPACE  0.560                          MEASURED ANGLES   143.00  124.00
          IDENTIFIED AS PLANE (-12-14  6)   DSPACE = 0.572    TRUE ANGLES   142.61  124.07   ORDER OF REFLECTION =  -6
          IDENTIFIED AS PLANE (-12-14  8)   DSPACE = 0.551    TRUE ANGLES   141.85  124.82   ORDER OF REFLECTION =  10


POINT  7  MEASURED DSPACE  0.737                          MEASURED ANGLES   125.00  142.00
          IDENTIFIED AS PLANE ( -5-13  5)   DSPACE = 0.749    TRUE ANGLES   124.02  142.65   ORDER OF REFLECTION =  -4
          IDENTIFIED AS PLANE ( -5-13  7)   DSPACE = 0.711    TRUE ANGLES   123.90  142.77   ORDER OF REFLECTION =  12


POINT  8  MEASURED DSPACE  1.169                          MEASURED ANGLES    98.50  168.20
          IDENTIFIED AS PLANE (  1 -9  3)   DSPACE = 1.162    TRUE ANGLES    98.12  168.55   ORDER OF REFLECTION =  -2


POINT  9  MEASURED DSPACE  1.089                          MEASURED ANGLES    67.50  160.50
          IDENTIFIED AS PLANE (  6 -8  2)   DSPACE = 1.087    TRUE ANGLES    67.82  161.15   ORDER OF REFLECTION =  -2


POINT 10  MEASURED DSPACE  1.014                          MEASURED ANGLES    33.00  127.00
          IDENTIFIED AS PLANE ( 10 -4  0)   DSPACE = 1.039    TRUE ANGLES    34.70  128.03   ORDER OF REFLECTION =  -2
```

Fig. 4.14 Output from program DSPACING corresponding to spots from Laue zones in Figure 4.12

(continued on next page)

```
POINT 11  MEASURED DSPACE  0.716                    MEASURED ANGLES    36.10   129.10
          IDENTIFIED AS PLANE ( 14 -6  0)  DSPACE = 0.728   TRUE ANGLES    36.00   129.33   ORDER OF REFLECTION =  -6
          IDENTIFIED AS PLANE ( 14 -6  2)  DSPACE = 0.721   TRUE ANGLES    38.75   132.07   ORDER OF REFLECTION =  12

POINT 12  MEASURED DSPACE  0.551                    MEASURED ANGLES    36.70   129.60
          IDENTIFIED AS PLANE ( 18 -8  0)  DSPACE = 0.563   TRUE ANGLES    36.71   130.04   ORDER OF REFLECTION =  -6
          IDENTIFIED AS PLANE ( 11 -5  2)  DSPACE = 0.560   TRUE ANGLES    38.83   132.16   ORDER OF REFLECTION =  10
          IDENTIFIED AS PLANE ( 19 -7  1)  DSPACE = 0.547   TRUE ANGLES    34.27   127.60   ORDER OF REFLECTION =   6
          IDENTIFIED AS PLANE ( 19 -9  1)  DSPACE = 0.527   TRUE ANGLES    38.99   132.32   ORDER OF REFLECTION =   0

POINT 13  MEASURED DSPACE  0.769                    MEASURED ANGLES    59.10   152.10
          IDENTIFIED AS PLANE ( 10-10  2)  DSPACE = 0.776   TRUE ANGLES    59.18   152.51   ORDER OF REFLECTION =  -6
          IDENTIFIED AS PLANE ( 10-10  4)  DSPACE = 0.754   TRUE ANGLES    61.74   155.06   ORDER OF REFLECTION =  12

POINT 14  MEASURED DSPACE  0.891                    MEASURED ANGLES    80.10   173.00
          IDENTIFIED AS PLANE (  5-11  3)  DSPACE = 0.890   TRUE ANGLES    80.20   173.53   ORDER OF REFLECTION =  -6

POINT 15  MEASURED DSPACE  0.695                    MEASURED ANGLES    81.50   174.50
          IDENTIFIED AS PLANE (  6-14  4)  DSPACE = 0.704   TRUE ANGLES    81.56   174.89   ORDER OF REFLECTION =  -6
          IDENTIFIED AS PLANE (  6-14  6)  DSPACE = 0.677   TRUE ANGLES    83.22   176.55   ORDER OF REFLECTION =  12

POINT 16  MEASURED DSPACE  0.596                    MEASURED ANGLES    88.70   178.20
          IDENTIFIED AS PLANE (  5-17  5)  DSPACE = 0.602   TRUE ANGLES    88.20   178.47   ORDER OF REFLECTION =  -6
          IDENTIFIED AS PLANE (  5-17  7)  DSPACE = 0.582   TRUE ANGLES    89.42   177.25   ORDER OF REFLECTION =  10

POINT 17  MEASURED DSPACE  0.579                    MEASURED ANGLES   104.80   162.00
          IDENTIFIED AS PLANE ( -1-17  7)  DSPACE = 0.602   TRUE ANGLES   107.65   159.02   ORDER OF REFLECTION =   4
          IDENTIFIED AS PLANE (  0-18  6)  DSPACE = 0.584   TRUE ANGLES   104.10   162.57   ORDER OF REFLECTION =  -6
          IDENTIFIED AS PLANE (  0-18  8)  DSPACE = 0.563   TRUE ANGLES   104.74   161.93   ORDER OF REFLECTION =  10
          IDENTIFIED AS PLANE ( -1-19  7)  DSPACE = 0.547   TRUE ANGLES   107.12   159.56   ORDER OF REFLECTION =  -2

POINT 18  MEASURED DSPACE  1.217                    MEASURED ANGLES    17.70   110.50
          IDENTIFIED AS PLANE (  9 -1 -1)  DSPACE = 1.216   TRUE ANGLES    18.03   111.36   ORDER OF REFLECTION =  -2

POINT 19  MEASURED DSPACE  0.802                    MEASURED ANGLES     2.20    90.60
          IDENTIFIED AS PLANE ( 13  3 -3)  DSPACE = 0.810   TRUE ANGLES     2.06    91.26   ORDER OF REFLECTION =  -2

POINT 20  MEASURED DSPACE  0.626                    MEASURED ANGLES     7.80   100.60
          IDENTIFIED AS PLANE ( 17  1 -1)  DSPACE = 0.650   TRUE ANGLES    10.00   103.33   ORDER OF REFLECTION =  12
          IDENTIFIED AS PLANE ( 17  1 -3)  DSPACE = 0.641   TRUE ANGLES     7.74   101.06   ORDER OF REFLECTION =  -6
          IDENTIFIED AS PLANE ( 18  2 -2)  DSPACE = 0.608   TRUE ANGLES     6.21    99.54   ORDER OF REFLECTION =   8
```

Fig. 4.14 continued.

checking of the inter-relationships between adjacent spots and adjacent zones is minimal. The lack of identification of a diffracting spot by this technique, when the zero order zone has been positively identified, provides evidence that the diffraction pattern cannot be interpreted as arising from a single crystal fragment.

CHAPTER 5

PARTICULATE OXIDE FORMATION ON IRON

5.1 TYPES OF FILAMENTARY GROWTH OBSERVED

Filamentary crystals are observed to grow on iron surfaces following oxidation at temperatures between 300°C and 800°C, but the nature of the filamentary particles is shown in Fig. 5.1 to be critically dependent on the oxidising temperature. This figure contains transmission electron micrographs, obtained by the silhouette technique, from the edges of iron specimens after oxidation for three hours in air at temperature intervals of 50°C over the range for which filamentary growth is observed. No filamentary crystals were observed at 250°C or 900°C.

High purity (99.99%) electron beam melted iron strip, supplied by Metals Research Corporation to MARZ grade, was used for all experiments. The specimens shown in Figure 5.1 were cut from a single strip of material which was cold-rolled to a thickness of 0.1 mm, annealed in air at approximately 700°C, descaled in warm 10% H_2SO_4, and washed in ethyl alcohol prior to oxidation. Other specimens have shown that the form of the oxide filaments does not appear to be significantly affected by the method of surface preparation, similar particles being observed at any given temperature on electropolished, mechanically-polished, as rolled, or annealed surfaces. These observations are in agreement with those of Talbot and Bigot[39] who showed that the length and density of filaments formed at 400°C were identical for cold worked and recrystallised iron. The purity of the iron was found to have more effect than the crystal form.

Two fundamentally different growth morphologies are observed in Figure 5.1. At lower temperatures, from 300°C to 500°C, the oxide crystals form as blade-shaped platelets which taper towards the tip. These platelets

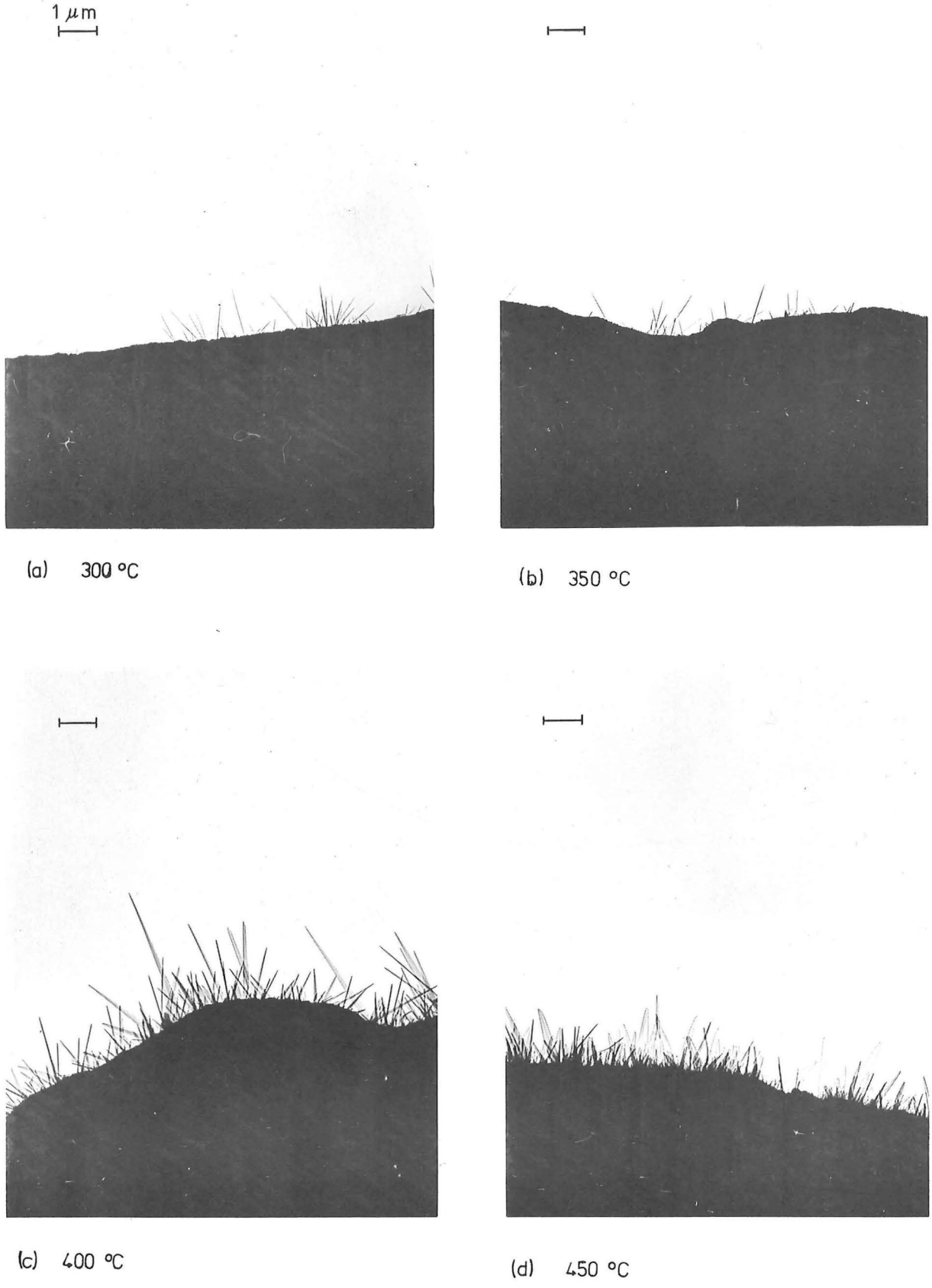

Fig. 5.1 Filamentary oxide growth on iron surfaces after 3 hours in air at atmospheric pressure at temperatures ranging from 300°C to 850°C.

(Continued on next page)

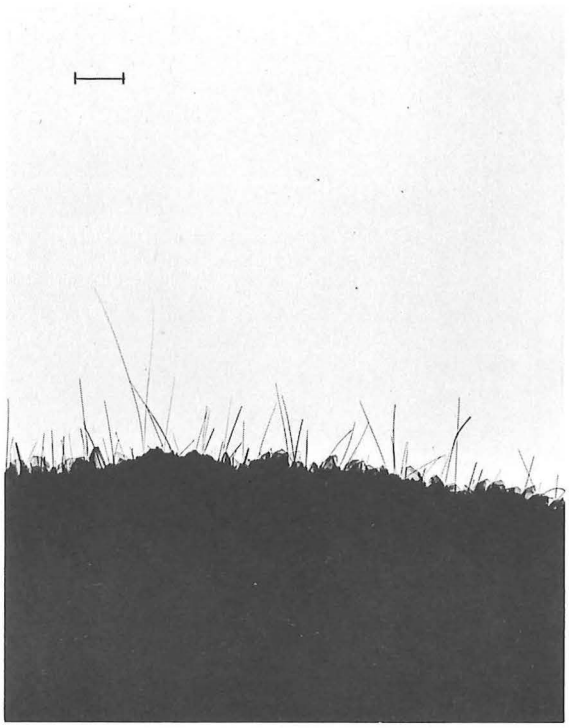

(e) 500 °C

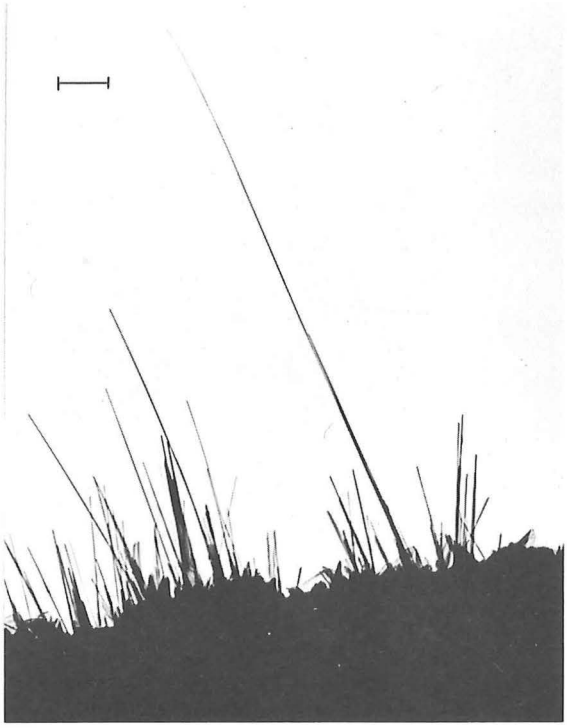

(f) 550 °C

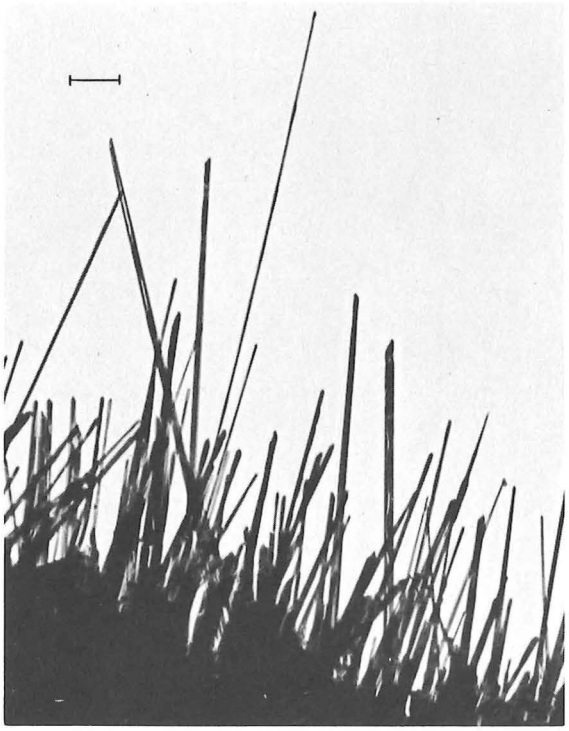

(g) 600° C

(h) 650° C

Fig. 5.1 Continued

(Continued on next page)

(i) 700 °C

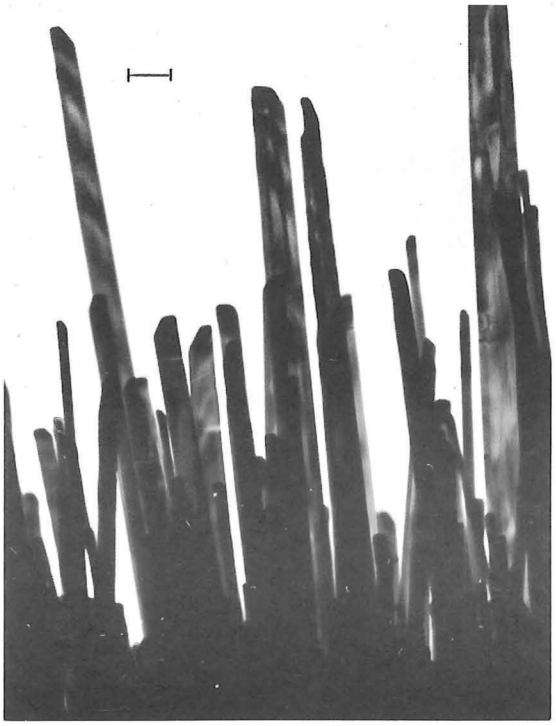

(j) 750 °C

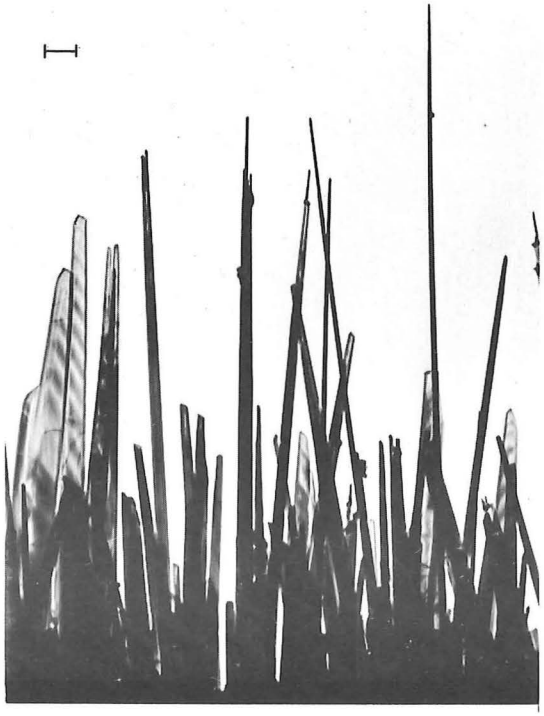

(k) 800° C

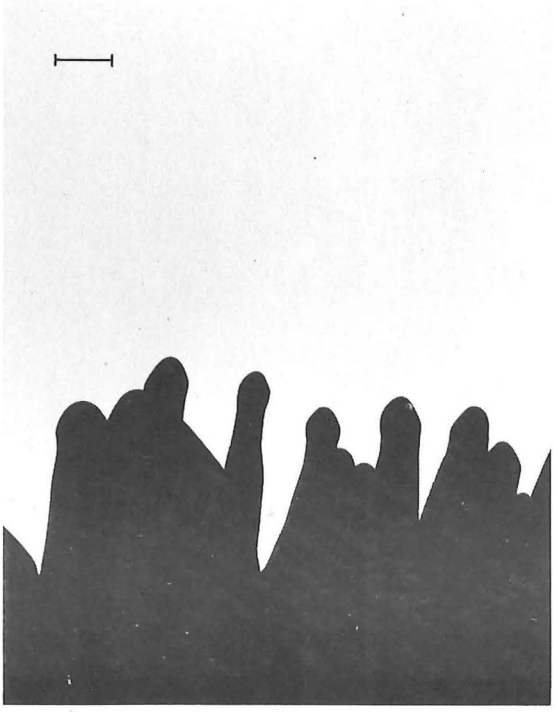

(l) 850 °C

Fig. 5.1 Continued

are transparent to electrons and appear of thin and uniform cross-section. Above 470°C a second crystal form becomes apparent. Whisker-like particles of constant cross-section become the predominant growth form, these particles broadening and assuming ribbon profiles of much larger size as the temperature is further increased. Although these crystals display a variety of different features under different oxidising conditions, all crystals of this type with relatively constant cross-section from base to tip will be referred to as "whiskers" to distinguish them from the "platelets" formed at lower temperature.

5.1.1 Platelets

Figure 5.1 shows that the ratio of platelet length to width at the base is relatively constant at any one temperature; but this ratio decreases with increasing temperature from approximately 50:1 at 300°C to 1:1 at 550°C. A maximum length is reached at approximately 400°C and the platelets become broader and decrease in length as the temperature increases above this point. They can no longer be observed at 600°C although their existence may be obscured by the profusion of whiskers at this temperature.

Accurate measurement of the filament length is difficult as the base region is obscured by localised surface roughness so that only the outer portions of the longer platelets are normally observed by the silhouette technique. The orientation of the particles to the electron beam is also not known. Measurements on 150 platelets after 3 hours of oxidation at 400°C have established that the filaments exhibit a maximum length of 4.0 μm, an average length of approximately 1.0 μm, a length:width ratio of 20:1, thickness of 10 nm to 30 nm and a surface density of $10^9 cm^{-2}$ (determined by scanning electron microscopy).

A number of additional features of the platelet morphology are observed in the high magnification photograph of Figure 5.2. The

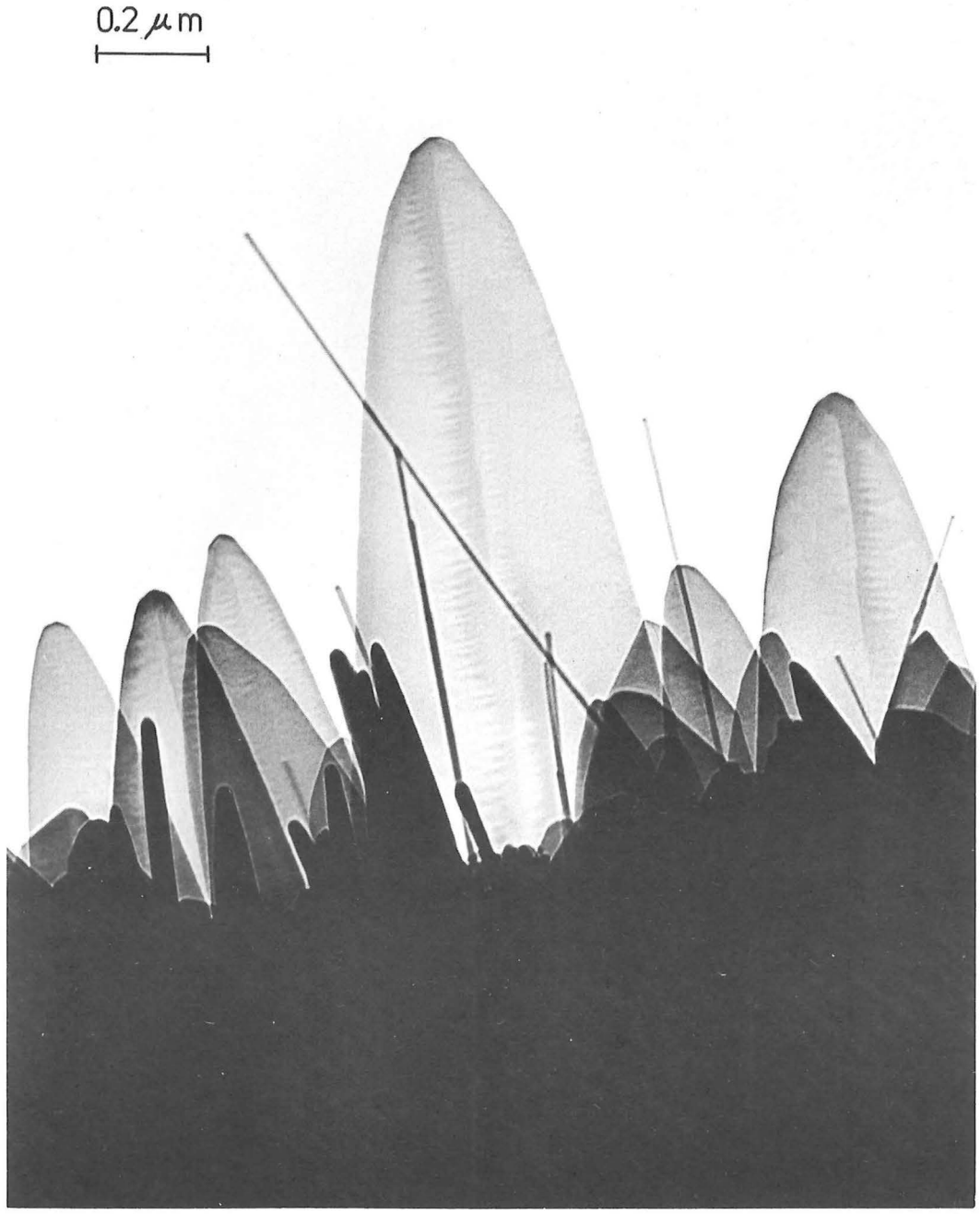

Fig. 5.2 Platelet formation on iron after 4½ hours at 500°C.

characteristic tip shape is composed of a number of different crystal faces, but the wide variation in length:width ratio at different temperatures is accompanied by a corresponding variety of tip profiles. Most crystals exhibit striated growth patterns on their faces as a result of thickness contrast, and many crystals also display bands of enhanced contrast around their perimeters or radiating from the centre of the base to the outer edges of the crystal. These effects are identified as bend contours, or occasionally as separate grains, in dark field images.

A striking feature of many blade images is an irregular line along the centre of the blade from base to tip which appears to be a trace of the growth of the pointed tip. A marked difference in contrast is frequently observed between the two halves of the platelet at either side of this line, and similar lines and contrast variation may also be associated with other changes of orientation of the whisker tip. Tallman and Gulbransen[46], observed similar features in platelets grown at similar temperatures in H_2O atmospheres containing a trace of oxygen, and attributed these contrast effects to thickness variations. The thickness variations were assumed to result from asymmetrical growth of the two halves of the crystal by a growth mechanism which assumed that the platelets consist of twinned αFe_2O_3 crystals. Examination of dark field images reveals that this contrast change cannot be attributed to such thickness variation but results from a change in lattice orientation due to either elastic bending or a grain boundary. Figure 5.3 shows a bright field image of a platelet formed at 550^{o}C and three dark field images from three different diffracted beams. It is observed that the line from point A to the base is associated with a contrast change for each of the three diffracted beams, which indicates an abrupt change of crystal orientation along this line. A bend contour would not be visible in dark field images from several different reflections since the contrast effects from a bend in a thin section originate from electrons which satisfy just one particular Bragg reflection.

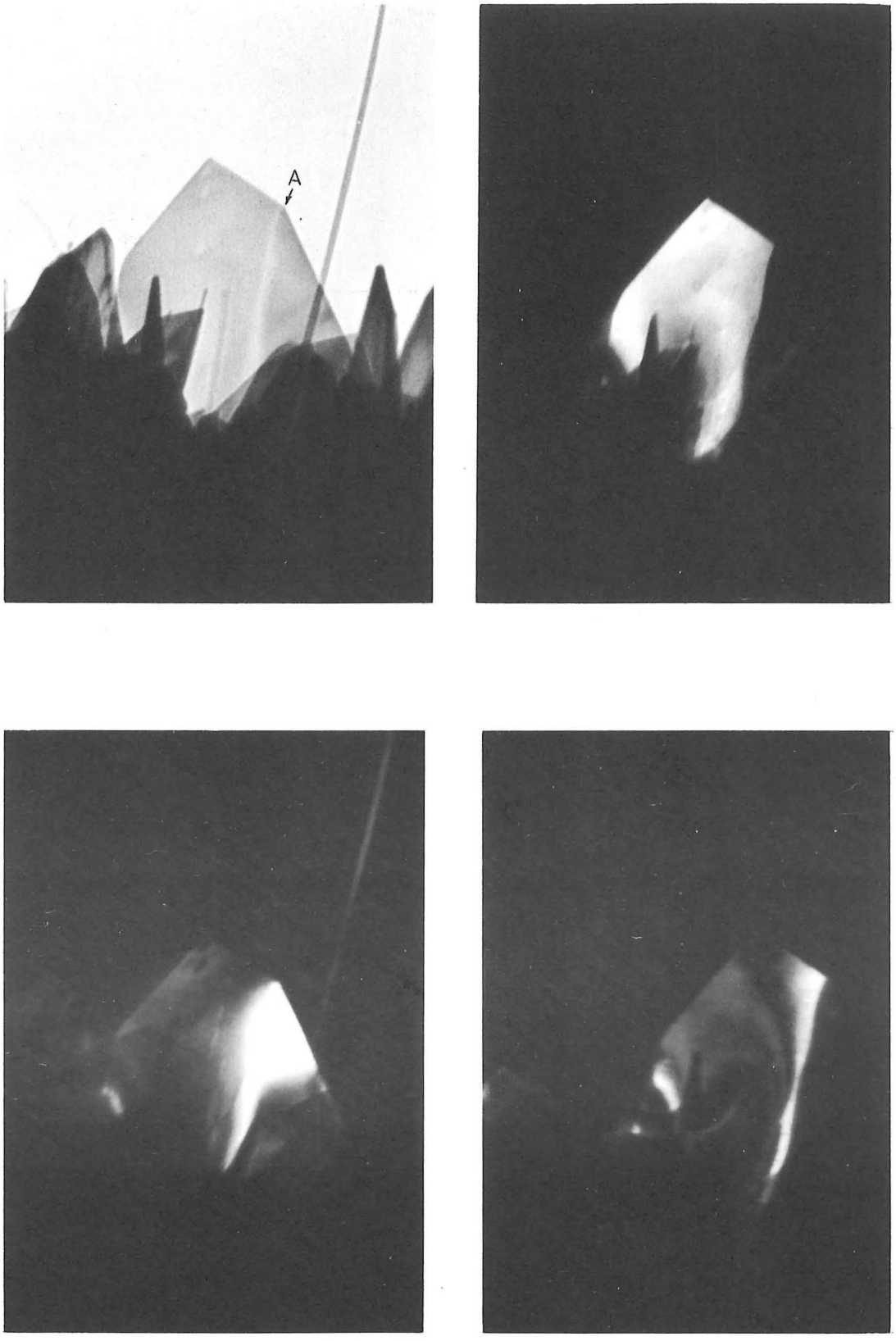

Fig. 5.3 Bright field and dark field images showing grain boundary in platelet formed at 550°C.

Extinction contours are also normally observed as gradations in intensity over a broad region rather than the abrupt contrast change observed here.

The change of contrast associated with a grain boundary along the axis of many platelets and the observation of the occasional platelet with a V-shaped notch at the tip suggest that the crystals may be folded at the centre with growth in two planes; however, scanning electron microscope observations do not support this suggestion. Specimens oxidised at temperatures from 400°C - 550°C have been examined using a number of different scanning electron microscopes but interpretation of the images is difficult as the resolution is barely sufficient to observe crystals of this size. Despite this limitation, the images do indicate that most platelets grow as flat sheets in a single plane from base to tip and intersect the oxide surface in a straight line. The platelets also appear to be randomly oriented to the base oxide layer.

5.1.2 Whiskers

The whisker crystals formed between 470°C and 850°C possess a variety of shapes and sizes which are dependent on the oxidising temperature. At 500°C fine filaments of approximately 15 nm thickness and lengths up to 5 μm are formed. At higher temperatures the whiskers broaden into ribbon-like profiles which remain transparent to electrons but which increase in size with increasing temperature. After three hours of oxidation a maximum size is reached at approximately 750°C when lengths of 30 μm and widths of 1 - 2 μm are observed. Above this temperature a slight decrease in size occurs and at 850°C the whisker profile is replaced by electron-dense mounds of oxide which are shown in Figure 5.1 (ℓ).

High resolution imaging of the finest whiskers is difficult as they are in constant motion under the impact of residual gas molecules in the electron microscope, and rapidly become covered by a sheath of contamination while under observation. High magnification bright field and dark field images of a whisker section are shown in Figure 5.4.

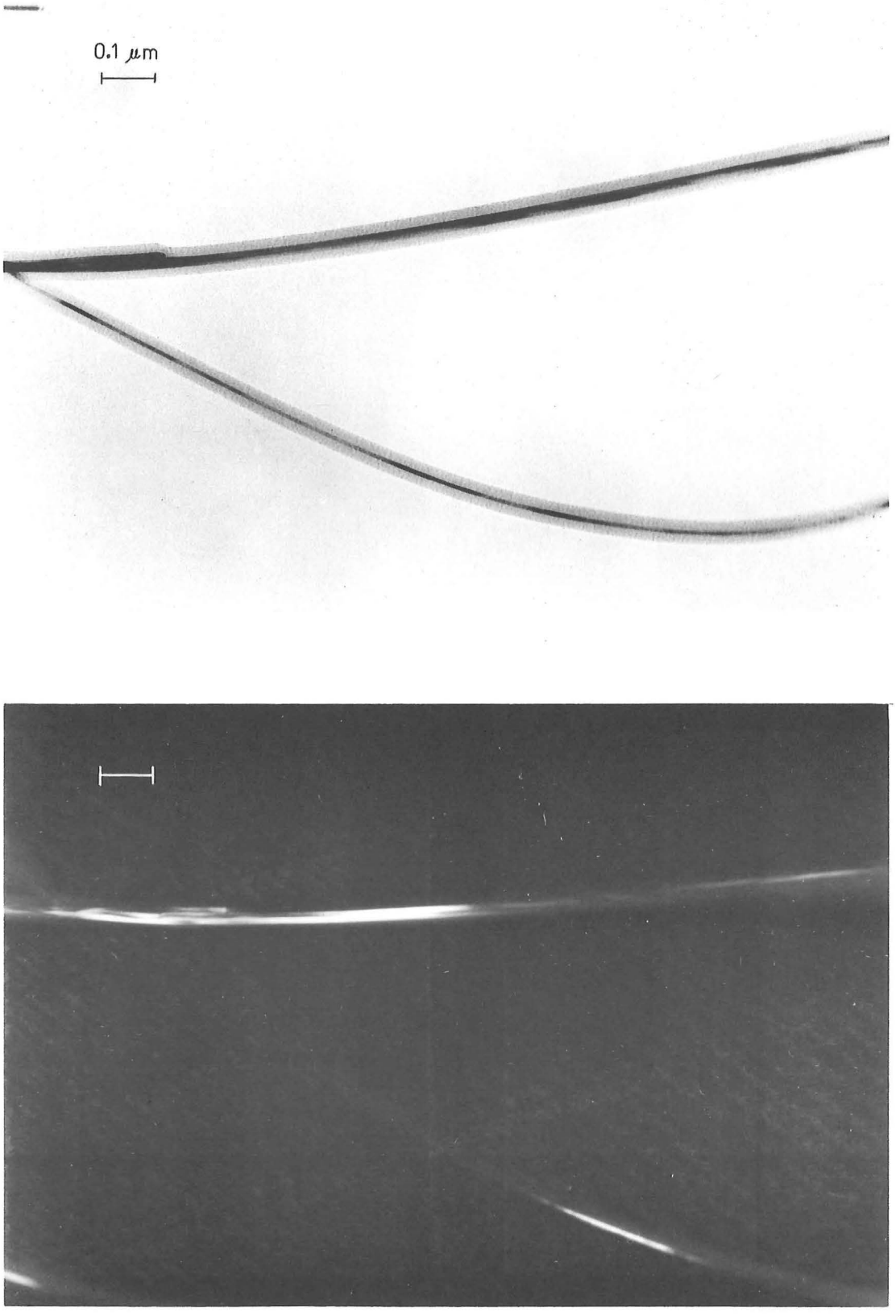

Fig. 5.4 High magnification bright field and dark field images of two fine whiskers showing bend contours and dual crystal nature of the top whisker. A contamination sheath surrounds both crystals.

The effect of the contamination sheath is a general reduction in resolution; but bend contours are clearly observed and the top whisker is clearly shown to consist of dual crystals growing together.

A number of features of the structure of the larger ribbon crystals formed at higher temperatures are revealed by diffraction contrast effects in Figure 5.1. At 750°C the ribbons are slightly tapered towards the tip and often display regularly spaced contrast bands along their length accompanied by localised bulging of the whisker sides. A likely cause of such effects is thickness variation resulting from the cyclic temperature fluctuation of approximately ± 20°C which is associated with thermostatic control of the oxidation furnace. In addition to these contours sharply defined dark lines are observed running parallel to the axis of many crystals, and a change of tip orientation is frequently associated with the termination of these lines at the whisker tips. Lasko and Tice[53] have observed similar features in copper oxide whiskers and have suggested that the lines are the images of axial screw dislocations; but a number of features of the contrast effects observed in the iron oxide whiskers suggest that the majority of such contrast lines are images of grain boundaries. The kinematical theory of image contrast predicts that contrast at screw dislocations should appear as thin dark lines in bright field images and that the line contrast should be reversed in dark field images.

A contrast reversal of this type has been detected in only a small proportion of the ribbons examined, indicating that most such ribbons do not contain axial screw dislocations. A discontinuous change of contrast is commonly observed across the contrast lines, however, which suggests that most ribbons consist of two or more parallel crystals growing together. Whiskers which split into two at the tip are a relatively common phenomenon above 700°C and may be readily explained in terms of multiple crystals of this type. An unusual ribbon which shows the existence of both dislocations and grain boundaries near the tip is shown in Figure 5.5.

Figure 5.6 shows that the larger whiskers may also contain transverse grain boundaries and networks of dislocations associated with

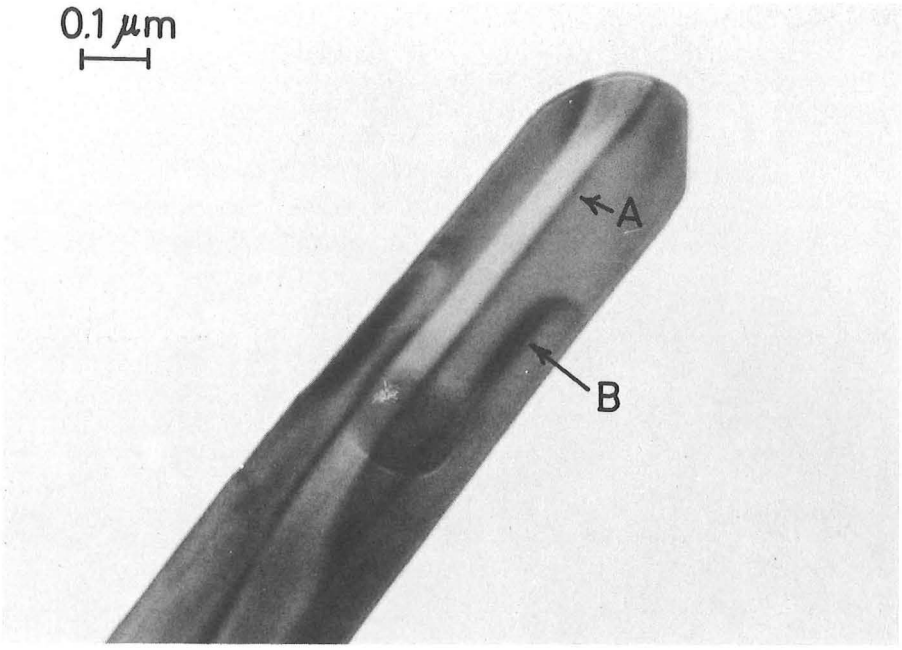

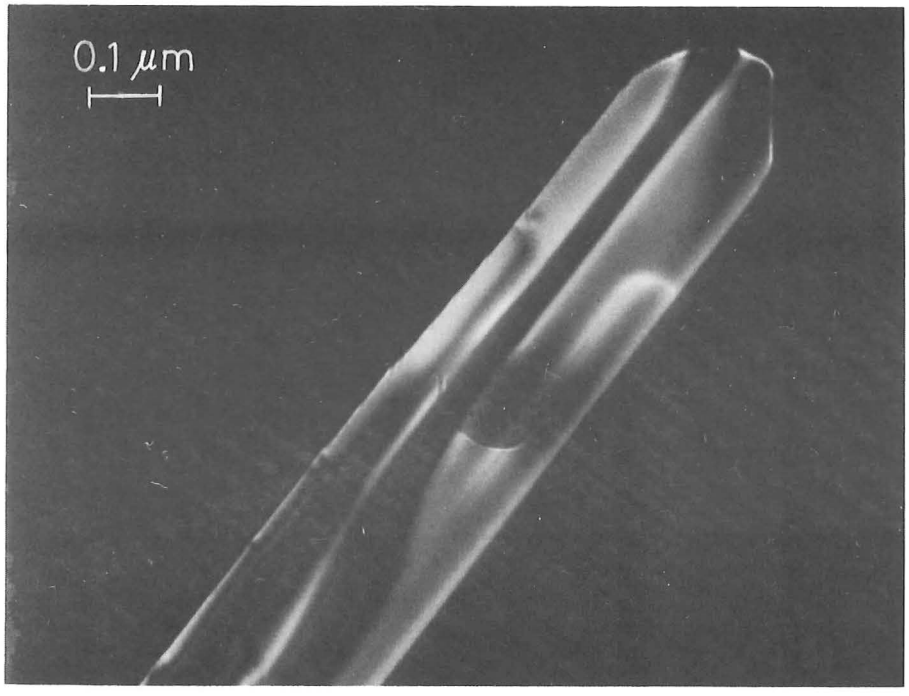

Fig. 5.5 Bright field and dark field images of ribbon tip showing both grain boundaries (A) and dislocations (B).

Fig. 5.6 Oxide whisker growth at 700°C exhibiting grain boundaries, extinction bend contours and dislocations.

lattice strain. Dark field observation is generally necessary to distinguish between these features and contrast effects resulting from bending or changes of thickness.

The higher temperature filaments are of sufficient size to be satisfactorily imaged by scanning electron microscopy. Figure 5.7 contains three images of different areas of a single iron specimen oxidised for three hours at 800°C. A large proportion of the surface was observed to be covered with mounds of oxide of irregular cross-section as shown in Figure 5.7(c), while other parts of the specimen showed whisker growth with a surface density of 10^8 cm^{-2}. The transition between areas of the surface bearing whiskers and those bearing mounds was abrupt and very few areas of the specimen contained mixtures of both types of surface particle. The abrupt transition between the two types of crystals suggests that orientation relationships within the oxide layer may have a strong influence over the nature of the surface growth. The bases of the whiskers are observed to blend smoothly into the surface oxide layer with an accumulation of material at this point. The tips of many of the whisker crystals are the nucleation sites for finer whiskers which reinforces the transmission electron microscope observations that the ribbons consist of bundles of crystals lying in a single plane.

5.2 *IN SITU* OBSERVATION OF GROWING FILAMENTS

A number of experiments have been performed using the controlled atmosphere gas reaction chamber to observe the formation of the oxide filaments *in situ*. All specimens have been oxidised in medical grade tank oxygen atmospheres at a pressure of 2.67 kPa (20 mm Hg) with the exception of one experiment using a 5% H_2 - 95% O_2 atmosphere at the same pressure. The specimens were given similar pretreatments to those described in Section 5.1 and were directly heated by the passage of electric current. Experiments have been performed at constant temperature to observe the nature of the growth process and to measure the rate of growth. Following

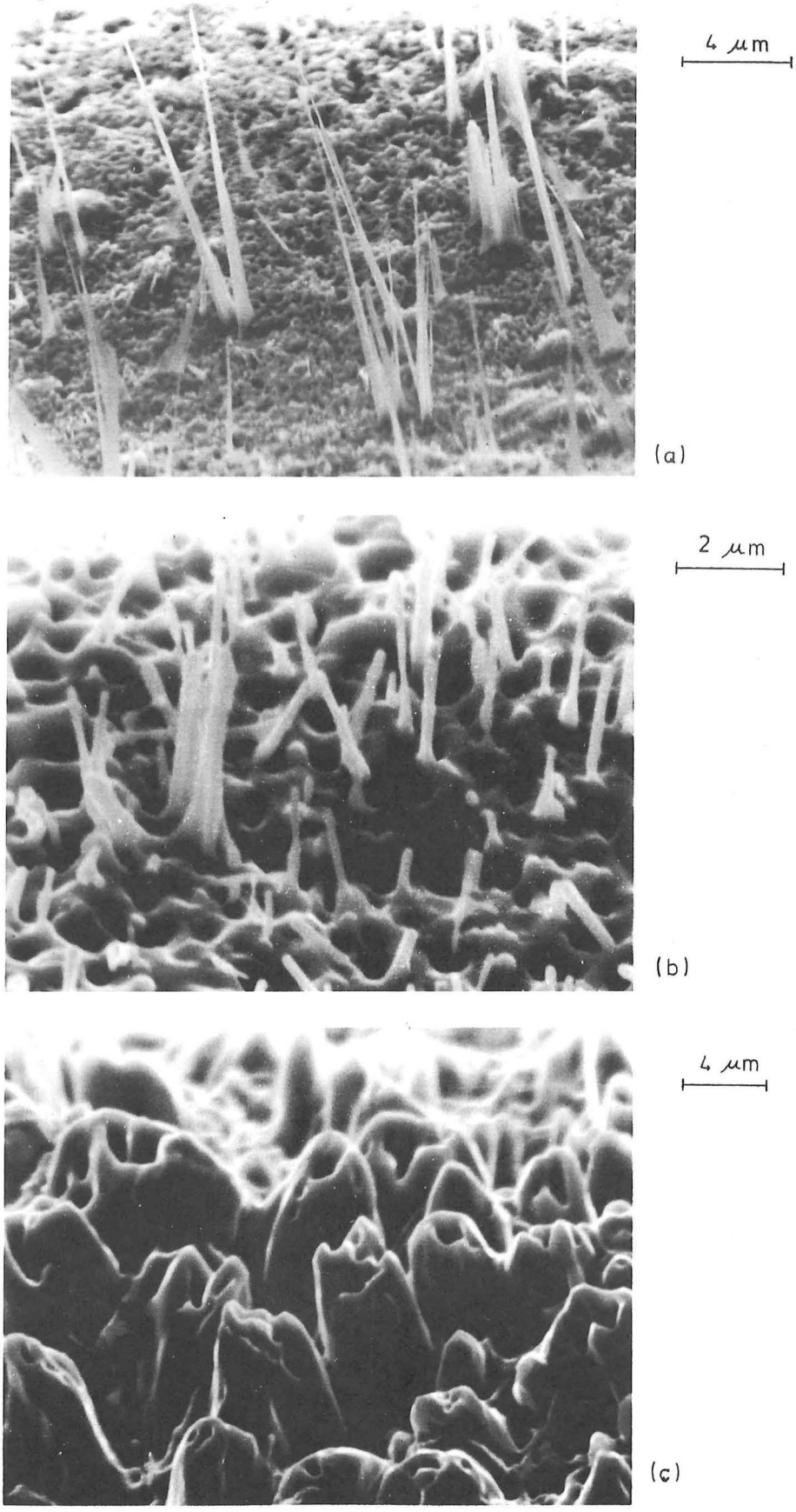

Fig. 5.7 Scanning electron micrographs of iron surface following oxidation for 3 hours at 800°C.

constant temperature oxidation the temperature of a number of specimens has been altered to observe the changes which occur. One of the experimental problems associated with this technique is that it is difficult to predict the time and place where activity of interest will occur, and to a certain extent the photographic sequences showing features of interest have been obtained fortuitously.

5.2.1 Oxidation at 500°C

An oxide growth sequence at a constant temperature of approximately 500°C in oxygen at 2.67 kPa is shown in Figure 5.8. The temperature of this specimen was steadily increased from room temperature over a period of approximately 30 minutes until filament growth was observed to be occurring on areas of the specimen. Oxidising conditions were then stabilised at that temperature and the photographic sequence of a chosen area of the specimen was commenced. The elapsed times in Fig. 5.8 refer to the period after the temperature was stabilised.

Growth does not occur simultaneously at all points on the surface. Localised clusters of whiskers are observed to form initially, and the surrounding areas eventually nucleate whiskers so that a relatively uniform surface density, estimated at $10^8 cm^{-2}$, is achieved after approximately 20 minutes of oxidation at this temperature. The whiskers grow by addition of material at the tip and appear to be preferentially nucleated on the points of projections from the oxide surface. A feature of the whisker growth which was not appreciated from *post situ* observation is that many of the whiskers grow as bundles of small filaments which nucleate side by side. Many of these whiskers continue to grow together and give the appearance of a leader filament which propagates first, followed by an overgrowth of the outer surfaces leading to apparent thickening of the crystal near the base. In the gas - reaction stage observations the separation of these crystals is occasionally observed, as in the case of whisker A in Figure 5.8 (f). This bundle consists of at least four

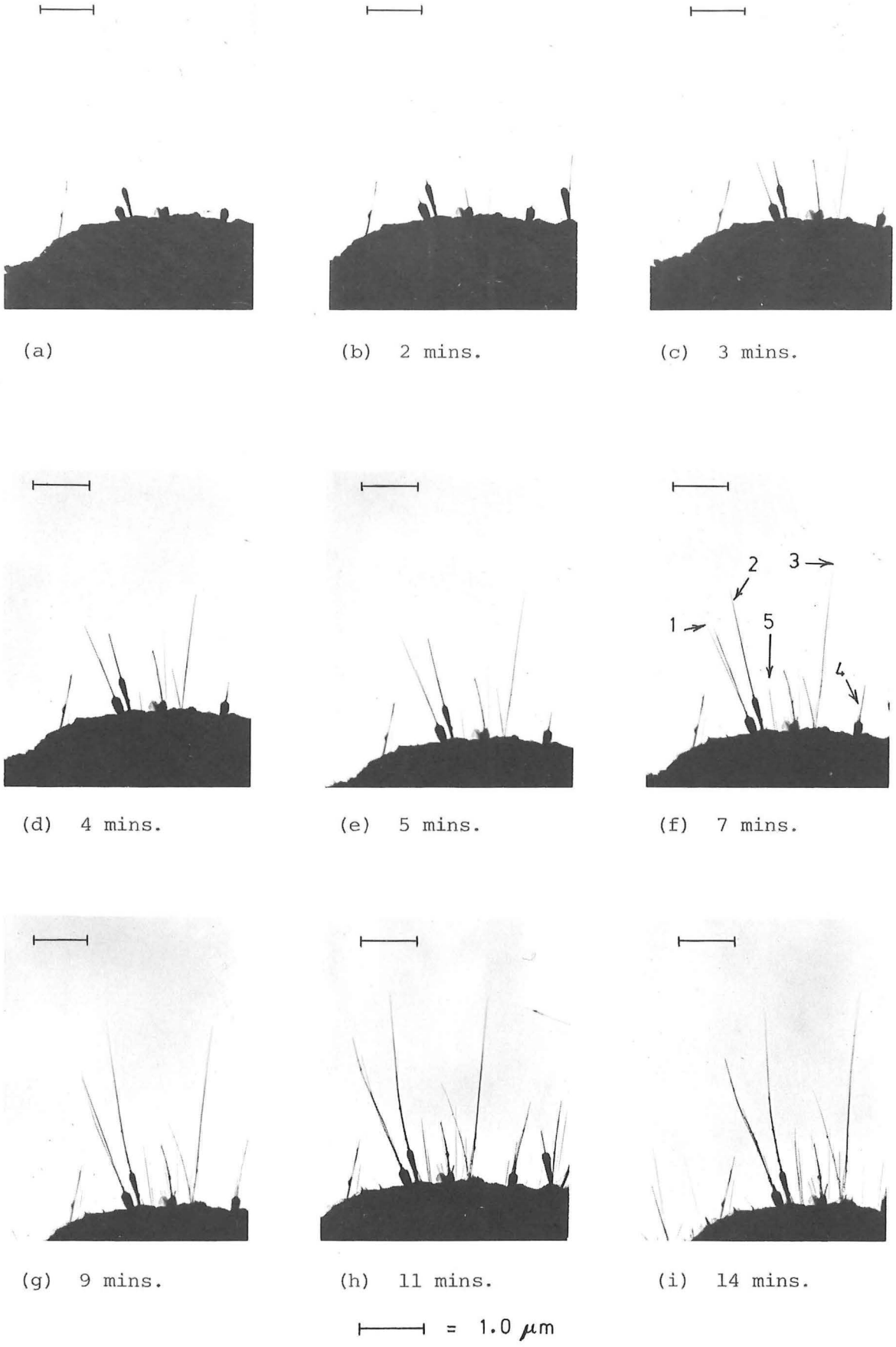

(a) (b) 2 mins. (c) 3 mins.

(d) 4 mins. (e) 5 mins. (f) 7 mins.

(g) 9 mins. (h) 11 mins. (i) 14 mins.

⟵⟶ = 1.0 μm

Fig. 5.8 Gas reaction stage observation of the growth of iron oxide whiskers at 500^{o}C (approx.) in oxygen.

(Continued on next page)

(j) 18 mins.

(k) 22 mins.

(l) 28 mins.

(m) 42 mins.

(n) 51 mins.

(o) 61 mins.

(p) 73 mins.

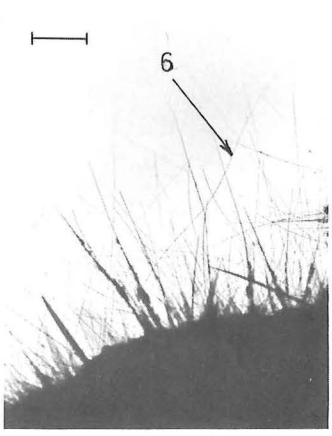

(q) 85 mins.

(r) 94 mins.

Fig. 5.8 continued

separate whiskers but its true nature as a multiple crystal was not apparent until separation occurred.

Many of the crystals which are formed early in the oxidation process are covered with considerable contamination and overgrowth in the form of bulbous irregularities and small platelets which grow on their surfaces as the reaction proceeds. Irregular overgrowths of oxide are not uncommon on specimens oxidised external to the electron microscope but the degree of contamination on this specimen is greater than is normally observed. It is possible that the contamination may be a function of the electron beam irradiation of the specimen or some feature of the oxidising atmosphere. The electron beam will certainly cause temperature fluctuations in the whiskers, as the condenser lens is adjusted for photographic purposes and the beam alignment is altered, but the magnitude of the effect is not known. Preferred sites for accumulation of material appear to be the points of contact between two whiskers and the region between the bases of whiskers which are nucleated close together. This suggests surface transport of the oxidising species.

5.2.2 Measurement of Growth Rate

The growth rates of 20 whiskers and five platelets grown on four specimens at different temperatures have been measured. The rates of growth of the whiskers labelled 1 - 5 in Figure 5.8 (h) are plotted in Figure 5.9 and are typical of the growth observed on all specimens. It is clear from this figure that after an initial induction period most whiskers exhibit a linear growth rate with respect to time followed by an abrupt cessation of growth at a variety of different lengths. After this transition point no further increase in length is observed for the majority of whiskers over the remainder of the experiment, which continued for 99 minutes. A few whiskers continue to grow at a rate slower than that initially observed after departure from the linear portion of the growth curve, but this growth may also be abruptly terminated.

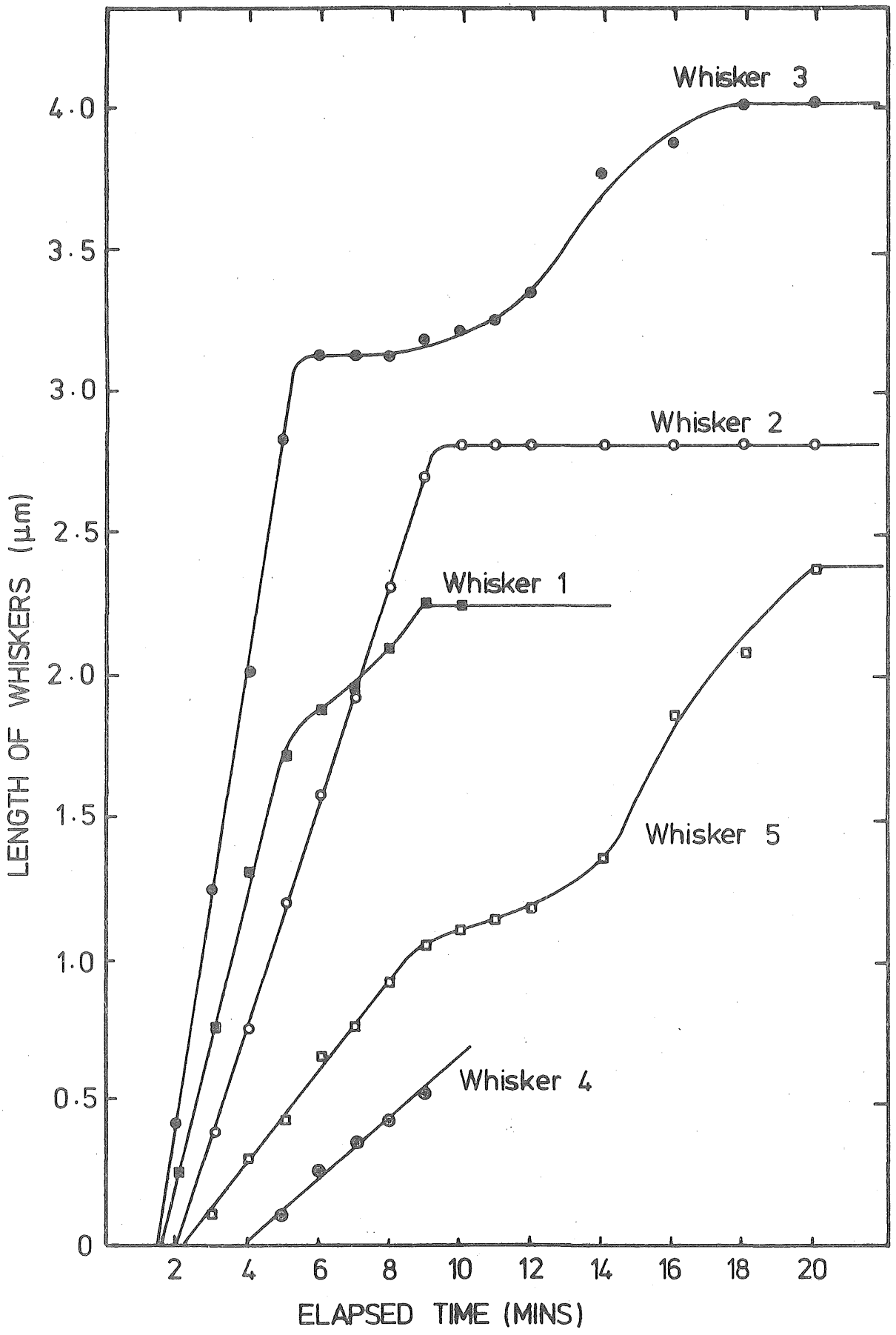

Fig. 5.9 Measured growth of whiskers labelled in Fig. 5.8(f) at 500°C.

A variation in rates of growth between 1.6 μm/min and 0.1 μm/min is observed on this one specimen, which is unlikely to be accounted for by different orientations of the crystals to the electron beam. Whiskers growing together in clusters do not necessarily lengthen at the same speed which also indicates that a true variation of growth rate does exist between different whisker crystals at the same temperature.

The extreme linearity of most of the plotted growth rates in Figure 5.9 is most surprising as it is generally assumed that cation diffusion from the base oxide to the whisker tip will provide the rate-controlling step for filament formation. Both internal diffusion and surface diffusion mechanisms would normally be expected to lead to a parabolic time law for the growth of whiskers of constant cross-section at constant temperature; that is

$$\ell = Kt^{0.5} \qquad \ldots.(5.1)$$

where ℓ is the whisker length, t is the elapsed time, and K is a rate constant which depends on the oxidising temperature.

It is, therefore, necessary to consider the accuracy and representativeness of the measured rates of growth and examine possible growth mechanisms which could account for the variable induction period, linear growth rate and abrupt cessation of growth which are observed.

Some anomalies in the measured growth rates are to be expected as a result of change of orientation of the filaments with respect to the electron beam as growth proceeds and localised temperature variation in the whiskers which are irradiated by the electron beam. The first of these effects is not considered significant as consistently linear results have been obtained for a number of different whiskers, but it is possible that localised heating by the electron beam and thermal conduction into the surface oxide could lead to a temperature gradient within each whisker. It is not possible to evaluate effects such as this but it is unlikely that effects related to the electron beam will show

any regularity or consistency as the beam intensity is subject to considerable fluctuation over the course of the experiment.

The representativeness of the whiskers whose growth rates are plotted in Figure 5.9 is certainly open to question. Insufficient experiments have been performed to state with certainty that all whiskers increase in length with a linear relationship with time. Experimental difficulties have limited the number of measurements of whisker length although several specimens have been observed at constant temperature for periods exceeding one hour. The lengths of the longest whisker crystals cannot be determined with accuracy owing to their movement under Brownian motion, and a large proportion of whiskers grow to terminal length in a shorter interval than can be recorded in a series of images on glass photographic plates. To examine the representativeness of the linear relationship the measured growth rates of a number of whiskers which have been observed on four different specimens under different oxidising conditions are plotted in Figure 5.10. Of the twenty five filaments measured the only whisker or platelet which shows a gradual reduction in growth rate with time is whisker 6 in Figure 5.8(q). It is plain that orientation effects could readily account for the deviation from a linear rate which is observed for this whisker as its direction of growth is observed to change several times during the photographic sequence.

No difference is observed between the growth behaviour of platelets compared with that of whiskers. A nucleation period of similar length is required and a similar range of growth rates exists. The platelets maintain a constant length : breadth ratio, and remain of constant shape as growth proceeds.

5.2.3 The Effect of Temperature Change

After 99 minutes of oxidation at 500°C the temperature of the specimen shown in Figure 5.8 was rapidly increased to 800°C for approximately 30 seconds and then returned to 500°C. During this short period

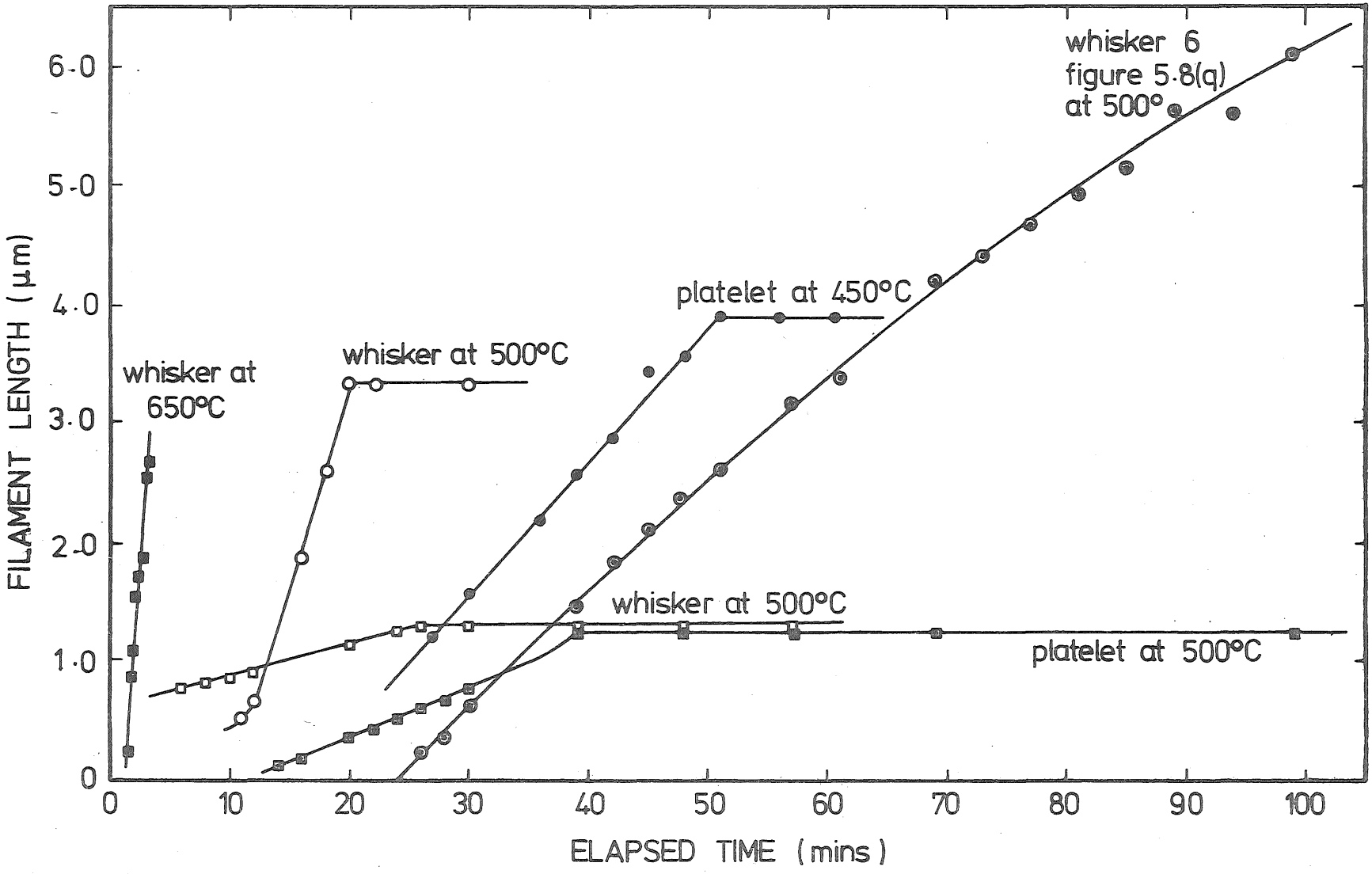

Fig. 5.10 Measured growth rates of assorted whiskers and platelets

at elevated temperature the ribbon-like whiskers shown in Figure 5.11(a) grew from the surface and the previously observed whisker and platelet crystals were completely obscured. The ribbons have a maximum length of 7.5μm which indicates a growth rate of 15 μm per minute at this temperature. The ribbon crystals are very thin, as indicated by their transparency to electrons, and provide very low contrast images on the photographic plates.

The results of an attempt to repeat the rapid growth process are observed in Figure 5.11(b). Heating at 1000°C for 15 seconds resulted in the formation of a high contrast band at the tip of each ribbon suggesting either severe thickening of the crystal at the tip or melting of the crystal. When the temperature was subsequently reduced to the original level of 500°C continued growth of the ribbon tips was observed as illustrated in Figure 5.11(c) - (f). Pointed crystals grew initially at the outer edges of the ribbon followed by growth of a sheet of parallel crystals which grew together to fill in the ribbon section so that the original crystal profile was restored. Careful examination of photographs of the original ribbon crystals reveals up to 20 weak contrast bands parallel to the axis of each ribbon which correspond to the multiple crystals which continue to form on the tips at lower temperature.

The effects of further temperature changes are illustrated in Figures 5.12 and 5.13. Figure 5.12 shows a reaction chamber growth sequence in a 5% H_2:95% O_2 atmosphere at 2.67 kPa (20 mm Hg) following a temperature increase from approximately 500°C to 800°C. The growth of whiskers at 500°C appeared to have terminated, as indicated by photographs (a) and (b) taken 7 minutes apart, and the temperature was increased immediately subsequent to photograph (b). No change was observed for a further 6½ minutes following the temperature increase until a rapid growth of irregular ribbon crystals took place. The growing crystals advanced at approximately 4.0 μm per minute and rapidly overtook

a. Iron oxide ribbons formed at 800°C from whiskers and platelets grown previously at 500°C.

b. Ribbon tips melted by heating momentarily to 1000°C.

c. Continued growth at ribbon tips after 1½ minutes at 500°C.

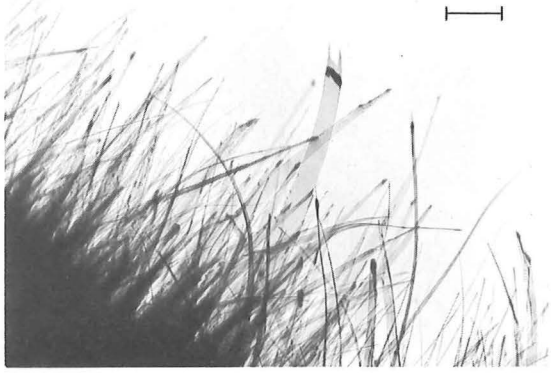

d. Growth after 2½ minutes at 500°C.

e. Growth after 4½ minutes at 500°C

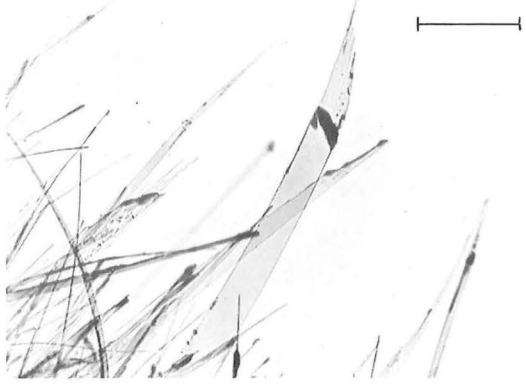

f. Growth after 10 minutes at 500°C.

Fig. 5.11 Continued growth at ribbon tips following apparent melting of tips by overheating.

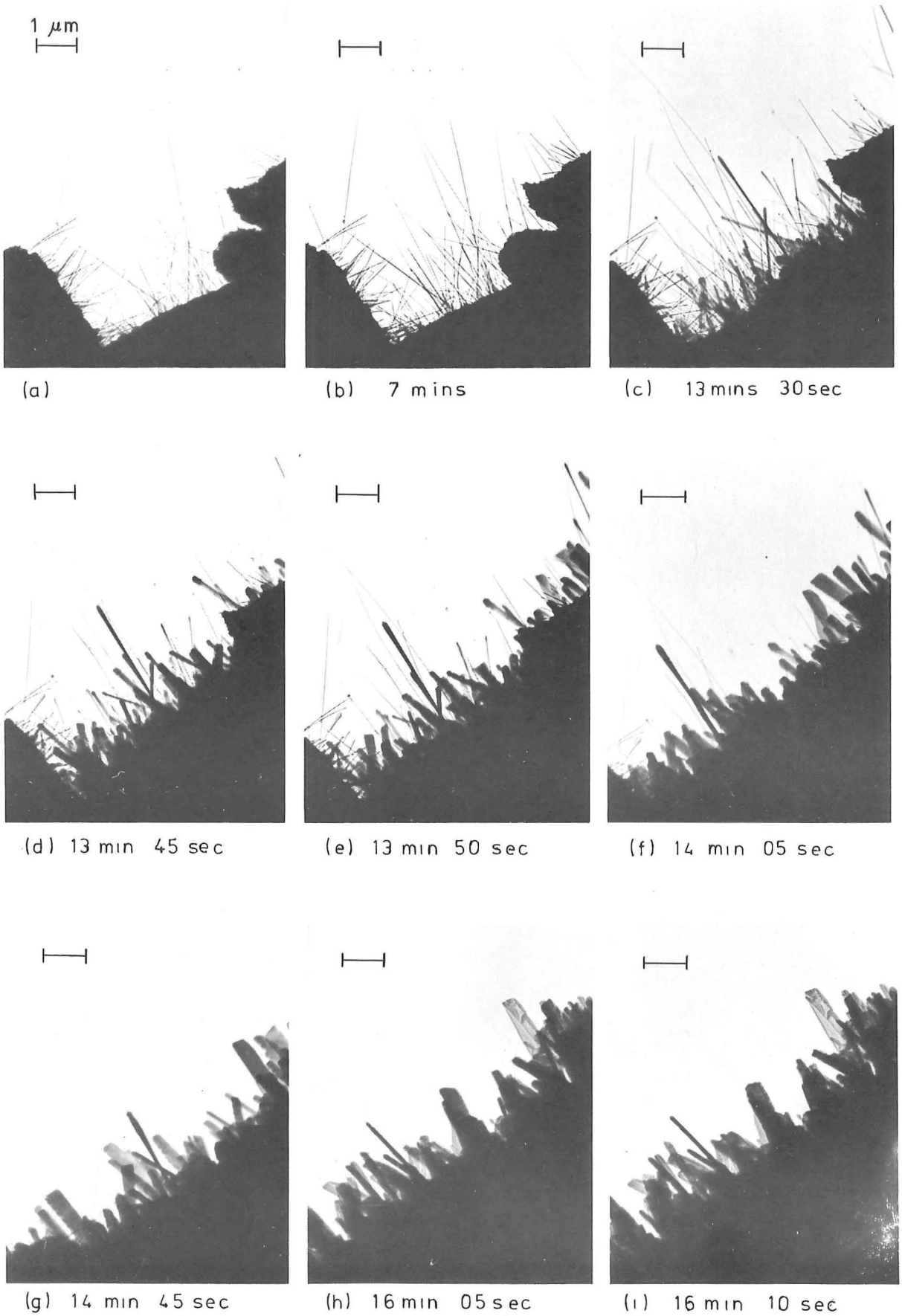

Fig. 5.12 Renewed whisker growth following a temperature increase. Micrographs (a) and (b) taken 7 mins. apart demonstrate effective cessation of growth at 500°C. A temperature increase (after 7 mins. elapsed time) leads to renewed growth following an induction period.

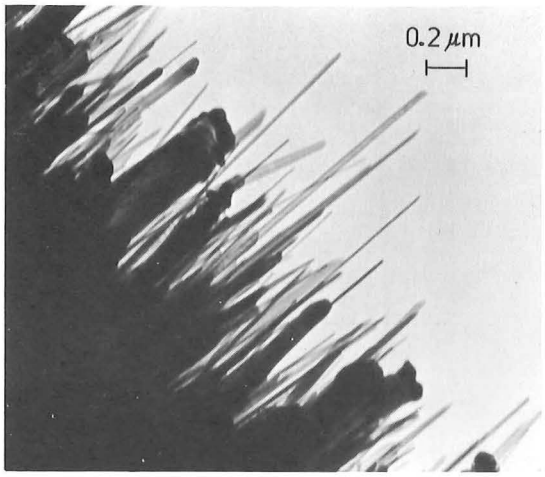

(a) 1.50 mins elapsed following temperature decrease.

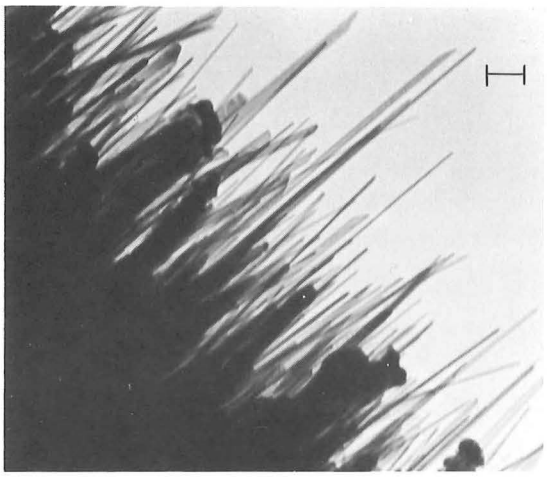

(b) 1.57 mins.

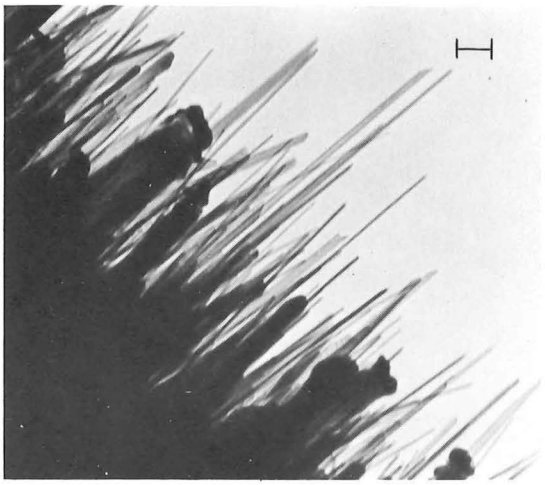

(c) 1.67 mins.

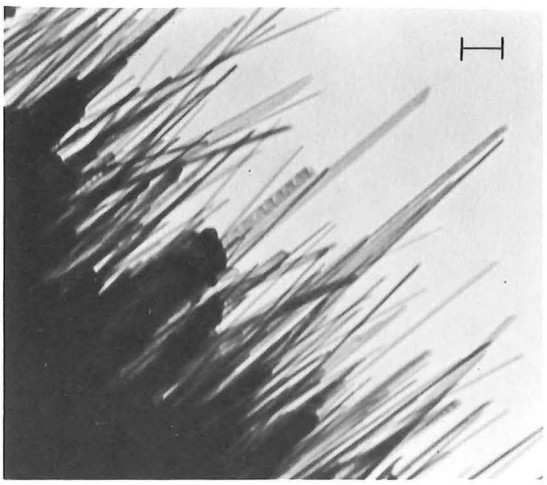

(d) 2.00 mins.

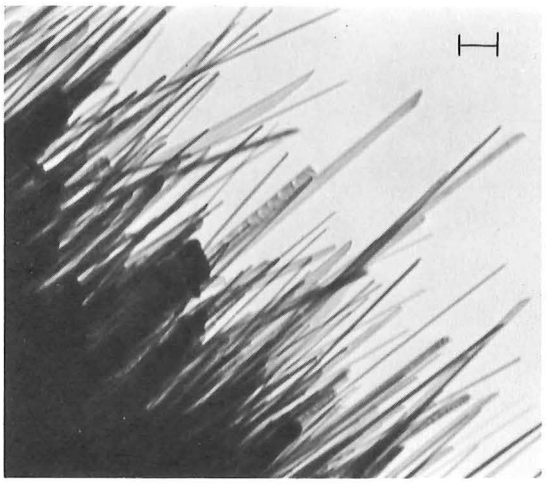

(e) 2.08 mins.

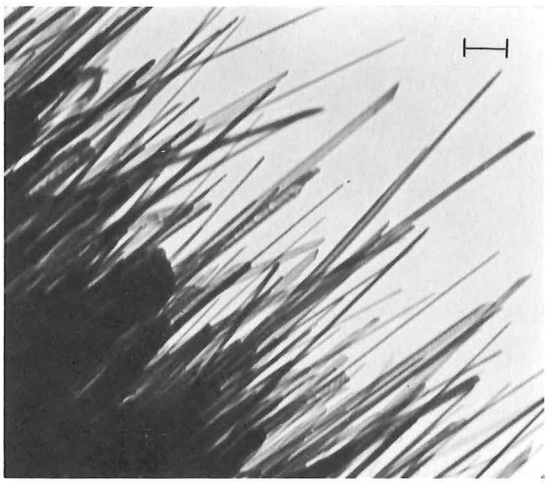

(f) 2.33 mins.

Fig. 5.13 Renewed growth of more regular whisker crystals following a temperature decrease from approx. 800°C to approx. 700°C.

the whiskers formed previously which did not show any change of form at the elevated temperature. The ribbons formed at the higher temperature are highly irregular and of variable thickness. Growth occurs simultaneously on a number of crystal faces so that the tip profiles remain constant and grain boundaries may be observed in many crystals associated with each change in tip profile.

When the majority of these crystals had reached their terminal length a reduction in the temperature to approximately 700^{o}C led to a further renewed growth of more regular shaped ribbons which are shown in Figure 5.13. Growth rates up to 4.5 μm per minute are observed, and narrow ribbons continue to advance from the tips of broad crystals whose growth has ceased. The observed rates of growth are approximately linear over the period of observation but the timing of the photographic sequence is not sufficiently accurate to detect small deviations from a linear relationship.

5.3 MULTIPLE WHISKER GROWTH

Many authors state that whisker growth consists of a series of stages involving propagation of a fine leader crystal which is followed up by secondary thickening or overgrowth on the outer surfaces. The gas reaction stage observations indicate multiple whiskers are frequently nucleated adjacent to one another and may grow together giving the appearance of overgrowth of a fine lead whisker when, in fact, they are forming as independent filamentary crystals. When the existence of these bundles of whiskers was recognised a closer study of many specimens revealed that most small iron oxide filaments propagate as multiple whiskers and that few single crystal whiskers exist.

The smallest whisker crystals may be attracted together from some distance apart, as is demonstrated in Figures 5.14 to 5.17. The filaments shown in these figures have been grown external to the electron

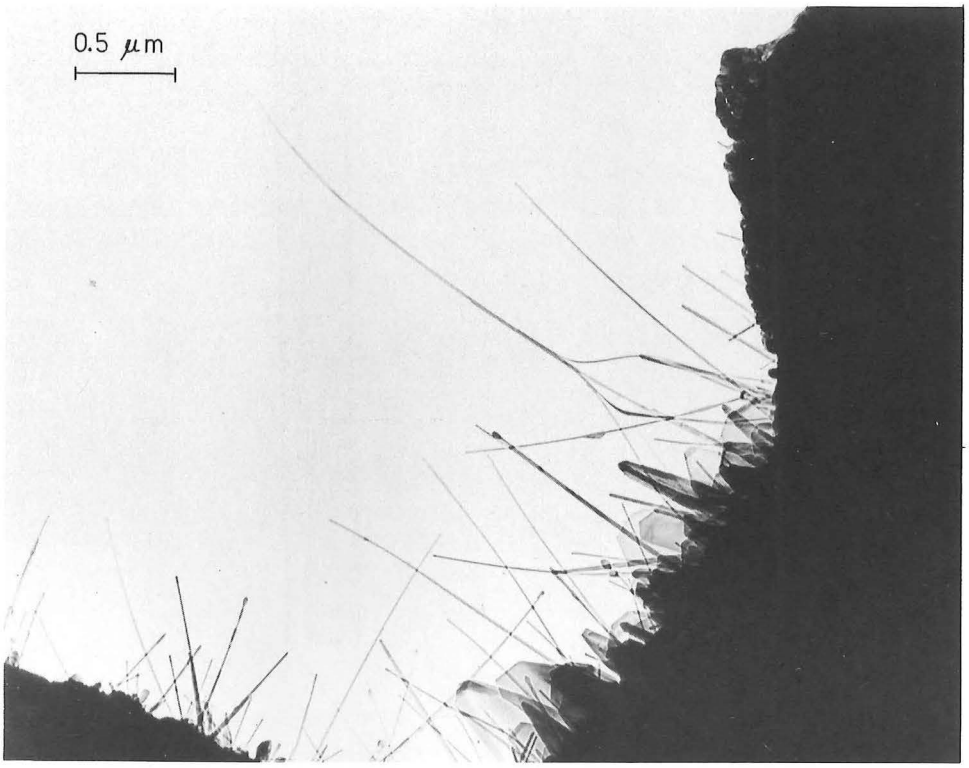

Fig. 5.14 Four whisker crystals nucleated some distance apart are attracted together to continue growth in a common direction. The ribbon-like nature of the whiskers is revealed by apparent changes of thickness at bends.

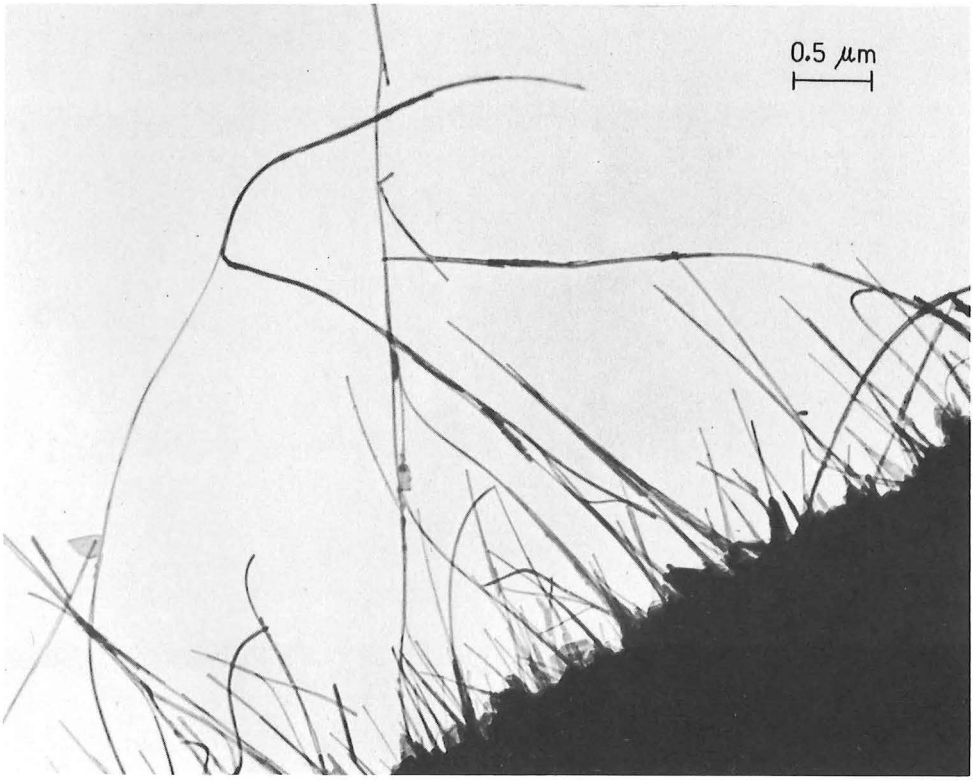

Fig. 5.15 Whisker crystals overheated by the electron beam reveal their multiple crystal structure.

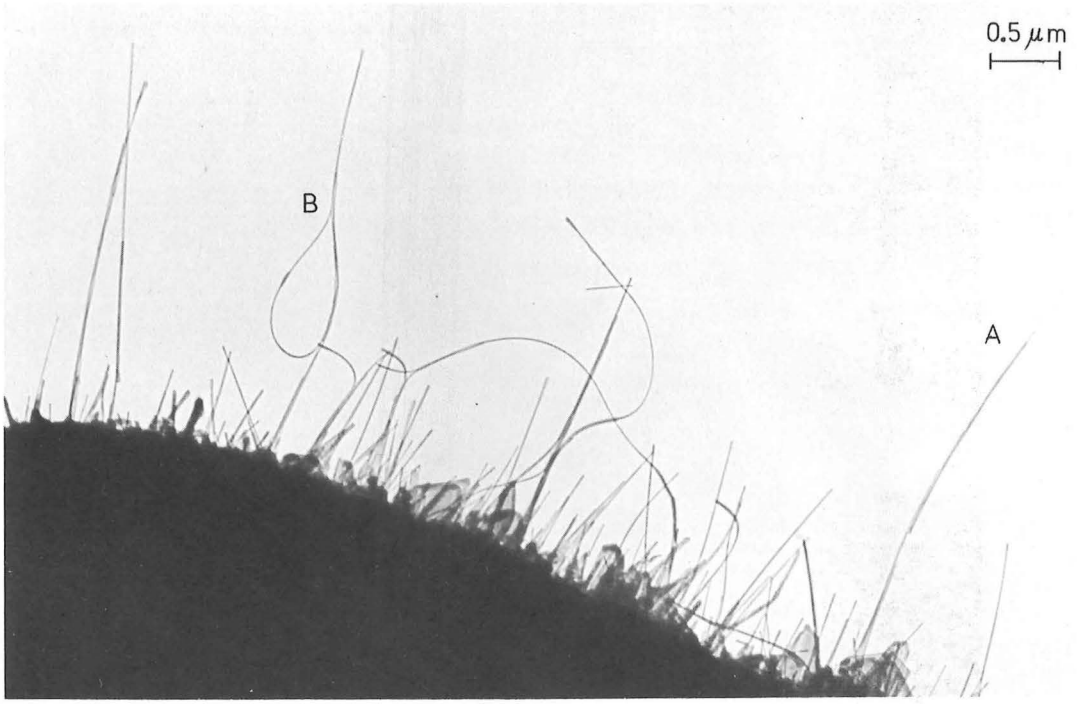

Fig. 5.16 Growth of a fragmented crystal (whisker A) at 470°C and fracture of whiskers attracted by intermolecular forces.

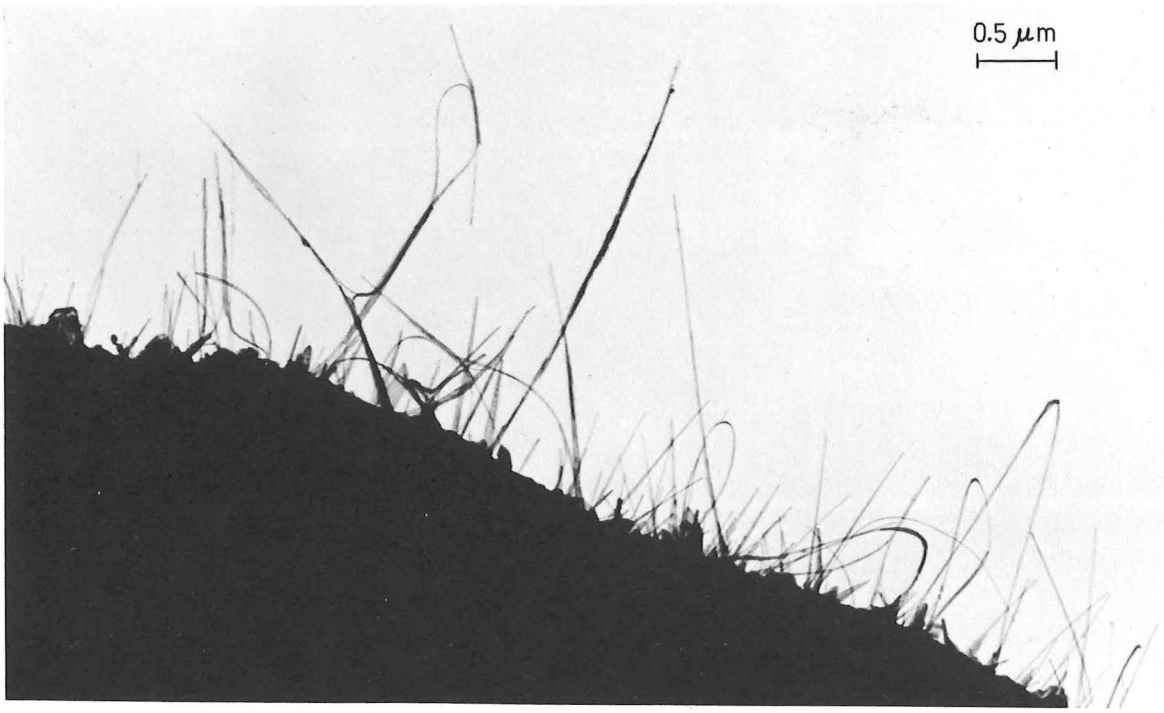

Fig. 5.17 Further examples of multiple whisker growth and the effects of intermolecular forces.

microscope at temperatures near the lower limit for iron oxide whisker formation, and few resemble the perfect single crystals of circular cross-section which are normally assumed in the literature. The most commonly observed type of multiple growth is shown in Figure 5.14. Two or more whiskers nucleated up to 1.5 μm apart may be attracted together to continue growth in a common direction, the misalignment of the crystals being accommodated by elastic deformation. Less regular crystals are shown in Figures 5.15 to 5.17. Whiskers may join at many positions down their length to produce a variety of irregular shapes, and may fracture or deform under load. Whisker A in Figure 5.16 appears to have grown as a fragmented crystal, and a small platelet appears to have formed on the side of a whisker in Figure 5.15.

Crystal B in Figure 5.16 will be used to estimate the forces required to draw crystals together into the configurations which are observed. The method of formation of the crystal is not known but simple elastic bend theory should enable a rough estimate of the forces required to produce the observed radius of curvature in terms of the simplified model of Figure 5.18. The bending moment (M) is related to the radius of curvature of the whisker (R) by the relation

$$M = \frac{EI}{R} \qquad \ldots.(5.2)$$

where I is the second moment of area of the whisker cross-section and E is the elastic modulus.

The minimum radius of curvature is estimated as 0.2 μm although the orientation of the whisker loop with respect to the electron beam is not known. This radius corresponds to the maximum bending moment ($M_{max} = F\ell$) exerted by the force of attraction F between the two whisker sections. Mehan and Herzog[124] indicate that the elastic modulus of whisker crystals is similar to that of bulk crystalline material, and in the absence of data for αFe_2O_3 at the oxidising temperature, a value of $E = 300 \times 10^9$ N/m^2 will be chosen. This figure is representative of materials of similar

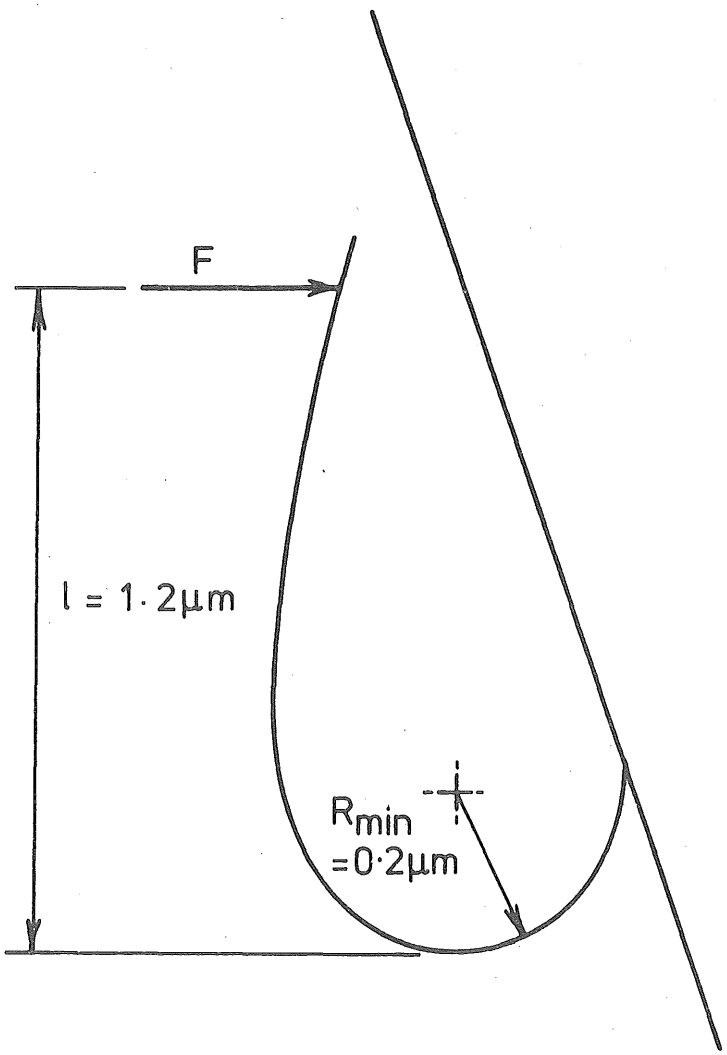

Fig. 5.18 Simplified model of whisker bending under the influence of attractive force F.

structure such as αAl_2O_3.

The whisker cross-section is a further property which is difficult to determine. A change in whisker profile is frequently observed at points where bending occurs, these points being indicated by arrows in Figure 5.16. Such images would be expected from a ribbon crystal of breadth:depth ratio of approximately 1.5:1. The depth (d) of the whisker under consideration is measured as 10.0 nm and a rectangular cross-section of breadth (b) 15.0 nm is assumed. The second moment of area of this section is given by

$$I = \frac{bd^3}{12}$$

Substitution of these values into Equation (5.2) provides a value for the maximum bending moment of 2.5×10^{-15} Nm which corresponds to an attractive force between the whiskers of 2.1×10^{-9} N.

> It is interesting to examine the elastic stress in the whisker represented by the measured radius of curvature. At a distance y from the neutral axis the stress (f) is given by
>
> $$f = \frac{Ey}{R} \qquad \ldots.(5.4)$$
>
> therefore $f_{max} = 0.03E$ at the outer surface of the whisker. This value is very close to the theoretical cohesive strength of solid matter which lies in the range 0.03E to 0.17E[124], and suggests a high degree of crystalline perfection in the observed whisker.

Intermolecular forces of electromagnetic origin (Van der Waals forces) are felt to account for the observed attraction of adjacent whisker crystals. Derjaguin[125] showed that electromagnetic forces of comparable magnitude exist between macroscopic crystals at distances up to 0.2 μm, the forces depending on the shape of the crystals and many other factors.

Although electromagnetic forces between individual molecules would be expected to decrease according to the inverse 7th power of the separation distance, measured values indicate an inverse 3rd or 4th power relationship exists for most macroscopic bodies. Gravitational forces would be negligible by comparison but it is possible that electrostatic effects which decrease according to an inverse square law may be significant.

The existence of molecular forces of this magnitude leads to speculation regarding the reason for separation of the occasional bundle of whiskers which are growing together, as was observed in the gas reaction chamber growth recorded in Figure 5.8. Repulsive electrostatic forces generated by the electron beam could possibly counter the attractive electromagnetic effects but movement of adjacent whiskers as a result of irradiation by the electron beam is not normally observed.

5.4 INFLUENCE OF THE OXIDISING ATMOSPHERE AND STATE OF THE METAL SUBSTRATE.

Gulbransen *et al*[11,33,35,36] have demonstrated that the oxidising atmosphere and state of the metal substrate may influence the type of filamentary growth observed on the oxide surface. The oxidation of annealed iron at temperatures of 400-500^{o}C in oxygen previously dried by cooling to -196^{o}C, produced a preponderance of fine whiskers with very few platelet crystals. The addition of traces of water vapour, however, led to a mixture of pointed blade-shaped platelets and whiskers similar to those observed in this study. When cold worked iron was oxidised under similar conditions a similar result was produced in atmospheres containing water vapour; but in dry O_2 a new crystal habit consisting of broad rounded platelets was observed after 48 hours oxidation at 400^{o}C. A further crystal habit, that of blunted blade-shaped platelets, was observed on annealed iron oxidised at 400^{o}C in an atmosphere of 10% H_2O + 90% (He + 1000 ppm O_2).

The preponderance of platelet growth on annealed specimens oxidised in the presence of water vapour was tentatively suggested by Gulbransen *et al* to demonstrate that the point growth sites for whiskers are transformed into linear sites by the direct action of hydrogen; this behaviour was assumed to be similar to the ordering of growth sites by hydrogen described in Section 1.4. No attempt has been made in this study to examine the effects of variation of the composition of the oxidising atmosphere using the gas reaction chamber, but observations of platelet growth have demonstrated that all such crystals remain essentially of constant shape and become broader as their length increases. Consequently, a long linear growth site on the oxide surface is not initially required for platelets pointed at their tips.

The observation that the crystalline state of the iron substrate can influence subsequent filamentary growth from the outer oxide layers introduces a complication which requires further study. Iron in both cold worked and annealed conditions has been examined by the author following oxidation for periods from 3 - 6 hours over a variety of temperatures and no significant difference has been observed between the oxidation products from the two metal states. Similar observations have been made by Talbot and Bigot[39] and it is possible that a variation in metal purity or some other factor may have led to the change of crystal habit reported.

CHAPTER 6

DETERMINATION OF FILAMENT STRUCTURE

6.1 INTRODUCTION

Selected area electron diffraction patterns have been used to determine the nature of both whisker and platelet crystals. Diffraction patterns may be obtained with little difficulty from the large ribbon-like whisker crystals formed at temperatures above 600°C and from the smaller platelets formed between 300°C and 550°C. However, a number of experimental problems are associated with electron diffraction from the fine whisker crystals which are obtained during the oxidation of iron between 460°C and approximately 500°C, and it is this crystal habit which is of most interest.

The first of these problems relates to movement of the whisker crystals while they are being observed. The finest filaments are of such a size that they are in constant vibration under the impact of gas molecules, and the heating effect of the electron beam causes them to bend during observation. The vibration leads to a severe reduction of resolution in high magnification images but is of lesser significance in selected area diffraction. The change of orientation of the tips of the vibrating whiskers with respect to the electron beam may be of the order of one or two degrees which will produce unusual intensity profiles about the reciprocal lattice points and some broadening of the diffraction spots in a direction perpendicular to the whisker axis. Bending of the whisker crystals when irradiated by the electron beam tends to be a greater problem. As the intensity of illumination is altered a number of diffraction patterns may be successively observed, each arising from a short section of the bent whisker. It is, therefore, often necessary to view the crystal at a low level of illumination and to obtain diffraction

patterns with the minimum alteration of the condenser settings. These difficulties become particularly significant when attempts are made to obtain a series of diffraction patterns at different orientations using the goniometer specimen stage.

Further difficulties arise from the density of the whisker growth. Only a few whiskers on any specimen grow significantly longer than their neighbouring crystals and can be isolated for selected area diffraction. To reduce the number of surrounding crystals disc specimens were electrochemically perforated to provide a central hole with a sharp edge from which only a few filaments would grow during subsequent oxidation. Despite this precaution it is rare that a number of selected area diffraction patterns may be obtained along the length of a single whisker without influence from neighbouring crystals.

The camera constant has been calibrated against objective lens current as it is not generally possible to position a diffraction standard in the same plane of focus as an oxidation specimen. Changes in objective lens current are minimised by the use of electrochemically thinned specimens, as described above, and the camera constant obtained by this method is normally accurate to within ± 2%.

Difficulties in interpretation of the selected area patterns arise from the nature of the patterns themselves. Pronounced reciprocal lattice streaks exist perpendicular to the whisker and platelet growth directions. Although these streaks assist in determining the orientation relationships between diffraction patterns the intersection of the streaks may lead to considerable displacement of the diffraction spots from their expected positions. The magnitude of this effect in the fine whisker crystals is demonstrated in Figure 6.1 which is a textured ring type diffraction pattern from a number of adjacent whiskers. The streaks are perpendicular to the whisker axis in every case so that the distribution of angles of the projections of the streaks in the diffraction pattern represents the

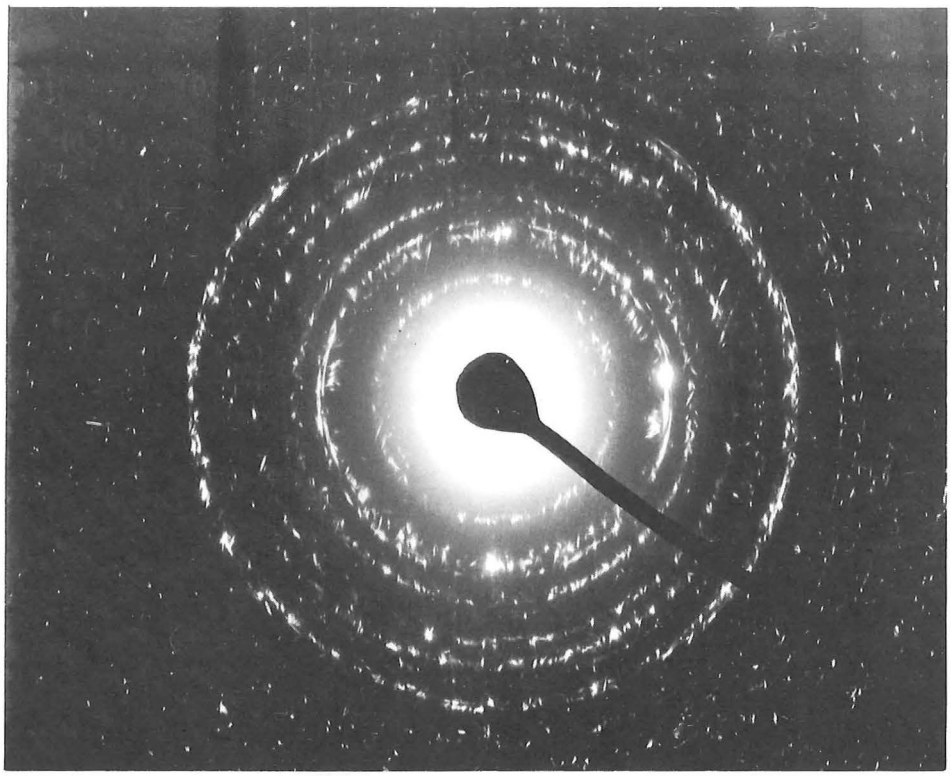

Fig. 6.1 Ring type diffraction pattern from iron oxide whiskers showing extent of reciprocal lattice streaks.

Fig. 6.2 Typical selected area diffraction pattern from a single whisker showing multiple diffracting zones.

distribution of whisker orientations with respect to the oxide surface.

6.2 STRUCTURE OF THE FINE WHISKER CRYSTALS

6.2.1 Structure and Growth Direction

The structure of the fine whiskers has been determined from a number of spot patterns, obtained from sections of individual whiskers, which have been indexed using program XIDENT. Only a small proportion of whiskers provide simple single crystal patterns which may be readily indexed, most patterns observed being of the multiple diffracting zone type shown in Figure 6.2 even when no contrast effects exist in the bright field images to indicate the existence of multiple crystals. Without exception the whiskers have been shown to consist of αFe_2O_3 with $<10\bar{1}>$ growth direction. A summary of the diffracting zones exhibited by these patterns is given in Table 6.1, all patterns being indexed using the αFe_2O_3 structural rhombohedral unit cell described in Appendix 4 with the cell parameters given by Pearson[126]:

$$a = b = c = 0.5427\,\text{nm}$$

$$\alpha = \beta = \gamma = 55.26^{\circ}$$

In all further discussion of αFe_2O_3 the structural rhombohedral cell will be used, the results of published work being converted to this cell where necessary by application of the transformation rules given in the International Tables for X-ray Crystallography[131].

The nature of typical selected area diffraction patterns from fine whiskers is demonstrated in Figure 6.3. The three patterns shown are from whiskers grown at 500°C of approximately 15 nm width and with a length of approximately 1.5 μm within the selected area. In each pattern the electron beam is perpendicular to the whisker axis, the whisker growth direction being indicated by an arrow on each pattern. Most well-defined diffraction patterns from the whiskers are obtained with the electron beam approximately perpendicular to the whisker axis, the [111]

PATTERN NUMBER	ZONE AXIS	ANGLE BETWEEN ZONE AXIS OF PATTERN AND $[10\bar{1}]$	STREAK DIRECTION	ANGLE BETWEEN PROJECTION OF STREAKS AND $[10\bar{1}]$	ANGLE BETWEEN ZONE AXES ON MULTIPLE PATTERNS
1164 H	$[111]$	90.00°	$\perp$ to $(\bar{1}2\bar{1})$	90.00°	
1174 H	$[\bar{1}\bar{3}5]$	45.26°	$\perp$ to (343)	90.00°	
5406	$[1\bar{1}2]$	102.14°	$\perp$ to (131)	90.00°	) 62.51°
	$[1\bar{5}3]$	103.57°	$\perp$ to (545)	90.00°	)
5415	$[1\bar{1}1]$	90.00°	$\perp$ to (121)	90.00°	
5424	$[111]$	90.00°	$\perp$ to $(\bar{1}2\bar{1})$	90.00°	) 32.38°
	$[010]$	90.00°	$\perp$ to (101)	90.00°	)
5442	$[2\bar{1}2]$	90.00°	$\perp$ to (141)	90.00°	
5447	$[1\bar{1}1]$	90.00°	$\perp$ to (121)	90.00°	
5502	$[1\bar{1}1]$	90.00°	$\perp$ to (121)	90.00°	
6016	$[010]$	90.00°	$\perp$ to (101)	90.00°	
6033	$[\bar{3}\bar{3}1]$	66.93°	$\perp$ to $(3\bar{2}3)$	90.00°	) 94.61°
	$[1\bar{3}4]$	67.72	$\perp$ to (353)	90.00°	)
6041	$[\bar{1}5\bar{1}]$	90.00°	$\perp$ to (525)	90.00°	
6091	$[101]$	90.00°	$\perp$ to $(\bar{1}1\bar{1})$	90.00°	

TABLE 6.1 Summary of indexed electron diffraction patterns from iron oxide whiskers. (All patterns indexed for αFe_2O_3 structural rhombohedral unit cell

$a_o = 0.5427$ nm

$\alpha = 55.26^{\circ}$)

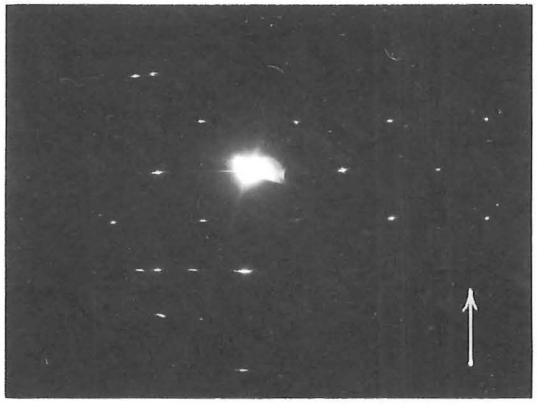

(a)

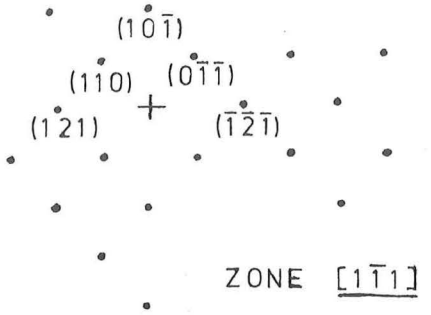

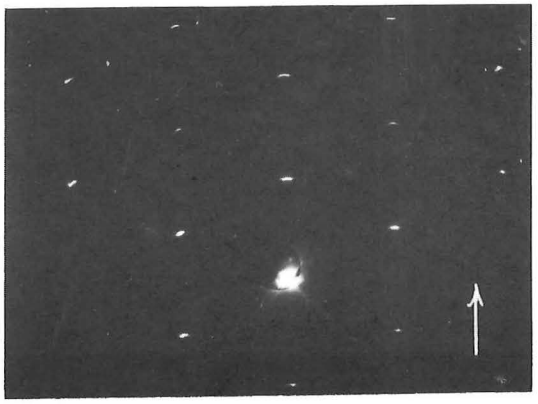

(b)

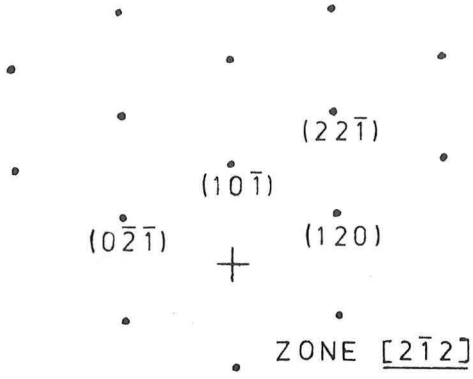

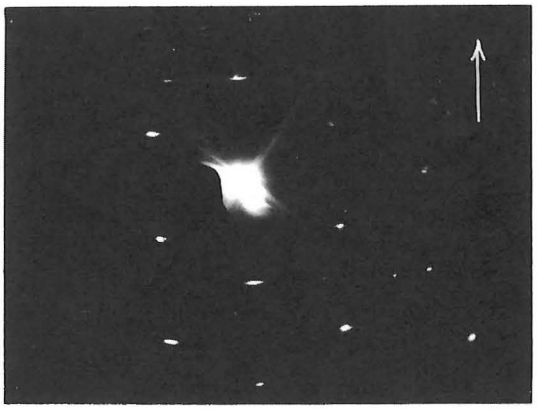

(c)

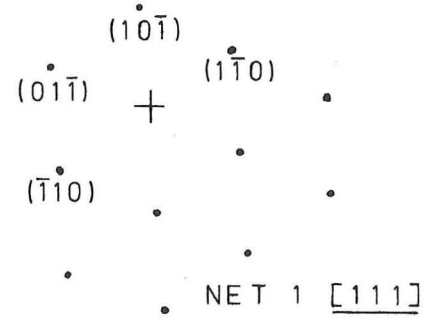

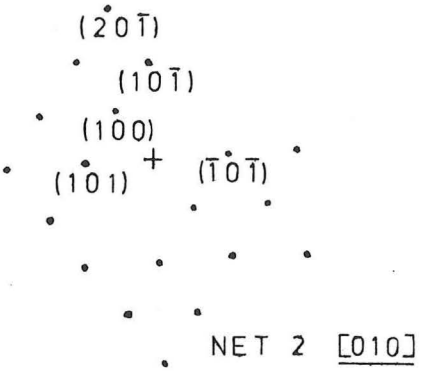

Fig. 6.3 Typical selected area electron diffraction patterns from iron oxide whiskers formed at 500°C. Indexing is in terms of the αFe_2O_3 structural rhombohedral cell.

and [1$\bar{1}$1] orientations being most commonly observed, but in all patterns the projection of the strong reciprocal lattice streaks remains perpendicular to the whisker axis. In each pattern the streaks lie along a reciprocal lattice vector which is in turn perpendicular to a set of direct lattice planes. The angle between these reciprocal vectors and the [10$\bar{1}$] direction has been calculated in Table 6.1, and is shown to be 90.00° in every case.

Forbidden reflections in αFe_2O_3 diffraction result only from the c-glide plane in the case of the primitive rhombohedral unit cell. Reflections of type hhℓ are forbidden where $\ell = 2n$. Despite the small size of the diffracting crystal, which results in all diffraction spots being weak, these forbidden reflections are frequently present as a result of multiple diffraction although they are normally of lower intensity than the surrounding spots. Examples of such reflections are found in spots 22$\bar{1}$ and 1$\bar{2}\bar{2}$ in Figure 6.3 (b).

6.2.2 Absence of evidence of axial twist

Gulbransen *et al*[11,38,41] have extensively studied iron oxide filament growth and the above determination of whisker structure and growth direction is in agreement with their work. However, they did not recognise the multiple crystal nature of the majority of αFe_2O_3 whiskers, and interpreted multiple crystal diffraction patterns as evidence of lattice twist and support for a screw dislocation growth mechanism. The diffraction pattern shown in Figure 6.3 (c), showing a reciprocal lattice net normal to [111] and a second net normal to [010], is identical to a pattern described by Gulbransen *et al*. Both nets include the origin and the spot 10$\bar{1}$ and from this it was concluded that the whisker was twisted about the [10$\bar{1}$] growth axis, which is normal to plane (10$\bar{1}$), such that the two patterns were given by two sections of the same whisker which lie within the selected area. The angle of rotation between the two zone axes is 32.4° which suggested a lattice twist over the 1.5 μm length of whisker

within the selected area of the same order of magnitude as that predicted by the application of the Eshelby theory described in Section 2.3.1 and assuming the presence of an axial screw dislocation. Two other patterns were found by Gulbransen *et al* which exhibited two diffracting zones rotated about $[10\bar{1}]$ and it was assumed that the probability that a small number of untwisted crystals might lie in the special orientations in the beam indicated by these patterns was negligible. The existence of axial screw dislocations was, therefore, assumed to be verified.

In this study three diffraction patterns from sections of fine whiskers have been indexed showing two reciprocal lattice zones rotated about $[10\bar{1}]$ and patterns showing three or more clearly defined superimposed nets of diffraction spots have been observed. Despite the fact that no grain boundaries were revealed by diffraction contrast in the micrographs of these whiskers it is concluded that the whiskers are composed of two or more separate untwisted grains each with $[10\bar{1}]$ growth direction. The three patterns are listed in Table 6.1 and show a lattice rotation about $[10\bar{1}]$ of 32.4°, 62.5° and 94.6°. No common orientation relationship is observed, the parallel planes in each of these dual crystals being $(\bar{1}2\bar{1})//(101)$, $(131)//(545)$, $(353)//(3\bar{2}3)$. Figure 6.4 shows a series of dual crystal patterns which were obtained along the length of a single whisker providing positive evidence that the whisker consists of a pair of untwisted crystals over the 1.5 μm length examined. Spots related to both the reciprocal lattice nets are obtained in all four patterns shown. Further evidence for the lack of axial twist is provided by dark field images formed by diffraction spots from crystal planes parallel to the whisker growth direction. The diffracting conditions for these planes are frequently satisfied over the complete length of a whisker which would not be the case if axial twist of the lattice existed. The many dark field images in which diffraction is limited to a small length of crystal may be interpreted in terms of the

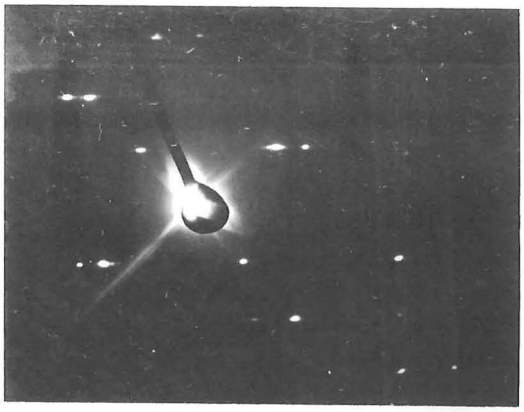

(a)

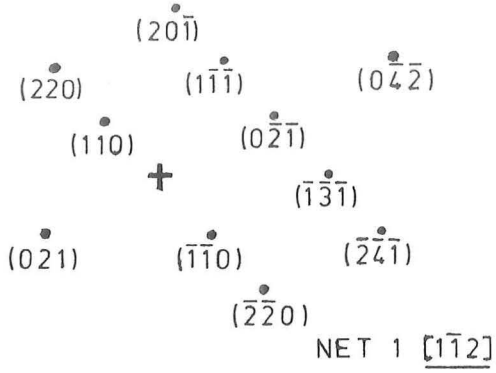

(b)

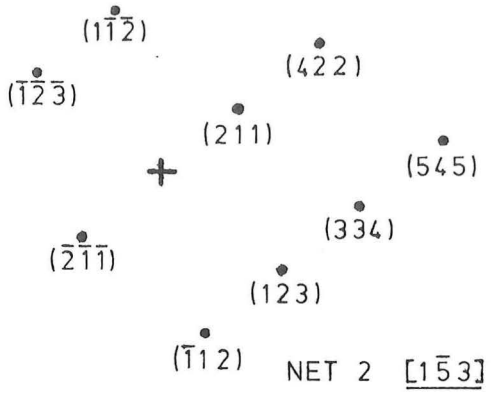

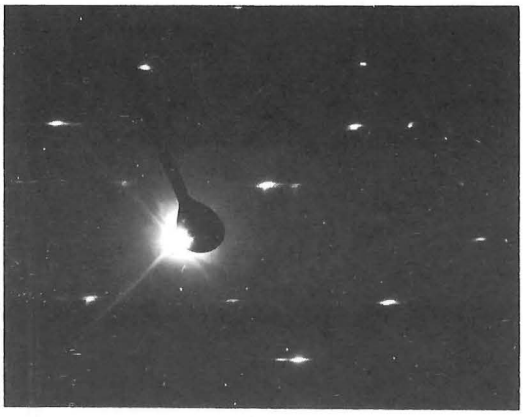

(c)

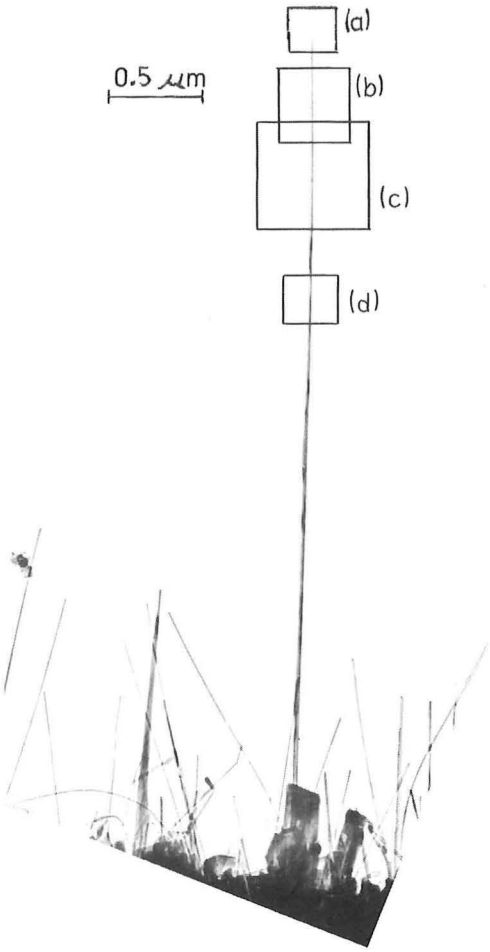

(d)

Fig. 6.4 A series of four selected area diffraction patterns from a section of an αFe_2O_3 whisker formed at 500°C.

observed whisker bending without the requirement for axial twist.

One diffraction pattern has been obtained which suggests that a twin relationship may exist between two crystals composing a whisker. This pattern is shown in Figure 6.5 and may be interpreted within the limits of experimental error as arising from one of two different diffracting zones, namely $[\bar{1}5\bar{2}]$ or $[\bar{1}\bar{3}5]$. The $[\bar{1}5\bar{2}]$ zone axis lies almost perpendicular to the $[10\bar{1}]$ whisker growth direction, the angle of inclination being 83.2°. However, if the pattern is indexed in this way the reciprocal lattice streaks lie parallel to the reciprocal vector corresponding to the lattice plane (423), and hence are not perpendicular to $[10\bar{1}]$ as in all other indexed patterns. The alternative indexing assumes the electron beam to be parallel to $[\bar{1}\bar{3}5]$ which lies at an angle of 45.3° to the $[10\bar{1}]$ whisker axis and which places the streaks perpendicular to $[10\bar{1}]$. Examination of the bright field images of this whisker does not give any indication that such a large angle of inclination exists between the normal to the whisker axis and the electron beam, and the pattern was obtained with a high resolution specimen stage in the JEM 100B microscope which does not have tilting facilities to enable the angle of inclination to be observed. This indexing of the pattern has been chosen and it may be observed that the electron beam is parallel to the (343) twin plane which is perpendicular to the $[10\bar{1}]$ growth direction. The pattern is rotated 180° about the axis [141] which is within 0.1° of the normal to plane (343) and which also lies normal to $[10\bar{1}]$. The length of the reciprocal lattice streaks exhibited by this pattern suggests that multiple twin bands may exist in the whisker, while dark field images from the two nets of spots favour the interpretation that the diffraction pattern arises from two separate crystals growing together with an orientation similar to the twin relationship described. This twin orientation is not supported by any other diffraction pattern.

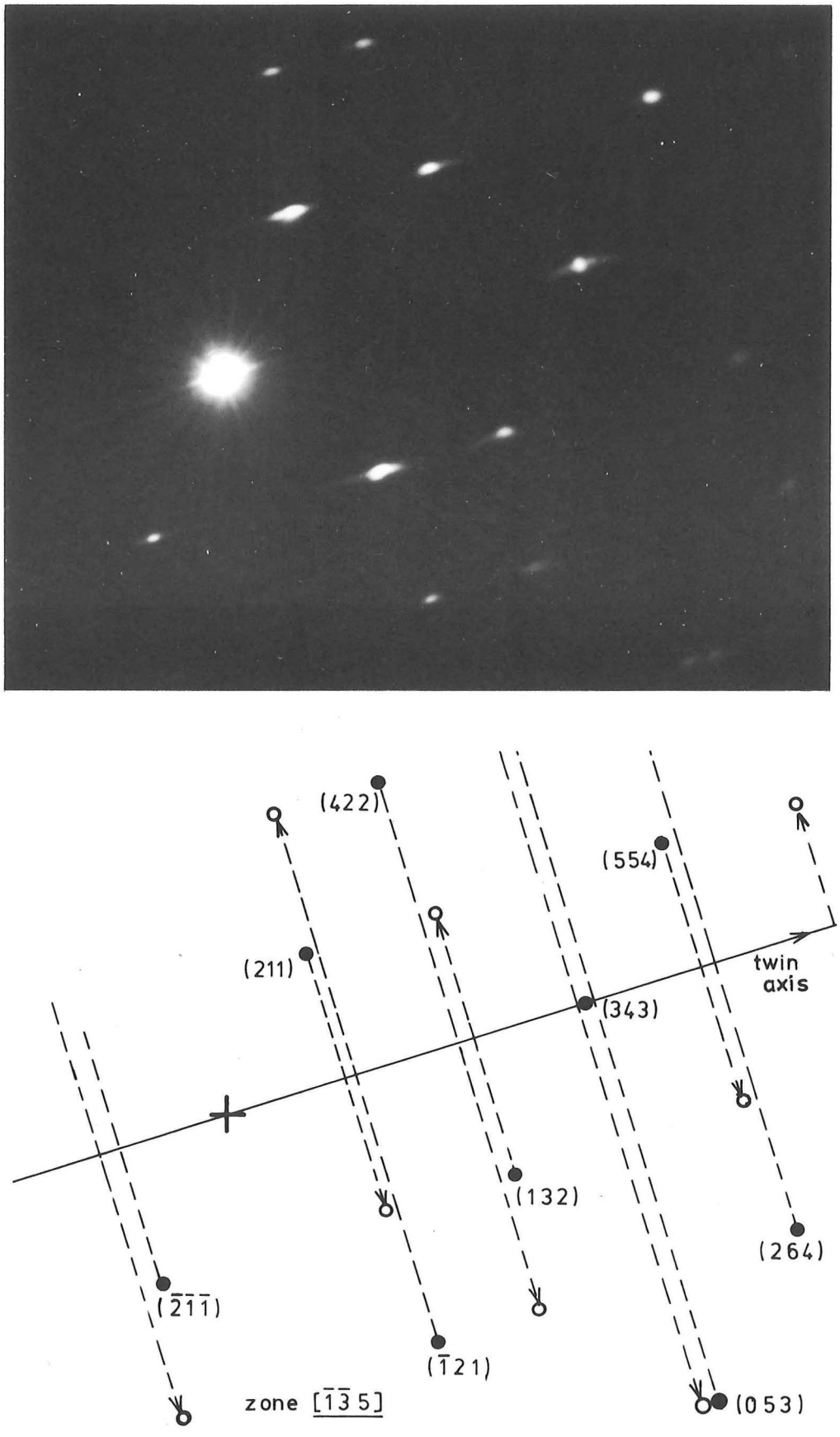

Fig. 6.5 Section of a selected area diffraction pattern from a fine αFe_2O_3 whisker showing twin relationship.

6.2.3 Interpretation of Reciprocal Lattice Streaks

The existence of pronounced extension of the reciprocal lattice points is evidenced by streaking of the diffraction spots normal to the whisker axis in most diffraction patterns. The streak length varies considerably between the diffraction spots but the maximum streak length measured is plotted on a stereographic projection with the $[10\bar{1}]$ growth axis as pole in Figure 6.6. It is observed from this figure that the streaks do not lie exclusively in a single crystallographic direction but the reciprocal lattice points are extended by a disc-like distribution of intensity perpendicular to the whisker axis. Although a disc-shaped intensity distribution in reciprocal space is predicted for a needle-shaped crystal, the external dimensions of the whisker would not be expected to create an intensity region of the magnitude observed. If it is assumed that the observable intensity region extends no further than the first intensity minimum in the diffraction function, the diameter of the reciprocal lattice disc may be considered inversely proportional to the whisker diameter, and the streak length in any single direction as inversely proportional to the crystal dimension normal to the streak[128]. On this basis the observed streak lengths represent crystal dimensions ranging from 5 nm to as small as 0.75 nm which is an order of magnitude smaller than observed whisker diameters. Hence, although the smallest whisker dimensions approach 5 nm the existence of planar defects within the whisker crystal is revealed. These defects lie in a number of different crystal planes parallel to the growth direction and may have a separation distance as small as 0.75 nm.

The nature of these defects has not been determined. The results of an attempt to resolve the faults in high resolution dark field images using a JEM 100B microscope are shown in Figure 6.7. In forming these images the effect of spherical aberration on the resolution was minimised by tilting the diffracted beam so that it passed directly along the axis of the microscope viewing system. It is observed that a number of whisker

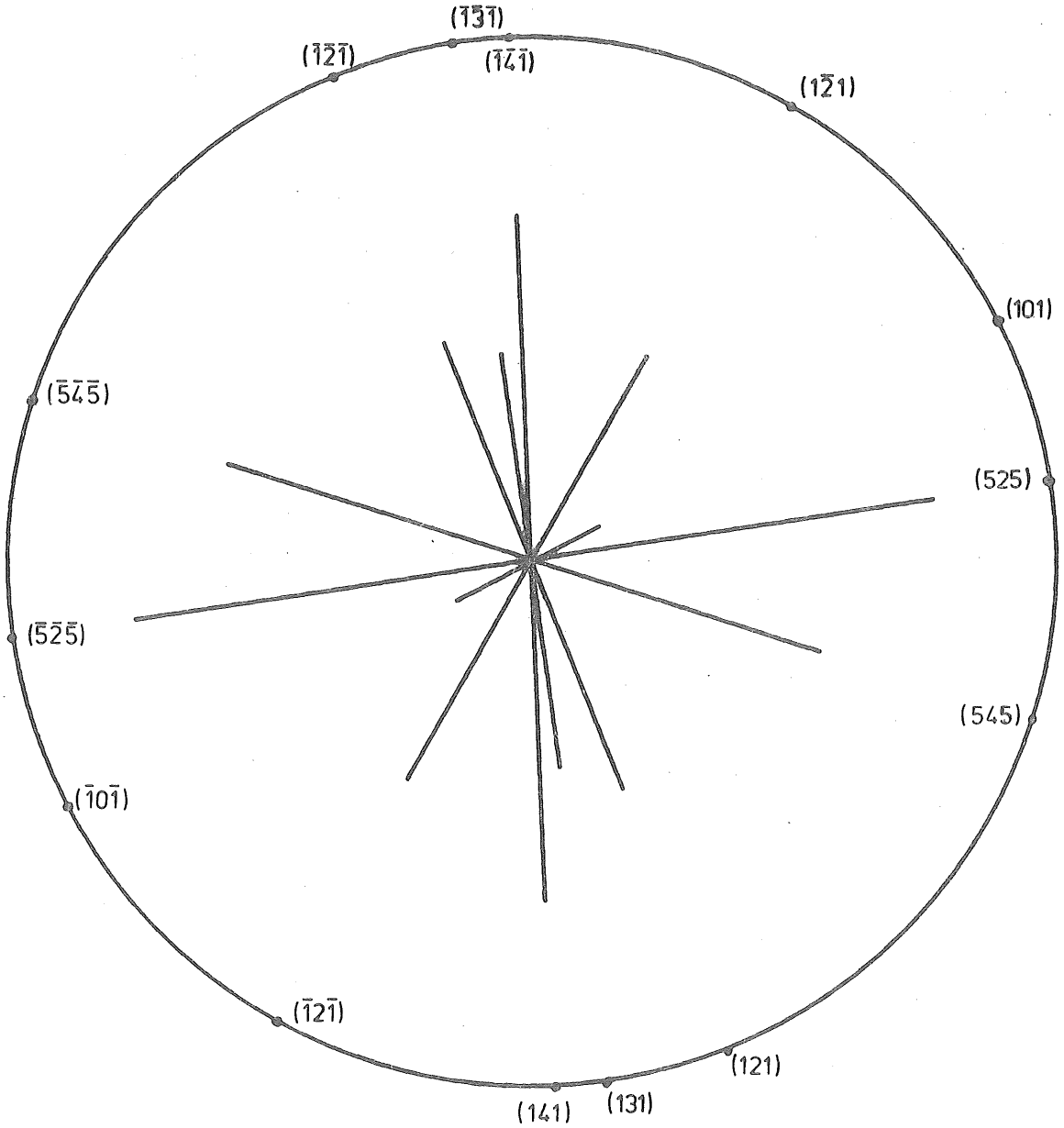

Fig. 6.6 Magnitude of reciprocal lattice streaks as measured in diffraction patterns from fine αFe_2O_3 whiskers. The streaks all lie in a plane normal to the $[10\bar{1}]$ growth direction and have been superimposed on a $[10\bar{1}]$ stereographic projection to demonstrate the two-dimensional nature of the extended interference region about the reciprocal lattice points. The scale of the streaks is 20 x maximum measured streak length on the photographic plates.

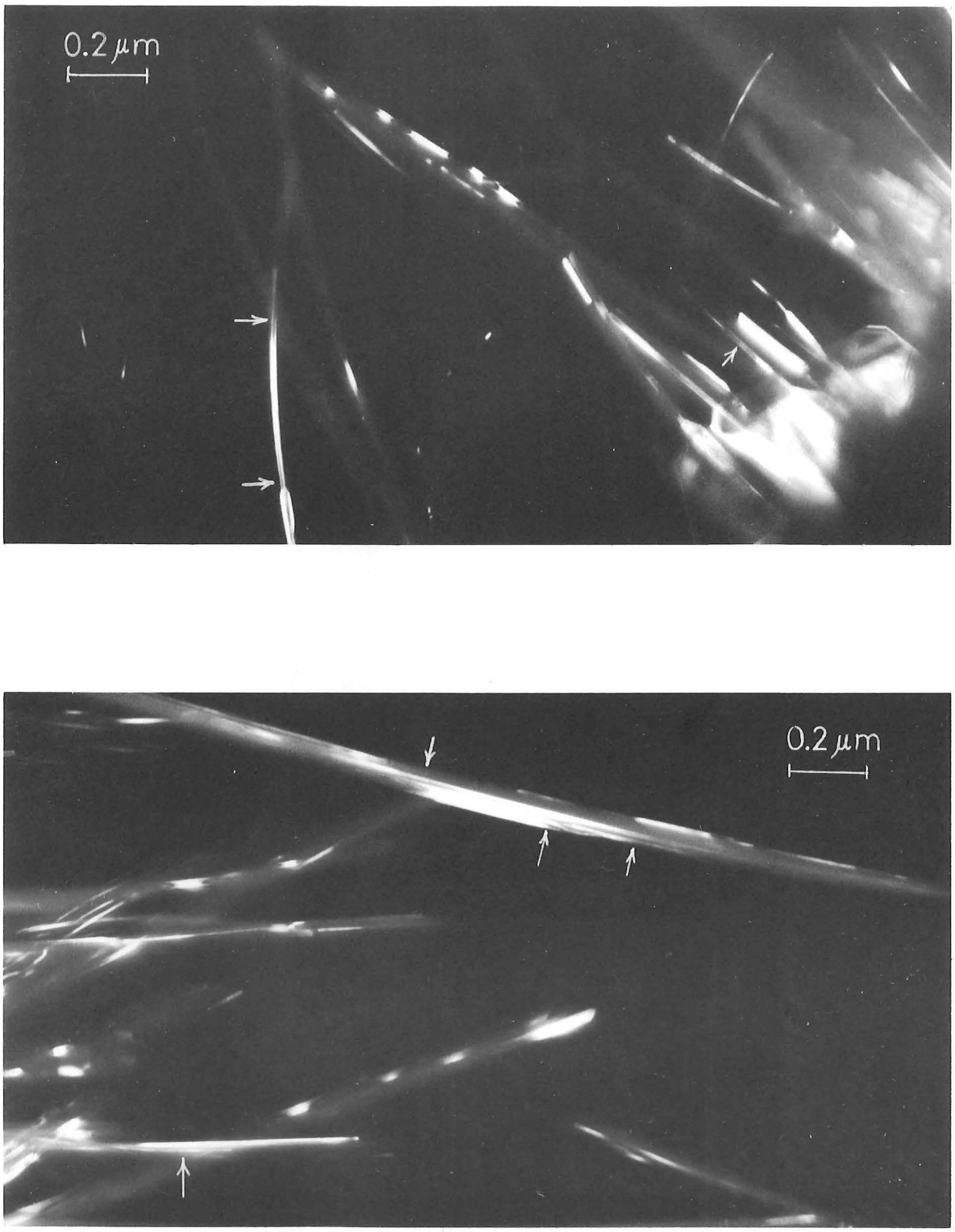

Fig. 6.7 High resolution dark field images reveal faults in fine whiskers.

sections (arrowed) show diffracting regions parallel to the growth direction which are separated by faults of approximately one nanometer thickness.

The contribution of whisker vibration to fine structure in the diffraction patterns is not known. When the electron beam is not parallel to the sheets of intensity which surround the reciprocal lattice points in a plane perpendicular to the $[10\bar{1}]$ growth direction, it is expected that the intersection of these sheets with the sphere of reflection will result in the formation of curved streaks in the diffraction pattern[129]. However, curved streaks are also observed in a number of diffraction patterns obtained with the electron beam perpendicular to the growth direction such as the diffraction pattern from the $2\bar{1}2$ zone shown in Figure 6.3 (b). This curvature may be introduced by the small changes in orientation resulting from whisker vibration.

6.3 STRUCTURE OF THE LARGER WHISKERS OF RIBBON SECTION

6.3.1 Nature of the Diffraction Patterns from Ribbon Crystals

Diffraction patterns are readily obtained from the larger whisker crystals grown above 600°C. The crystals are stable under the electron beam and are of sufficient size that their tips are often separated from those of neighbouring crystals. Two selected area diffraction patterns from sections of these larger whiskers are shown in Figure 6.8, the patterns indicating an αFe_2O_3 structure with $\langle 10\bar{1} \rangle$ growth direction which is identical to that of the fine whiskers formed at lower temperatures.

The most striking feature of the diffraction patterns is the existence of rows of weak additional spots in layer lines normal to the $[10\bar{1}]$ growth direction. These extra spots have been observed by Takagi[34], Talbot and Bigot[39], and Gulbransen *et al*[11] but no explanation of their presence has been given. The number of extra spots which lie on the reciprocal lattice vectors normal to $[10\bar{1}]$ varies according to the

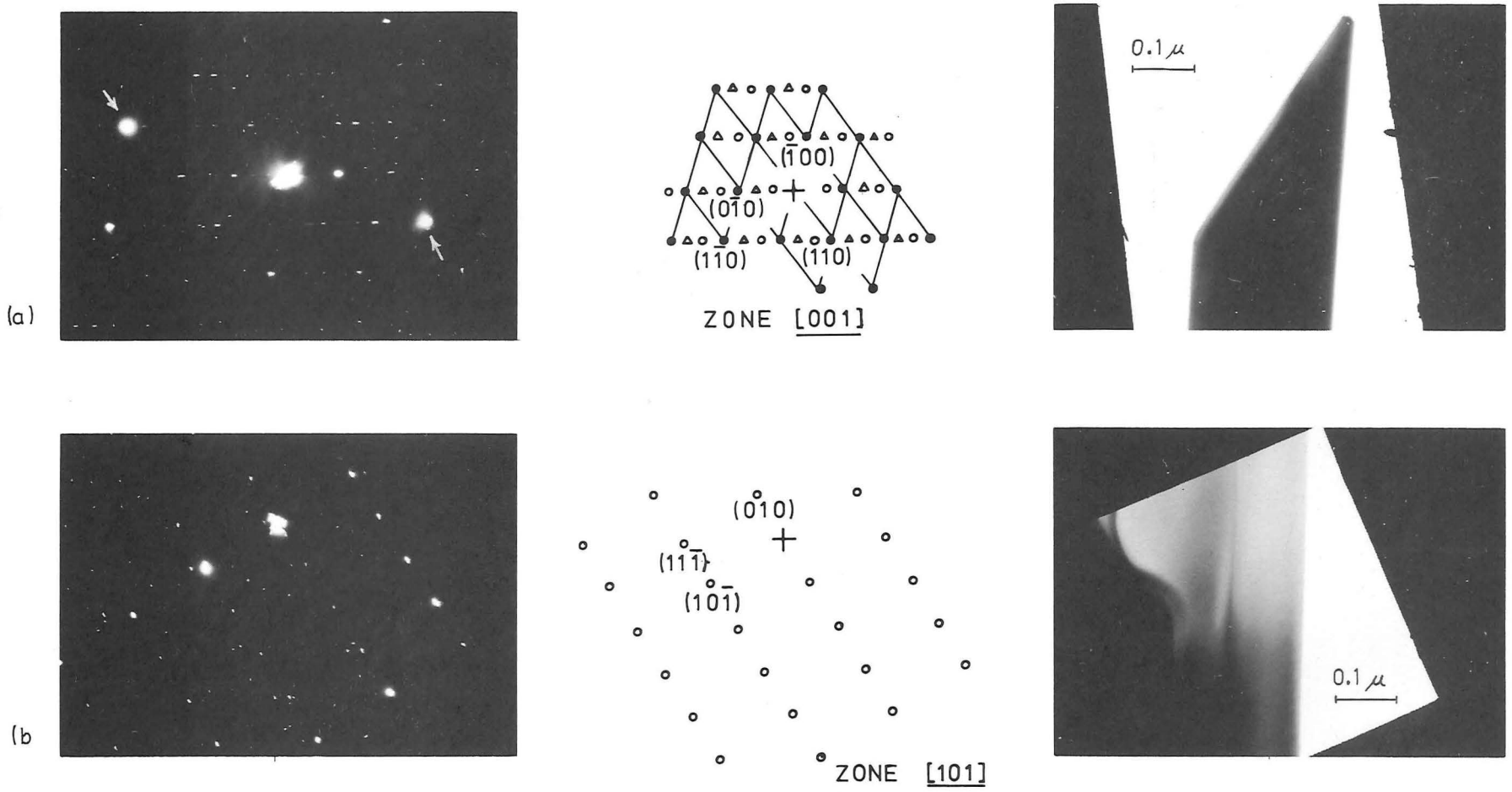

Fig. 6.8 Selected area diffraction patterns from large whiskers of ribbon section showing extra spots due to multiple diffraction.

orientation of the electron beam. Two equally spaced extra spots are found on the 010 reciprocal vector in Figure 6.8 (a) which shows the diffraction pattern corresponding to the 001 reciprocal lattice plane; six extra spots lie on the $1\bar{1}1$ reciprocal vector in Figure 6.8 (b) which shows the 011 diffracting zone; and in the commonly observed 111 diffracting zone nine additional spots have been observed along the $1\bar{2}1$ reciprocal vector.

The additional reflections cannot be indexed normally and are assumed to result from multiple diffraction. In Figure 6.8 (a) a number of primary diffraction spots of considerable intensity (arrowed) are displaced by reciprocal lattice rods which lie perpendicular to the (111) ribbon face. The rediffracted beams from these reflections produce a set of secondary reflection spots which are marked with open circles. The positions of these reflections may be obtained by displacing the origin of the pattern to coincide with one of the strong displaced primary spots. The remaining reflections, which are identified with open triangles, are the result of threefold or higher order diffraction. These spots are very weak as the intensity of the diffraction spots decreases as the order of diffraction increases.

A number of diffraction patterns from the whisker crystals of smaller dimensions formed at temperatures between $500^{o}C$ and $550^{o}C$ have exhibited similar extra spots on layer lines normal to the growth direction. It is assumed that the whisker structure at higher temperature is essentially the same as that for the finest whiskers with the exception that large numbers of defects may be readily observed in the larger crystals as is shown in Figure 5.6. The source of the reciprocal lattice rods has not been determined but the existence of a high density of faults parallel to the whisker axis is assumed. No twin relationship has been observed.

6.3.2 Measurement of Ribbon Tip Angles

Considerable uniformity of the angularity of the ribbon tips is observed for crystals grown within a temperature range from 600°C to 800°C. This uniformity of growth behaviour is demonstrated by Figure 6.9 which shows the tips of two whiskers growing side by side in the gas reaction chamber at a temperature of 650°C. These ribbons appear to be growing with their flat surfaces approximately normal to the electron beam and the angles associated with their growing tips have been measured from the photographs and compared with those of ten other whiskers lying in a similar orientation. The mean tip angles of all measured whiskers are shown in Figure 6.10 (a). Consideration of these angles and of selected area diffraction patterns from three whisker tips, such as is shown in Figure 6.8 (a), suggests that growth occurs on the $\{20\bar{1}\}$ and $\{20\bar{1}\}$ planes as shown in Figure 6.10 (b). The tip planes shown in this figure $(\bar{1}0\bar{2})$, $(20\bar{1})$ and (201), all lie in the 010 zone, the axis of which is normal to the growth axis $[10\bar{1}]$ and lies at an angle of 32.4° to [111] which is normal to the flat ribbon face. The calculated angles between the tip planes normal to the [010] zone axis are shown in Figure 6.10 (b) and may be compared with the measured angles. The small discrepancies between measured and calculated values may be accounted for by variation of the orientation of the observed whiskers to the electron beam.

A small proportion of ribbon crystals provide single crystal diffraction patterns, most ribbons consisting of a number of parallel crystals growing together with a change of tip orientation occurring at the grain boundary such as is observed in Figure 6.9. The orientation relationships existing between the grains have not been determined.

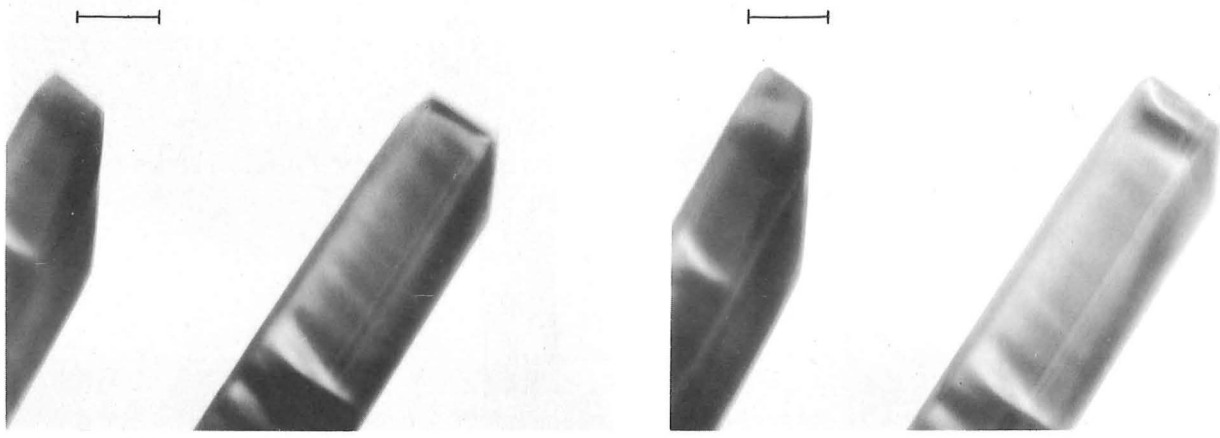

(a) Tip growth after 47 mins at 650°C (b) + 20 seconds

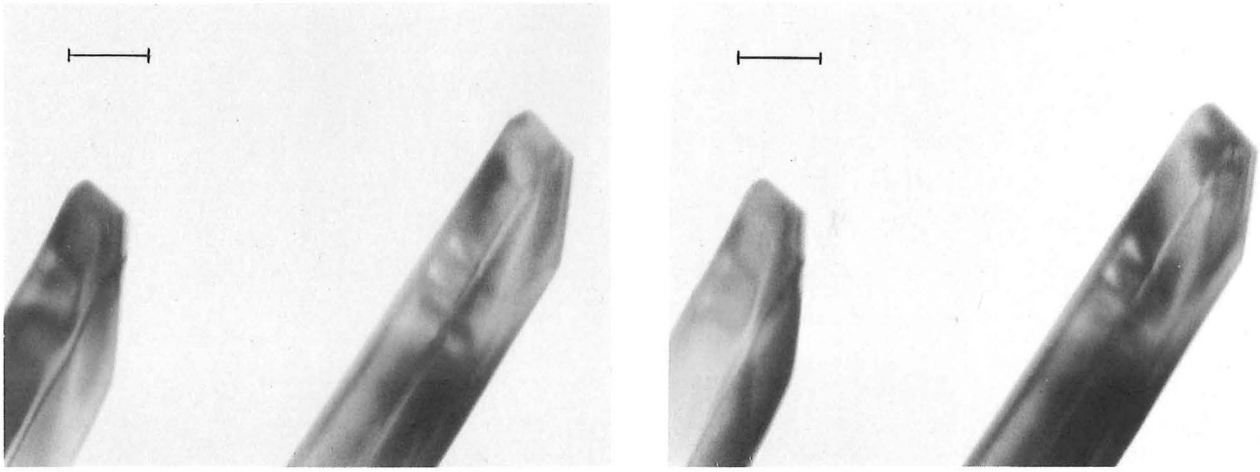

(c) + 35 seconds (d) + 95 seconds

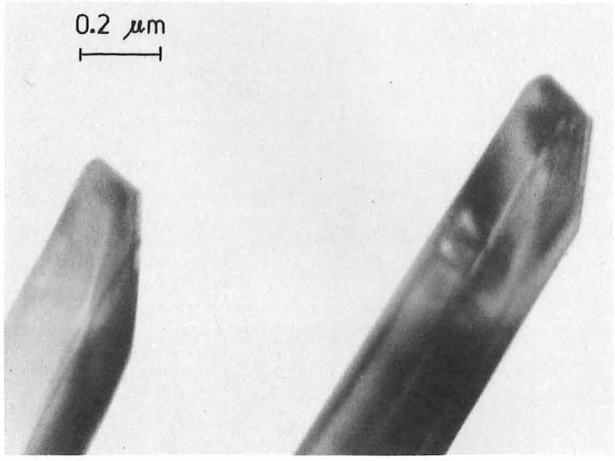

(e) + 100 seconds

Fig. 6.9 High magnification images of the tips of two ribbons growing side by side in the gas reaction chamber at 650°C.

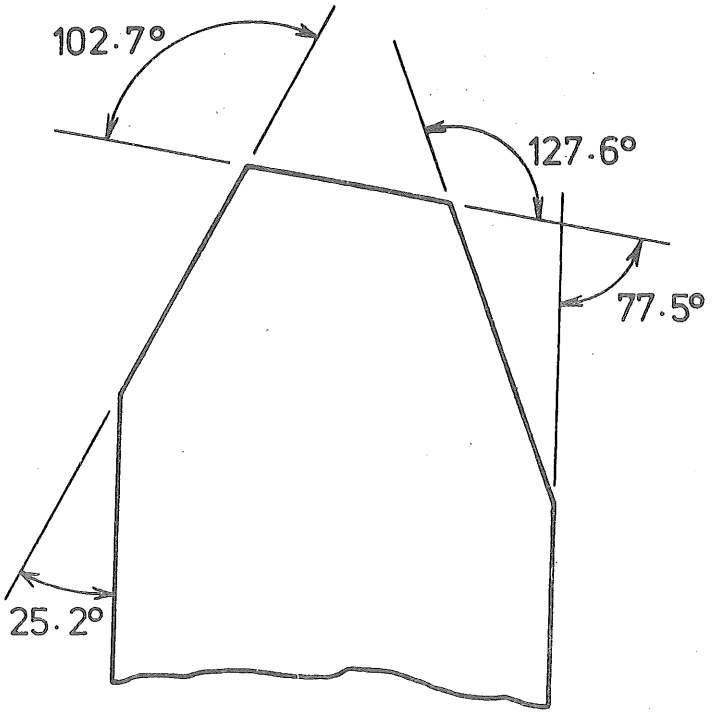

(a) Mean of 20 measurements of the angles associated with the growing tips of ribbon-like whiskers formed at 650°C.

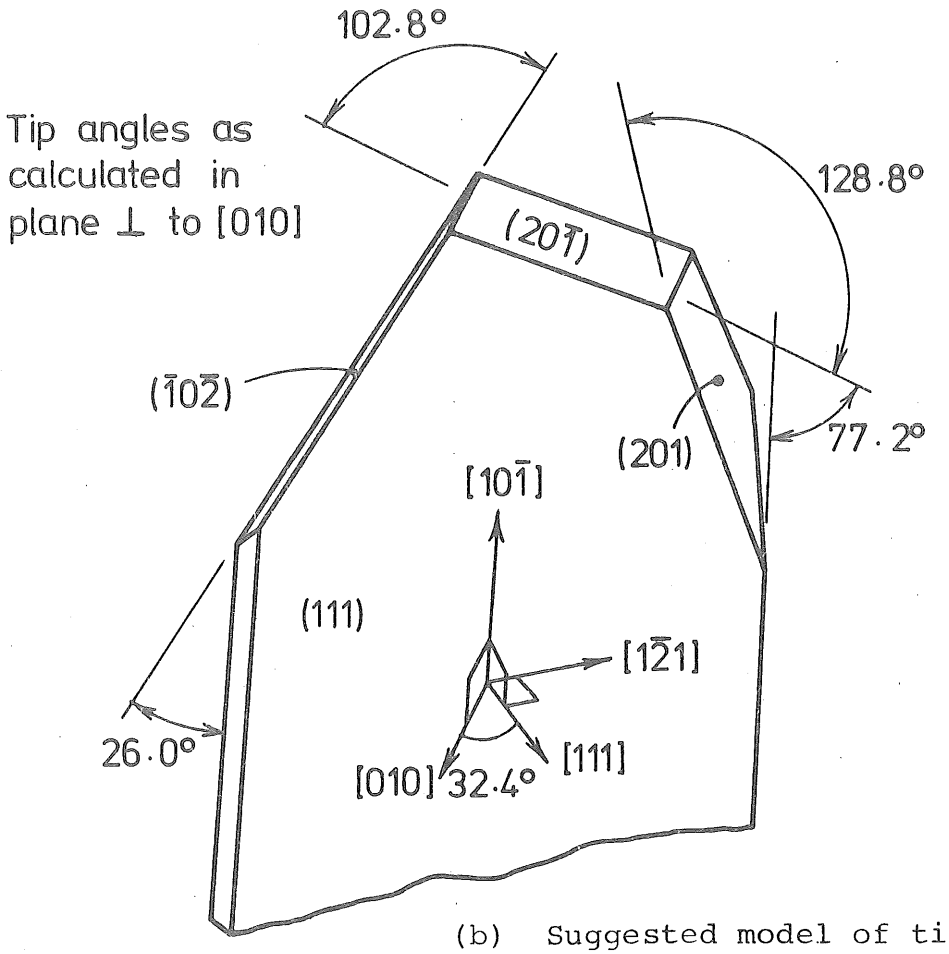

(b) Suggested model of tip growth.

Fig. 6.10 Comparison of measured angles at whisker tips and proposed model of the structure of ribbon-like whiskers.

6.4 STRUCTURE OF PLATELETS FORMED AT LOWER TEMPERATURES

6.4.1 Basic Structure of the Platelets

Selected area electron diffraction patterns from the blade-like platelets formed below 550^{o}C are characterised by continuous reciprocal lattice streaks which link the reciprocal lattice points in a direction perpendicular to the platelet face. These streaks or rods cause considerable distortion of the expected diffraction geometry and give rise to additional spots in diffraction patterns from many orientations of the crystals.

Eight selected area diffraction patterns have been indexed to determine that the platelets consist of αFe_2O_3 with a $[10\bar{1}]$ growth direction similar to that of the whiskers described above. This interpretation is confirmation of the basic structure described by Gulbransen *et al*[11,46] who first recognised the existence of the reciprocal lattice streaks. Previous workers[37,39] had interpreted the distorted patterns with additional spots as arising from the γFe_2O_3 phase. A comprehensive examination of the diffraction patterns obtained using program XIDENT reveals that many patterns can be indexed for γFe_2O_3 within normal experimental limits, but there is no satisfactory correlation between patterns obtained with controlled changes of the beam orientation and no common growth direction is found.

Indexed patterns are shown in Figures 6.11 and 6.12 to demonstrate the effects of the αFe_2O_3 reciprocal lattice rods. These rods lie perpendicular to the $(0\bar{1}0)$ platelet face in a distorted hexagonal pattern corresponding to the projection of the 010 reciprocal lattice plane into a plane lying normal to the streak direction. This plane has no low index indices but is almost parallel to the $1\bar{3}1$ reciprocal lattice plane. The diffraction pattern corresponding to the $[1\bar{3}1]$ zone, with the electron beam almost parallel to the streaks, is shown in Figure 6.11 (a). As the beam is tilted with respect to the streaks considerable distortion of

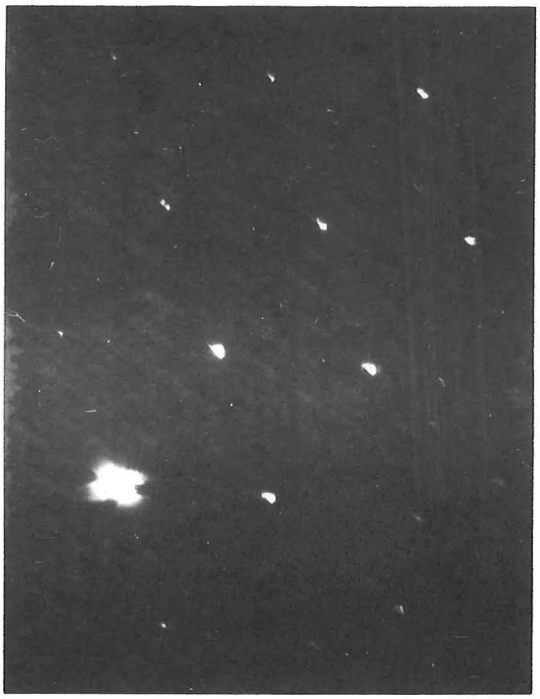

(310) ⟷ = 0.2 μm

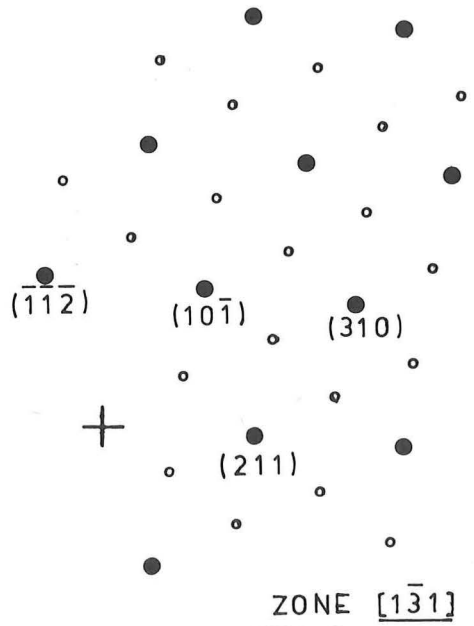

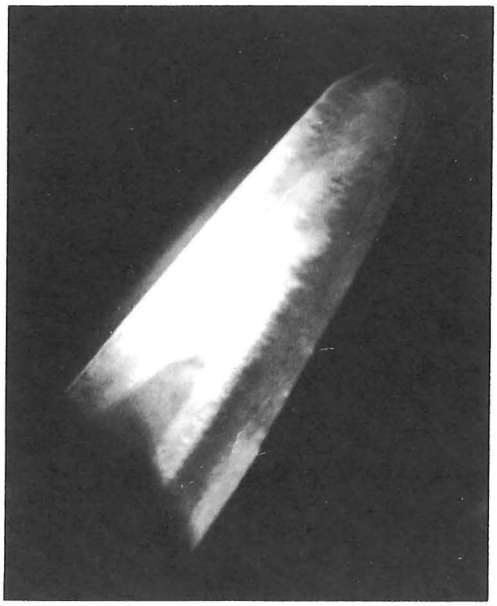

(211)

Fig. 6.11 Selected area diffraction pattern and dark field images from a rounded platelet formed at 500°C.

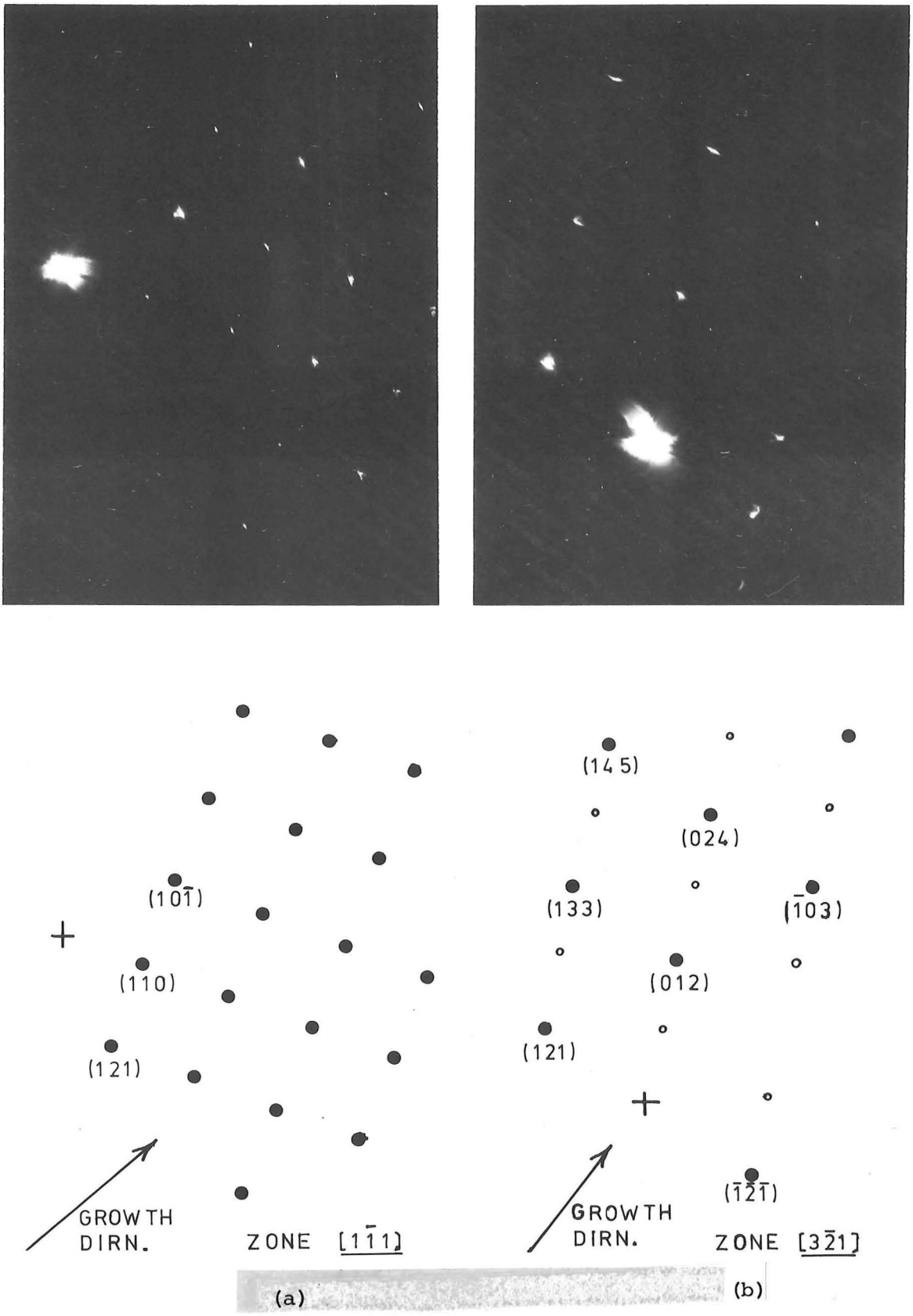

Fig. 6.12 Selected area diffraction patterns from αFe_2O_3 platelets formed at 450°C.

the hexagonal pattern occurs as a result of intersection of the streaks with the reciprocal lattice, but the hexagonal pattern continues to be viewed over a wide range of inclination of the electron beam to the streaks. Considerable curvature of the rows of diffraction spots is commonly observed, the curvature of the reflecting sphere resulting in the rows of the pattern being concave in the direction of tilt of the streaks relative to the beam.

Indexing of the diffraction patterns and examination of the effects of the reciprocal lattice streaks has been accomplished with the aid of a model of the αFe_2O_3 reciprocal lattice. The manner by which the reciprocal lattice streaks produce the extra spots along the layer lines of the diffraction pattern in Figure 6.11 corresponding to the $[1\bar{3}1]$ zone is demonstrated in Figure 6.13.

Additional spots are also produced by the streaks in the diffraction pattern from the $[3\bar{2}1]$ zone shown in Figure 6.12 (a) when the electron beam is inclined to both the platelet face and the $[10\bar{1}]$ growth direction. The orientation may be observed in the stereographic projection in Figure 6.14 on which all zone axes and the poles of crystal planes mentioned in this chapter have been plotted. The reciprocal lattice plane represented by the diffraction pattern shown in Figure 6.12 (b) does not display extra spots. In this instance the electron beam is almost parallel to $[1\bar{1}1]$ which is normal to the streak direction. The continuous streaks are not imaged in this pattern owing to a small misorientation between the electron beam and $[1\bar{1}1]$.

6.4.2 Interpretation of the Reciprocal Lattice Streaks

The platelet crystals are so thin that diffraction is expected to be essentially kinematic, and the continuity of the streaks from one reciprocal lattice point to the next indicates that the lattice perpendicular to the streak direction (i.e. parallel to the platelet face)

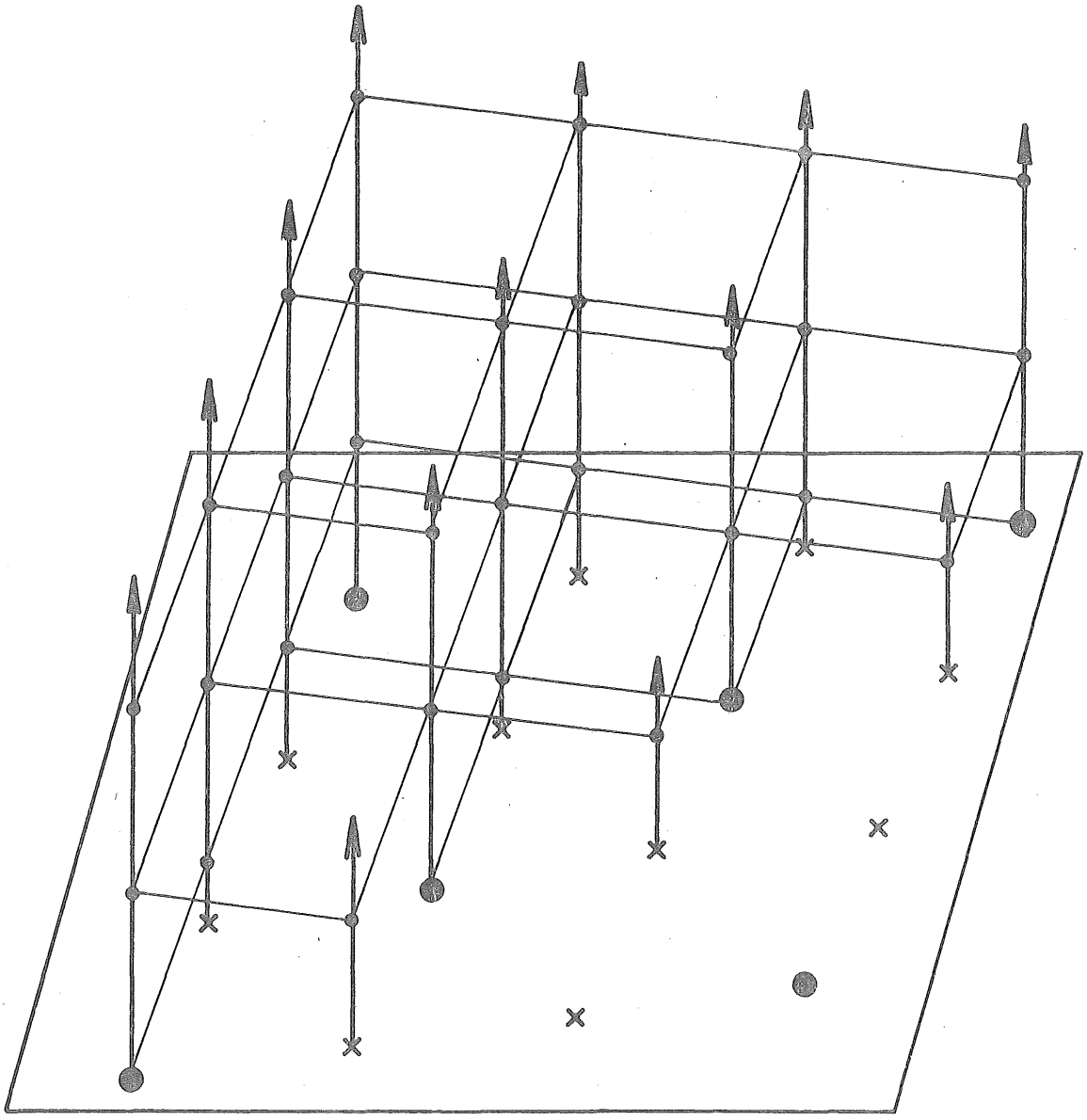

Figure 6.13. The formation of extra diffraction spots in the diffraction pattern corresponding to zone $1\bar{3}1$. The extra spots marked by crosses are caused by the intersection of the continuous reciprocal lattice streaks with the sphere of reflection, which is represented by a plane in the diagram. Normal diffraction spots are shown as large dots.

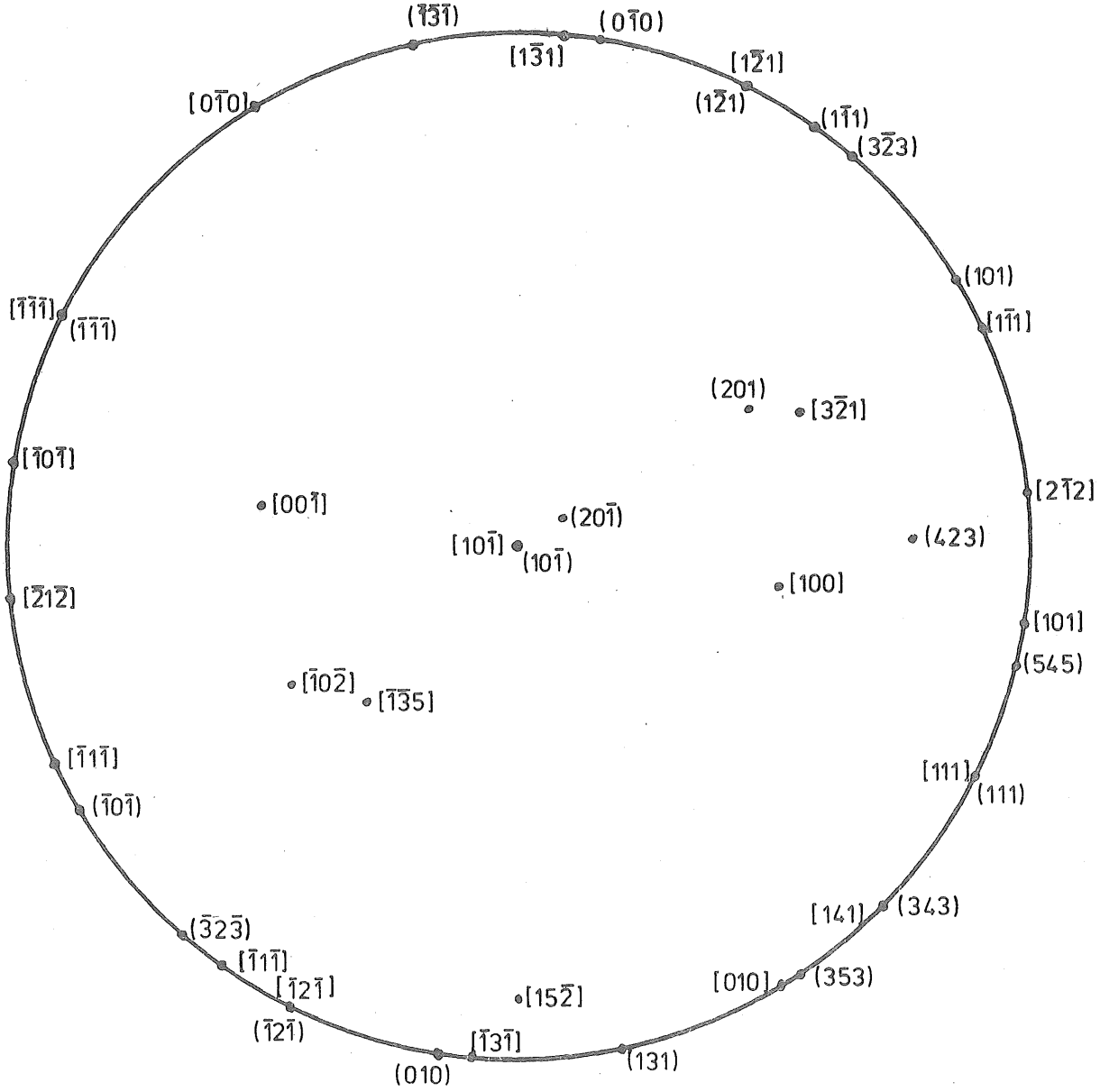

Fig. 6.14 Stereographic projection of αFe_2O_3 with $[10\bar{1}]$ as pole showing all zone axes and poles of crystal planes discussed in this chapter.

must be interrupted every few crystal planes. Gulbransen *et al*[11,46] attribute the high intensity associated with many of the extra spots to twinning, the two crystal orientations being related by mirroring on the blade face plane (010). This mirror plane intersects each reciprocal lattice net in a mirror line normal to the reciprocal lattice rods, and hence the mirror twin of a reciprocal lattice point would lie on the same rod. The indexing of the diffraction patterns obtained in this study does not confirm or refute the existence of such a twinned structure as most patterns do not possess extra spots on the reciprocal lattice rods with sufficiently high intensity to be attributed to any effect other than the intersection of an extended interference region (i.e. reciprocal lattice streak) with the sphere of reflection. The intense spots observed by Gulbransen *et al* may be attributable to the effect of curvature of the sphere of reflection to intersect the primary intensity region of a spot on an adjacent reciprocal lattice plane. The twinning may be present but is not required to index most of the diffraction patterns obtained. It is clear that a high density of twinned crystals or planar faults exists parallel to the platelet surface to create the continuous streaks.

In a small proportion of the diffraction patterns pairs of weak spots are observed which correspond to the anomalous diffraction reported by Gulbransen *et al*. These spots appear as satellite streaks lying at one sixth of the repeat distance between the continuous reciprocal lattice streaks. Their presence may be the result of multiple diffraction effects.

6.4.3 Dark field platelet images

Many dark field images have been examined in an attempt to determine the nature of changes in lattice orientation associated with the contrast effects which are observed in the bright field images of

many platelets. Figure 5.4 demonstrates that if a grain boundary is associated with a change in tip orientation it may be readily identified by dark field observation; but in general the dark field images obtained with the JEM 7A microscope are of limited resolution owing to the lack of beam tilt facilities and the results are often difficult to interpret. Distinct changes in lattice orientation along the centre of the platelets are unambiguously observed in only a small proportion of crystals, the images shown in Figure 6.15 being typical of most pointed crystals. These images are obtained with the electron beam almost parallel to [010] and reveal that elastic bending or buckling is prevalent, particularly in the region of the platelet tip. The change of contrast along the centre of the crystal also appears to be related to bending rather than an abrupt change in lattice orientation, as a change of position of the line of contrast occurs between the images from different beams. An unusual feature of this crystal is the appearance of dark spots of approximately 10 nm diameter which are randomly positioned over the platelet surface. Such spots have not been observed on freshly oxidised specimens and it is possible that they are nuclei of oxide formed at room temperature, this specimen having been stored for 12 weeks subsequent to high temperature oxidation and prior to observation.

The change of contrast along the centre of the platelets is not normally observed in crystals with more rounded tips. The dark field images from a rounded platelet in Figure 6.11 suggest that the contrast effects in these crystals are the result of thickness variation and that overgrowth of the flat surfaces has occurred.

An attempt has been made to obtain dark field images from the weak extra reflections formed by the intersection of the continuous reciprocal lattice rods with the sphere of reflection and also from the anomalous spots described in the previous section. Hirsch *et al*[130]

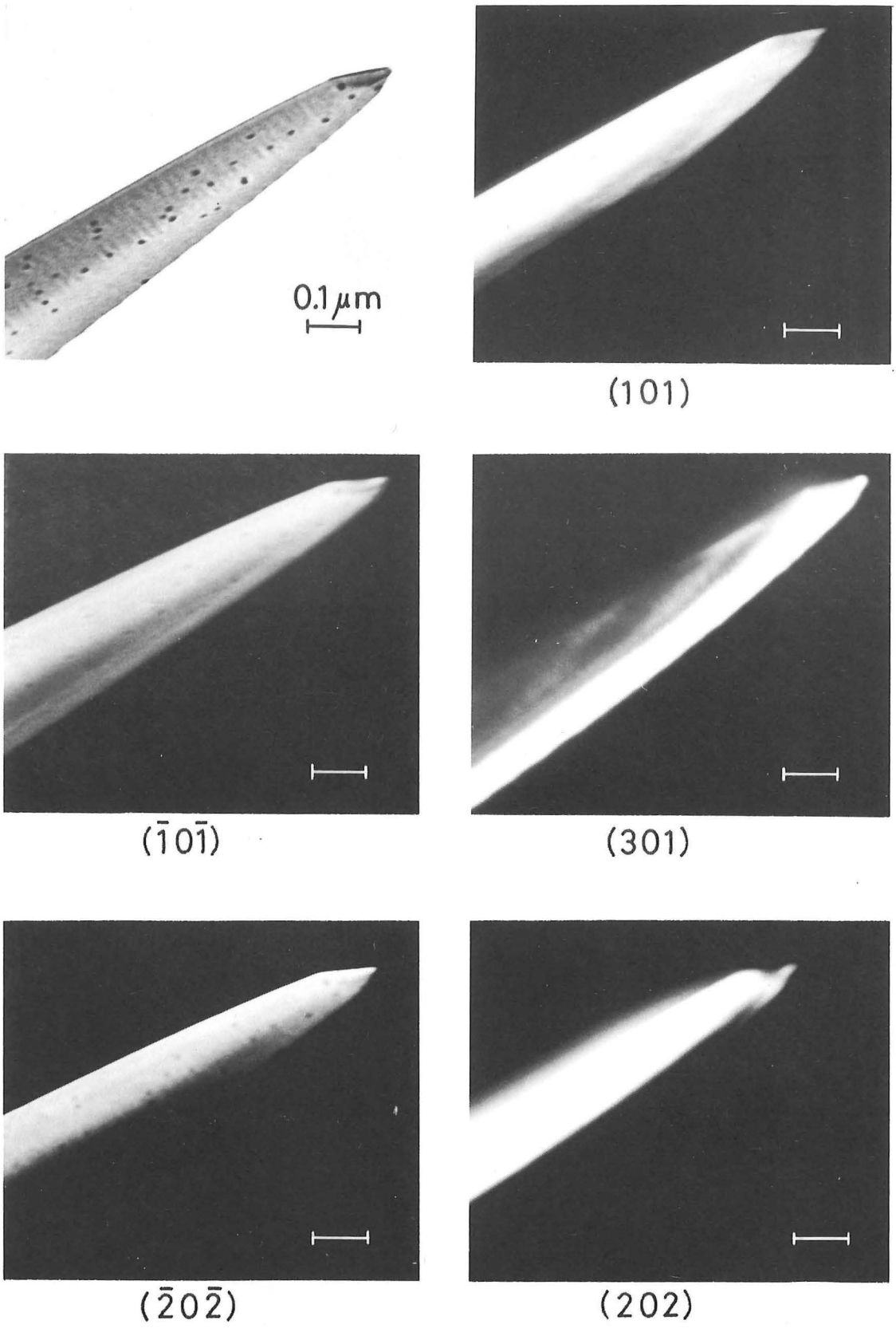

Fig. 6.15 A series of dark field images from an αFe_2O_3 platelet grown at 450°C. The images are obtained from beams corresponding to planes in the 010 zone.

show that anomalous spots in diffraction from gold foils may arise from double-positioning twin boundaries as a result of double diffraction, and Pashley and Stowell[132] have demonstrated that dark field images of the boundaries may be obtained from these spots. The boundaries described by Pashley and Stowell are essentially parallel to the electron beam and hence form highly localised images, whereas the boundaries in the αFe_2O_3 which give rise to the reciprocal lattice streaks lie parallel to the platelet face and imaging is more difficult. The weak diffraction spots from the platelets do not arise from a highly localised region and the intensity of the dark field images is too low for detail to be observed; consequently, a uniformly low intensity image of the complete platelet is normally observed.

CHAPTER 7

DISCUSSION OF RESULTS AND CONCLUSIONS

This project was commenced with the objective of determining the structure and growth mechanism of filamentary oxide crystals, and the degree to which this objective has been achieved will be discussed in this chapter. The results of Chapters 5 and 6 are examined in the light of existing theories of filamentary growth and recommendations for the direction of future work are made. Much of the effort applied to this study has involved the development of experimental techniques for the analysis of structure by electron diffraction and the construction of a versatile reaction chamber to enable direct observation of filament formation in the electron microscope; and the effectiveness of these techniques and their further development and application is also considered.

7.1 COMPUTER ANALYSIS OF ELECTRON DIFFRACTION PATTERNS

Program XIDENT has proved a valuable aid for the direct indexing of electron diffraction spot patterns. All the patterns discussed in Chapter 6 have been indexed by this technique; and in identifying the diffracting phase it has been possible to examine all known iron oxides and, where appropriate, hydrated iron oxides. The major advantage of a direct computer technique is that all possible phases which might exist under the experimental conditions may be examined.

Indexing of the diffraction patterns from the αFe_2O_3 platelets which are described in Section 6.4, demonstrates the ability of the technique to handle experimental error resulting from a number of factors inherent in selected area electron diffraction

with an electron microscope. The diffraction patterns obtained from these platelets may display a highly distorted representation of the reciprocal lattice planes as a result of inclination of the electron beam to the continuous reciprocal lattice streaks which exist as a result of twinning or faulting of the crystals. Extension of the error tolerances of program XIDENT enabled patterns to be indexed in less than 30 seconds processing time on the Burroughs B6718 computer, even though measured diffracted distances were in error by up to 10% and angular relationships between the diffraction spots deviated by as much as six degrees from the angles between the crystal planes which they represent.

One problem associated with the use of a computer program based on a search routine is the difficulty in predicting the computation time required to examine a particular crystal structure. Some experience is necessary to determine the extent to which error limits may be relaxed without excessive expenditure of computation time or generation of a multitude of erroneous solutions. The most precise match of a diffraction pattern to the geometry of the reciprocal lattice plane is frequently not the correct indexing, but erroneous solutions may often be identified by inspection or by comparison with additional patterns obtained from the same crystal by the use of a goniometer.

Limited experience with a variety of computer programs to assist diffraction analysis suggests that a need exists for a computer program capable of producing perspective views of a three-dimensional lattice from any desired orientation. Despite the aid of computer-produced stereographic directions, considerable difficulty was experienced in visualising orientation relationships for the rhombohedral αFe_2O_3 structure without the aid of a reciprocal lattice model. Such a development is a relatively simple extension of current techniques; and the utilisation of interactive computer graphics facilities should permit the display of a variety of relationships such as transformation of unit cells, the geometry of twin

relationships, intersection of the reciprocal lattice by the sphere of reflection, etc. A development of this type is felt to be of greater practical application than further automation of spot pattern measurement and indexing techniques. The extension of program XIDENT to examine specified twin relationships would also prove useful.

7.2 PERFORMANCE OF THE TILTING GAS REACTION STAGE

A limited experimental programme has demonstrated that the tilting high-temperature gas reaction chamber is capable of providing images of useful resolution and contrast while maintaining all normal viewing modes on the JEM 7A microscope. The full potential of this instrument has not yet been utilised owing to the time required for development and solution of the initial operational problems described in Section 3.6.

The range of operation of the specimen chamber would be extended by further development of two features: namely, recording of the electron images and measurement and control of specimen temperature. An improvement in image recording is the most obvious need. Dynamic experiments cannot be successfully recorded on glass photographic plates owing to the slow speed of manipulation of the plates and limited camera capacity, and the limited resolution of images obtained by photographing of the fluorescent screen is unsatisfactory. An image intensifier in association with video-tape recording facilities would seem the most suitable solution to this problem provided accurate measurement of electron diffraction patterns can be retained; although a direct recording 16 mm cine camera may be a suitable low cost alternative. The limited accuracy of specimen temperature measurement is a more difficult problem. It is possible to calibrate a particular platinum heater ribbon-thermocouple combination by standard techniques involving observation of phase changes or the melting points of standard materials; however, a lack of knowledge of the heating effects of the electron beam and the distribution

of temperature in the specimen precludes precise temperature measurement. The use of furnace-type specimen chambers, in which the specimen is heated indirectly by radiation, may stabilise temperature fluctuations but will not necessarily lead to more precise temperature measurement. Electron beam heating is characteristic of the *in situ* observation technique.

7.3 SIGNIFICANCE OF GROWTH RATE MEASUREMENTS

The gas reaction chamber has enabled the first accurate measurements, of which the author is aware, of the rate of growth of iron oxide filaments. Previous estimates of the rate of growth have been made by observation of the average terminal lengths of filaments following periods of oxidation at constant temperature for varying periods of time; but it has been clearly demonstrated with the reaction chamber that the terminal lengths of the crystals have little relationship to the rate of growth. One such observation by Takagi[34] suggested that the rate of growth was approximated by

$$\ell = kt^{0.3} \qquad \ldots\ldots 7.1$$

where ℓ is the whisker length, t is time of oxidation and k is a constant which depends on the temperature and which has a maximum value at 700°C - 750°C.

It was assumed that the difference between the measured rate and that expected for a diffusion-limited process ($\ell = kt^{0.5}$) was attributable to radial diffusion leading to whisker thickening. Most other proposed mechanisms for growth of oxide whiskers also assume that the growth rate will be limited by the rate of diffusion of the oxidising species to the whisker tip.

The reaction chamber observations have clearly established that, following an initial incubation period, a linear relationship exists

between the lengths of both whisker and platelet iron oxide crystals and time of oxidation at constant temperature. This linear growth is observed to terminate abruptly at a variety of filament lengths and no further growth is subsequently observed for most crystals. At 500°C a range of growth rates from 0.1 μm/min to 1.6 μm/min has been observed on a single specimen and a growth rate as high as 15 μm/min has been detected at approximately 800°C.

These observations suggest that the rate-limiting step of the growth processes of oxide whiskers and platelets is not diffusion of metal ions to the filament tips as has been previously assumed. The concentration profile which exists for such a diffusion-limited process to proceed must lead to a reduction in the rate of transport as the whisker length increases and the consequent reduction in growth rate should have been readily detected by the experimental method used. It is assumed, therefore, that over the range of whisker lengths observed the diffusion processes are capable of maintaining a sufficiently high concentration of iron at the whisker tips for growth to continue at a rate determined by generation of growth steps, rate of arrival of oxygen atoms, or some other constant rate process.

7.3.1 Rate of Impingement of Oxygen Molecules on the Whisker Tips

A brief examination shows that the rate of arrival of oxygen molecules on the whisker tips is unlikely to provide the rate-limiting step of the growth process. At 500°C a growth rate of 1.6 μm/min was observed in oxygen at a pressure of 2.67 kPa (20 mm Hg). The mass rate of impingement of oxygen atoms ($\overset{o}{W}$) on a whisker tip may be estimated by application of the kinetic theory of gases and is given by[77]

$$\overset{o}{W} = Ap \left(\frac{m}{2\pi kT}\right)^{\frac{1}{2}} \qquad \ldots\ 5.2$$

where A is the cross-sectional area of the whisker, p is the pressure of oxygen over the whisker, m is the mass of an oxygen molecule, k is the molecular gas constant, and T is the absolute temperature of the gaseous phase.

If it is assumed that every molecule which strikes the whisker end is incorporated into the oxide lattice, and if the whisker radius is constant, it can be written that

$$A\rho\overset{o}{\ell} = \frac{\overset{o}{W}}{c}$$

where $\overset{o}{\ell}$ is the rate of length increase, ρ is the density of oxide produced, and c is the proportion by weight of oxygen in the oxide.

By combining equations 5.2 and 5.3 and solving for $\overset{o}{\ell}$

$$\overset{o}{\ell} = \frac{p}{\rho c}\left(\frac{m}{2\pi kT}\right)^{\frac{1}{2}} \quad \ldots\ldots 5.4$$

The density of αFe_2O_3 [133] is approximately 5.24×10^3 kg/m^3, and the proportion by weight of oxygen in αFe_2O_3 is estimated from the phase diagram of Figure 1.1 as 0.30.

$$m(O_2) = \frac{\text{molecular weight}}{\text{Avogadro's number}}$$

$$= 53.13 \times 10^{-27} \text{ kg/molecule}$$

$$k = 1.38 \times 10^{-23} \text{ joules/molecule } K^o$$

Hence at a pressure of 2.67 kPa and temperature of 500^{o}C (773^{o}K) the rate of length increase

$$\overset{o}{\ell} = \frac{2.76 \times 10^{3}}{5.24 \times 10^{3} \times 0.30} \left(\frac{53.13 \times 10^{-27}}{2\pi \times 1.38 \times 10^{-23} \times 773} \right)^{\frac{1}{2}} \text{m/sec}$$

$$= 1.5 \times 10^{-3} \text{ m/sec.}$$

Comparison of this figure with the observed growth rate of 1.6×10^{-6} m/min shows that the supply of oxygen to the whisker tips is not a limiting factor in the growth process, and any concentration profile of oxygen in the atmosphere surrounding the whisker will be insignificant at this pressure.

7.3.2 Growth by Vapour Deposition

A number of authors[77,96,134-138] have examined the problem of whisker growth by deposition from the vapour by considering the impingement of atoms on the whisker surfaces, temporary adsorption of the impinging atoms, and diffusion of atoms along the lateral surfaces to a sink at the whisker tip which is generally assumed to be provided by a screw dislocation. Steady-state growth laws have been derived to describe the characteristics of whisker growth from the vapour, many of which are similar to those observed for the growth of oxide whiskers. An initial exponential growth normally occurs when the length of the whisker is small and most atoms adsorbed on the whisker sidewalls near the base can diffuse to the tip before re-evaporation occurs. As the whisker increases in length these atoms are not able to reach the tip before re-evaporation and a linear growth rate results which is eventually followed by an abrupt termination of growth. This termination of growth is explained in terms of a number of possible factors which include:

a) Poisoning of the tip by adsorption of impurities on growth steps.

b) Accumulation of vacancies at the dislocation which enable it to slip or climb from the whisker.

c) The onset of two-dimensional nucleation on the whisker sidewalls.

The feasibility of a vapour transport mechanism for growth of the αFe_2O_3 whiskers and platelets can be considered by examination of reported measurements of the vapour pressures of the iron oxides which are summarised by Samsonov[139]. The total vapour pressures (metal + oxide + oxygen) are as follows:

FeO	(750°C)	2.14×10^{-15} Pa	(1.6×10^{-17} mm Hg)
Fe_2O_3	(427°C)	2.99×10^{-24} Pa	(2.2×10^{-26} mm Hg)
Fe_3O_4	(725°C)	5.66×10^{-15} Pa	(4.2×10^{-17} mm Hg)

Substitution of the largest of these values in Equation 5.4, with appropriate changes to other factors, yields a value for the whisker growth rate of $\dot{\ell}^{o} = 2 \times 10^{-21}$ m/sec. This calculated value is based on the assumption that only oxide molecules striking the advancing whisker end will contribute to axial growth. The actual growth rate observed is 10^{13} times greater than this value, which suggests that all molecules striking the oxide surface within a radius of 30 mm from the whisker would be required to diffuse to the whisker tip for growth to occur at the measured rate. Clearly, vapour transport is not a significant factor to be considered.

7.3.3 Nucleation and Growth Processes

The linear growth rate provides strong evidence that the nucleation and growth processes which occur at the whisker tip determine the rate of crystal formation, rather than the transport of the reaction components to the growth site. A detailed examination of these crystal growth processes is beyond the scope of this thesis; and in view of the lack of understanding of the nature of the diffusing species, the movement of

growth steps and the effect of atmospheric contaminants, such an examination may not yet be possible. It has been shown that growth of the larger whisker crystals occurs on the {201} and {20$\bar{1}$} crystal faces which are not normal to the [10$\bar{1}$] whisker axis. Any model of whisker growth must, therefore, explain why growth continues in the [10$\bar{1}$]direction and not normal to the growing faces.

It is likely that crystal defects play an important role in such a mechanism. It is generally assumed that the filamentary profile is initially established by poisoning of the growth site so that growth occurs preferentially in certain directions; two dimensions in the case of platelet growth, and one dimension for whisker formation. Maintenance of the filamentary profile as crystal dimensions increase is attributed to the perfection of the crystal side faces, since the growth rate is greatly enhanced by the presence of defects such as dislocations, grain boundaries and re-entrant twin boundaries. The planar faults, which have been detected by the existence of reciprocal lattice streaks, may provide a suitable defect structure for rapid growth on the {201}and {20$\bar{1}$} planes; while, conversely, the perfect crystal faces which comprise the whisker and platelet sidewalls will be unable to grow until very high supersaturations are reached. The high mechanical strength of the filamentary crystals is an indication of the surface perfection of these lateral sidewalls; since imperfections on the surface, such as growth steps would provide stress concentrations which will result in a local reduction in strength.

7.4 WHISKER AND PLATELET STRUCTURE

The structure of both whisker and platelet crystals has been confirmed to be αFe_2O_3, and a common <10$\bar{1}$> growth direction has been determined for all filaments studied by electron diffraction. When iron

is oxidised in air or O_2 the type of filament observed is primarily a function of the oxidising temperature; a predominance of platelets with (010) flat surfaces being observed below approximately 470^{o}C, and a predominance of whisker crystals of ribbon-like cross-section with (111) surfaces being formed above this temperature.

The majority of the whiskers consist of two or more crystals growing together and are not single crystals as has been generally assumed in the literature; but single crystal filaments also exist. Two distinct types of multiple crystals are observed. The first type relates to crystals nucleated together at the base and which grow together at the same rate as a single discrete filament as shown in Figure 5.4; the second type involves whiskers nucleated as separate crystals, often some distance apart, and which grow as separate filaments until they are attracted together by intermolecular forces to continue growth in a common direction. Whiskers of this second type are shown in Figures 5.14 to 5.17.

It is not always possible to distinguish between these two forms of multiple whisker, and it is possible that diffraction patterns from whiskers of the second type have obscured orientation relationships which would be expected to exist between crystals growing together from nucleation. No single clearly defined orientation relationship has been observed in the limited number of multiple crystal diffraction patterns which have been studied; however, the rotation relationship which is observed in the diffraction pattern of Figure 6.3 (c) was also observed by Gulbransen *et al*[11] although it was wrongly interpreted as lattice rotation in a single crystal. This orientation shows $(\bar{1}2\bar{1})$ parallel to (101) in dual crystals with $[10\bar{1}]$ growth direction, and the lattice rotation of 32.4^{o} is the same as that required to bring the (010) and (111) planes parallel to one another. These two planes are the platelet and whisker face planes and a relatively small distortion of the rhombohedral geometry is required to accommodate the lattice mismatch between them.

The description of the αFe_2O_3 platelet structure described by Gulbransen *et al* has been basically confirmed although the twin relationship described by these authors has not been verified. The interpretation of contrast effects, which are peculiar to these crystals, as thickness contours resulting from asymmetrical growth about the tip is shown to be an erroneous interpretation; most of such contrast effects being the result of elastic bending or buckling of the crystals. Grain boundaries have also been observed within the platelet crystals.

7.5 CATION TRANSPORT - SCREW DISLOCATION, GRAIN BOUNDARY or SURFACE DIFFUSION?

Any growth mechanism for oxide filaments must provide for the transport of iron from the base oxide layer or metal surface to the whisker tips at a rate which is consistent with the observed rates of growth. In the absence of suitable vapour transport a short circuit diffusion mechanism is required based on either surface diffusion on the whisker sidewalls, which are of high crystalline perfection, or internal diffusion by way of an axial screw dislocation or grain boundary. The literature has tended to favour transport mechanisms based on an axial screw dislocation, which provides an internal diffusion path with protection from the oxidising atmosphere, but a number of difficulties exist for such proposals. The first of these is the lack of experimental evidence of the existence of such dislocations. In view of the ease with which dislocations may be imaged in both bright field and dark field images of the larger iron oxide whiskers, it would be expected that continuous axial screw dislocations would be readily detected; but they are not observed in most whiskers. The absence of lattice twist in the finer whiskers is further evidence to suggest that such dislocations do not exist. Although two or more dislocations of opposite sign, of the type described in Section 2.3.1 might provide a source of continuous growth steps at the whisker tip

without resultant twist of the crystal lattice, their mutual annihilation would result in a dislocation-free crystal with no short circuit diffusion path from base to tip.

An examination of the rate of diffusion required within a single axial screw dislocation to account for a whisker growth rate of 0.6 μm/min has been made by Gulbransen *et al* [11]. The driving force for migration of cations to the whisker tip was assumed to be the oxidation of Fe_3O_4 to Fe_2O_3 assisted by compressive stress in the oxide layer, and the whisker was assumed to be of 10 nm diameter with an effective dislocation core diameter of 0.6 nm. A diffusion coefficient for iron transport within the dislocation core of 4×10^{-9} cm^2/sec was shown to be required. This diffusion coefficient was compared with measured data for the bulk diffusion of iron in αFe_2O_3 at similar temperatures by assuming the bulk diffusion to take place through screw dislocations with a density of 10^8 cm^{-2} lying normal to the cross-section under consideration. If it is assumed that all such dislocations have a diffusion coefficient similar to that estimated for the dislocations in the αFe_2O_3 whiskers, then the bulk diffusion coefficient should be 10^{10} times higher than is actually observed. Hence, it is clear that normal screw dislocations in αFe_2O_3 do not possess diffusion properties such as would be required to account for the observed rates of whisker growth. It seems unlikely that discrepancies of this magnitude can be explained in terms of a different dislocation core structure or the existence of multiple axial dislocations within the whiskers.

Similar arguments may be used to show that grain boundary diffusion is also unlikely to provide a sufficient flux of iron to account for the observed rates of growth. Grain boundaries are observed in many, but not all, whisker crystals; and the existence of planar defects such as faults or twin boundaries has been demonstrated in the platelet crystals by the

existence of continuous reciprocal lattice streaks. The mobility of oxygen on such boundaries would also be expected to be high and diffusing cations would not receive protection from the oxidising atmosphere.

In view of these inadequacies of internal diffusion mechanisms, and the strong evidence for surface diffusion activity which is provided by the meniscus-shaped accumulation of material at the whisker bases and at points of filament contact, it is concluded that surface diffusion provides the predominant mode of cation transport to the whisker tips. The nature of such a diffusion process in the presence of a high pressure of oxygen is a matter of conjecture as the knowledge of surface diffusion under such conditions is not well developed. It is assumed that oxide molecules adsorbed on the whisker and platelet surfaces will provide mass transport under the influence of a concentration gradient created by the effective sink at the filament tip where growth occurs. It is difficult to imagine a long distance migration of oxide molecules over the base oxide layer without an alternative growth site being encountered, but a high mobility would be expected on the perfect filament sidewalls. It is convenient to assume the existence of perpetual growth steps at the filament tips provided by the emergence of defects, but further work is required to determine the nature of such defects and the reason for the abrupt termination of growth.

7.6 RECOMMENDATIONS FOR FUTURE WORK

The limited test programme using the gas reaction stage has illustrated a number of important features of filamentary oxide growth which require further examination. A closer examination of the defect structure of both whisker and platelet crystals is required to determine the relationship of defects to the growth mechanism. High resolution cine images from the growing tips of the larger whisker filaments may provide considerable information on the generation and propagation of growth steps in relation

to grain boundaries, twin interfaces, dislocations and other defects, and the means by which growth is abruptly terminated may be observed. Determination of the temperature dependence of the growth rate, the effect of different oxidising atmospheres, the introduction of atmospheric contaminants and other variation of the oxidising conditions, may also provide additional information.

Preliminary investigations into the oxidation of copper reveal a very similar filament growth behaviour to that of iron. Streaking of the diffraction patters from CuO whiskers and platelets suggests that similar defects exist in these crystals to those observed in the αFe_2O_3 filaments, and extension of the gas reaction chamber studies to such metals may provide further information regarding filamentary growth processes.

Preliminary investigations have been made into the feasibility of observing the initial nucleation stage of filament formation by *in situ* oxidation of thin foils in the reaction chamber. Foils of iron have been found to adhere readily to a platinum heater ribbon when collected on the ribbon from a water surface, and formation of an initial oxide layer has been detected by observation of selected area diffraction patterns; however, further development of the technique is required before it will be possible to observe the nucleation of filaments and relate growth sites to features such as surface defects in the foil or oxide layer.

REFERENCES

1. LANDER, J.J. Chemisorption and ordered surface structures. Surf. Sci. 1, 1964: 125.

2. RHODIN, T.N. *et al* Nucleation and growth of oxide on metals. Mem. Sci. Rev. Metall. 62, 1965: 67.

3. KOFSTAD, P. High-temperature oxidation of metals. New York Wiley, 1966. 340p.

4. BENARD, J. The oxidation of metals and alloys. Metall. Rev. 9 1964: 473.

5. KUBASCHEWSKI, O. and HOPKINS, B.E. Oxidation of metals and alloys. London, Butterworths, 1962. 319p.

6. Boggs, W.E. *et al* The effect of oxygen pressure on the oxidation of zone-refined iron. J. Electochem. Soc. 112, 1965: 539.

7. WAGNER, C. The formation of thin oxide films on metals. Corros. Sci. 13, 1973: 23.

8. WAGNER, C. Theory of the tarnishing process. Z. Phys. Chem. B.21, 1933: 25.

9. WAGNER, C. Diffusion and high temperature oxidation of metals. *In* American Society for Metals. Atom movements. Cleveland, Am. Soc. Metal, 1951, p. 153-173.

10. HAUFFE, K. Oxidation of metals. New York, Plenum Pr., 1965. 452p.

11. GULBRANSEN, E.A. and TALLMAN, R.L. Chemical physics of surface reactions on metals. Pittsburgh, Pa. Westinghouse Electric Corp., 1967. 127p. AD-653723

12. BARDOLLE, J. and BENARD, J. On the effect of the crystalline orientation of iron on the surface formation of oxide nuclei at low pressures of oxygen and high temperatures. c.r. Acad. Sci., Paris, 239, 1954: 706.

13. HONDROS, E.D. On the presence of oxide nuclei and dislocations on the surfaces of pure iron at 500°C. Mem. Sci. Rev. Metall. 62 suppl., 1965: 57.

14. RÖNNQUIST, A. and THOMAS, K. Nucleation of oxide on thin films of pure iron. Br. Corros. J. 1, 1965: 47.

15. BOGGS, W.E. *et al* The effects of crystallographic orientation and oxygen pressure on the oxidation of iron. J.Electochem. Soc. 114, 1967: 32.

16. SEWELL, P.B. and COHEN, M. An electron diffraction study of thin oxide films on iron single crystals. J. Electrochem. Soc. 111, 1964: 58.

17. LAUKONIS, J.V. and COLEMAN, R.V. High temperature oxidation of iron whiskers. J. Appl. Phys. 30, 1959: 1364.

18. COLEMAN, R.V. The growth and properties of whiskers. Metall. Rev. 35, 1964: 261.

19. BUDNIKOV, P.P. and SANDULOV, D.B. Preparation and investigation of filamentary single crystals (whiskers) of beryllium oxide. J.Appl. Chem. U.S.S.R. 43, 1970: 1667.

20. ARNOLD, S.M. and KOONCE, S.E. Filamentary growths on metals at elevated temperatures. J. Appl. Phys. 27, 1964: 964.

21. NABARRO, F.R.N. and JACKSON, P.J. Growth of crystal whiskers, a review. *In* Doremus, R.H., *et al*, eds. Growth and perfection of crystals. New York, Wiley, 1958. p.11-101.

22. HARGREAVES, C.M. On the growth of sapphire microcrystals. J.Appl. Phys. 32, 1961: 936.

23. EDWARDS, P.L. and HAPPEL, R.J. Alumina whisker growth on a single crystal alumina substrate. J. Appl. Phys. 33, 1962: 826.

24. WEBB, W.W. *et al* Dislocations in whiskers. Phys. Rev. 108, 1957: 498.

25. WEBB, W.W. Dislocation structure of whiskers. *In* Doremus, R.H. *et al*, eds. Growth and perfection of crystals. New York, Wiley, 1958. p.230-238.

26. DRAGSDORF, R.D. and WEBB, W.W. Detection of screw dislocations in αAl_2O_3 whiskers. J. Appl. Phys. 29, 1958: 817.

27. SEARS, G.W. and DEVRIES, R.C. Morphological development of aluminium oxide crystals grown by vapour deposition. J.Chem. Phys. 39, 1963: 2837.

28. CAMPBELL, W.B. Growth of whiskers by Vapor-phase reactions. *In* Levitt, A.D. ed. Whisker technology. New York, Wiley, 1970. p.15-46.

29. WIEDEMANN, H.G. *et al*. Growth morphology of alumina whiskers. Naturw. 61, 1974: 65.

30. BARBER, D.J. Electron microscopy and diffraction of aluminium oxide whiskers. Phil. Mag. 8th ser.10, 1964: 75.

31. HART, R.K. Morphology of corundum films on aluminium. International congress for electron microscopy, 5th, Philadelphia, 1962. Electron microscopy. New York, 1962. 2v. p.C-10.

32. HURLEN, T. Oxidation of titanium. J. Inst. Metals. 89, 1960: 128.

33. GULBRANSEN, E.A. and COPAN, T.P. Effect of stress and environment on the microtopology of the corrosion product. *In* Rhodin, T.N. ed. Physical metallurgy of stress corrosion fracture. New York, Wiley-Interscience, 1959. p.155-180.

34. TAKAGI, R. Growth of oxide whiskers on metals at high temperatures. J. Phys. Soc. Japan, 12, 1957:1212.

35. GULBRANSEN, E.A. and COPAN, T.P. Microtopology of the surface reactions of oxygen and water vapour with metals. Discuss. Faraday Soc. 28, 1959: 229.

36. GULBRANSEN, E.A. *et al* Oxide growths formed on pure iron in oxygen, water vapour and carbon dioxide atmospheres. *In* International congress for electron microscopy, 5th,Philadelphia, 1962. Electron microscopy. New York, 1962. 2v. p.C-1.

37. BIGOT, J. Préparation et étude des whiskers d'oxyde de fer. Mem. Sci. Rev. Metall. 60, 1963: 541.

38. GULBRANSEN, E.A. Model of oxidation processes occurring in oxide whiskers and platelets on iron at 400°C to 500°C. Mem. Sci. Rev. Metall. 62 suppl., 1965: 253.

39. TALBOT, S. and BIGOT, J. Sur la formation des whiskers par oxydation du fer. Mem. Sci. Rev. Metall. 62 suppl., 1965: 261.

40. PFEFFERKORN, G. and VAHL, J. Die Kombination lichtmikroskopischer, electronenoptischer sowie röntgenographischer Methoden zur Untersuchung von Metalloxyd -Whiskern und-Deckschichten. Werkstoffe Korros. 12, 1963: 1021.

41. TALLMAN, R.L. and GULBRANSEN, E.A. Crystal morphology and mechanisms of growth of alpha-Fe_2O_3 whiskers on iron. J.Electrochem. Soc. 114, 1967: 1227.

42. JANSSON, L. and VANNERBERG, N. The effect of oxygen pressure and the growth of whiskers on the oxidation of pure Fe. Oxidat. Metals. 3, 1971: 453.

43. SVEDUNG, I. *et al* The effect of recrystallisation on the oxide scale composition and growth of whiskers during the oxidation of pure iron. Oxidat. Metals. 6, 1973:21.

44. GOURSAT, A.G. and SMELTZER, W.W. Kinetics and morphological development of the oxide scale on iron at high temperatures in oxygen at low pressure. Oxidat. Metals 6, 1973: 101.

45. PFEFFERKORN, G. and VAHL, J. Beobachtungen zum Whiskerwachstum bei der Metallkorosion. Mem. Sci. Rev. Metall. 62, 1965: 223.

46. TALLMAN, R.L. and GULBRANSEN, E.A. Selected area electron diffraction study of twinned αFe_2O_3 bladelike platelet growths on iron. J. Electrochem. Soc. 115, 1968: 770.

47. GULBRANSEN, E.A. and TALLMAN, R.L. Selected area electron diffraction study of αFe_2O_3 platelet growths twinned on twist grain boundaries. J. Electrochem. Soc. 117, 1970: 250.

48. VIJAYAKAR, S.J. and AGARWALA, R.P. Electron microscopic studies of oxide whiskers. *In* Congrès internationale de microscopie électronique, 7th, Grenoble, 1970. Microscopie électronique. Paris, Societé Française de Microscopie Électronique, 1970. 2v v.2: p.469.

49. AHMAD, I. and CAPSIMALIS, G.P. Growth and some mechanical properties of filamentary single crystals (whiskers) of NiO, WO_3, $W_{20}O_{58}$, $W_{18}O_{49}$ and WO_2. *In* Peiser, H.S. Crystal growth.Oxford, Pergamon, 1967 p.325-331.

50. COWLEY, J.M. Intensity Anomalies in electron diffraction patterns of CuO. J. Electochem. Soc. 101, 1954: 277.

51. GULBRANSEN, E.A. *et al.* Oxidation of copper between 250°C and 450°C and growth of CuO whiskers. J.Electrochem. Soc. 108, 1961: 119.

52. LASKO, W.R. *et al.* Oxide whisker formations on copper. *In* International conference for electron microscopy, 5th, Philadelphia, 1962. Electron microscopy. New York, 1962. 2v. p.C-10.

53. LASKO, W.R. and TICE, W.K. Electron microscope investigation of extinction line contours in copper oxide whiskers. J. Appl. Phys. 33, 1962: 2045.

54. LASKO, W.R. and TICE, W.K. An electron optical study of the effect of temperature and environment on the growth of oxide whiskers on cold-rolled and annealed copper. J. Electrochem. Soc. 109, 1962:211.

55. LASKO, W. R. and TICE, W.K. Unusual corrosion growth products formed on copper. Corros. 18, 1962: 116.

56. JAENICKE, W. *et al.* Mechanical stresses during the oxidation of copper and their influence on oxidation kinetics. Mem.Sci.Rev. Metall. 62 suppl., 1965: 231.

57. ISHII, M. and HASHIMOTO, H. Electron microscopic observation of oxides formed on thin films of copper at elevated temperatures. Jap. J. Appl. Phys. 6, 1967: 173.

58 SHARMA, S.D. and KASHYAP, S.C. Growth of ZnO whiskers, platelets and dendrites. J. Appl. Phys. 42, 1971: 5302.

59. HASHIMOTO, H. *et al.* Bundle structure of needle crystal of tungsten oxide. Acta. Metall. 6, 1958: 557.

60. HASHIMOTO, H. *et al.* Electron microscopic study by cine film on the formation of thin oxide films. *In* Neugebauer, C.A. *et al*, eds. Structure and properties of thin films. New York, Wiley, 1959. p.71-86.

61. HASHIMOTO, H. *et al.* Drops of oxides on tungsten oxide needles and nuclei of dendritic crystals. J. Cryst. Growth, vol. 7, p.113.

62. MARKALI, J. *In* Kriegel, W.W. and Palmour, H. eds. Mechanical properties of engineering ceramics. New York, Wiley-Interscience, 1963. p.93.

63. PFEFFERKORN, G. Elektronenmikroskopische Untersuchungen zum Kristallwachstum von Oxyden. Z.Wiss.Mikrosk. 62, 1954: 109.

64. ERKER, L. Treatice on ores and assaying. 2d. ed. Translated by A.G. Sisco and C.S. Smith, Chicago, University of Chicago Press, 1951. p.177. First published 1574; 2d ed. 1580.

65. HERRING, C. and GALT, J.K. Elastic and plastic properties of very small metal specimens. Phys. Rev. 85, 1952:1060.

66. CAMPBELL, W.B. Growth of whiskers by vapour-phase reactions. *In* Levitt, A.P., ed. Whisker technology, New York, Wiley, 1970. p.15-46.

67. BRENNER, S.S. Properties of whiskers, a review. *In* Doremus, R.H. *et al*, eds. Growth and perfection of crystals. New York, Wiley, 1958. p.157-190.

68. BRENNER, S.S. *In* Gilman, J.J. The art and science of growing crystals. New York, Wiley, 1963. p.30-54.

69. FRANK, F.C. On tin whiskers. Phil. Mag. 7th ser. 44, 1953: 854.

70. ESHELBY, J.D. A tentative theory of metallic whisker growth. Phys. Rev. 91, 1953: 755.

71. AMELINCKX, S. *et al*. Formation and properties of helical dislocations. Phil. Mag. 8th ser. 2, 1957: 355.

72. ELLIS, W.C. *et al*. Growth of metal whiskers from the solid. *In* Doremus, R.H. *et al*, eds. Growth and perfection of crystals. New York, Wiley, 1958. p.102-120.

73. BURTON, W.K. *et al*. Growth of crystals and the equilibrium structure of their surfaces. Phil. Trans. Roy. Soc. 234A, 1951: 299.

74. FRANK, F.C. The influence of dislocations on crystal growth. Discuss. Faraday Soc. 5, 1949: 48.

75. SEARS, G.W. Mercury whiskers. Acta. Metall. 1, 1953: 457.

76. SEARS, G.W. A mechanism of whisker growth. Acta. Metall. 3, 1955: 367.

77. SEARS, G.W. A growth mechanism for mercury whiskers. Acta. Metall. 3, 1955: 361.

78. GOMER, R. Field emission from mercury whiskers. J. Chem. Phys. 26, 1957: 1333.

79. MELMED, A.J. and GOMER, R. Field emission from whiskers. J. Phys. Chem. 34, 1961: 1802.

80. ESHELBY, J.D. Screw dislocations in thin rods. J.Appl. Phys. 24, 1953: 176.

81 ESHELBY, J.D. The twist in a crystal whisker containing a dislocation. Phil. Mag. 8th ser. 3, 1958: 440.

82. WEBB, W.W. Dislocation structure and the formation and strength of sodium chloride whiskers. J. Appl. Phys. 31, 1960: 194

83. WEBB, W.W. and BERTELONE, N.P. Novel mechanism for mass transport during whisker growth - cesium chloride from aqueous films. J. Appl. Phys. 31, 1960: 207.

84. WEBB,W.W. Dislocation mechanisms in the growth of palladium whisker crystals. J. Appl. Phys. 36, 1965: 214.

85. SHLICHTA, P.J. Comparison of copper whiskers with ultrafine wires. *In* Doremus, R.H. *et al*, eds. Growth and perfection of crystals. New York, Wiley, 1958. p.214-218.

86. LAL, K. and PENEVA, S.K. Study of shapes of diffracting planes by X-ray Laue techniques. J. Appl. Phys. 39, 1968:5474.

87. VERMA, A.R. and PENEVA, S.K. X-ray investigations on the growth of cadmium whiskers. J. Cryst. Growth. 3(4), 1968: 700.

88. HAMILTON, D.R. Interferometric determination of twist and polytype in silicon carbide whiskers. J. Appl. Phys. 31, 1960: 112.

89. SEARS, G.W. *et al*. Twist in alumina whiskers. J. Chem. Phys. 34, 1961: 2142.

90 WAGNER, R.S. *et al*. Study of the filamentary growth of silicon crystals from the vapour. J. Appl. Phys. 35, 1964: 2993.

91. TANAKA, K. *et al*. Lattice defects in zinc sulfide whiskers. Jap. J. Appl. Phys. 4, 1965: 493.

92. YAMAMOTO, M. *et al.* Transmission electron-microscopic study on the growth of copper whiskers by halide reduction. J. Cryst. Growth. 3(4), 1968: 705.

93. REGIS, M. Absence de la dislocation - vis axiale dans les trichites metalliques preparees a partir d'halogenures solides. Acta. Metall. 17, 1969: 1281.

94. HASIGUTI, R.R. *et al.* An axial dislocation in copper whiskers. J. Cryst. Growth. 7, 1970: 117.

95. AMELINCKX, S. Dislocations in alkali halide whiskers. *In* Doremus, R.H. *et al*, eds. Growth and perfection of crystals. New York, Wiley, 1958. p.139-153.

96. GOMER, R. Some observations in field emission from mercury whiskers. *In* Doremus, R.H. *et al*, eds. Growth and perfection of crystals. New York, Wiley, 1958. p.126-132.

97. MÜLLER, E.W. Observation of paired screw dislocations in iron whiskers. J. Appl. Phys. 30, 1959: 1843.

98. WAGNER, R.S. and ELLIS, W.C. Vapour-liquid-solid mechanism of single crystal growth. Appl. Phys. Lett. 4, 1964: 89.

99. WAGNER, R.S. VLS mechanism of crystal growth. *In* Levitt, A.P. ed. Whisker technology. New York, Wiley, 1970. p.47-119.

100. SCHWOEBEL, R.L. A diffusion model for filamentary crystal growth. J. Appl. Phys. 38, 1967: 1759.

101. SCHWOEBEL, R.L. and SHIPSEY, E. Step motion on crystal surfaces. J. Appl. Phys. 37, 1966: 3682.

102. PRICE, P.B. *et al* On the growth and properties of electrolytic whiskers. Acta. Metall. 6, 1958: 524.

103. CABRERA, N. and COLEMAN, R.V. Theory of crystal growth from the vapour. *In* Gilman, J.J. The art and science of growing crystals. New York, Wiley, 1963. p.3-28.

104. DROTT, J. Growth of silver sulphide whiskers. Acta.Metall. 8, 1960: 19.

105. HASHIMOTO, H. *et al.* High temperature gas reaction specimen chamber for an electron microscope. Jap. J. Appl. Phys. 7, 1968: 946.

106. HASHIMOTO, H. *et al.* Electron cinematographic observations of whisker growth of molybdenum oxides and copper. *In* International congress for electron microscopy, 6th, Kyoto, 1966. Electron microscopy. Tokyo, Maruzen, 1966. 2v v.1: p.495.

107. FISCHMEISTER, H. Mechanism and kinetic effects of particulate oxide growth. Part I: Whiskers. Mem. Sci. Rev. Metall. 62, 1965: 211.

108. PEACH, M.O. Mechanism of growth of whiskers on cadmium. J. Appl. Phys. 23, 1952: 1401.

109. FLOWER, H.M. High voltage electron microscopy of environmental reations. J. Microscopy. 97, 1973: 171.

110 PAI, S.I. Fluid dynamics of jets. New York, Van Nostrand, 1954. 227p.

111. SWANN, P.R. High voltage microscope studies of environmental reactions. *In* Thomas, G. ed. Electron microscopy and structure of metals, Berkeley, University of California Press, 1972. p. 878.

112. MARTIN, C.J. and BOYD, J.D. A method of calibrating a specimen heating stage in the electron microscope. J. Phys. E.; J. Sci. Instrum. ser.2.6, 1973: 21.

113. BAKER, R.T.K. and HARRIS, P.S. Controlled atmosphere electron microscopy. J. Phys. E.; J. Sci. Instrum. ser. 2. 5, 1972:793.

114. ANDREWS, K.W. *et al.* Interpretation of electron diffraction patterns. 2d. ed. London, Hilger, 1971. p.226.

115. PLOC, R.A. and KEECH, G.H. Computer assisted analysis of transmission electron diffraction. Congrès internationale de microscopie électronique, 7th Grenoble, 1970. Microscopie électronique. Paris, Societe Française de Microscopie Électronique, 1970. 2v. v.2: p.203.

116. VILLAGRANA, R.E. and WHITE, P.H. Computer generated electron diffraction patterns. *ibid* p.205.

117. MEAKIN, J.D. Computer generation and automatic plotting of electron diffraction patterns. Trans. Metall. Soc. A.I.M.E. 245, 1969: 170.

118. MAUCIONE, C.M. *et al.* Computer generation and automatic plotting of perfect and twinned electron diffraction patterns for cubic crystal structures. Metall. Trans. 2, 1971: 2289.

119 VAINSHTEIN, B.K. Structure analysis by electron diffraction. Translated by E. Feigl and J.A. Spink. London, Pergamon, 1964. p.61.

120. WILKES, P. Complete indexing of electron diffraction patterns by computer. J. Mater. Sci. 9, 1974: 517.

121. BOOTH, M. *et al.* A general program for interpreting electron diffraction patterns. Metall. Trans. 5, 1974: 775.

122. HIRSCH, P.B. *et al.* Electron microscopy of thin crystals. London, Butterworths, 1965. p.112-116.

123. ANDREWS, K.W. *et al.* Interpretation of electron diffraction patterns. 2d ed. London, Hilger, 1971. 224p.

124. MEHAN, R.L. and HERZOG, J.A. Mechanical properties of whiskers. *In* Levitt, A.P. ed. Whisker technology. New York, Wiley, 1970. p.157-195.

125. DERJAGUIN, B.V. The force between molecules. Scient. Am. 203, 1960: 47.

126. PEARSON, W.B. A handbook of lattice spacings and structures of metals and alloys. Oxford, Pergamon, 1967. v.2.

127. SMITHELLS, C.J. Metals reference book. 4th Ed. London, Butterworths, 1967. v.2.

128. HIRSCH, P.B. *et al.* Electron Microscopy of thin crystals. London, Butterworths, 1965. p.129-130.

129. *ibid* p.137-141

130. *ibid* p.305-307

131. International Union of Crystallography. International tables for X-ray crystallography. Birmingham, Kynoch Press, 1952-62. v.2.

132. PASHLEY, D.W. and STOWELL, M. J. Electron microscopy and diffraction of twinned structures in evaporated films of gold. Phil. Mag. 8th ser. 8, 1963: 1605.

133. SAMSONOV, G.V. The oxide handbook. New York, Plenum, 1973. p.34.

134. BLAKELEY, J.M. and JACKSON, K.A. Growth of crystal whiskers. J. Chem. Phys. 37, 1962: 428.

135. GOMER, R. Comments on "Growth of crystal whiskers" by Blakeley and Jackson. J. Chem. Phys. 38, 1963: 273.

136. SIMMONS, J.A. *et al.* Theory of whisker growth and evaporation. J. Appl. Phys. 35, 1964: 2271.

137. RUTH, V. and HIRTH, J.P. Kinetics of diffusion controlled whisker growth. J. Chm. Phys. 41, 1964: 3139.

138. SIMMONS, J.A. *et al.* On the solution of the Stefan problem for whisker growth. *In* Peiser, S.H. ed. Crystal growth. Oxford, Pergamon, 1967. p.255-264.

139. SAMSONOV, G.V. The oxide handbook. New York, Plenum, 1973. p.193.

140. SMAILL, J.S. Metallurgical stereographic projections. London, Hilger, 1972. 262p.

141. ASTM. X-ray Powder Data File card 17-536.

142. ASTM. X-ray Powder Data File card 8-98.

APPENDIX 1

LISTING OF PROGRAM XIDENT

```
C     PROGRAM CRYSTAL IDENTIFICATION                                          00001000
C                                                                             00002000
C     IDENTIFIES AND INDEXES ELECTRON DIFFRACTION SPOT PATTERNS               00003000
C                                                                             00004000
C                                                                             00005000
C                                                                             00006000
C     FORM OF INPUT DATA                                                      00007000
C                                                                             00008000
C        DATA CARD 1   PHOTO DESCRIPTION                    (20A4)          00009000
C                  2   CAMCO,TOL,IOUT                (F8.4,F6.3,I1)          00010000
C     N.B. CAMCO IS A DIAMETER BASED CAMERA CONSTANT, TOL IS POSITION         00011000
C     TOLERANCE IN MILLIMETERS, IOUT =1 IF PRINTOUT OF SYMMETRICAL SOLNS      00012000
C     IS REQUIRED OTHERWISE LEAVE BLANK                                       00013000
C                  3   DIFFRACTED DISTANCES               (5F8.3)           00014000
C                  4   ANGLES BETWEEN SPOTS               (4F8.2)           00015000
C                  5   SYM,TITLE OF MATERIAL          (I1,19A4)             00016000
C                                                                             00017000
C     N.B. FOR SYM WRITE 0 FOR PRIMITIVE CELL TYPE P                          00018000
C                        1 FOR ALL FACES CENTRED TYPE F                       00019000
C                        2 FOR BODY CENTRED CELL TYPE I                       00020000
C                        3 FOR A FACE CENTRED CELL TYPE A                     00021000
C                        4 FOR B FACE CENTRED CELL TYPE B                     00022000
C                        5 FOR C FACE CENTRED CELL TYPE C                     00023000
C                        6 FOR OBVERSE RHOMB (HEX CELL) TYPE R                00024000
C                        7 FOR REVERSE RHOMB (HEX CELL) TYPE R                00025000
C                                                                             00026000
C        DATA CARD 6   A,B,C,ALPHA,BETA,GAMMA       (3F10.3,3F10.2)          00027000
C                  7   ICARD                                                  00028000
C                                                                             00029000
C     N.B. IF NEW MATL. FOLLOWING        ICARD=1 AND REPEAT CARDS 5-7         00030000
C     N.B. IF NEW PHOTO FOLLOWING        ICARD=2 AND REPEAT CARDS 1-7         00031000
C                                                                             00032000
C                                                                             00033000
C                                                                             00034000
C     PROGRAM XIDENT                                                          00035000
C                                                                             00036000

      INTEGER READR,PRINTR,H,HMAX,PMAX,QMAX,RMAX,SMAX,TMAX,SYM,SYMI           00037000
      DOUBLE PRECISION DSQ2,DSQ4                                              00038000
      DOUBLE PRECISION A,B,C,PI180,V,DMAX,DSQ,ASTAR,BSTAR                     00039000
      DOUBLE PRECISION CSTAR,SINA,SINB,SING,COSA,COSB,COSG,COSAS              00040000
      DOUBLE PRECISION COSBS,COSGS,A11,A12,A13,A22,A23,A33,DMIN               00041000
      COMMON RADIX(5,50),ANGIX(4,50),IZONES(3,50,50),IHP(5,50,50),            00042000
     1IKP(5,50,50),ILP(5,50,50),KSETS,KP(50),RAD(3,801),KS,ANGLES(4),         00043000
     2IZOS(3,50),IOUT,DIST(5),DISTIX(5,50),ANGACT(4),CAMKO(50),CAMCO,         00044000
     3LE,LES,ADEVN(50),DEVSQ(50),KT,D2,D4                                     00045000
      DIMENSION TITLE(19),IND(3,3,801),DISTN(5),DISTX(5),PHOTO(20),IH(5)      00046000
     1 ,IK(5),IL(5)                                                           00047000
      AMTOL=0.05                                                              00048000
      PAMTOL=AMTOL*100.                                                       00049000
      ANGTOL=3.0                                                              00050000
      DPR=57.295780                                                           00051000
   12 PI180=3.1415926535897932/180.                                           00052000
C                                                                             00053000
C     ****READ DETAILS OF DIFFRACTION PATTERN                                 00054000
C                                                                             00055000
    2 READR=5                                                                 00056000
      PRINTR=6                                                                00057000
      WRITE (6,533)                                                           00058000

   11 READ(5,101)(PHOTO(I),I=1,20)                                            00059000

      READ(READR,102) CAMCO,TOL,IOUT                                          00060000
      READ(READR,103)(DIST(N),N=1,5 )                                         00061000
      IF(DIST(4).EQ.0.0) GO TO 120                                            00062000
  110 LE=5                                                                    00063000
      GO TO 130                                                               00064000
  120 LE=3                                                                    00065000
  130 LES=LE-1                                                                00066000
      READ(READR,106)(ANGLES(MM),MM=1,4)                                      00067000
      DO 135 MM=1,LES                                                         00068000
      COSANG=COS(ANGLES(MM)/DPR)                                              00069000
  135 ANGLES(MM)=(ARCOS(COSANG))*DPR                                          00070000
    3 DO 5 N=1,5                                                              00071000
      IF(TOL-(DIST(N)*AMTOL)) 14,4,4                                          00072000
   14 DISTN(N)=DIST(N)-(DIST(N)*AMTOL)                                        00073000
      DISTX(N)=DIST(N)+(DIST(N)*AMTOL)                                        00074000
      GO TO 5                                                                 00075000
    4 DISTN(N)=DIST(N)-TOL                                                    00076000
      DISTX(N)=DIST(N)+TOL                                                    00077000
    5 CONTINUE                                                                00078000
      WRITE(6,201) PHOTO                                                      00079000
      WRITE (PRINTR,221)                                                      00080000
      WRITE (PRINTR,221)                                                      00081000
      WRITE (PRINTR,221)                                                      00082000
      WRITE(PRINTR,202) CAMCO                                                 00083000
      WRITE(6,203) TOL,PAMTOL                                                 00084000
      WRITE(PRINTR,204)(DIST(K),K=1,5)                                        00085000
      WRITE(PRINTR,219) ANGTOL                                                00086000
      WRITE(PRINTR,220) (ANGLES(MM),MM=1,4)                                   00087000
```

```
C                                                                       00088000
C     ****READ DETAILS OF MATERIALS                                     00089000
C                                                                       00090000
   10 KONST=1                                                           00091000
      READ(5,107)SYM,(TITLE(J),J=1,19)                                  00092000
      SYMI=SYM+1                                                        00093000
      READ(READR,104) A,B,C,ALPHA,BETA,GAMMA                            00094000
      WRITE(PRINTR,205) TITLE                                           00095000
      WRITE(6,221)                                                      00096000
      WRITE(PRINTR,206)                                                 00097000
      WRITE(PRINTR,207) A,B,C,ALPHA,BETA,GAMMA                          00098000
C                                                                       00099000
C     ****COMPUTE RECIPROCAL CONSTANTS                                  00100000
C                                                                       00101000
      SINA=DSIN(ALPHA*PI180)                                            00102000
      SINB=DSIN(BETA*PI180)                                             00103000
      SING=DSIN(GAMMA*PI180)                                            00104000
      COSA=DCOS(ALPHA*PI180)                                            00105000
      COSB=DCOS(BETA*PI180)                                             00106000
      COSG=DCOS(GAMMA*PI180)                                            00107000
      V=1./(A*B*C*DSQRT(1.+2.*COSA*COSB*COSG-COSA*COSA-COSB*COSB-COSG*CO 00108000
     1SG))                                                              00109000
      ASTAR=B*C*V*SINA                                                  00110000
      BSTAR=A*C*V*SINB                                                  00111000
      CSTAR=A*B*V*SING                                                  00112000
      COSAS=(COSB*COSG-COSA)/(SINB*SING)                                00113000
      COSBS=(COSA*COSG-COSB)/(SINA*SING)                                00114000
      COSGS=(COSA*COSB-COSG)/(SINA*SINB)                                00115000
      A11=ASTAR*ASTAR                                                   00116000
      A22=BSTAR*BSTAR                                                   00117000
      A33=CSTAR*CSTAR                                                   00118000
      A12=2.*ASTAR*BSTAR*COSGS                                          00119000
      A13=2.*ASTAR*CSTAR*COSBS                                          00120000
      A23=2.*BSTAR*CSTAR*COSAS                                          00121000
C                                                                       00122000
C     ****DETERMINE LIMITS OF INDICES                                   00123000
C                                                                       00124000
    6 DISTMX=DISTX(1)                                                   00125000
    7 DO 9 N=2,5                                                        00126000
    8 IF(DISTMX.GT.DISTX(N)) GO TO 9                                    00127000
      DISTMX=DISTX(N)                                                   00128000
    9 CONTINUE                                                          00129000
      DMIN=CAMCO/(2.*DISTMX)                                            00130000
      DMIN=DMIN*DMIN                                                    00131000
      DMAX=DSQRT(1/DMIN)                                                00132000
      HMAX=(DMAX/(ASTAR*DSQRT(1.-COSBS*COSBS)*SING))+1.                 00133000
      KMAX=(DMAX/(BSTAR*DSQRT(1.-COSGS*COSGS)*SINA))+1.                 00134000
      LMAX=(DMAX/(CSTAR*DSQRT(1.-COSAS*COSAS)*SINB))+1.                 00135000
  503 WRITE(PRINTR,532)HMAX,KMAX,LMAX                                   00136000
C                                                                       00137000
C     ****GENERATE RECIPROCAL VECTORS                                   00138000
C                                                                       00139000
      PMAX=0                                                            00140000
      RMAX=0                                                            00141000
      TMAX=0                                                            00142000
      LIST3=0                                                           00143000
      NHMAX=-HMAX                                                       00144000
      NKMAX=-KMAX                                                       00145000
      NLMAX=-LMAX                                                       00146000
      DO 70 NH=NHMAX,HMAX                                               00147000
      DO 70 NK=NKMAX,KMAX                                               00148000
      DO 70 NL=NLMAX,LMAX                                               00149000
      H=-NH                                                             00150000
      K=-NK                                                             00151000
      L=-NL                                                             00152000
      IF(H.EQ.0.AND.K.EQ.0.AND.L.EQ.0) GO TO 15                         00153000
      CALL PROHIB (SYMI,H,K,L,INC)                                      00154000
      IF (INC-1) 17,70,70                                               00155000
   15 LIST3=1                                                           00156000
      GO TO 70                                                          00157000
   17 DSQ=H*H*A11+H*K*A12+H*L*A13+K*K*A22+K*L*A23+L*L*A33               00158000
      D=SNGL(DSQRT(1./DSQ))                                             00159000
      RADI=CAMCO/(2.*D)                                                 00160000
      DO 70 N=1,5,2                                                     00161000
   18 IF(RADI-DISTN(N)) 70,19,19                                        00162000
   19 IF(RADI-DISTX(N)) 20,20,70                                        00163000
   20 IF(N-1) 40,21,22                                                  00164000
   21 PMAX=PMAX+1                                                       00165000
      M=PMAX                                                            00166000
      GO TO 40                                                          00167000
   22 IF(N-3) 40,25,26                                                  00168000
   25 IF(LIST3.EQ.1) GO TO 70                                           00169000
      RMAX=RMAX+1                                                       00170000
      M=RMAX                                                            00171000
      GO TO 40                                                          00172000
   26 TMAX=TMAX+1                                                       00173000
      M=TMAX                                                            00174000
   40 NN=(N+1)/2                                                        00175000
      IND(NN,1,M)=H                                                     00176000
      IND(NN,2,M)=K                                                     00177000
      IND(NN,3,M)=L                                                     00178000
      RAD(NN,M)=D                                                       00179000
      IF(PMAX.GT.800.OR.RMAX.GT.800.OR.TMAX.GT.800) GO TO 1003          00180000
   70 CONTINUE                                                          00181000
```

```
      GO TO 71                                                          00182000
 1003 WRITE(PRINTR,218)                                                 00183000
      GO TO 1004                                                        00184000
   71 WRITE(PRINTR,208)PMAX,RMAX,TMAX                                   00185000
      GO TO (38,31,32,33,34,35,36,37),SYMI                              00186000
   31 WRITE(6,534)                                                      00187000
      GO TO 38                                                          00188000
   32 WRITE(6,535)                                                      00189000
      GO TO 38                                                          00190000
   33 WRITE(6,536)                                                      00191000
      GO TO 38                                                          00192000
   34 WRITE(6,537)                                                      00193000
      GO TO 38                                                          00194000
   35 WRITE(6,538)                                                      00195000
      GO TO 38                                                          00196000
   36 WRITE(6,539)                                                      00197000
      GO TO 38                                                          00198000
   37 WRITE(6,540)                                                      00199000
   38 IF(DIST(4)) 43,43,44                                              00200000
   43 IF(PMAX.EQ.0.OR.RMAX.EQ.0) GO TO 1007                             00201000
   44 IF(PMAX.EQ.0.OR.RMAX.EQ.0.OR.TMAX.EQ.0) GO TO 1007                00202000
C                                                                       00203000
C     ****DETERMINE INDICES OF POINT '2'                                00204000
C                                                                       00205000
   92 DO 1002 I=1,PMAX                                                  00206000
   95 DO 1002 K=1,RMAX                                                  00207000
      ZHB=(IND(1,1,I)+IND(2,1,K))/2.                                    00208000
      NHB=ZHB                                                           00209000
      AZHB=NHB                                                          00210000
      IF(ZHB-AZHB) 1002,96,1002                                         00211000
   96 ZKB=(IND(1,2,I)+IND(2,2,K))/2.                                    00212000
      NKB=ZKB                                                           00213000
      AZKB=NKB                                                          00214000
      IF(ZKB-AZKB) 1002,97,1002                                         00215000
   97 ZLB=(IND(1,3,I)+IND(2,3,K))/2.                                    00216000
      NLB=ZLB                                                           00217000
      AZLB=NLB                                                          00218000
      IF(ZLB-AZLB) 1002,98,1002                                         00219000
   98 IF(NHB.EQ.0.AND.NKB.EQ.0.AND.NLB.EQ.0) GO TO 1002                 00220000
      CALL PROHIB (SYMI,NHB,NKB,NLB,INC)                                00221000
      IF(INC-1) 99,1002,1002                                            00222000
C                                                                       00223000
C     ****CHECK POINT '2' IS WITHIN LIMITS OF RADIUS                    00224000
C                                                                       00225000
   99 DSQ2=NHB*NHB*A11+NHB*NKB*A12+NHB*NLB*A13+NKB*NKB*A22+NKB*NLB*A23+ 00226000
     1NLB*NLB*A33                                                       00227000
      D2=SNGL(DSQRT(1./DSQ2))                                           00228000
      RADI2=CAMCO/(2.*D2)                                               00229000
      IF(RADI2.GE.DISTN(2).AND.RADI2.LE.DISTX(2)) GO TO 151             00230000
      GO TO 1002                                                        00231000
C                                                                       00232000
C     ****DETERMINE INDICES OF POINT '4'                                00233000
C                                                                       00234000
  151 IF(DIST(4).EQ.0.0) GO TO 159                                      00235000
      DO 1001 M=1,TMAX                                                  00236000
      ZHD=(IND(2,1,K)+IND(3,1,M))/2.                                    00237000
      NHD=ZHD                                                           00238000
      AZHD=NHD                                                          00239000
      IF(ZHD-AZHD) 1001,153,1001                                        00240000
  153 ZKD=(IND(2,2,K)+IND(3,2,M))/2.                                    00241000
      NKD=ZKD                                                           00242000
      AZKD=NKD                                                          00243000
      IF(ZKD-AZKD) 1001,154,1001                                        00244000
  154 ZLD=(IND(2,3,K)+IND(3,3,M))/2.                                    00245000
      NLD=ZLD                                                           00246000
      AZLD=NLD                                                          00247000
      IF(ZLD-AZLD) 1001,155,1001                                        00248000
  155 IF(NHD.EQ.0.AND.NKD.EQ.0.AND.NLD.EQ.0) GO TO 1001                 00249000
      CALL PROHIB (SYMI,NHD,NKD,NLD,INC)                                00250000
      IF (INC-1) 156,1001,1001                                          00251000
C                                                                       00252000
C     ****CHECK POINT '4' IS WITHIN LIMITS OF RADIUS                    00253000
C                                                                       00254000
  156 DSQ4=NHD*NHD*A11+NHD*NKD*A12+NHD*NLD*A13+NKD*NKD*A22+NKD*NLD*A23+ 00255000
     1NLD*NLD*A33                                                       00256000
      D4=SNGL(DSQRT(1./DSQ4))                                           00257000
      RADI4=CAMCO/(2.*D4)                                               00258000
      IF(RADI4.GE.DISTN(4).AND.RADI4.LE.DISTX(4)) GO TO 158             00259000
      GO TO 1001                                                        00260000
```

```
C                                                                       00261000
C     ****SORT PLANES INTO ARRAYS                                       00262000
C                                                                       00263000
  159 L=1                                                               00264000
      M=1                                                               00265000
  158 IH(1)=IND(1,1,I)                                                  00266000
      IH(2)=NHB                                                         00267000
      IH(3)=IND(2,1,K)                                                  00268000
      IH(4)=NHD                                                         00269000
      IH(5)=IND(3,1,M)                                                  00270000
      IK(1)=IND(1,2,I)                                                  00271000
      IK(2)=NKB                                                         00272000
      IK(3)=IND(2,2,K)                                                  00273000
      IK(4)=NKD                                                         00274000
      IK(5)=IND(3,2,M)                                                  00275000
      IL(1)=IND(1,3,I)                                                  00276000
      IL(2)=NLB                                                         00277000
      IL(3)=IND(2,3,K)                                                  00278000
      IL(4)=NLD                                                         00279000
      IL(5)=IND(3,3,M)                                                  00280000
C                                                                       00281000
C     ****CALCULATE ANGLES BETWEEN PLANES                               00282000
C                                                                       00283000
      MM=0                                                              00284000
      II=1                                                              00285000
  160 IF(DIST(4)) 161,161,162                                           00286000
  161 NZ=3                                                              00287000
      GO TO 163                                                         00288000
  162 NZ=5                                                              00289000
  163 DO 170 NN=2,NZ                                                    00290000
      S=((IH(II)*IH(NN)*ASTAR*ASTAR)+(IK(II)*IK(NN)*BSTAR*BSTAR)+(IL(II) 00291000
     1*IL(NN)*CSTAR*CSTAR)+((IK(II)*IL(NN)+IL(II)*IK(NN))*BSTAR*CSTAR*CO 00292000
     2SAS)+((IL(II)*IH(NN)+IL(NN)*IH(II))*CSTAR*ASTAR*COSBS)+((IH(II)*IK 00293000
     3(NN)+IK(II)*IH(NN))*ASTAR*BSTAR*COSGS))                           00294000
      T=((IH(II)*IH(II)*ASTAR*ASTAR)+(IK(II)*IK(II)*BSTAR*BSTAR)+(IL(II) 00295000
     1*IL(II)*CSTAR*CSTAR)+(2.0*IH(II)*IK(II)*ASTAR*BSTAR*COSGS)+(2.0*IL 00296000
     2(II)*IH(II)*CSTAR*ASTAR*COSBS)+(2.0*IK(II)*IL(II)*BSTAR*CSTAR*COSA 00297000
     3S))                                                               00298000
      U=((IH(NN)*IH(NN)*ASTAR*ASTAR)+(IK(NN)*IK(NN)*BSTAR*BSTAR)+(IL(NN) 00299000
     1*IL(NN)*CSTAR*CSTAR)+(2.0*IH(NN)*IK(NN)*ASTAR*BSTAR*COSGS)+(2.0*IL 00300000
     2(NN)*IH(NN)*CSTAR*ASTAR*COSBS)+(2.0*IK(NN)*IL(NN)*BSTAR*CSTAR*COSA 00301000
     3S))                                                               00302000
      W=SQRT(T*U)                                                       00303000
      YY=ARCOS(S/W)                                                     00304000
      YY=YY*DPR                                                         00305000
      MM=MM+1                                                           00306000
      IF(YY.GT.(ANGLES(MM)+ANGTOL).OR.YY.LT.(ANGLES(MM)-ANGTOL)) GO TO 1 00307000
     1001                                                               00308000
      ANGACT (MM)=YY                                                    00309000
  170 CONTINUE                                                          00310000
      CALL OARRAY(KONST,IH,IK,IL,I,J,K,L,M,PI180)                       00311000
 1001 CONTINUE                                                          00312000
 1002 CONTINUE                                                          00313000
 1007 KONST=3                                                           00314000
      CALL OARRAY(KONST,IH,IK,IL,I,J,K,L,M,PI180)                       00315000
 1004 READ(READR,105) ICARD                                             00316000
      IF (ICARD-1.) 11,10,11                                            00317000
C                                                                       00318000
C     **** FORMAT STATEMENTS ----INPUT                                  00319000
C                                                                       00320000
  101 FORMAT(20A4)                                                      00321000
  102 FORMAT(F8.4,F6.3,I1)                                              00322000
  103 FORMAT(5F8.2)                                                     00323000
  104 FORMAT(3F10.3,3F10.2)                                             00324000
  105 FORMAT(I1)                                                        00325000
  106 FORMAT(4F8.2)                                                     00326000
  107 FORMAT(I1,19A4)                                                   00327000
C                                                                       00328000
C     ****FORMAT STATEMENTS ---- OUTPUT                                 00329000
C                                                                       00330000
  201 FORMAT(1H1,20A4)                                                  00331000
  202 FORMAT(1HO,'CAMERA CONSTANT=',F8.4)                               00332000
  203 FORMAT(1HO,'POSITION TOLERANCE =',F6.3,' MILLIMETRES  (MINIMUM OVE 00333000
     1R-RIDING TOLERANCE OF + OR - ',F3.1,' PERCENT OF DIFF. DISTANCE PR 00334000
     2EVAILS)')                                                         00335000
  204 FORMAT(1HO,'DIFFRACTED DISTANCES OF SPOTS ARE',//5F10.2,'   (MILLI 00336000
     1METRES)')                                                         00337000
  205 FORMAT(1HO,///////1X,19A4)                                        00338000
  206 FORMAT(1HO,20X,'REAL CELL CONSTANTS'//26X,'A',8X,'B',8X,'C',6X,'AL 00339000
     1PHA',5X,'BETA',4X,'GAMMA'/)                                       00340000
  207 FORMAT(20X,6F9.3)                                                 00341000
  208 FORMAT(1HO,20X,'MAXIMUM DIMENSIONS OF ARRAYS ARE  ',516)          00342000
  218 FORMAT(1HO,'ARRAY LIMITS EXCEEDED---MATERIAL CHECK CANCELLED')    00343000
  219 FORMAT(1HO,'ANGLE TOLERANCE = ',F5.2,' DEGREES')                  00344000
  220 FORMAT(1HO,'MEASURED ANGLES BETWEEN SPOTS ARE',// 4F10.2)         00345000
  221 FORMAT(55H*******************************************************) 00346000
  532 FORMAT(1HO,20X,19HMAXIMUM INDICES ARE,3I4)                        00347000
  533 FORMAT(1HO,6X,30HPROGRAM CRYSTAL IDENTIFICATION)                  00348000
```

```
534 FORMAT(1HO,20X,'PROHIBITED REFLECTIONS FOR THE FACE CENTRED CELL T 00349000
     1YPE F HAVE BEEN OMITTED')                                        00350000
535 FORMAT(1HO,20X,'PROHIBITED REFLECTIONS FOR THE BODY CENTRED CELL T 00351000
     1YPE I HAVE BEEN OMITTED')                                        00352000
536 FORMAT(1HO,20X,'PROHIBITED REFLECTIONS FOR THE FACE CENTRED CELL T 00353000
     1YPE A HAVE BEEN OMITTED')                                        00354000
537 FORMAT(1HO,20X,'PROHIBITED REFLECTIONS FOR THE FACE CENTRED CELL T 00355000
     1YPE B HAVE BEEN OMITTED')                                        00356000
538 FORMAT(1HO,20X,'PROHIBITED REFLECTIONS FOR THE FACE CENTRED CELL T 00357000
     1YPE C HAVE BEEN OMITTED')                                        00358000
539 FORMAT(1HO,20X,'PROHIBITED REFLECTIONS FOR THE OBVERSE RHOMBOHEDRO 00359000
     1N (HEXAGONAL CELL) TYPE R HAVE BEEN OMITTED')                    00360000
540 FORMAT(1HO,20X,'PROHIBITED REFLECTIONS FOR THE REVERSE RHOMBOHEDRO 00361000
     1N (HEXAGONAL CELL) TYPE R HAVE BEEN OMITTED')                    00362000
      END                                                              00363000
```

```
      SUBROUTINE PROHIB (SYMI,H,K,L,INC)                               00364000
C                                                                      00365000
C     TEST INDICES AND ELIMINATE PROHIBITED REFLECTIONS                00366000
C                                                                      00367000
      INTEGER H,SYMI                                                   00368000
      GO TO (68,13,15,61,62,13,63,64),SYMI                             00369000
   13 AKH=(K+H)/2.                                                     00370000
      KH=AKH                                                           00371000
      BKH=KH                                                           00372000
      IF(AKH.NE.BKH) GO TO 70                                          00373000
      IF(SYMI.NE.2) GO TO 68                                           00374000
   62 ALH=(L+H)/2.                                                     00375000
      LH=ALH                                                           00376000
      BLH=LH                                                           00377000
      IF(ALH.NE.BLH) GO TO 70                                          00378000
      IF(SYMI.NE.2) GO TO 68                                           00379000
   61 AKL=(K+L)/2.                                                     00380000
      KL=AKL                                                           00381000
      BKL=KL                                                           00382000
      IF(AKL.NE.BKL) GO TO 70                                          00383000
      GO TO 68                                                         00384000
   15 AKHL=(H+K+L)/2.                                                  00385000
      GO TO 66                                                         00386000
   63 AKHL=(K+L-H)/3.                                                  00387000
      GO TO 66                                                         00388000
   64 AKHL=(H+L-K)/3.                                                  00389000
   66 KHL=AKHL                                                         00390000
      BKHL=KHL                                                         00391000
      IF(AKHL.NE.BKHL) GO TO 70                                        00392000
   68 INC=0                                                            00393000
   69 GO TO 75                                                         00394000
   70 INC=1                                                            00395000
   75 RETURN                                                           00396000
      END                                                              00397000
```

```
      SUBROUTINE OARRAY(KONST,IH,IK,IL,IA,JA,KA,LA,MA,PI180)                    00398000
C                                                                               00399000
C     SUBROUTINE 'OARRAY' SORTS SOLUTIONS AND PRINTS RESULTS                    00400000
C                                                                               00401000
      COMMON RADIX(5,50),ANGIX(4,50),IZONES(3,50,50),IHP(5,50,50),              00402000
     1IKP(5,50,50),ILP(5,50,50),KSETS,KP(50),RAD(3,801),KS,ANGLES(4),           00403000
     2IZOS(3,50),IOUT,DIST(5),DISTIX(5,50),ANGACT(4),CAMKO(50),CAMCO,           00404000
     3LE,LES,ADEVN(50),DEVSQ(50),KT,D2,D4                                       00405000
      DIMENSION IH(5),IK(5),IL(5),ANG(5),                                       00406000
     1IZON(3),IZO(3),DIV(3),ADIV(3),JDIV(3),DEVN(5),DEV(50),HSUM(50)            00407000
      DOUBLE PRECISION PI180                                                    00408000
      IF(KONST-3) 1030,600,1030                                                 00409000
C                                                                               00410000
C     CALCULATE LOWEST ORDER ZONE AXES                                          00411000
C                                                                               00412000
 1030 IZON(1)=IK(1)*IL(2)-IK(2)*IL(1)                                           00413000
 1031 IZON(2)=IL(1)*IH(2)-IL(2)*IH(1)                                           00414000
 1032 IZON(3)=IH(1)*IK(2)-IH(2)*IK(1)                                           00415000
      DO 1033 I=1,3                                                             00416000
      IZO(I)=IZON(I)                                                            00417000
 1033 CONTINUE                                                                  00418000
 1040 IF(IABS(IZO(1))-IABS(IZO(2)))1041,1042,1042                               00419000
 1041 INV=IZO(2)                                                                00420000
      IZO(2)=IZO(1)                                                             00421000
      IZO(1)=INV                                                                00422000
 1042 IF(IABS(IZO(2))-IABS(IZO(3)))1043,1045,1045                               00423000
 1043 INV=IZO(3)                                                                00424000
      IZO(3)=IZO(2)                                                             00425000
      IZO(2)=INV                                                                00426000
      GO TO 1040                                                                00427000
 1045 INCMAX=IABS(IZO(1))                                                       00428000
 1083 DO 1061 INC=1,INCMAX                                                      00429000
      DO 1060 IZ=1,3                                                            00430000
 1046 DIV(IZ)=IABS(IZO(IZ))/((INCMAX+1.)-INC)                                   00431000
      JDIV(IZ)=DIV(IZ)+0.001                                                    00432000
      ADIV(IZ)=JDIV(IZ)                                                         00433000
 1060 CONTINUE                                                                  00434000
      IF(DIV(1).EQ.ADIV(1).AND.DIV(2).EQ.ADIV(2).AND.DIV(3).EQ.ADIV(3))G        00435000
     1O TO 1063                                                                 00436000
 1061 CONTINUE                                                                  00437000
 1063 DO 1070 I=1,3                                                             00438000
      IF(IZON(I))64,65,65                                                       00439000
   64 IZON(I)=IZON(I)/((INCMAX+1)-INC)-0.001                                    00440000
      GO TO 1070                                                                00441000
   65 IZON(I)=IZON(I)/((INCMAX+1)-INC)+0.001                                    00442000
 1070 CONTINUE                                                                  00443000
C                                                                               00444000
C     LOAD SOLUTIONS INTO OUTPUT ARRAYS                                         00445000
C                                                                               00446000
      GO TO (100,400,600,400) KONST                                             00447000
  100 KONST=2                                                                   00448000
      DO 110 I=1,50                                                             00449000
  110 KP(I)=0                                                                   00450000
      KT=0                                                                      00451000
      KSETS=0                                                                   00452000
  200 IF(KT.LT.50) GO TO 208                                                    00453000
  900 KONST=4                                                                   00454000
      GO TO 350                                                                 00455000
  208 KT=KT+1                                                                   00456000
      KSETS=KSETS+1                                                             00457000
      RADIX(1,KT)=RAD(1,IA)                                                     00458000
      RADIX(2,KT)=D2                                                            00459000
      RADIX(3,KT)=RAD(2,KA)                                                     00460000
      RADIX(4,KT)=D4                                                            00461000
      RADIX(5,KT)=RAD(3,MA)                                                     00462000
      DO 210 I=1,4                                                              00463000
  210 ANGIX(I,KT)=ANGACT(I)                                                     00464000
      DO 220 I=1,5                                                              00465000
      DISTIX(I,KT)=DIST(I)                                                      00466000
  220 CONTINUE                                                                  00467000
      KS=KT                                                                     00468000
  300 KP(KS)=KP(KS)+1                                                           00469000
```

```
                                                                      00470000
      CALCULATE MEAN DEVIATION OF SPOTS FROM TRUE POSITIONS           00471000
                                                                      00472000
      DEV(KS)=0.                                                      00473000
      DEVSQ(KS)=0.                                                    00474000
      RADTOT=0.                                                       00475000
      DISTOT=0.                                                       00476000
   30 DO 50 N=1,LE                                                    00477000
      RADTOT=RADTOT+RADIX(N,KS)                                       00478000
   50 DISTOT=DISTOT+(CAMCO/(2*DISTIX(N,KS)))                          00479000
      CAMINC=((RADTOT-DISTOT)/DISTOT)+1.                              00480000
      CAMKO(KS)=CAMCO*CAMINC                                          00481000
      ANGDEV=0.                                                       00482000
      DO 55 N=1,LES                                                   00483000
   55 ANGDEV=ANGDEV+(ANGIX(N,KS)-ANGLES(N))                           00484000
      ANGDE=ANGDEV/LE                                                 00485000
      ANG(1)=0.-ANGDE                                                 00486000
      DO 56 N=1,LES                                                   00487000
      M=N+1                                                           00488000
   56 ANG(M)=(ANGIX(N,KS)-ANGLES(N))-ANGDE                            00489000
      DO 58 N=1,LE                                                    00490000
      X1=DISTIX(N,KS)-((CAMKO(KS)/(2.*RADIX(N,KS)))*DCOS(ANG(N)*PI180)) 00491000
      X2=(CAMKO(KS)/(2.*RADIX(N,KS)))*DSIN(ANG(N)*PI180)              00492000
   58 DEVSQ(KS)=DEVSQ(KS)+SQRT((X1*X1)+(X2*X2))                       00493000
      IF(KP(KS).GT.50) GO TO 1000                                     00494000
      K=KP(KS)                                                        00495000
      DO 310 I=1,3                                                    00496000
      IZONES(I,K,KS)=IZON(I)                                          00497000
  310 IZOS(I,KS)=JDIV(I)                                              00498000
      DO 320 I=1,5                                                    00499000
      IHP(I,K,KS)=IH(I)                                               00500000
      IKP(I,K,KS)=IK(I)                                               00501000
  320 ILP(I,K,KS)=IL(I)                                               00502000
      GO TO 1000                                                      00503000
C                                                                     00504000
C     CHECK FOR SYMMETRICAL EQUIVALENT SOLUTIONS                      00505000
C                                                                     00506000
  400 DO 410 KS=1,KT                                                  00507000
      IF(RAD(1,IA).EQ.RADIX(1,KS).AND.   D2    .EQ.RADIX(2,KS).AND.RAD(2 00508000
     1,KA).EQ.RADIX(3,KS).AND.   D4    .EQ.RADIX(4,KS).AND.RAD(3,MA).EQ. 00509000
     2RADIX(5,KS)) GO TO 420                                          00510000
      GO TO 410                                                       00511000
  420 DO 430 L=1,4                                                    00512000
      IF(ANGIX(L,KS).NE.ANGACT(L)) GO TO 410                          00513000
  430 CONTINUE                                                        00514000
      DO 440 I=1,3                                                    00515000
      IF(IZOS(I,KS).NE.JDIV(I)) GO TO 410                             00516000
  440 CONTINUE                                                        00517000
      GO TO 300                                                       00518000
  410 CONTINUE                                                        00519000
      GO TO 200                                                       00520000
  600 IF(KSETS) 1600,1600,350                                         00521000
C                                                                     00522000
C     SORT SETS OF RESULTS INTO ORDER OF ACCURACY                     00523000
C                                                                     00524000
  350 N=KT                                                            00525000
      M=N                                                             00526000
 1120 M=M/2                                                           00527000
      IF(M) 1130,1140,1130                                            00528000
 1130 K=N-M                                                           00529000
      J=1                                                             00530000
 1141 I=J                                                             00531000
 1149 L=I+M                                                           00532000
      IF(DEVSQ(I)-DEVSQ(L)) 1160,1160,1150                            00533000
 1150 B=DEVSQ(I)                                                      00534000
      DEVSQ(I)=DEVSQ(L)                                               00535000
      DEVSQ(L)=B                                                      00536000
      CAM=CAMKO(I)                                                    00537000
      CAMKO(I)=CAMKO(L)                                               00538000
      CAMKO(L)=CAM                                                    00539000
      DO 1153 NM=1,5                                                  00540000
      AR=RADIX(NM,I)                                                  00541000
      RADIX(NM,I)=RADIX(NM,L)                                         00542000
      RADIX(NM,L)=AR                                                  00543000
      AD=DISTIX(NM,I)                                                 00544000
      DISTIX(NM,I)=DISTIX(NM,L)                                       00545000
      DISTIX(NM,L)=AD                                                 00546000
      DO 1153 KK=1,50                                                 00547000
      IP=IHP(NM,KK,I)                                                 00548000
      IHP(NM,KK,I)=IHP(NM,KK,L)                                       00549000
      IHP(NM,KK,L)=IP                                                 00550000
      IP=IKP(NM,KK,I)                                                 00551000
      IKP(NM,KK,I)=IKP(NM,KK,L)                                       00552000
      IKP(NM,KK,L)=IP                                                 00553000
      IP=ILP(NM,KK,I)                                                 00554000
      ILP(NM,KK,I)=ILP(NM,KK,L)                                       00555000
 1153 ILP(NM,KK,L)=IP                                                 00556000
```

```
      DO 1154 NN=1,3                                                    00557000
      IQ=IZOS(NN,I)                                                     00558000
      IZOS(NN,I)=IZOS(NN,L)                                             00559000
      IZOS(NN,L)=IQ                                                     00560000
      DO 1154 KK=1,50                                                   00561000
      IP=IZONES(NN,KK,I)                                                00562000
      IZONES(NN,KK,I)=IZONES(NN,KK,L)                                   00563000
 1154 IZONES(NN,KK,L)=IP                                                00564000
      DO 1155 NA=1,4                                                    00565000
      AA=ANGIX(NA,I)                                                    00566000
      ANGIX(NA,I)=ANGIX(NA,L)                                           00567000
 1155 ANGIX(NA,L)=AA                                                    00568000
      KZ=KP(I)                                                          00569000
      KP(I)=KP(L)                                                       00570000
      KP(L)=KZ                                                          00571000
      I=(I-M)                                                           00572000
      IF(I-1) 1160,1149,1149                                            00573000
 1160 J=J+1                                                             00574000
      IF(J-K) 1141,1141,1120                                            00575000
 1140 IF (KONST.NE.4) GO TO 1180                                        00576000
      KT=30                                                             00577000
      DO 1165 LS=31,50                                                  00578000
 1165 KP(LS)=0                                                          00579000
      GO TO 208                                                         00580000
C                                                                       00581000
C     SORT ZONEAXES WITHIN EACH SET INTO ORDER                          00582000
C                                                                       00583000
 1180 IF(KT.LE.30) GO TO 1185                                           00584000
      KT=30                                                             00585000
 1185 DO 1300 KS=1,KT                                                   00586000
      N=KP(KS)                                                          00587000
      DO 1210 KK=1,N                                                    00588000
 1210 HSUM(KK)=IZONES(1,KK,KS)+IZONES(2,KK,KS)+IZONES(3,KK,KS)          00589000
      M=N                                                               00590000
 1220 M=M/2                                                             00591000
      IF(M) 1230,1240,1230                                              00592000
 1230 K=N-M                                                             00593000
      J=1                                                               00594000
 1241 I=J                                                               00595000
 1249 L=I+M                                                             00596000
      IF(HSUM(L)-HSUM(I)) 1260,1260,1250                                00597000
 1250 HB=HSUM(I)                                                        00598000
      HSUM(I)=HSUM(L)                                                   00599000
      HSUM(L)=HB                                                        00600000
      DO 1252 NN=1,3                                                    00601000
      IP=IZONES(NN,I,KS)                                                00602000
      IZONES(NN,I,KS)=IZONES(NN,L,KS)                                   00603000
 1252 IZONES(NN,L,KS)=IP                                                00604000
      DO 1254 NN=1,5                                                    00605000
      IP=IHP(NN,I,KS)                                                   00606000
      IHP(NN,I,KS)=IHP(NN,L,KS)                                         00607000
      IHP(NN,L,KS)=IP                                                   00608000
      IP=IKP(NN,I,KS)                                                   00609000
      IKP(NN,I,KS)=IKP(NN,L,KS)                                         00610000
      IKP(NN,L,KS)=IP                                                   00611000
      IP=ILP(NN,I,KS)                                                   00612000
      ILP(NN,I,KS)=ILP(NN,L,KS)                                         00613000
 1254 ILP(NN,L,KS)=IP                                                   00614000
      I=(I-M)                                                           00615000
      IF(I-1)1260,1249,1249                                             00616000
 1260 J=J+1                                                             00617000
      IF(J-K)1241,1241,1220                                             00618000
 1240 DO 1293 IPZ=1,N                                                   00619000
      IPZN=IPZ-1                                                        00620000
      IF (IPZ.EQ.1) GO TO 1242                                          00621000
      IF(HSUM(IPZ).LT.HSUM(IPZN)) GO TO 1300                            00622000
 1242 IF(IZONES(1,IPZ,KS).LE.IZONES(2,IPZ,KS).AND.                      00623000
     1IZONES(2,IPZ,KS).LE.IZONES(3,IPZ,KS))GO TO 1290                   00624000
      GO TO 1293                                                        00625000
 1290 DO 1291 NN=1,3                                                    00626000
      IP=IZONES(NN,IPZ,KS)                                              00627000
      IZONES(NN,IPZ,KS)=IZONES(NN,1,KS)                                 00628000
 1291 IZONES(NN,1,KS)=IP                                                00629000
      DO 1292 NN=1,5                                                    00630000
      IP=IHP(NN,IPZ,KS)                                                 00631000
      IHP(NN,IPZ,KS)=IHP(NN,1,KS)                                       00632000
      IHP(NN,1,KS)=IP                                                   00633000
      IP=IKP(NN,IPZ,KS)                                                 00634000
      IKP(NN,IPZ,KS)=IKP(NN,1,KS)                                       00635000
      IKP(NN,1,KS)=IP                                                   00636000
      IP=ILP(NN,IPZ,KS)                                                 00637000
      ILP(NN,IPZ,KS)=ILP(NN,1,KS)                                       00638000
 1292 ILP(NN,1,KS)=IP                                                   00639000
 1293 CONTINUE                                                          00640000
 1300 CONTINUE                                                          00641000
```

```
C                                                                       00642000
C     WRITE OUT RESULTS                                                 00643000
C                                                                       00644000
      IF(KSETS-1) 1295,1295,1294                                        00645000
 1294 WRITE(6,1001) KSETS                                               00646000
 1295 DO 1500 KS=1,KT                                                   00647000
      IF(KP(KS)-1)1302,1302,1301                                        00648000
 1301 WRITE(6,1002)KS,(IZONES(NN,1,KS),NN=1,3),KS,KP(KS)                00649000
      WRITE(6,1016)                                                     00650000
      GO TO 1305                                                        00651000
 1302 WRITE(6,1003)KS,(IZONES(NN,1,KS),NN=1,3)                          00652000
      WRITE(6,1016)                                                     00653000
 1305 WRITE(6,1004)                                                     00654000
      DO 1308 I=1,LE                                                    00655000
      DISTIX(I,KS)=CAMKO(KS)/(2.*DISTIX(I,KS))                          00656000
 1308 WRITE(6,1005)I,IHP(I,1,KS),IKP(I,1,KS),ILP(I,1,KS),RADIX(I,KS),   00657000
     1DISTIX(I,KS)                                                      00658000
      WRITE(6,1008)CAMKO(KS)                                            00659000
      WRITE(6,1009)CAMCO                                                00660000
      ADEVN(KS)=DEVSQ(KS)/LE                                            00661000
      WRITE(6,1010)ADEVN(KS)                                            00662000
      WRITE(6,1007)                                                     00663000
      DO 1390 I=2,LE                                                    00664000
      LES=I-1                                                           00665000
 1390 WRITE(6,1006)I,ANGIX(LES,KS),ANGLES(LES)                          00666000
      IF(IOUT-1)1500,1395,1500                                          00667000
 1395 IF(KP(KS).LE.1) GO TO 1500                                        00668000
      WRITE(6,1011)KS                                                   00669000
      KKMAX=KP(KS)                                                      00670000
      IF(LE-3)1440,1396,1440                                            00671000
 1396 WRITE(6,1013)                                                     00672000
      DO 1400 I=2,KKMAX                                                 00673000
 1400 WRITE(6,1015)(IZONES(L,I,KS),L=1,3),IHP(1,I,KS),                  00674000
     1IKP(1,I,KS),ILP(1,I,KS),IHP(2,I,KS),IKP(2,I,KS),                  00675000
     2ILP(2,I,KS),IHP(3,I,KS),IKP(3,I,KS),ILP(3,I,KS)                   00676000
      GO TO 1500                                                        00677000
 1440 WRITE(6,1012)                                                     00678000
      DO 1460 I=2,KKMAX                                                 00679000
 1460 WRITE(6,1014)(IZONES(L,I,KS),L=1,3),IHP(1,I,KS),                  00680000
     1IKP(1,I,KS),ILP(1,I,KS),IHP(2,I,KS),IKP(2,I,KS),                  00681000
     2ILP(2,I,KS),IHP(3,I,KS),IKP(3,I,KS),ILP(3,I,KS),                  00682000
     3IHP(4,I,KS),IKP(4,I,KS),ILP(4,I,KS),IHP(5,I,KS),                  00683000
     4IKP(5,I,KS),ILP(5,I,KS)                                           00684000
 1500 CONTINUE                                                          00685000
      KS=0                                                              00686000
      KSETS=0                                                           00687000
      GO TO 1000                                                        00688000
 1600 WRITE(6,1017)                                                     00689000
      GO TO 1000                                                        00690000
 1000 RETURN                                                            00691000
C                                                                       00692000
C     FORMAT STATEMENTS----OUTPUT                                       00693000
C                                                                       00694000
 1001 FORMAT(1HO,I3,' SETS OF POSSIBLE ZONE AXES INDEX WITHIN SPECIFIED  00695000
     1LIMITS')                                                          00696000
 1002 FORMAT(1HO,/////11X,'SET ',I2,'    ZONE AXIS (',3I3,')',10X,'(SET  00697000
     1',I2,' HAS ',I2,' SYMMETRICAL EQUIVALENT SOLUTIONS)')             00698000
 1003 FORMAT(1HO,/////11X,'SET ',I2,'    ZONE AXIS (',3I3,')',10X,'(THER 00699000
     1E ARE NO SYMMETRICAL EQUIVALENT SOLUTIONS)')                      00700000
 1004 FORMAT(1HO,20X,'POINT',10X,'PLANE',10X,'DSPACE',10X,'ESTIMATED ',' 00701000
     1DSPACE FROM DIFF. PATTERN'/)                                      00702000
 1005 FORMAT(1H ,22X,I1,9X,'(',3I3,')',7X,F6.3,15X,F6.3)                00703000
 1006 FORMAT(1H ,20X,'ANGLE BETWEEN PLANES 1 & ',I1,                    00704000
     1' = ',F6.2,'  MEASURED ',F6.2,' DEGREES')                         00705000
 1007 FORMAT(1H )                                                       00706000
 1008 FORMAT(1HO,20X,'N.B. BEST FIT CAMERA CONSTANT USED ',             ' 00707000
     1IN ABOVE ESTIMATES OF D SPACINGS = ',F7.3)                        00708000
 1009 FORMAT(1H ,65X,'(INPUT CAMERA CONSTANT = ',F7.3,')')              00709000
 1010 FORMAT(1HO,20X,'MEAN DEVIATION OF MEASURED SPOTS ',               ' 00710000
     1FROM TRUE POSITIONS = ',F5.3,' MILLIMETRES')                      00711000
 1011 FORMAT(1HO,20X,'SYMMETRICAL EQUIVALENT SOLUTIONS ',               ' 00712000
     1FOR SET ',I2)                                                     00713000
 1012 FORMAT(1HO,21X,'ZONE AXIS',10X,'POINT 1',10X,'POINT 2',           00714000
     110X,'POINT 3',10X,'POINT 4',10X,'POINT 5',/)                      00715000
 1013 FORMAT(1HO,21X,'ZONE AXIS',10X,'POINT 1',10X,'POINT 2',           00716000
     110X,'POINT 3',/)                                                  00717000
 1014 FORMAT(1H ,20X,'(',3I3,')',7X,'(',3I3,')',6X,'(',                 00718000
     13I3,')',6X,'(',3I3,')',6X,'(',3I3,')',6X,'(3I3,')')               00719000
 1015 FORMAT(1H ,20X,'(',3I3,')',7X,'(',3I3,')',6X,'(',                 00720000
     13I3,')',6X,'(',3I3,')')                                           00721000
 1016 FORMAT(1H ,10X,'*******    **********************')               00722000
 1017 FORMAT(1HO,20X,'NO IDENTIFICATION',/21X,'********************')     00723000
      END                                                               00724000
```

APPENDIX 2

LISTING OF PROGRAM ANGLE

```
FTN4
      PROGRAM ANGLE
C     CALCULATES ANGLE BETWEEN ZONE AXES WHEN IPLAN=0,
C     CALCULATES ANGLE BETWEEN PLANE NORMAL AND ZONE AXIS WHEN
C     IPLAN=1, CALCULATES ANGLE BETWEEN TWO PLANES WHEN IPLAN=2.
C
      DIMENSION U(2),V(2),W(2),IU(2),IV(2),IW(2)
      WRITE(1,201)
      READ(1,101)
      WRITE(1,202)
      READ(1,102)A,B,C,ALPHA,BETA,GAMMA
      WRITE(6,101)
      WRITE(6,203)A,B,C,ALPHA,BETA,GAMMA
      ALPHA=ALPHA/57.29578
      BETA=BETA/57.29578
      GAMMA=GAMMA/57.29578
      WRITE(1,204)
    5 READ(1,103) IPLAN,IU(1),IV(1),IW(1),IU(2),IV(2),IW(2)
   10 IF(IPLAN-1)40,20,20
   20 S11=B*B*C*C*SIN(ALPHA)*SIN(ALPHA)
      S22=A*A*C*C*SIN(BETA)*SIN(BETA)
      S33=A*A*B*B*SIN(GAMMA)*SIN(GAMMA)
      S12=A*B*C*C*((COS(ALPHA)*COS(BETA))-(COS(GAMMA)))
      S23=A*A*B*C*((COS(BETA)*COS(GAMMA))-COS(ALPHA))
      S31=A*B*B*C*((COS(GAMMA)*COS(ALPHA))-COS(BETA))
      DO 30 I=1,2
      U(I)=IU(I)*S11+IV(I)*S12+IW(I)*S31
      V(I)=IU(I)*S12+IV(I)*S22+IW(I)*S23
      W(I)=IU(I)*S31+IV(I)*S23+IW(I)*S33
      IF(IPLAN.EQ.1) GO TO 50
   30 CONTINUE
      GO TO 60
   40 U(1)=IU(1)
      V(1)=IV(1)
      W(1)=IW(1)
   50 U(2)=IU(2)
      V(2)=IV(2)
      W(2)=IW(2)
   60 AIUVW1=(A*A*U(1)*U(1))+(B*B*V(1)*V(1))+(C*C*W(1)*W(1))+(2.*B*C*V
     1(1)*W(1)*COS(ALPHA))+(2.*C*A*W(1)*U(1)*COS(BETA))+(2.*A*B*U(1
     2)*V(1)*COS(GAMMA))
      AIUVW1=SQRT(AIUVW1)
      AIUVW2=(A*A*U(2)*U(2))+(B*B*V(2)*V(2))+(C*C*W(2)*W(2))+(2.*B*C*
     1W(2)*W(2)*COS(ALPHA))+(2.*C*A*W(2)*U(2)*COS(BETA))+(2.*A*B*U(2)
     2*V(2)*COS(GAMMA))
      AIUVW2=SQRT(AIUVW2)
   70 AL=(A*A*U(1)*U(2))+(B*B*V(1)*V(2))+(C*C*W(1)*W(2))+(B*C*(V(1)*
     1W(2)+W(1)*V(2))*COS(ALPHA))+(A*C*(W(1)*U(2)+U(1)*W(2))*COS(BETA
     2))+(A*B*(U(1)*V(2)+V(1)*U(2))*COS(GAMMA))
      COSRO=AL/(AIUVW1*AIUVW2)
   80 CORO=(SQRT(1-COSRO*COSRO))/COSRO
      RO=ATAN(CORO)
      ROANG=RO*57.29578
      IF(COSRO)81,82,82
   81 ROANG=180+ROANG
   82 IF(IPLAN-1)85,90,95
   85 WRITE(6,205) IU(1),IV(1),IW(1),IU(2),IV(2),IW(2),ROANG
      GO TO 5
   90 WRITE(6,206) IU(1),IV(1),IW(1),IU(2),IV(2),IW(2),ROANG
      GO TO 5
   95 WRITE(6,207) IU(1),IV(1),IW(1),IU(2),IV(2),IW(2),ROANG
      GO TO 5
  101 FORMAT(1H ,40HTHIS SPACE RESERVED FOR THE TITLE        )
  102 FORMAT(3F10.3,3F10.2)
  103 FORMAT(I1,6I3)
  201 FORMAT(1H ,"INPUT NAME OF CRYSTAL   TO FORMAT 20A4")
  202 FORMAT(1H ,"INPUT A,B,C,ALPHA,BETA,GAMMA, TO FORMAT 3F10.3",
     1",3F10.2")
  203 FORMAT(/6F9.3)
  204 FORMAT(1H ,"INPUT IPLAN, INDICES OF PLANE (OR ZONE) 1, AND",/
     1" INDICES OF PLANE (OR ZONE) 2   TO FORMAT I1,6I3",/"N.B.",
     2" IPLAN=0 FOR ANGLE BETWEEN TWO ZONE AXES",/11X,"1 FOR ",
     3"ANGLE BETWEEN PLANE NORMAL AND ZONE AXIS",/11X,"2 FOR ",
     4"ANGLE BETWEEN TWO PLANES")
  205 FORMAT(1H ,"ANGLE OF ZONE AXIS     ",3I3," TO ZONE AXIS "
     1,3I3," IS ",F7.2," DEG")
  206 FORMAT(1H ,"ANGLE OF PLANE NORMAL ",3I3," TO ZONE AXIS "
     1,3I3," IS ",F7.2," DEG")
  207 FORMAT(1H ,"ANGLE OF PLANE         ",3I3," TO PLANE     "
     1,3I3," IS ",F7.2," DEG")
      END
     END$
```

```
ALPHA FE2O3     STRUCTURAL RHOMBOHEDRAL

    5.427     5.427     5.427    55.260    55.260    55.260

 ANGLE OF ZONE AXIS      1   0  -1 TO ZONE AXIS      1   1   1 IS    90.00 DEG
 ANGLE OF ZONE AXIS      1   1   1 TO ZONE AXIS      0   1   0 IS    32.38 DEG
 ANGLE OF PLANE NORMAL   1   0   1 TO ZONE AXIS      1   1   1 IS    57.62 DEG
 ANGLE OF PLANE NORMAL   1   1   1 TO ZONE AXIS      1   1   1 IS      .03 DEG
 ANGLE OF PLANE          1   0   1 TO PLANE         1   0  -1 IS    90.00 DEG
 ANGLE OF PLANE          0   1   0 TO PLANE         1   1   1 IS    72.41 DEG
```

Fig. A2.1 Sample of output from program ANGLE

Small discrepancy of 0.03° indicates level of error which may accumulate in the angular determination as a result of accumulated computation error on the HP2100 minicomputer. Such errors can be readily reduced by specification of double precision variables or by detailed attention to the manner in which transformations between direct and reciprocal lattices are performed.

APPENDIX 3

Listing of Program DSPACING

```
C     PROGRAM DSPACING          B.L. RHOADES                                    00001000
C                                                                               00002000
C     TO DETERMINE D SPACINGS FOR PERMISSIBLE REFLECTIONS FROM ANY              00003000
C     CRYSTAL STRUCTURE   ***   OR TO INDEX LOOSE SPOTS ON SINGLE               00004000
C     CRYSTAL PATTERNS                                                          00005000
C                                                                               00006000
C     FORM OF INPUT DATA                                                        00007000
C                                                                               00008000
C                                                                               00009000
C     DATA CARD 1   SYM,TITLE                              (I1,19A4)          00010000
C                                                                               00011000
C     N.B. FOR SYM WRITE 0 FOR PRIMITIVE CELL TYPE P                            00012000
C                        1 FOR ALL FACES CENTRED TYPE F                         00013000
C                        2 FOR BODY CENTRED CELL TYPE I                         00014000
C                        3 FOR A FACE CENTRED CELL TYPE A                       00015000
C                        4 FOR B FACE CENTRED CELL TYPE B                       00016000
C                        5 FOR C FACE CENTRED CELL TYPE C                       00017000
C                        6 FOR OBVERSE RHOMB (HEX CELL) TYPE R                  00018000
C                        7 FOR REVERSE RHOMB (HEX CELL) TYPE R                  00019000
C                                                                               00020000
C     DATA CARD 2   A,B,C,ALPHA,BETA,GAMMA              (3F10.3,3F10.2)       00021000
C     DATA CARD 3   MIN D SPACING REQUIRED                  (F6.3)              00022000
C     DATA CARD 4   ICNTRL                                                      00023000
C                                                                               00024000
C                FOR ICNTRL WRITE 1 IF DSPACE LISTING ONLY IS REQD.             00025000
C                                 2 IF LOOSESPOTS IDENTIFICATION REQD.          00026000
C                                 3 IF DSPACE LISTING AND LOOSESPOTS            00027000
C                                   ARE BOTH REQD.                              00028000
C                                                                               00029000
C     IF ICNTRL = 2 OR 3 THE FOLLOWING DATA CARDS ARE REQUIRED TO               00030000
C       PROVIDE DETAILS OF LOOSE SPOTS TO BE INDEXED                            00031000
C                                                                               00032000
C     DATA CARD 5   PHOTO                                  (20A4)             00033000
C     DATA CARD 6   NSP, CAMCO, TOL , ANGTOL   (I2,F8.4,2F6.3)                 00034000
C     DATA CARD 7   INDICES OF DATUM SPOTS          (2* (3I3,2X))               00035000
C     DATA CARD 8   DIST, ANGLES                   (3F8.3)                      00036000
C                                                                               00037000
C        (N.B.   ONE CARD FOR EACH OF NSP SPOTS)                                00038000
C                                                                               00039000
C     PROGRAM DSPACING                                                          00040000
C                                                                               00041000

      COMMON PRINTR,IND(3,15000),DSPACE(15000),SYM,TITLE                        00042000
      COMMON/CELL/A,B,C,COSA,COSB,COSG                                          00043000
      COMMON/RCELL/ASTAR,BSTAR,CSTAR,COSAS,COSBS,COSGS                          00044000
      INTEGER READR,PRINTR,H,HMAX                                               00045000
      DIMENSION TITLE(19)                                                       00046000
      DIMENSION FORMA(21)                                                       00047000
      DOUBLE PRECISION A,B,C,PI180,V,DMAX,DSQ,ASTAR,BSTAR                       00048000
      DOUBLE PRECISION CSTAR,SINA,SINB,SING,COSA,COSB,COSG,COSAS                00049000
      DOUBLE PRECISION COSBS,COSGS,A11,A12,A13,A22,A23,A33,DMIN                 00050000
      DOUBLE PRECISION ALPHA,BETA,GAMMA                                         00051000
    2 READR=5                                                                   00052000
      PRINTR=6                                                                  00053000
      DATA FORMA/6H(//6X,,6H'H  K  ,6H L',7X,6H,'DSPA,6HCE'    ,6H,14X,',      00054000
     16HH  K   ,6HL',7X,,6H'DSPAC,6HE'     ,6H,14X,',6HH  K   ,6HL',7X,,       00055000
     26H'DSPAC,6HE'     ,6H,14X,',6HH  K   ,6HL',7X,,6H'DSPAC,6HE'     ,       00056000
     36H///)  /                                                                 00057000
      DATA LEFT,RIGHT,ASPEC,FSPEC,BLANKS,ISPEC,XSPEC,AISPEC/6H(4X,   ,          00058000
     16H)      ,6HA13,   ,6HF13.3,,6H       ,6H3I3,   ,6H12X,   ,6H3A3,   /   00059000
C                                                                               00060000
C     ****READ DETAILS OF MATERIALS                                             00061000
C                                                                               00062000
   10 READ(5,101)SYM,(TITLE(J),J=1,19)                                          00063000

      SYMI=SYM+1                                                                00064000
      READ(READR,104) A,B,C,ALPHA,BETA,GAMMA                                    00065000
    4 READ (5,107)DMIN                                                          00066000
      READ(5,112) ICNTRL                                                        00067000
      WRITE (6,205) TITLE                                                       00068000

      WRITE (PRINTR,221)                                                        00069000
      WRITE (PRINTR,221)                                                        00070000
      WRITE (PRINTR,221)                                                        00071000
      WRITE(PRINTR,206)                                                         00072000
      WRITE(PRINTR,207) A,B,C,ALPHA,BETA,GAMMA                                  00073000
      WRITE (6,208)DMIN                                                         00074000
C                                                                               00075000
C     ****COMPUTE RECIPROCAL CONSTANTS                                          00076000
C                                                                               00077000
   12 PI180=3.1415926535897932/180.                                             00078000
      SINA=DSIN(ALPHA*PI180)                                                    00079000
      SINB=DSIN(BETA*PI180)                                                     00080000
      SING=DSIN(GAMMA*PI180)                                                    00081000
      COSA=DCOS(ALPHA*PI180)                                                    00082000
      COSB=DCOS(BETA*PI180)                                                     00083000
      COSG=DCOS(GAMMA*PI180)                                                    00084000
      V=1./(A*B*C*DSQRT(1.+2.*COSA*COSB*COSG-COSA*COSA-COSB*COSB-COSG*CO        00085000
     1SG))                                                                      00086000
      ASTAR=B*C*V*SINA                                                          00087000
      BSTAR=A*C*V*SINB                                                          00088000
      CSTAR=A*B*V*SING                                                          00089000
```

```
      COSAS=(COSB*COSG-COSA)/(SINB*SING)                                    00090000
      COSBS=(COSA*COSG-COSB)/(SINA*SING)                                    00091000
      COSGS=(COSA*COSB-COSG)/(SINA*SINB)                                    00092000
      A11=ASTAR*ASTAR                                                       00093000
      A22=BSTAR*BSTAR                                                       00094000
      A33=CSTAR*CSTAR                                                       00095000
      A12=2.*ASTAR*BSTAR*COSGS                                              00096000
      A13=2.*ASTAR*CSTAR*COSBS                                              00097000
      A23=2.*BSTAR*CSTAR*COSAS                                              00098000
C                                                                           00099000
C     ****DETERMINE LIMITS OF INDICES                                       00100000
C                                                                           00101000
      HMAX=DSQRT(1./(ASTAR*ASTAR*DMIN*DMIN))                                00102000
      KMAX=DSQRT(1./(BSTAR*BSTAR*DMIN*DMIN))                                00103000
      LMAX=DSQRT(1./(CSTAR*CSTAR*DMIN*DMIN))                                00104000
      NHMAX=-HMAX                                                           00105000
      NKMAX=-KMAX                                                           00106000
      NLMAX=-LMAX                                                           00107000
      M=0                                                                   00108000
      DO 70 H=NHMAX,HMAX                                                    00109000
      DO 70 K=NKMAX,KMAX                                                    00110000
      DO 70 L=NLMAX,LMAX                                                    00111000
      IF(H.EQ.0.AND.L.EQ.0.AND.K.EQ.0) GO TO 70                             00112000
      DSQ=H*H*A11+H*K*A12+H*L*A13+K*K*A22+K*L*A23+L*L*A33                   00113000
      D=SNGL(DSQRT(1./DSQ))                                                 00114000
      IF (D.LT.DMIN) GO TO 70                                               00115000
C                                                                           00116000
C     ****TEST INDICES AND ELIMINATE PROHIBITED REFLECTIONS                 00117000
C                                                                           00118000
      GO TO (17,13,15,61,62,13,63,64),SYMI                                  00119000
   13 AKH=(K+H)/2.                                                          00120000
      KH=AKH                                                                00121000
      BKH=KH                                                                00122000
      IF(AKH.NE.BKH) GO TO 70                                               00123000
      IF(SYMI.NE.2) GO TO 17                                                00124000
   62 ALH=(L+H)/2.                                                          00125000
      LH=ALH                                                                00126000
      BLH=LH                                                                00127000
      IF(ALH.NE.BLH) GO TO 70                                               00128000
      IF(SYMI.NE.2) GO TO 17                                                00129000
   61 AKL=(K+L)/2.                                                          00130000
      KL=AKL                                                                00131000
      BKL=KL                                                                00132000
      IF(AKL.NE.BKL) GO TO 70                                               00133000
      GO TO 17                                                              00134000
   15 AKHL=(H+K+L)/2.                                                       00135000
      GO TO 66                                                              00136000
   63 AKHL=(K+L-H)/3.                                                       00137000
      GO TO 66                                                              00138000
   64 AKHL=(H+L-K)/3.                                                       00139000
   66 KHL=AKHL                                                              00140000
      BKHL=KHL                                                              00141000
      IF(AKHL.NE.BKHL) GO TO 70                                             00142000
   17 M=M+1                                                                 00143000
      IF (M.GT.15000) GO TO 1003                                            00144000
      IND(1,M)=H                                                            00145000
      IND(2,M)=K                                                            00146000
      IND(3,M)=L                                                            00147000
      DSPACE(M)=D                                                           00148000
   70 CONTINUE                                                              00149000
      NUMAX=M                                                               00150000
      CALL SORT (M)                                                         00151000
      IF(ICNTRL-2) 90,80,90                                                 00152000
   90 CALL OUTPUT (LEFT,RIGHT,ASPEC,FSPEC,BLANKS,ISPEC,XSPEC,NUMAX,FORMA   00153000
     1,AISPEC,SYMI)                                                         00154000
      IF(ICNTRL-2) 95,95,80                                                 00155000
   80 CALL LSPOTS (M,ASTAR,BSTAR,CSTAR,COSAS,COSBS,COSGS,ICNTRL)            00156000
   95 GO TO 10                                                              00157000
 1003 WRITE(PRINTR,218)                                                     00158000
      GO TO 10                                                              00159000
 1004 STOP                                                                  00160000
C                                                                           00161000
C     **** FORMAT STATEMENTS                                                00162000
C                                                                           00163000
  101 FORMAT(I1,19A4)                                                       00164000
  104 FORMAT(3F10.3,3F10.2)                                                 00165000
  107 FORMAT(F6.3)                                                          00166000
  112 FORMAT(I1)                                                            00167000
  205 FORMAT(1HI,19A4)                                                      00168000
  206 FORMAT(1HO,'REAL CELL CONSTANTS'//6X,'A',8X,'B',8X,'C',6X,'ALPHA',    00169000
     15X,'BETA',4X,'GAMMA'/)                                                00170000
  207 FORMAT(6F9.3)                                                         00171000
  208 FORMAT(1HO,'MINIMUM DSPACE DESIRED =',F6.3,' ANGSTROMS')              00172000
  218 FORMAT(1HO,'ARRAY LIMITS EXCEEDED---MATERIAL CHECK CANCELLED')        00173000
  221 FORMAT(55H*******************************************************)    00174000
      END                                                                   00175000
```

```
      SUBROUTINE SORT (N)                                                   00176000
                                                                            00177000
C                                                                           00178000
C     SORT ARRAY INTO DESCENDING ORDER OF DSPACE                            00179000
C                                                                           00180000
       COMMON PRINTR,IND(3,15000),DSPACE(15000),SYM,TITLE                   00181000
      M=N                                                                   00182000
 1020 M=M/2                                                                 00183000
      IF (M) 1030,1040,1030                                                 00184000
 1030 K=N-M                                                                 00185000
      J=1                                                                   00186000
 1041 I=J                                                                   00187000
 1049 L=I+M                                                                 00188000
      IF (DSPACE(L)-DSPACE(I)) 1060,1060,1050                               00189000
 1050 B=DSPACE(I)                                                           00190000
      DSPACE(I)=DSPACE(L)                                                   00191000
      DSPACE(L)=B                                                           00192000
      DO 1055 NM=1,3                                                        00193000
      IB=IND(NM,I)                                                          00194000
      IND(NM,I)=IND(NM,L)                                                   00195000
      IND(NM,L)=IB                                                          00196000
 1055 CONTINUE                                                              00197000
      I=(I-M)                                                               00198000
      IF (I-1) 1060,1049,1049                                               00199000
 1060 J=J+1                                                                 00200000
      IF(J-K) 1041,1041,1020                                                00201000
 1040 RETURN                                                                00202000
      END
```

```
      SUBROUTINE OUTPUT (LEFT,RIGHT,ASPEC,FSPEC,BLANKS,ISPEC,XSPEC,NUMAX 00203000
     1,FORMA,AISPEC,SYMI)                                                   00204000
                                                                            00205000
C                                                                           00206000
C     SUPPRESSES REPEATED D-SPACINGS AND FORMATS OUTPUT                     00207000
C                                                                           00208000
       COMMON PRINTR,IND(3,15000),DSPACE(15000),SYM,TITLE                   00209000
      DIMENSION FORM(13),DSP(4),TITLE(19)                                   00210000
      DIMENSION FORME(21),FORMA(21)                                         00211000
      FORM(1)=LEFT                                                          00212000
      FORM(2)=ISPEC                                                         00213000
      FORM(4)=XSPEC                                                         00214000
      FORM(5)=ISPEC                                                         00215000
      FORM(7)=XSPEC                                                         00216000
      FORM(8)=ISPEC                                                         00217000
      FORM(10)=XSPEC                                                        00218000
      FORM(11)=ISPEC                                                        00219000
      FORM(13)=RIGHT                                                        00220000
   10 IM=0                                                                  00221000
      ANT=(NUMAX/200.)+0.999                                                00222000
      NT=ANT                                                                00223000
   20 DO 90 NTIMES=1,NT                                                     00224000
      IF (NTIMES.EQ.1) GO TO 22                                             00225000
      WRITE (6,205) TITLE                                                   00226000
   22 WRITE (PRINTR,209) NTIMES,NT                                          00227000
      GO TO (38,31,32,33,34,35,36,37),SYMI                                  00228000
   31 WRITE(6,534)                                                          00229000
      GO TO 38                                                              00230000
   32 WRITE(6,535)                                                          00231000
      GO TO 38                                                              00232000
   33 WRITE(6,536)                                                          00233000
      GO TO 38                                                              00234000
   34 WRITE(6,537)                                                          00235000
      GO TO 38                                                              00236000
   35 WRITE(6,538)                                                          00237000
      GO TO 38                                                              00238000
   36 WRITE(6,539)                                                          00239000
      GO TO 38                                                              00240000
   37 WRITE(6,540)                                                          00241000
   38 NLAST=(NUMAX-(NTIMES-1)*200)                                          00242000
      DO 5 LE=1,21                                                          00243000
      FORME(LE)=FORMA(LE)                                                   00244000
    5 CONTINUE                                                              00245000
   11 IF(NLAST-50) 14,14,12                                                 00246000
   12 IF (NLAST-100) 15,15,13                                               00247000
   13 IF (NLAST-150) 16,16,29                                               00248000
   14 DO 114 L=6,10                                                         00249000
      FORME(L)=BLANKS                                                       00250000
  114 CONTINUE
```

```
   15 DO 115 L=11,15                                                    00251000
      FORME(L)=BLANKS                                                   00252000
  115 CONTINUE                                                          00253000
   16 DO 116 L=16,20                                                    00254000
      FORME(L)=BLANKS                                                   00255000
  116 CONTINUE                                                          00256000
   29 WRITE(6,FORME)                                                    00257000
   30 DO 80 IMI=1,50                                                    00258000
      IMM=IM+IMI                                                        00259000
      IMMA=IMM+50                                                       00260000
      IMMB=IMM+100                                                      00261000
      IMMC=IMM+150                                                      00262000
      IZ=IMM-1                                                          00263000
      IZA=IMMA-1                                                        00264000
      IZB=IMMB-1                                                        00265000
      IZC=IMMC-1                                                        00266000
      FORM(3)=FSPEC                                                     00267000
      FORM(6)=FSPEC                                                     00268000
      FORM(9)=FSPEC                                                     00269000
      FORM(12)=FSPEC                                                    00270000
      DSP(1)=DSPACE(IMM)                                                00271000
      DSP(2)=DSPACE(IMMA)                                               00272000
      DSP(3)=DSPACE(IMMB)                                               00273000
      DSP(4)=DSPACE(IMMC)                                               00274000
   40 IF (IMM.GT.NUMAX) GO TO 141                                       00275000
      IF(IMI.EQ.1) GO TO 42                                             00276000
      IF (DSPACE(IMM).EQ.DSPACE(IZ)) GO TO 142                          00277000
   42 IF (IMMA.GT.NUMAX) GO TO 144                                      00278000
      IF(IMI.EQ.1) GO TO 44                                             00279000
      IF (DSPACE(IMMA).EQ.DSPACE(IZA)) GO TO 145                        00280000
   44 IF (IMMB.GT.NUMAX) GO TO 147                                      00281000
      IF(IMI.EQ.1) GO TO 46                                             00282000
      IF (DSPACE(IMMB).EQ.DSPACE(IZB)) GO TO 148                        00283000
   46 IF (IMMC.GT.NUMAX) GO TO 150                                      00284000
      IF(IMI.EQ.1) GO TO 48                                             00285000
      IF (DSPACE(IMMC).EQ.DSPACE(IZC)) GO TO 151                        00286000
      GO TO 48                                                          00287000
  141 DO 143 NZ=1,3                                                     00288000
      IND(NZ,IMM)=BLANKS                                                00289000
  143 CONTINUE                                                          00290000
      FORM(2)=AISPEC                                                    00291000
  142 FORM(3)=ASPEC                                                     00292000
      DSP(1)=BLANKS                                                     00293000
      GO TO 42                                                          00294000
  144 DO 146 NZ=1,3                                                     00295000
      IND(NZ,IMMA)=BLANKS                                               00296000
  146 CONTINUE                                                          00297000
      FORM(5)=AISPEC                                                    00298000
  145 FORM(6)=ASPEC                                                     00299000
      DSP(2)=BLANKS                                                     00300000
      GO TO 44                                                          00301000
  147 DO 149 NZ=1,3                                                     00302000
      IND(NZ,IMMB)=BLANKS                                               00303000
  149 CONTINUE                                                          00304000
      FORM(8)=AISPEC                                                    00305000
  148 FORM(9)=ASPEC                                                     00306000
      DSP(3)=BLANKS                                                     00307000
      GO TO 46                                                          00308000
  150 DO 152 NZ=1,3                                                     00309000
      IND(NZ,IMMC)=BLANKS                                               00310000
  152 CONTINUE                                                          00311000
      FORM(11)=AISPEC                                                   00312000
  151 FORM(12)=ASPEC                                                    00313000
      DSP(4)=BLANKS                                                     00314000
   48 WRITE (PRINTR,FORM)(IND(IZ,IMM),IZ=1,3),DSP(1),(IND(IZ,IMMA),IZ=1, 00315000
     13),DSP(2),(IND(IZ,IMMB),IZ=1,3),DSP(3),(IND(IZ,IMMC),IZ=1,3),DSP(4 00316000
     2)                                                                 00317000
   80 CONTINUE                                                          00318000
      IM=IM+200                                                         00319000
   90 CONTINUE                                                          00320000
  100 RETURN                                                            00321000
C                                                                       00322000
C     FORMAT STATEMENTS                                                 00323000
C                                                                       00324000
  205 FORMAT(1H1,20A4)                                                  00325000
  209 FORMAT(1HO,'LIST OF D SPACINGS  (UNIT = ANGSTROMS)',43X,'SHEET',I2 00326000
     1,' OF',I2,' SHEETS'///)                                           00327000
  534 FORMAT(1HO,    'PROHIBITED REFLECTIONS FOR THE FACE CENTRED CELL T 00328000
     1YPE F HAVE BEEN OMITTED')                                         00329000
  535 FORMAT(1HO,    'PROHIBITED REFLECTIONS FOR THE BODY CENTRED CELL T 00330000
     1YPE I HAVE BEEN OMITTED')                                         00331000
  536 FORMAT(1HO,    'PROHIBITED REFLECTIONS FOR THE FACE CENTRED CELL T 00332000
     1YPE A HAVE BEEN OMITTED')                                         00333000
  537 FORMAT(1HO,    'PROHIBITED REFLECTIONS FOR THE FACE CENTRED CELL T 00334000
     1YPE B HAVE BEEN OMITTED')                                         00335000
  538 FORMAT(1HO,    'PROHIBITED REFLECTIONS FOR THE FACE CENTRED CELL T 00336000
     1YPE C HAVE BEEN OMITTED')                                         00337000
  539 FORMAT(1HO,    'PROHIBITED REFLECTIONS FOR THE OBVERSE RHOMBOHEDRO 00338000
     1N (HEXAGONAL CELL) TYPE R HAVE BEEN OMITTED')                     00339000
  540 FORMAT(1HO,    'PROHIBITED REFLECTIONS FOR THE REVERSE RHOMBOHEDRO 00340000
     1N (HEXAGONAL CELL) TYPE R HAVE BEEN OMITTED')                     00341000
      END                                                               00342000
```

```
      SUBROUTINE LSPOTS (NI,ASTAR,BSTAR,CSTAR,COSAS,COSBS,COSGS,ICNTRL)  00343000
C                                                                        00344000
C     COMPARES ANGLES BETWEEN RECIPROCAL VECTORS                         00345000
C                                                                        00346000
       COMMON PRINTR,IND(3,15000),DSPACE(15000),SYM,TITLE                00347000
      DOUBLE PRECISION ASTAR,BSTAR,CSTAR,COSAS,COSBS,COSGS,S,T,Y,X       00348000
      DIMENSION INDS(3,2),DIST(50),ANG(2,50),                            00349000
     1IH(2),IK(2),IL(2),ANGIX(2),PHOTO(20)                               00350000
      INTEGER POINTS,POSTVS                                              00351000
      INTEGER U,V,W                                                      00352000
      DOUBLE PRECISION AHZERO,AKZERO,ALZERO,DH,DK,DL                     00353000
   10 READ (5,901)(PHOTO(J),J=1,20)                                      00354000
      READ(5,902)NSP,CAMCO,TOL,ANGTOL                                    00355000
      READ(5,903)((INDS(N,M),N=1,3),M=1,2)                               00356000
      AMTOL=0.05                                                         00357000
      PAMTOL=AMTOL*100.                                                  00358000
      DPR=57.295780                                                      00359000
   30 DO 40 M=1,NSP                                                      00360000
   40 READ(5,904)DIST(M),(ANG(I,M),I=1,2)                                00361000
      DO 20 M=1,NSP                                                      00362000
      DO 20 I=1,2                                                        00363000
      COSANG=COS(ANG(I,M)/DPR)                                           00364000
   20 ANG(I,M)=(ARCOS(COSANG))*DPR                                       00365000
      IF(ICNTRL-3) 45,42,45                                              00366000
   42 WRITE(6,959)                                                       00367000
   45 WRITE(6,952)PHOTO                                                  00368000
      WRITE(6,953)                                                       00369000
      WRITE(6,954)CAMCO,ANGTOL,TOL                                       00370000
      WRITE(6,961) PAMTOL                                                00371000
      WRITE(6,958)((INDS(N,M),N=1,3),M=1,2)                              00372000
      IF(NSP.GT.50) GO TO 1000                                           00373000
C                                                                        00374000
C     SORT THROUGH LIST OF DSPACES AND CHECK ALL POINTS                  00375000
C     WITHIN TOLERANCE                                                   00376000
C     N.B. ALL ANGLES MUST COME WITHIN ANGLE TOLERANCE OR                00377000
C     SPOT IS REJECTED                                                   00378000
C                                                                        00379000
      CALL ZONES (U,V,W,INDS,DH,DK,DL)                                   00380000
      WRITE(6,960) U,V,W                                                 00381000
      DO 50 I=1,2                                                        00382000
      IH(I)=INDS(1,I)                                                    00383000
      IK(I)=INDS(2,I)                                                    00384000
   50 IL(I)=INDS(3,I)                                                    00385000
      ICHECK=0                                                           00386000
      DO 75 N=1,NSP                                                      00387000
      DSPCE=CAMCO/(2.*DIST(N))                                           00388000
      WRITE(6,949)N,DSPCE,(ANG(KZ,N),KZ=1,2)                             00389000
      IF(TOL-(DIST(N)*AMTOL)) 54,55,55                                   00390000
   54 DISTN=DIST(N)-(DIST(N)*AMTOL)                                      00391000
      DISTX=DIST(N)+(DIST(N)*AMTOL)                                      00392000
      GO TO 56                                                           00393000
   55 DISTN=DIST(N)-TOL                                                  00394000
      DISTX=DIST(N)+TOL                                                  00395000
   56 DSPX=CAMCO/(2.*DISTN)                                              00396000
      DSPN=CAMCO/(2.*DISTX)                                              00397000
      DO 70 NA=1,NI                                                      00398000
      IF(DSPACE(NA).GT.DSPX)GO TO 70                                     00399000
      IF(DSPACE(NA).LT.DSPN)GO TO 72                                     00400000
      NH=IND(1,NA)*U+IND(2,NA)*V+IND(3,NA)*W                             00401000
      IF (NH.GT.12.OR.NH.LT.-12) GO TO 70                                00402000
      AHZERO=IND(1,NA)-NH*DH                                             00403000
      AKZERO=IND(2,NA)-NH*DK                                             00404000
      ALZERO=IND(3,NA)-NH*DL                                             00405000
```

```
C                                                                       00406000
C     CALCULATE AND CHECK ANGLES                                        00407000
C                                                                       00408000
      DO 65 NN=1,2                                                      00409000
      S=((AHZERO*IH(NN)*ASTAR*ASTAR)+(AKZERO*IK(NN)*BSTAR*BSTAR)+(ALZERO 00410000
     1*IL(NN)*CSTAR*CSTAR)+((AKZERO*IL(NN)+ALZERO*IK(NN))*BSTAR*CSTAR*CO 00411000
     2SAS)+((ALZERO*IH(NN)+IL(NN)*AHZERO)*CSTAR*ASTAR*COSBS)+((AHZERO*IK 00412000
     3(NN)+AKZERO*IH(NN))*ASTAR*BSTAR*COSGS))                           00413000
      T=((AHZERO*AHZERO*ASTAR*ASTAR)+(AKZERO*AKZERO*BSTAR*BSTAR)+(ALZERO 00414000
     1*ALZERO*CSTAR*CSTAR)+(2.0*AHZERO*AKZERO*ASTAR*BSTAR*COSGS)+(2.0*AL 00415000
     2ZERO*AHZERO*CSTAR*ASTAR*COSBS)+(2.0*AKZERO*ALZERO*BSTAR*CSTAR*COSA 00416000
     3S))                                                               00417000
      Y=((IH(NN)*IH(NN)*ASTAR*ASTAR)+(IK(NN)*IK(NN)*BSTAR*BSTAR)+(IL(NN) 00418000
     1*IL(NN)*CSTAR*CSTAR)+(2.0*IH(NN)*IK(NN)*ASTAR*BSTAR*COSGS)+(2.0*IL 00419000
     2(NN)*IH(NN)*CSTAR*ASTAR*COSBS)+(2.0*IK(NN)*IL(NN)*BSTAR*CSTAR*COSA 00420000
     3S))                                                               00421000
      Z=DSQRT(T*Y)                                                      00422000
      YZ=SNGL(S/Z)                                                      00423000
      YY=ARCOS(YZ)                                                      00424000
      YY=YY*DPR                                                         00425000
      ANGMAX=ANG(NN,N)+ANGTOL                                           00426000
      ANGMIN=ANG(NN,N)-ANGTOL                                           00427000
      IF(YY.GT.ANGMAX.OR.YY.LT.ANGMIN) GO TO 70                         00428000
   65 ANGIX(NN)=YY                                                      00429000
      WRITE(6,955) (IND(K,NA),K=1,3),DSPACE(NA),(ANGIX(NN),NN=1,2),NH   00430000
      ICHECK=ICHECK+1                                                   00431000
   70 CONTINUE                                                          00432000
   72 IF(ICHECK)73,73,74                                                00433000
   73 WRITE(6,957)                                                      00434000
   74 WRITE(6,956)                                                      00435000
   75 ICHECK=0                                                          00436000
      GO TO 1001                                                        00437000
C                                                                       00438000
C     FORMAT STATEMENTS                                                 00439000
C                                                                       00440000
  901 FORMAT(20A4)                                                      00441000
  902 FORMAT(I2,F8.4,F6.3,F6.3)                                         00442000
  903 FORMAT(3I3,2X,3I3)                                                00443000
  904 FORMAT(3F8.3)                                                     00444000
  949 FORMAT(1HO,////1X,'POINT',I3,'  MEASURED DSPACE ',F6.3,30X,'MEASU 00445000
     1RED ANGLES',2F10.2)                                               00446000
  951 FORMAT(1HO,'ERROR CONDITION EXISTS FOR INPUT TO '                 00447000
     1'LOOSESPOTS SUBROUTINE   RERUN DATA')                             00448000
  952 FORMAT(1HO,///1X,20A4)                                            00449000
  953 FORMAT(1H ,40H**********************************************)      00450000
  954 FORMAT(1HO,20X,'CAMERA CONSTANT =',F8.3,5X,'ANGLE TOLERANCE =',   00451000
     1F6.2,' DEGREES',5X,'POSITION TOLERANCE =',F6.2,' MILLIMETRES')    00452000
  955 FORMAT(1HO,9X,' IDENTIFIED AS PLANE (',3I3,')     DSPACE =',F6.3,4 00453000
     1X,' TRUE ANGLES ',2F10.2,5X,'ORDER OF REFLECTION = ', I3)         00454000
  956 FORMAT(1HO,//)                                                    00455000
  957 FORMAT(1HO,10X,'NO IDENTIFICATION FOR THIS SPOT')                 00456000
  958 FORMAT(1HO,20X,'DATUM PLANES ARE',10X,3I3,6X,3I3)                 00457000
  959 FORMAT(1H1)                                                       00458000
  960 FORMAT(1HO,20X,'ZONE REPRESENTED BY DATUM PLANES IS   ',3I3)      00459000
  961 FORMAT(1HO,30X,'(N.B.  MINIMUM OVER-RIDING TOLERANCE OF + OR - ', 00460000
     1F3.1,' PERCENT OF DIFF. DISTANCE PREVAILS)')                      00461000
      GO TO 1001                                                        00462000
 1000 WRITE(6,951)                                                      00463000
 1001 RETURN                                                            00464000
      END                                                               00465000
```

```
      SUBROUTINE ZONES(U,V,W,INDS,DH,DK,DL)                                  00466000
                                                                             00467000
C
C     DETERMINES VECTOR C(UVW) TO CONVERT HKL RECIPROCAL VECTORS INTO        00468000
C     ZERO ORDER PLANE                                                       00469000
C                                                                            00470000
       COMMON PRINTR,IND(3,15000),DSPACE(15000),SYM,TITLE                    00471000
      COMMON/CELL/A,B,C,COSA,COSB,COSG                                       00472000
      COMMON/RCELL/ASTAR,BSTAR,CSTAR,COSAS,COSBS,COSGS                       00473000
      DOUBLE PRECISION A,B,C,COSA,COSB,COSG,DH,DK,DL,CC                      00474000
      DOUBLE PRECISION UDASH,VDASH,WDASH                                     00475000
      DOUBLE PRECISION ASTAR,BSTAR,CSTAR,COSAS,COSBS,COSGS                   00476000
      DIMENSION INDS(3,2)                                                    00477000
      DIMENSION IZON(3),IZO(3),DIV(3),ADIV(3),JDIV(3)                        00478000
      INTEGER U,V,W                                                          00479000
C                                                                            00480000
C     DETERMINE LOWEST ORDER ZONE FOR REFERENCE SPOTS                        00481000
C                                                                            00482000
      IZON(1)=INDS(2,1)*INDS(3,2)-INDS(2,2)*INDS(3,1)                        00483000
      IZON(2)=INDS(3,1)*INDS(1,2)-INDS(3,2)*INDS(1,1)                        00484000
      IZON(3)=INDS(1,1)*INDS(2,2)-INDS(1,2)*INDS(2,1)                        00485000
      DO 1033 I=1,3                                                          00486000
      IZO(I)=IZON(I)                                                         00487000
 1033 CONTINUE                                                               00488000
 1040 IF(IABS(IZO(1))-IABS(IZO(2)))1041,1042,1042                            00489000
 1041 INV=IZO(2)                                                             00490000
      IZO(2)=IZO(1)                                                          00491000
      IZO(1)=INV                                                             00492000
 1042 IF(IABS(IZO(2))-IABS(IZO(3)))1043,1045,1045                            00493000
 1043 INV=IZO(3)                                                             00494000
      IZO(3)=IZO(2)                                                          00495000
      IZO(2)=INV                                                             00496000
      GO TO 1040                                                             00497000
 1045 INCMAX=IABS(IZO(1))                                                    00498000
 1083 DO 1061 INC=1,INCMAX                                                   00499000
      DO 1060 IZ=1,3                                                         00500000
 1046 DIV(IZ)=IABS(IZO(IZ))/((INCMAX+1.)-INC)                                00501000
      JDIV(IZ)=DIV(IZ)+0.001                                                 00502000
      ADIV(IZ)=JDIV(IZ)                                                      00503000
 1060 CONTINUE                                                               00504000
      IF(DIV(1).EQ.ADIV(1).AND.DIV(2).EQ.ADIV(2).AND.DIV(3).EQ.ADIV(3))G     00505000
     1O TO 1063                                                              00506000
 1061 CONTINUE                                                               00507000
 1063 DO 1070 I=1,3                                                          00508000
      IF(IZON(I))64,65,65                                                    00509000
   64 IZON(I)=IZON(I)/((INCMAX+1)-INC)-0.001                                 00510000
      GO TO 1070                                                             00511000
   65 IZON(I)=IZON(I)/((INCMAX+1)-INC)+0.001                                 00512000
 1070 CONTINUE                                                               00513000
      U=IZON(1)                                                              00514000
      V=IZON(2)                                                              00515000
      W=IZON(3)                                                              00516000
C                                                                            00517000
C     DETERMINE VECTOR C(UVW)                                                00518000
      UDASH=A*A*U+A*B*V*COSG+A*C*W*COSB                                      00519000
C                                                                            00520000
      VDASH=A*B*U*COSG+B*B*V+B*C*W*COSA                                      00521000
      WDASH=C*A*U*COSB+B*C*V*COSA+C*C*W                                      00522000
      CC=(U*U*A*A+2.*U*V*A*B*COSG+2.*U*W*A*C*COSB+V*V*B*B+2.*V*W*B*C*COS     00523000
     1A+W*W*C*C)*(UDASH*UDASH*ASTAR*ASTAR+VDASH*VDASH*BSTAR*BSTAR+WDASH*     00524000
     2WDASH*CSTAR*CSTAR)                                                     00525000
      CC=1/DSQRT(CC)                                                         00526000
      DH=CC*UDASH                                                            00527000
      DK=CC*VDASH                                                            00528000
      DL=CC*WDASH                                                            00529000
      RETURN                                                                 00530000
      END                                                                    00531000
```

APPENDIX 4

STRUCTURE AND PROPERTIES OF SELECTED IRON OXIDES

A4.1 FeO (Wustite)

Structure:- Cubic (f.c.c.) a_o = 0.428 to 0.431 nm[136]

FeO is a p-type conducter and has an unusually high concentration of lattice defects which consist of vacant cation sites and an equivalent number of electron defects represented chemically by Fe^{3+} ions. A relatively high rate of cation diffusion is possible, essentially via cation vacant sites.

FeO is not stable in bulk below 570°C although it may continue to be present as a thin film adjacent to the iron surface down to 400°C.

A4.2 Fe_3O_4 (Magnetite)

Structure:- Cubic (f.c.c.) a_o = 0.8394 nm[136]

Magnetite has the spinel ($MgAl_2O_4$) structure. In this structure the oxygen atoms are cubic close packed and the metal ions occupy both the tetrahedral and octahedral interstitial sites. The unit cell consists of 32 oxygen atoms and hence contains 32 octahedral and 64 tetrahedral sites. Fe_3O_4 is an example of an inverse spinel. One eighth of the tetrahedral sites are occupied by trivalent cations and half the octahedral sites are shared by the divalent and trivalent ions.

A4.3 γFe_2O_3 (Maghemite)

Structure:- Cubic a_o = 0.832 nm[136]

γFe_2O_3 is a pseudospinel probably having the $LiFe_5O_8$ type structure. γFe_2O_3 has all the reflections of the Fe_3O_4 spinel structure plus additional reflections which probably result from ordered vacancies or ordered substitution of protons for ferrous ions in certain positions of the structure. This substitution has the effect of reducing the structure to primitive cubic. In some γFe_2O_3 preparations faint extra reflections can be detected which can be indexed using a tetragonal cell with $c_o = 3a_o$; Hence γFe_2O_3 can be identified from Fe_3O_4 by the extra spots and by its slightly lower lattice parameter.

A4.4 αFe_2O_3 (Hematite)

Structure:- Rhombohedral $a_o = 0.5427$

$\alpha = 55.25^{o}$ [136]

Fe_2O_3 may be a p-type or n-type conductor, and iron and oxygen ions diffuse at approximately the same rate in Fe_2O_3 at high temperatures.

Figure A4.1 shows plan and elevation views for the common unit cells used for αFe_2O_3 and its isomorphs. The structural and morphological hexagonal and rhombohedral unit cells are all four in common use, and the face-centred rhombohedral cell has been found useful as it approximates to a distorted cubic cell with 85.7^{o} angles. The structural unit cells provide the lattice points necessary to predict the diffraction patterns, whereas the morphological cells have proved useful for morphological work.

A4.5 $\alpha FeO(OH)$ (Goethite)

Structure:- Orthorhombic $a = 0.4596$ nm

$b = 0.9957$ nm

$c = 0.3021$ nm [141]

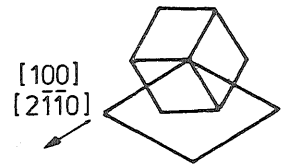

Conventional Structural
Rhombohedral a = 5.4228Å, α = 55.273°
Hexagonal a = 5.0317Å, c = 13.737Å

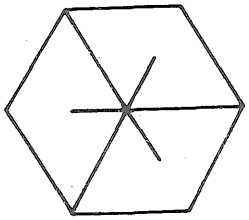

Face Centred Rhombohedral
Structural
a = 7.3976Å, α = 85.715°

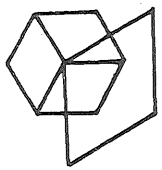

Conventional Morphological
a = 3.6988Å, α = 85.715°

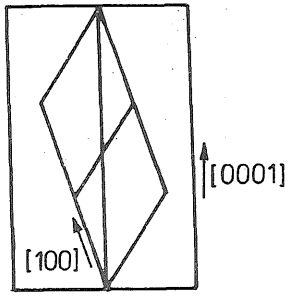

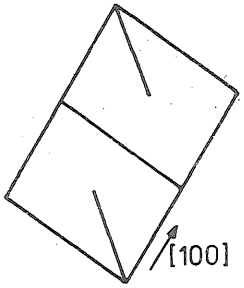

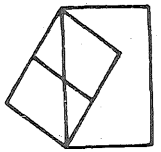

Fig. A4.1 Plan and elevation views of commonly used unit cells for αFe_2O_3.
From Gulbransen *et al*

A4.6 γFeO(OH) (Lepidocrocite)

Structure:- Orthorhombic

a = 0.389 nm

b = 1.254 nm

c = 0.307 nm [142]